Sustainable recovery of gold using glycine

By

Mohammadreza Azadi

MEng

This thesis is presented for the degree of

Doctor of Philosophy

of The University of Western Australia

Supervisors:

Associate Professor Dr. Ali Karrech (Coordinating and principal)
Dr. Mohamed Elchalakani

THE UNIVERSITY OF WESTERN AUSTRALIA

Department of Civil, Environmental and Mining Engineering
School of Engineering
Faculty of Engineering and Mathematical Sciences

2021

Abstract

Identifying a non-toxic solution to recover metals such as gold, silver and copper from ores is of ultimate significance to the mining industry and its stakeholders. Recently, new studies have been conducted on the leaching of gold and copper using alkaline glycine as an environmentally friendly lixiviant. The results are promising and may sparkle considerable interests by the mining industry. However, it is important to understand the behaviour of glycine in aqueous solutions in the presence of various metals.

Glycine has been used in hydrometallurgy as a buffer for many decades. However, its structure and behaviour as reagent are yet to be explored. In this study, the behaviour of glycine in aqueous solution is investigated using the revised Helgeson-Kirkham-Flowers (HKF) equations of state and temperature and pressure dependent thermodynamic data. Peptides of glycine, their ionisation states and their mutual equilibrium reactions are also investigated. Equilibrium constants are calculated for the glycine species and their corresponding reactions. Consequently, the mole fraction and stability of glycine and its peptides were identified as functions of pH and temperature.

It is important to identify the thermodynamic properties and stability domains of the metal-glycinate complexes. In previous studies the thermodynamic equilibrium has been investigated for divalent metal-glycinate formations only. Thermodynamic data of monovalent metal-glycinate are scarce in general and inexistent for most of precious metals including gold. To estimate the equilibrium constant of monovalent metal-glycinate formations, a data analysis has been conducted which correlates the standard partial molal properties of metal-glycinate complexes and the standard partial molal properties of metals at ambient conditions.

The potential of environmentally friendly glycine in the in-situ leaching of gold was investigated by employing a microfluidic system with controlled flow, temperature and fluid composition. This technique can provide real time measurements with low consumption of chemicals. Although the microfluidic fabrication is time consuming, the results can be obtained in a shorter period of time. In particular, electrokinetic in-situ leaching (EK-ISL) has been evaluated for gold using alkaline-glycine. By applying a voltage gradient, the transport of ions from low-permeable ore bodies is enhanced through the reagents. We examined the potential of alkaline glycine to leach gold through a low-permeability medium consisting of micro-silica sand and gold powder. The experiment was conducted in the different voltages: 0, 5, 10, 20 and 30 V. Each stage took 4 days irrespective of the level of leaching. In addition, the effects of copper and sulphides were evaluated by adding 10% chalcopyrite and pyrite, respectively. The results show that gold recovery increases when voltage increases. However, the gold recovery dramatically decreases in the presence of chalcopyrite and pyrite.

Acknowledgments

I would like to express my deep and sincere gratitude to my supervisor, Associate Professor Ali Karrech, for the continuous support and help throughout my Ph.D study. During the past three years, I have learnt a lot from him on both professionally and personally for his patience, encouragement, motivation and immense knowledge. I feel proud and lucky to be one of his students.

I would like to thank my co-supervisor, Dr. Mohamed Elchalakani for his support, guidance and encouragement in various parts and phases of this research.

Many thanks to my collaborators, and research team members: Mostafa Attar, Andrew van de Ven, Xiangjian Dong, and Professor Hakan Basir for their company and help during these years of study. We have shared several ideas through stimulating conversations which inevitably affected my academic development.

To friends and staff who supported me with their positive words during my Ph.D research: Hamidreza Ezadi, , Harry Watts, Karen Leers, Heather Gordon, and Michelle Wright.

The financial support from Robert and Maude Gledden Postgraduate Scholarships was highly appreciated.

Last year (2020) was the worst year in my life and for many others around the world due to pandemic. I lost my Dad and I could not go to Iran for his funeral. He spent all his life for his children. He always wanted to see my Ph.D degree. From the bottom of my heart, my gratitude goes to my Dad and Mom, for their love and encouragement.

Declaration

I, Mohammadreza Azadi, certify that:

This thesis has been substantially accomplished during enrolment in this degree. This thesis does not contain material which has been submitted for the award of any other degree or diploma in my name, in any university or other tertiary institution. In the future, no part of this thesis will be used in a submission in my name, for any other degree or diploma in any university or other tertiary institution without the prior approval of The University of Western Australia and where applicable, any partner institution responsible for the joint-award of this degree. This thesis does not contain any material previously published or written by another person, except where due reference has been made in the text and, where relevant, in the Authorship Declaration that follows. This thesis does not violate or infringe any copyright, trademark, patent, or other rights whatsoever of any person. This thesis contains published work, some of which has been co-authored.

[redacted] 20/08/2022

Authorship declaration: Co-authored publications

AUTHORSHIP DECLARATION: CO-AUTHORED PUBLICATIONS

This thesis contains work that has been published.

Details of the work:
Data analysis and estimation of thermodynamic properties of aqueous monovalent metal–glycinate complexes. Fluid Phase Equilibria, 480, 25–40.

Location in thesis:
Chapter 2

Student contribution to work:
70 %.

Co-author signatures and dates: 13/10/2021
[redacted]

Student signatu[redacted]

Date: 18/10/2021

I, Ali Karrech certify that the student's statements regarding their contribution to each of the works listed above are correct.

As all co-authors' signatures could not be obtained, I hereby authorise inclusion of the co-authored work in the thesis.

Coordinating supervisor signature: [redacted]

Date: 18/10/2021

AUTHORSHIP DECLARATION: CO-AUTHORED PUBLICATIONS

This thesis contains work that has been published.

Details of the work:
Microfluidic study of sustainable gold leaching using glycine solution. Hydrometallurgy, 185, 186–193.
Location in thesis:
Chapter 3

Student contribution to work:
70 %.

Co-author signatures and dates: 18/10/2021
[redacted]

Student signat[redacted]

Date: 18/10/2021

I, Ali Karrech certify that the student's statements regarding their contribution to each of the works listed above are correct.

As all co-authors' signatures could not be obtained, I hereby authorise inclusion of the co-authored work in the thesis.

Coordinating supervisor signature: [redacted]

Date: 18/10/2021

AUTHORSHIP DECLARATION: CO-AUTHORED PUBLICATIONS

This thesis contains work that has been prepared for publication.

Details of the work:
Electrokinetic study on leaching gold using alkaline glycine.
Location in thesis:
Chapter 5

Student contribution to work:
70 %.

Co-author signatures and dates: 18/10/2021
[redacted]

Student signat[redacted]

Date: 18/10/2021

I, Ali Karrech certify that the student's statements regarding their contribution to each of the works listed above are correct.

As all co-authors' signatures could not be obtained, I hereby authorise inclusion of the co-authored work in the thesis.

Coordinating supervisor signature: [redacted]

Date: [redacted] 18/10/2021

List of Figures

List of Tables

Chapter 1

Introduction

1.1 Introduction

Cyanide is the standard and robust substance that leaches gold from low grade secondary processing pads. However, it cannot be used for in-situ recovery because of its toxicity. Therefore, other reagents that have less toxicity and environmental footprint have been investigated through recent research initiative. For example, thiosulphate, acidic thiocyanate, halides, thiourea, organic reagents, and glycine have been examined as potential alternatives to cyanide [1–9]. In addition, [10] examined the effects of pH and impurities on gold solubility in amino acids; their results suggest that samples with higher copper contents produce higher gold and copper recoveries in the presence of hydrogen peroxide which facilitates the oxidative dissolution of metals. Since copper is known to dissolve easily in amino acid solutions [11], the enhanced solubility of gold could be due to the increased surface area exposed by the dissolving copper. [12] examined the effect of adding amino acids to thiosulphate for gold leaching and found that gold recovery increases as amino acids are added to thiosulphate solutions. At a later stage, [7] conducted experiments on the leaching copper from gold-copper concentrates in glycine solutions. They studied the effects of glycine concentration and pH in the presence and absence of hydrogen peroxide. [8] investigated the leaching of gold, silver, and their alloys in alkaline glycine with exposure to hydrogen peroxide. They found that glycine is a more effective gold/silver lixiviant in pH ranging from 10 to 11 and temperature of about 60^oC. They also examined the effect of glycine concentration and showed that it improves gold solubility. Despite the importance of glycine as a promising substance for the mining industry, its behaviour in aqueous solution has not been investigated comprehensively. Therefore, this chapter is intended to bridge this gap and evaluate the role of glycine in the leaching of base/precious metals.

There has been a considerable effort in collecting and documenting the thermodynamic data of various chemicals including glycine and its complexes during the last two decades [13–16]. These contributions were based on earlier work of Helgeson and coauthors [17–19] who predicted the behaviour of aqueous electrolytes at high temperature and pressure using some equations known as Helgeson-Kirkham-Flowers (HKF) equations of state. The revised HKF equations of state have been used to predict the thermodynamic properties of aqueous species at temperatures up to $1{,}000^oC$ and pressures up to 5 kb [19, 20]. Group additivity

equations of state for aqueous organic molecules have been generated by combining the revised HKF equations of state of chemical species [21–23]. The thermodynamic data and the revised HKF equations of state for many aqueous organic species including amino acids have been calculated [23–26]. The revised HKF equations of state have been used to predict the polymerisation behaviour of organic species as a function of temperature, pressure, pH, and redox state [27, 28]. The thermodynamic data collected to establish equations of state were not dedicated to the leaching applications and often need careful verification to ensure that all the relevant species exist in a given database before major simulations and/or important conclusions can be drawn. The above studies have addressed the thermodynamic behaviour of glycine but not for leaching applications, despite the existence of some experimental studies that document the reactions between glycine and Au/Cu [7, 8, 10, 29]. However, these contributions are empirical in nature. In this chapter, we apply the basic principles of thermodynamics to investigate the behaviour of glycine at various levels of pH and temperature. Therefore, systematic thresholds of stability will be obtained which may facilitate the leaching processes of base/precious metals. In other words, this chapter shows why alkaline is the best condition of glycine-based aqueous solutions to leach target metals using leaching techniques. Amino acids can react with a large range of metals [30]. Using amino acids to leach the metals from ores could be a new door for mining industries not only for the leaching process but also for any possible replacement of processes that involve lixiviant-metal interactions.

This chapter is to explain the basic structure of glycine and chemical reactions between glycine and its peptides. The governing equations and corresponding thermodynamic data will be well explained including the behaviour of glycine and its peptides in aqueous solution. Mole fraction and the behaviour of glycine under different pH and temperature conditions, and the importance of alkaline environment in such mixtures will be discussed. Objectives and outline of the thesis will be presented in the last parts.

1.2 Basic chemical reactions

Glycine (NH_2CH_2COOH) has three dissociation states in water, namely glycinium cation $^+H_3NCH_2COOH$ (Gly^+), zwitterion $^+H_3NCH_2COO^-$ ($Gly^\pm$), and glycinate anion H2NCH2COO$^-$ (Gly^-). The equilibrium concentration of non-zwitterionic forms is negligible at room temperature [35].

$$NH_2CH_2COOH + H_2O \Leftrightarrow H_2NCH_2COO^- + H_3O^+; \qquad K_a = \frac{[Gly^-][H_3O^+]}{[Gly]} \tag{1.1}$$

$$H_2NCH_2COO^- + H_2O \Leftrightarrow {}^+H_3NCH_2COO^- + OH^-; \qquad K_b = \frac{[Gly^\pm][OH^-]}{[Gly^-]} \tag{1.2}$$

$$H_3O^+ + OH^- \Leftrightarrow H_2O; \qquad K_w = [H_3O^+][OH^-] \tag{1.3}$$

Species	$\triangle_f \bar{G}^{o\,a}$	$\triangle_f \bar{H}^{o\,a}$	$\bar{S}^{o}_{Pr,Tr}{}^{b}$	$\bar{C}^{o\,b}_{P}$	$\bar{V}^{o\,c}$	$a^d_1 \times 10$	$a^e_2 \times 10^{-2}$	a^f_3	$a^g_4 \times 10^{-4}$	c^b_1	$c^g_2 \times 10^{-4}$	$\omega^e \times 10^{-5}$
$Gly^{\pm}$	-380.53^h	-522.08^h	164.39^h	39.33^h	43.19^h	48.54^h	-2.40^h	5.19^h	-10.71^h	70.76^h	-20.25^h	-1.07^h
$Gly^{\pm}$	-370.79^k	-513.92^k	158.53^k	38.91^i	43.20^i	47.28^i	2.97^i	16.69^i	-12.72^i	119.24^i	-35.15^i	0.96^i
Gly^{+}	-384.18^j	-517.94^j	190.12^j	166.10^o	49.90^o	65.15^p	-34.56^p	-27.70^p	1.97^p	165.27^p	-5.06^p	-1.38^p
Gly^{-}	-314.93^j	-469.74^j	119.54^j	-3.35^o	45.70^o	40.75^p	14.81^p	83.97^p	-19.79^p	90.37^p	-33.14^p	2.89^p
$GlyGly^{\pm}$	-489.53^p	-735.09^p	220.71^p	117.15^p	77.40^p	73.89^p	28.07^p	209.49^p	-66.57^p	289.95^p	-74.10^p	2.47^p
$GlyGly^{+}$	-507.45^j	-735.21^j	280.45^j	979.06^p	84.70^p	92.26^p	-33.47^p	-96.19^p	23.81^p	142.67^p	-0.42^p	-10.29^p
$GlyGly^{-}$	-442.33^j	-691.70^j	200.71^j	270.70^p	80.40^p	67.86^p	15.90^p	15.44^p	2.01^p	67.78^p	-28.49^p	-6.02^p
$GlyGlyGly^{\pm}$	-605.59^p	-949.64^p	295.93^p	184.93^i	112.10^i	101.00^i	29.16^i	140.96^i	-44.73^i	267.36^i	-69.45^i	-6.44^i
$GlyGlyGly^{+}$	-623.96^j	-950.48^j	354.80^j	302.08^p	119.40^p	119.34^p	-32.38^p	-164.72^p	45.65^p	120.08^p	4.23^p	-19.20^p
$GlyGlyGly^{-}$	-559.40^j	-907.93^j	280.91^j	132.63^p	115.10^p	94.93^p	16.99^p	-53.09^p	23.85^p	45.19^p	-23.85^p	-14.94^p
DKP	-240.33^k	-415.47^k	223.84^k	143.93^p	76.80^p	70.46^p	13.68^p	45.77^p	-21.51^p	119.24^p	-31.13^p	-9.62^p
OH^{-}	-157.30^l	-230.02^m	-10.71^m	-137.19^n	-4.18^n	5.24^l	0.31^l	7.71^l	-11.64^l	17.36^l	-43.29^l	7.22^l

Table 1.1: Standard molal thermodynamic data and the revised HKF equations of state for disociated states of glycine and its peptides. Disociated states of glycine include glycinium cation $^{+}H_3NCH_2COOH$ (Gly^{+}), zwitterion $^{+}H_3NCH_2COO^{-}$($Gly^{\pm}$), and glycinate anion H2NCH2COO^{-}(Gly^{-}). Glycine peptides can be synthesized by bonding Glycyl ($NH_2CH_2CO^{-}$) to glycine or disociated states of glycine to make $GlyGly^{-}$, $GlyGly^{\pm}$, and $GlyGly^{+}$. Accordingly, $GlyGlyGly^{-}$, $GlyGlyGly^{\pm}$, and $GlyGlyGly^{+}$ can be made by bonding Glycyl ($NH_2CH_2CO^{-}$) to two moles of glycine or disociated states of glycine. DKP (diktopeperazine)can be made from glycine peptides (GlyGly) by loosing one mole of H_2O with one extra linkage. DKP has a ring structure compared to normal peptides with chain structures. ^{a} kJ mol^{-1}, ^{b} J mol^{-1} K^{-1}, ^{c} Cm^3 mol^{-1}, ^{d} J mol^{-1} bar^{-1}, ^{e} J mol^{-1}, ^{f} J K mol^{-1} bar^{-1}, ^{g} J K mol^{-1}, ^{h} [23], ^{i} [24], ^{j} [31], ^{k} [13], ^{l} [21], ^{m} [32], ^{n} [20], ^{o} [33], ^{p} [34].

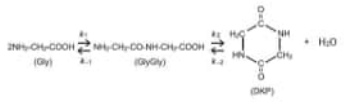

Figure 1.1: Reaction pathways between Gly, GlyGly, and DKP (diktopeperazine). DKP can be made from glycine peptides (GlyGly) by loosing one mole of H_2O with one extra linkage. DKP has a ring structure compared to normal peptides with chain structures.

$$NH_2CH_2COOH \Leftrightarrow {}^+H_3NCH_2COO^-; \qquad K = \frac{[Gly^{\pm}]}{[Gly]} = \frac{K_a K_b}{K_w} \tag{1.4}$$

The above equilibrium reactions (Eqs. 1.1 to 1.4) show the relations that govern the different states of glycine.

where [.] denotes concentration. The expressions of equilibrium constants so defined mean that the activity coefficients are close to unity, which is valid in the case of dilute solutions. The equilibrium constant K in Eq. 1.4 is equal to 4.91×10^5 at ambient conditions [36]. Since K is large, glycine exists predominantly as zwitterion in the neutral solution. By titration of glycine with NaOH, two equilibrium reactions can occur:

$$Gly^{\pm} \Leftrightarrow Gly^- + H^+; \qquad pK_{a1} = -log_{10}\frac{[Gly^-][H^+]}{[Gly^{\pm}]} \tag{1.5}$$

$$Gly^+ \Leftrightarrow Gly^{\pm} + H^+; \qquad pK_{a2} = -log_{10}\frac{[Gly^{\pm}][H^+]}{[Gly^+]} \tag{1.6}$$

It is also possible to produce Gly peptides and their ionization states in water by increasing the concentration of Gly. Gly peptides are formed as diketopiperazine (DKP), diglycine/glycylglycine (GlyGly), triglycine/glycylglycylglycine (GlyGlyGly), tetraglycine (GlyGlyGlyGly), pentaglycine (GlyGlyGlyGlyGly), hexaglycine (GlyGlyGlyGlyGlyGly) and so on. Glycine peptides can be synthesized by bonding Glycyl ($NH_2CH_2CO^-$) to Gly instead of H^+ as follows:

$$2(NH_2CH_2COOH) \Leftrightarrow NH_2CH_2CONHCH_2COOH + H_2O \tag{1.7}$$

$$3(NH_2CH_2COOH) \Leftrightarrow NH_2CH_2CONHCH_2CONHCH_2COOH + 2H_2O \tag{1.8}$$

$$nGly \Leftrightarrow peptides + (n-1)H_2O \tag{1.9}$$

In addition, Fig. 1.1 presents reaction pathways between Gly, GlyGly, and DKP as discussed [37].

Numerous thermodynamic studies have been conducted on Gly and its peptides at different temperatures [13, 38–43]. [44] claimed that the polymerisation of amino acids does not occur in the presence of liquid water at temperatures ranging from 150 to 180^{o}C. [45] claimed that the equilibrium reaction of n *aminoacids* $\Leftrightarrow$ *peptide* $+ (n-1)H_2O$ is unfavourable in the presence of liquid water at all temperatures. However, [46] indicated

that neither of these statements is accurate and both are in conflict with the experimental data reported by [47]. Many mineral dehydration reactions are documented in metamorphic rocks and have been widely studied by experimental petrologists. Dehydration reactions occur during the transformation of biochemicals into organic matter found in sedimentary rocks [46]. Many other transformations leading to biomarkers and polymerised compounds found in sedimentary rocks and petroleum involve dehydration reactions, which occur in the presence of aqueous solutions [48, 49]. The behaviour of Gly as a lixiviant in the leaching process of base and precious metals requires careful investigation to optimise its impact on recovery at various temperatures, pH levels and Gly concentrations.

1.3 Governing thermodynamic equations

The primary thermodynamic data and the parameters of revised HKF equations of state of glycine and its peptides including the updated data provided by [34] are presented in table 1.1. The following sections explain how to calculate the temperature dependence of standard partial molar Gibbs free energy, standard partial molar heat capacity, and the standard partial molar volume of Gly at various temperatures. The standard partial molar Gibbs free energy of a reaction is calculated using the following equation.

$$\Delta\bar{G}^o_r = \sum_i v_{i,r}\Delta\bar{G}^o_i \tag{1.10}$$

$\Delta\bar{G}^o_i$ [kJ mol] stands for standard partial molal Gibbs free energy of formation and $v_{i,r}$ the stoichiometric coefficient of the ith species in the reaction. $\Delta\bar{G}^o_i$ is calculated for Gly and its peptides at different temperatures using the thermodynamic data and the revised HKF equations of state of Gly. As shown by [19] and [20], the relations between the revised HKF equations of state and $\Delta\bar{G}^o$ can be written as follows:

$$\begin{aligned}
&\triangle\bar{G}^o = \triangle\bar{G}^o_r - \bar{S}^o_{P_r,T_r}(T - T_r) \\
&- c_1[Tln(\frac{T}{T_r})] - c_2[(\frac{1}{T-\theta}) - (\frac{1}{T_r-\theta})](\frac{\theta-T}{\theta}) + c_2(\frac{T}{\theta^2})ln[\frac{T_r(T-\theta)}{T(T_r-\theta)}] \\
&+ a_1(P - P_r) + a_2 ln(\frac{\Psi+P}{\Psi+P_r}) + (\frac{1}{T+\theta})[a_3(P-P_r) + a_4 ln(\frac{\Psi+P}{\Psi+P_r})] \\
&+ \omega[(\frac{1}{\varepsilon}) - 1] - \omega_{P_r,Tr}[Y_{P_r,T_r}(T_r - T) + (\frac{1}{\varepsilon_{P_r,T_r}}) - 1]
\end{aligned} \tag{1.11}$$

Therein, $\Delta\bar{G}^o_r$ represents the standard partial molal Gibbs energy of formation of the species at the reference temperature (T_r= 273 ^{o}K). $\Delta\bar{G}^o$ [kJ mol] and $\bar{S}^o_{P_r,T_r}$ [J mol^{-1} K^{-1}] represent the standard partial molal Gibbs energy and the standard partial molal entropy of formation of the species at the temperature T and pressure P of interest, respectively. The parameters a_1 [J mol^{-1} bar^{-1}], a_2 [J mol^{-1}], a_3 [J K mol^{-1} bar^{-1}], a_4 [J K mol^{-1} bar^{-1}], c_1 [J mol^{-1} K^{-1}], and c_2 [J K mol^{-1} bar^{-1}] are temperature and pressure independent properties of the species, the parameters θ = 228 ^{o}K and Ψ = 2600 bar are intrinsic to the solvent, ω [J mol^{-1}] denotes the Born coefficient of the species, and ε stands for the dielectric constant of H_2O, and Y represents the partial derivatives of the reciprocal dielectric constant of H_2O expressed by $-(\frac{\delta(\frac{1}{\varepsilon})}{\delta T})_P$. The subscripts P_r and T_r stand for the pressure and temperature of reference, respectively. The following expression can be

used to relate the equilibrium constant of a given reaction to its standard molal Gibbs free energy [23].

$$\Delta\bar{G}_r^o = -2.303RTlog_{10}K = \sum_i v_{i,r} log_{10}\alpha_i \tag{1.12}$$

where R is the gas constant (8.31447 J mol^{-1} K^{-1}), T is the temperature in Kelvin and α_i is the activity of the ith species, and K is equilibrium constant of the reaction. Numerous studies have been carried out to calculate the standard partial molar heat capacity $\bar{C}_p^o$ [J mol^{-1} K^{-1}] and the standard partial molar volume $\bar{V}^o$ [cm3 mol−1] of species [23, 33, 36, 41, 50–52]. In the case of Gly and its peptides, [24] proposed the following equations:

$$\bar{C}_p^o = c_1 + \frac{c_2}{T-\theta} + \omega TX \tag{1.13}$$

$$\bar{V}^o = \sigma + \frac{\xi}{T-\theta} + \omega Q \tag{1.14}$$

$$\sigma = a_1 + \frac{a_2}{\Psi + P} \tag{1.15}$$

$$\xi = a_3 + \frac{a_4}{\Psi + P} \tag{1.16}$$

where the terms Q, Y, and X represent the partial derivatives of the reciprocal dielectric constant of H_2O expressed by $-(\frac{\delta(\frac{1}{\varepsilon})}{\delta P})_T$, $-(\frac{\delta(\frac{1}{\varepsilon})}{\delta T})_P$, and $(\frac{\delta(Y)}{\delta T})_P$, respectively. σ and ξ are volumetric parameters defined by [24].

1.4 Behavior of Gly and its peptides

The standard molar Gibbs free energy and the subsequent equilibrium constant of the reactions between Gly, Gly peptides and their ionization states can be predicted at various temperatures. $\Delta\bar{G}_r^o$ has been calculated using Eq. 1.11 at various temperatures and atmospheric pressure. At ambient temperature (25^oC), $\Delta\bar{G}_f^o$ of H_2O is about -237.17 kJ mol^{-1} [53]. The thermodynamic data of water at higher temperatures provided by [54] can be used to calculate standard molar Gibbs free energy. Using Eq. 1.12, $\log_{10} K$ for Gly, its peptides and their ionization states also have been calculated at any temperature up to 100^oC. Eqs. 1.7 and 1.8 are used to calculate the standard molar Gibbs free energy of equilibrium reactions between Gly and its peptides for each dissociation state separately.

Fig. 1.2 shows the molar Gibbs free energy $\Delta\bar{G}_r^o$ of the equilibrium reaction of Gly and its peptides to their ionization states. The values of $\Delta\bar{G}_r^o$ obtained for the reactions involving Gly as represented by Eq. 1.5 (resp. A.3) are -55.86 (resp. -13.39) kJ mol^{-1} at 25^oC and -59 (resp. -16.49) kJ mol^{-1} at 100^oC. In the case of $GlyGly^{\pm}$ to $GlyGly^{-}$ (resp. $GlyGly^{+}$ to $GlyGly^{\pm}$), the values of molar Gibss free energy for reactions are -47.2 (resp. -17.91) kJ mol^{-1} at 25^oC and -50.14 (resp. -2.9 kJ) mol^{-1} at 100^oC. Similarly, $\Delta\bar{G}_r^o$ for $GlyGlyGly^{\pm}$ to $GlyGlyGly^{-}$ (resp. $GlyGlyGly^{+}$ to $GlyGlyGly^{\pm}$) reactions are -46.19 (resp. -18.37) kJ mol^{-1} at 25^oC and -49.14 (resp. -21.92) kJ mol^{-1} at 100^oC. Fig. 1.3 shows the variation of $\Delta\bar{G}_r^o$ with respect of temperature corresponding to different dissociation states of Gly into Gly peptides.

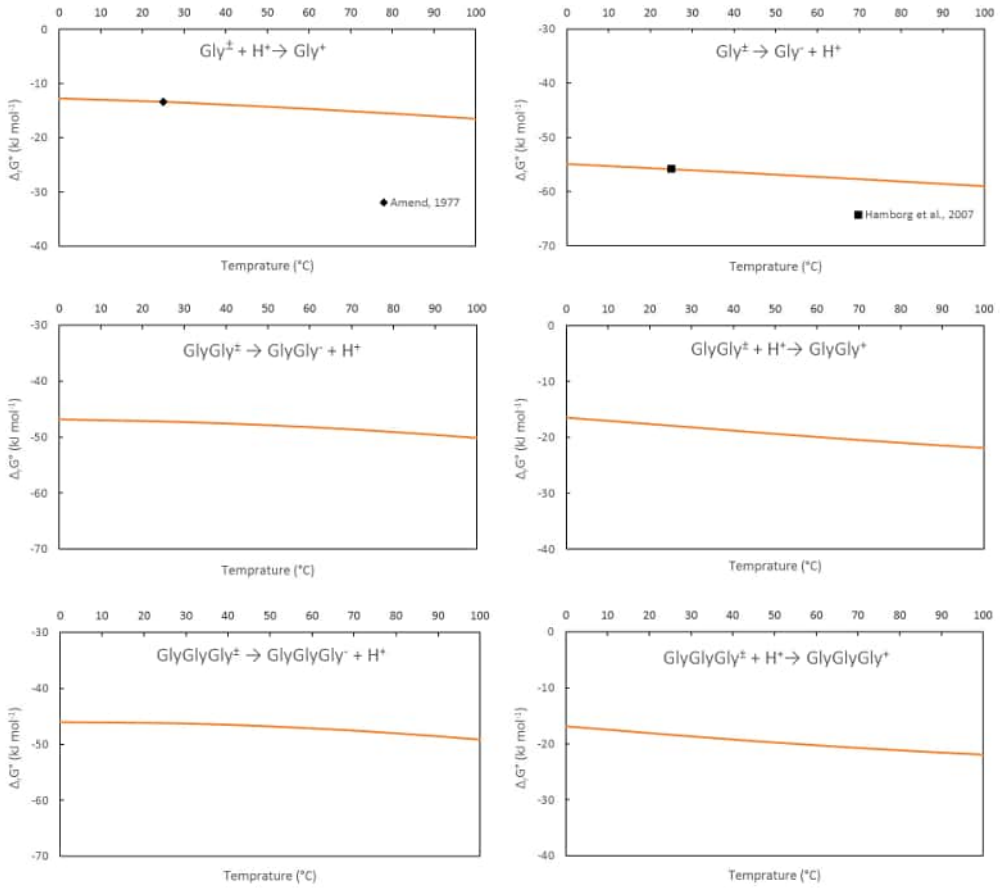

Figure 1.2: Standard partial molal Gibbs free energy ($\Delta\bar{G}_r^o$) for equilibrium reactions among ionization states of glycine and its peptides as a function of temperature. Continuous line represents the data generated in this study.

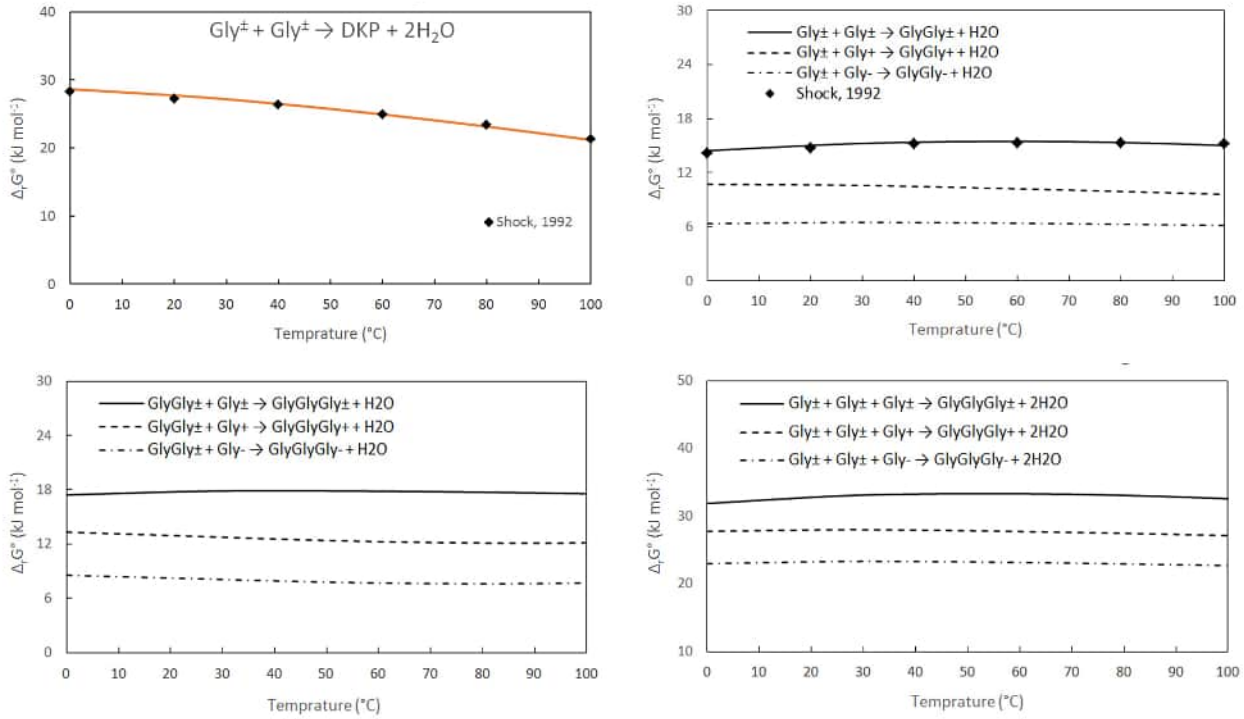

Figure 1.3: Standard partial molal Gibbs free energy ($\Delta\bar{G}_r^o$) for polymerisation of $Gly^{\pm}$ to DKP, Gly to GlyGly and Gly to GlyGlyGly as a function of temperature. Standard partial molal Gibbs free energy ($\Delta\bar{G}_r^o$) of the reactions for Gly to GlyGly and Gly to GlyGlyGly have been calculated separately for dissociated states of Gly and GlyGly. ($\Delta\bar{G}_r^o$) of the reactions with $Gly^{\pm}$ are higher than ($\Delta\bar{G}_r^o$) of the reactions with Gly^{+} and ($\Delta\bar{G}_r^o$)of the reactions with Gly^{+} are higher than ($\Delta\bar{G}_r^o$) of the reactions with Gly^{-}.

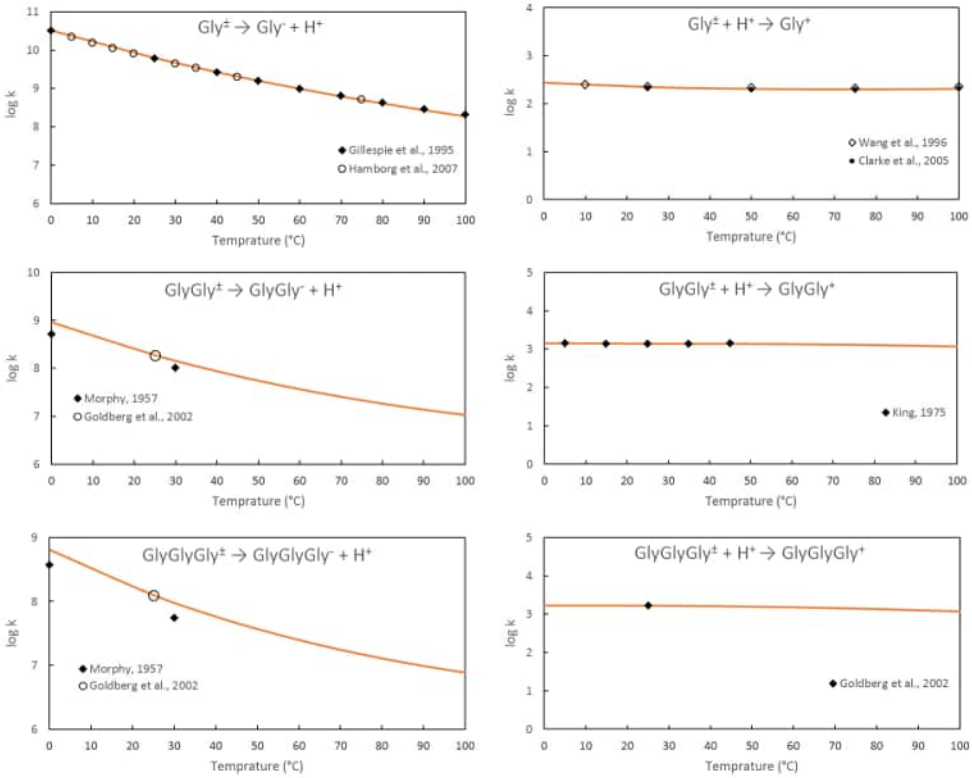

Figure 1.4: Standandard equilibrium constant $\log_{10} K$ for the reactions among disociated states of Gly and its peptides as a function of temperature. Continuous line represents the data generated in this study. The symbols pointed on the graphs are available data reported by previous researchers. The values of $\log_{10} K$ obtained in this study are consistent with those retrieved from literature.

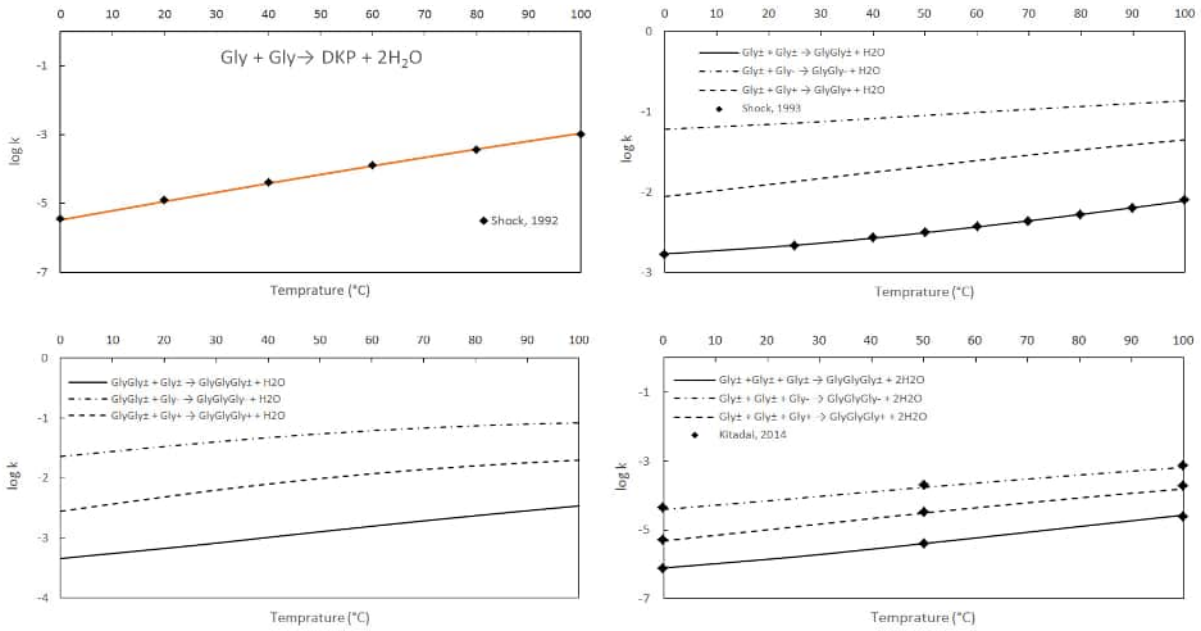

Figure 1.5: Standard equilibrium constant $\log_{10} K$ for polymerisation of Gly to DKP, Gly to GlyGly and Gly to GlyGlyGly as a function of temperature. Standard equilibrium constant $\log_{10} K$ of the reactions for Gly to GlyGly and Gly to GlyGlyGly have been calculated separately for dissociated states of Gly and GlyGly. As it is clear, $\log_{10} K$ of the reactions with Gly^- are higher than $\log_{10} K$ of the reactions with Gly^+ and $\log_{10} K$ of the reactions with Gly^+ are higher than $\log_{10} K$ of the reactions with $Gly^{\pm}$.

Fig. 1.4 shows the temperature variation of $\log_{10} K$ of the reaction between Gly and its peptides to produce ionization states. $\log_{10} K$ for the equilibrium reaction represented by Eq. 1.5 (resp. 1.6), is equal to 9.79 (resp. 2.34) at 25^oC . In the case of GlyGly, the values of $\log_{10} K$ corresponding to the reaction represented by Eq. 1.5 (resp. 1.6) is 8.27 (resp. 3.14) at 25^oC. Similarly, these values are respectively 8.1 and 3.22 for GlyGlyGly at 25^oC.

Fig. 1.5 presents the variation of $\log_{10} K$ with respect to temperature corresponding to various reactions of Gly and its peptides into ionization states. The value of $\log_{10} K$ in the case of chemical reactions following Eq. 1.7 at 25^oC is -2.66 (resp. -1.86 and -1.14) for $GlyGly^{\pm}$ (resp. $GlyGly^+$ and $GlyGly^-$). The value of $\log_{10} K$ is -4.82 at 25^oC for DKP. As it can be seen in Fig. 1.2 to 1.5, the thermodynamic data of $\Delta \bar{G}_r^o$ and $\log_{10} K$ calculated in this study are consistent with those provided previously [13, 23, 31, 34, 46, 55–59].

1.5 Mole fraction and stability of Gly, GlyGly and GlyGlyGly

An amino acid consists of a basic amino group, an acidic carboxyl group, and a characteristic side chain. The degree of protonation of these functional groups changes depending on the solution pH ($-NH_3^+ \Leftrightarrow -NH_2 + H^+$, $-COOH \Leftrightarrow -COO^- + H^+$). In addition, the net charge of the amino acid molecule changes accordingly [37]. Amino acids generally show the highest polymerisation reactivity under anionic state [60, 61]. Consequently, the zwitterion of Gly is more likely to give a proton away than to take another one. Therefore, the polymerisation of Gly intensifies as pH increases. This can be confirmed by verifying

that the $\log_{10} K$ of the reaction $Gly^{\pm} + Gly^{-} \rightarrow GlyGly^{-}$ is higher than its counterpart of $Gly^{\pm} + Gly^{\pm} \rightarrow GlyGly^{\pm}$. [34] graphed the equilibrium concentrations of GlyGly, DKP, and GlyGlyGly at different temperature and pH levels with an initial Gly concentration of 1mM. The likelihood of peptides occurrence is low at high pH where high Gly^{-} concentrations can exist. The maximum concentrations of GlyGly, DKP and GlyGlyGly are 2.2×10^{-5}, 2×10^{-8}, and 1.5×10^{-11}, respectively, at 25^{o}C. These concentrations change to 3.8×10^{-5}, 0.9×10^{-6}, and 1.2×10^{-10}, respectively when temperature increases to 100^{o}C.

Using the following equations and the relation between the standard equilibrium constant of the reactions, concentration of GlyGly can be estimated [37].

$$Gly + Gly \Leftrightarrow GlyGly + H_2O \tag{1.17}$$

$$Gly^{\pm} + Gly^{\pm} \Leftrightarrow GlyGly^{\pm} + H_2O \tag{1.18}$$

$$Gly^{\pm} + Gly^{-} \Leftrightarrow GlyGly^{-} + H_2O \tag{1.19}$$

$$Gly^{-} + Gly^{-} \Leftrightarrow GlyGly^{-} + OH^{-} \tag{1.20}$$

$$[GlyGly] = K'[Gly]^2 = K_1[Gly^{\pm}]^2 + K_2[Gly^{\pm}][Gly^{-}] + K_3[Gly^{-}]^2 \tag{1.21}$$

where K', K_1, K_2, K_3 are equilibrium constants referred to Eqs. 1.17, 1.18, 1.19 and 1.20, respectively. Eq. 1.21 presents the relation between equilibrium constant of the reactions represented by Eqs. 1.17 to 1.20. The sum of $[Gly^{\pm}]$ and $[Gly^{-}]$ is equal to [Gly] [37]. If the molar fraction of $[Gly^{\pm}]$ and $[Gly^{-}]$ are α and β respectively, then $\alpha[Gly^{-}]$= [Gly], $\beta[Gly^{\pm}]$= [Gly], and $\alpha + \beta = 1$. Hence, Eq. 1.21 becomes

$$k'[Gly]^2 = (k_1 - k_2 + k_3)\alpha^2 + (k_3 - 2k_2)\alpha + k_3[Gly]^2 \tag{1.22}$$

$$k' = (k_1 - k_2 + k_3)\alpha^2 + (k_3 - 2k_2)\alpha + k_3 \tag{1.23}$$

The concentration of GlyGly can be calculated from Eqs. 1.21 to Eq. 1.23.

Fig.1.6 shows the changes of dissociation states of Gly and GlyGly with respect to pH at temperatures 25^{o}C, 60^{o}C, and 100^{o}C. It can be seen that $Gly^{\pm}$ and Gly^{-} exist in approximately equal mole fractions at pH values of about 9.79, 8.98 and 8.26 corresponding to 25^{o}C, 60^{o}C, and 100^{o}C, respectively. Similarly, the mole fractions of $Gly^{p}m$ and Gly^{+} are equal at pH values of about 2.34, 2.30 and 2.30 corresponding to 25^{o}C, 60^{o}C and 100^{o}C. The same conditions exist for the GlyGly dissociation states. $GlyGly^{\pm}$ and $GlyGly^{-}$ are equal at pH values of about 8.27, 7.76 and 7.02 corresponding to 25^{o}C, 60^{o}C and 100^{o}C. Finally, the fraction of $GlyGly^{\pm}$ and $GlyGly^{+}$ are equal when pH reaches 3.14, 3.12 and 3.02 corresponding to 25^{o}C, 60^{o}C and 100^{o}C. It can be seen that the pH of the dissociation states of Gly shifts left by increasing the temperature which means that the reaction $Gly^{\pm} + Gly^{-} \rightarrow GlyGly^{-}$ occurs at lower pH as temperature increases. Using Fig. 1.6, each α can be attributed to a pH. To refine the proposed analysis, we now

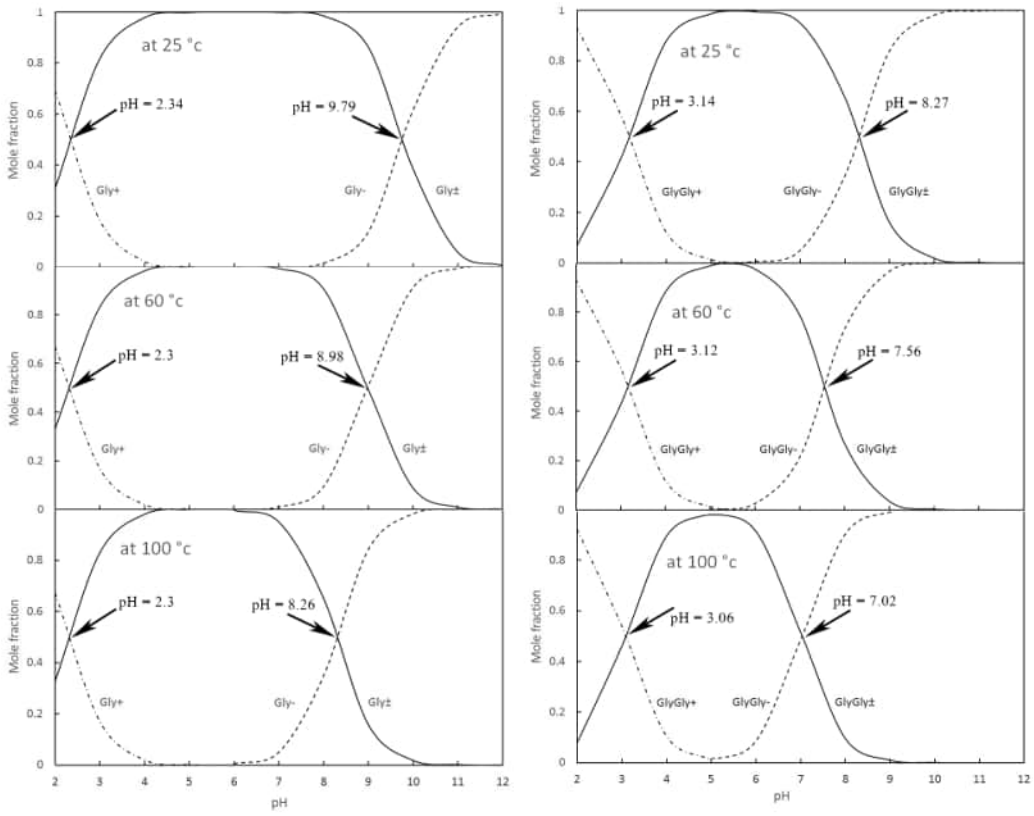

Figure 1.6: Mole fraction and dissociation change of Gly and GlyGly as a function of pH at 25^{o}C, 60^{o}C and 100^{o}C. It can be seen that $Gly^{\pm}$ and Gly^{-} exist in approximately equal mole fractions at pH values of about 9.79, 8.98 and 8.26 corresponding to 25^{o}C, 60^{o}C, and 100^{o}C, respectively. $GlyGly^{\pm}$ and $GlyGly^{-}$ are equal at pH values of about 8.27, 7.76 and 7.02 corresponding to 25^{o}C, 60^{o}C and 100^{o}C.

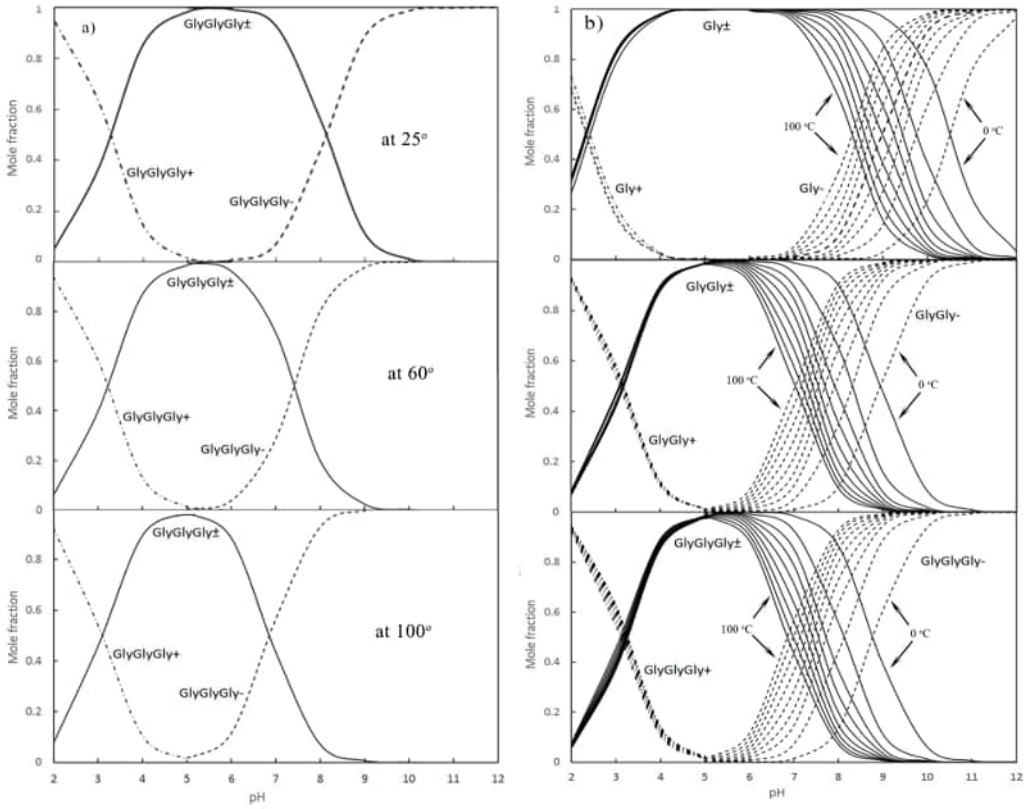

Figure 1.7: a) Mole fraction and dissociation change of GlyGlyGly as a function of pH at 25^{o}C, 60^{o}C and 100^{o}C. b) Mole fraction and dissociation change of Gly, GlyGly, and GlyGlyGly as a function of pH from 0^{o}C to 100^{o}C. b) shows that curves shift left by increasing the temperature.

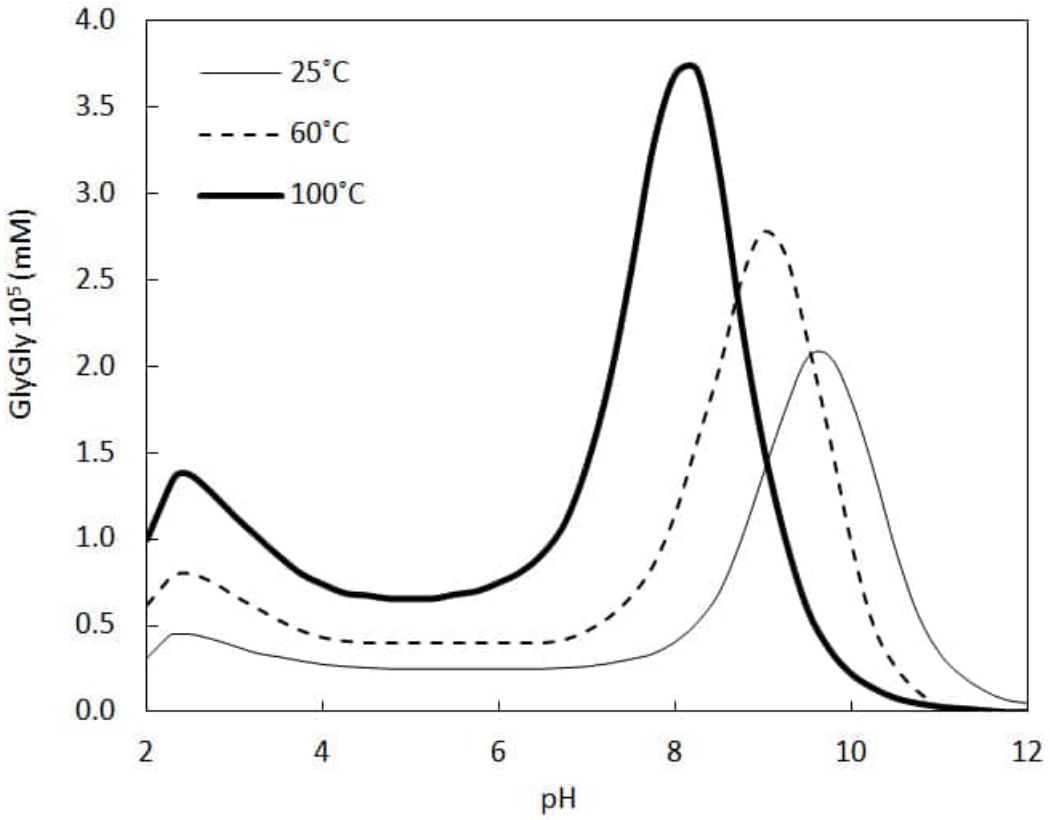

Figure 1.8: pH dependence of the equilibrium concentrations of GlyGly at 25^{o}C, 60^{o}C and 100^{o}C. The maximum concentration of GlyGly occurs at pH 9.79 (resp. 8.98 and 8.26) and 25^{o}C (resp. 60^{o}C and 100^{o}C). The concentration of GlyGly increases with temperature at lower pH and decreases with temperature at higher pH. The minimum concentration (about zero) of GlyGly occurs at pH higher than 12, 11 and 10.4 at temperatures 25^{o}C, 60^{o}C and 100^{o}C, respectively.

take into account the species activity coefficients. Using the thermodynamic data and the revised HKF parameters presented in Table 1.1, we calculate the pH dependence of GlyGly concentration at 25^{o}C, 60^{o}C, and 100^{o}C as shown in Fig.1.8. The initial concentration of Gly was set to 1 mM and the ionic strength to $\mu = 0.1$ given the presence of NaCl. The activity coefficients of aqueous species can be calculated using the extended $Debye - Huckel$ equation [19]. As shown in Fig.1.8, the GlyGly concentration increases with temperature at low pH and decreases with temperature at high pH. As mentioned before, the reaction $Gly^{\pm} + Gly^{-} \rightarrow GlyGly^{-}$ is more likely to occur than the reaction $Gly^{\pm} + Gly^{\pm} \rightarrow GlyGly^{\pm}$. The maximum concentration of GlyGly occurs at pH 9.79 (resp. 8.98 and 8.26) and 25^{o}C (resp. 60^{o}C and 100^{o}C).

Fig. 1.7-a shows the changes of dissociation states of GlyGlyGly as a function of pH at temperatures 25^{o}C, 60^{o}C, and 100^{o}C. Fig. 1.7-b also depicts the change of dissociation states of Gly, GlyGly, and GlyGlyGly as a function of pH at temperature 0^{o}C, 25^{o}C, and every 10^{o}C increment from 40^{o}C to 100^{o}C.

1.6 The importance of alkaline environment in the reaction between Gly and metals

Many studies have been conducted on the stability of metals and glycine complexes. Although metals can react with three dissociation states of Gly, existing studies have revealed that the reaction with the anion state of Gly (glycinate) is the most effective [62–64]. Some of these reactions may be slow and further kinetic studies need to be done to evaluate their likelihood in practice. [65] summarised the stability of metal-glycinate complexes such as complexes of Cu^{2+},Cd^{2+}, Zn^{2+} and Co^{2+} with one, two and three moles of glycinate. Following equations show the metal reactions with glycinate.

$$M^Z + Gly^- \rightarrow MGly^{Z-1} \tag{1.24}$$

$$M^Z + 2Gly^- \rightarrow MGly_2^{Z-2} \tag{1.25}$$

$$M^Z + 3Gly^- \rightarrow MGly_3^{Z-3} \tag{1.26}$$

where M represents a metal ion and Z is the charge of the metal. When the metal of interest in Eq. 1.25 is Au^+, $\log_{10} K$ is 15.4 according to [66] and 18 according to [67]. Similarly, when the metal is Cu^{2+}, $\log_{10} K$ is 8.57 for Eq. 1.24 and 15.64 for Eq. 1.25 as reported by [64] at room temperature 25^{o}C. The reaction of metals with different moles of Gly^- based on Eq. 1.25, 1.26 and 1.27, depends on Gly concentration. For instance, [68] showed that Eq. 1.26 is more likely to happen when Gly concentration is more than 1M. Gly^- peptides can also react with metals [69]. The following equations are some examples of reactions between Gly^- and metals;

$$M^Z + GlyGly^- \rightarrow MGlyGly^{Z-1} \tag{1.27}$$

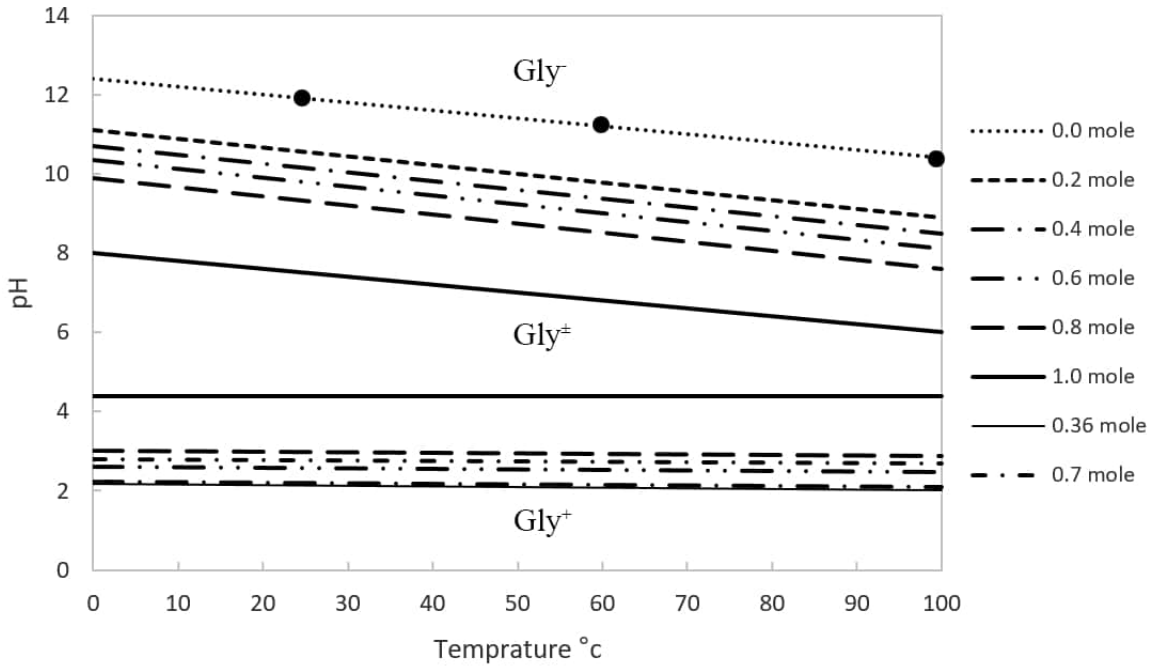

Figure 1.9: Dissociation change and stability of $Gly^{\pm}$ as a function of pH and temperature. The black circles indicate pH 12 at temperature 25^oC, pH 11 at temperature 60^oC and pH 10.4 at temperature 100^oC from left to right, respectively. At room temperature (25^oC), the maximum concentration of $Gly^{\pm}$ exists at pH values ranging from 4.4 to 7.6. The pH interval changes to 4.4-6 at a temperature 100^oC. The minimum amount of $Gly^{\pm}$ appears at pH 12 (resp. 10.4) and temperature 25^oC (resp. 100^oC) where Gly^- is more stable. This amount appears at pH 11 and temperature 60^oC.

$$M^Z + 2GlyGly^- \rightarrow MGlyGly_2^{Z-2} \tag{1.28}$$

$$M^Z + GlyGlyGly^- \rightarrow MGlyGlyGly^{Z-1} \tag{1.29}$$

The conditions of Gly^- and $Gly^{\pm}$ co-existence, and Gly^+ and $Gly^{\pm}$ co-existence are also favourable to the formation of Gly peptides (these conditions coincide with the maxima that can be seen in Fig. 1.8). As mentioned in the previous section, the likelihood of peptides occurrence is low at high pH where the concentration of Gly^- can be high. Fig. 1.8 shows that the concentration of GlyGly is relatively low at pH higher than 10.

The thermodynamic data and chemical reactions reported in this paper are instrumental to understand the role of Gly and its behaviour at different pH and temperature in leaching precious metals. To show the favourable conditions of high concentration and stability of Gly^- in aqueous solutions, stability of dissociation states of Gly are obtained at various temperatures and pH (Fig. 1.9).

Fig. 1.9 shows the stability zones and dissociation changes of $Gly^{\pm}$ with respect to pH and temperature. At room temperature (25^oC), the maximum concentration of $Gly^{\pm}$ occurs at pH values ranging from 4.4 to 7.6. The pH interval changes to 4.4-6 when temperature increases to 100^oC. The minimum amount of $Gly^{\pm}$ appears at pH 12 (resp. 10.4) and temperature 25^oC (resp. 100^oC) where Gly^- is more stable. Fig. 1.9 includes

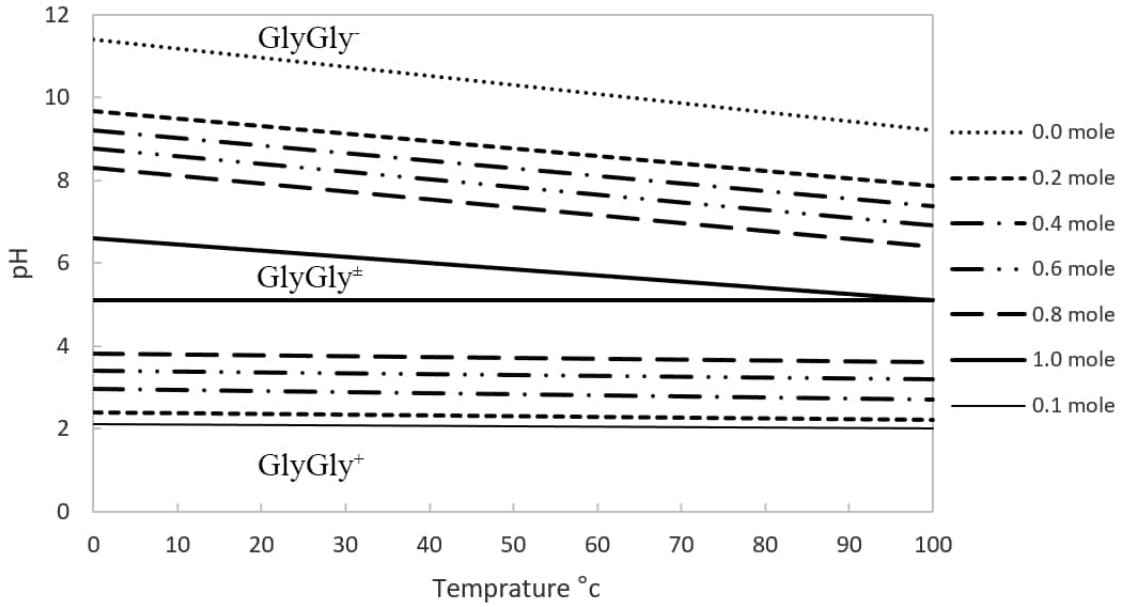

Figure 1.10: Dissociation change and stability of $GlyGly^{\pm}$ as function of pH and temperature. At room temperature (25^oC), the maximum concentration of $GlyGly^{\pm}$ occurs at pH values ranging from 5.1 to 6.7. The minimum amount of $GlyGly^{\pm}$ appears at pH 11.4 (resp. 9.2) and temperature 25^oC (resp. 100^oC) where $GlyGly^{-}$ is more stable.

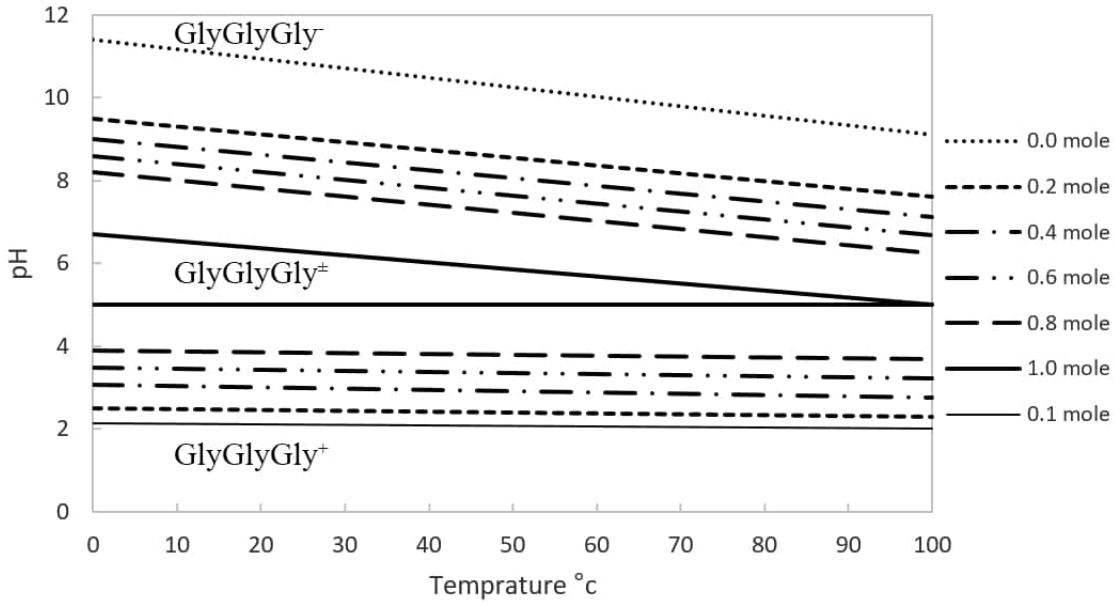

Figure 1.11: Dissociation change and stability of $GlyGlyGly^{\pm}$ as function of pH and temperature. At room temperature (25^oC), the maximum concentration of $GlyGlyGly^{\pm}$ exists at pH values ranging from 5 to 6.7. The minimum amount of $GlyGlyGly^{\pm}$ appears at pH 11.4 (resp. 9.1) and temperature 25^oC (resp. 100^oC) where $GlyGlyGly^{-}$ is more stable.

three dots that are positioned on the graph to delimit the stability zones of Gly^- at different temperatures and pH levels. The dots indicate pH 12 at 25^oC, pH 11 at 60^oC and pH 10.4 at 100^oC from the left to the right, respectively. Given the range of temperatures from 25^oC to 100^oC with pH 10.4 to 12, a temperature-pH domain centred around 60^oC and pH 11 is the optimal window where Gly can be used as a lixiviant for metals such as Au/Cu. Using high temperatures has its own shortcomings as water reaches its boiling point, but also because the process becomes more energy demanding and less cost-effective. However, for the purpose of in-situ leaching, temperature may play an important role depending on the orebody depth (as temperature increases with depth). As it can be seen in Fig. 1.9, increasing pH and temperature improves the process. Fig. 1.10 and Fig. 1.11 show the stability zones of GlyGly and GlyGlyGly with respect to pH and temperature. The species $GlyGly^-$ and $GlyGlyGly^-$ are sable at lower pH compared to Gly^-, in comparable ranges of temperatures. The equilibrium reaction of $GlyGly^-$ and Gly^- can be expressed by Eq. 1.20. [70] investigated the role of oxidation, dissolution and modification of Cu surface using hydrogen peroxide as an oxidiser and glycine as inhibitor during chemical-mechanical planarisation (CMP) of copper. They found that at the presence of 0.1 M glycine, copper removal rate was high in the solution containing 2.5 % of H_2O_2 at pH 4. They attributed this increase due to copper-glycine reaction. [7, 8] showed that copper can be leached from ores in glycine solutions in the presence of hydrogen peroxide. They also examined the glycine-peroxide system as a lixiviant of gold and silver. They demonstrated that increasing the pH from 10 to 11 at temperature 60^oC, increases the recovery of gold. However, the role of H_2O_2 in aqueous solutions goes beyond the adjustment of the equilibrium thresholds.

1.7 Thesis objectives

The main purpose of this PhD thesis is to investigate the potential of using alkaline-glycine as an environmentally friendly lixiviant for leaching gold. Although comprehensive empirical studies have been undertaken on leaching gold using glycine as an amino-acids, yet there is a gap for thermodynamic properties of gold glycinate complex in literature. The thermodynamic properties can help researchers to understand the stability of the glycine and metal-glycinate complexes in functions of pH, temperature and even pressure. In this thesis, this gap has been addressed and the fundamental thermodynamic properties for monovalent metal-glycinate complexes including gold glycinate have been calculated based on data analysis approach. To evaluate the rate of leaching gold using alkaline glycine in the real time, microfluidic chips have been employed. This part of research helps researchers to match the results with thermodynamic studies to understand the effect of pH and temperature. Microfluidic devises can mimic the in situ leaching in micro scale and simulate the leaching through crack crack. In situ leaching ISL is one of techniques that does not require operational activities in mining industries. Electro_Kinetic EK is one of proposed ISL by previous researchers. In this study, applicability of EK-ISL to alkaline glaycine to leach the gold has been evaluated. The study particularly focuses on:

- Thermodynamic properties and stability of glycine in aqueous solutions.
- Stability constants for metal glycinates including gold-glycinate that are scarce in

the literature.

- Gold recovery rate during leaching using alkaline glycine.
- Akaline glycine in in-situ leaching by applying electricity current through the low-permeable media.

1.8 Thesis outline

This thesis contains six chapters and is presented in three research papers. An introductory chapter was presented at the beginning of this thesis to provide the background of the research topic and also to explain the chemical structure of glycine as an amino acid. The papers form the main body of the thesis, which are categorised into three parts based on their topics. In the conclusions and recommendations, general remarks are presented to summarise the main outcomes of this research and open the horizons for future research .

Chapter 1: introduction to glycine and its behaviour in aqueous solutions

The behaviour of Gly in aqueous solutions was studied using the revised HKF equations of state and thermodynamic data that have been reported in the literature. Consequently, the variation of molar fractions of Gly, glycine dissociation states and glycine peptides have been investigated. The results show that $Gly^{\pm}$ and Gly^{-} can exist in approximately equal amounts at pH 9.79 (resp. 8.98 and 8.26) and temperature 25^{o}C (resp. 60^{o}C and 100^{o}C). In addition, the results indicate that $Gly^{\pm}$ and Gly^{+} have equal concentrations at pH 2.34, 2.30 and 2.30 corresponding to 25^{o}C, 60^{o}C and 100^{o}C, respectively. The stability of Gly was presented as a function of pH and temperature. The minimum amount of $Gly^{\pm}$ appears at pH 12 (resp. 10.4) and temperature 25^{o}C (resp. 100^{o}C) where Gly^{-} is more stable. This study shows that increasing temperature and pH can improve the solubility of various metals by Gly as Gly^{-} is more stable in this condition. As the polymerisation of Gly and its peptides may reduce the recovery through metal-glycinate reactions, increasing the pH and temperature can be advantageous. The reaction of metals with Gly can be more effective in the presence of hydrogen peroxide which facilitates the oxidative dissolution of metals.

Chapter 2: Data analysis and estimation of thermodynamic properties of aqueous monovalent metal-glycinate complexes. The purpose of this chapter is to estimation of gold-glycinate equilibrium constant using thermodynamic equations.

Paper 1: *Data analysis and estimation of thermodynamic properties of aqueous monovalent metal-glycinate complexes. Fluid Phase Equilibria, 480, 25-40.*

Chapter 3: Microfluidic study of sustainable gold leaching using glycine solution. The purpose of this chapter is to evaluating the gold recovery using alkaline glycine.

Paper 2: *Microfluidic study of sustainable gold leaching using glycine solution. Hydrometallurgy, 185, 186-193.*

In this paper, microchannel was employed to conduct a real time monitoring of the

leaching process by injecting the lixiviant through a micro scale channel where a layer of gold was coated. The experiment was helpful to evaluate the potential of alkaline glycine in in-situ leaching of precious metals.

Chapter 4: Advantage of using microchannel.

It is useful to compare microchannels to other laboratory leaching methods. In this chapter, the advantages and disadvantages of using microchannels are discussed.

Chapter 5: Electrokinetic study on leaching gold using alkaline glycine. The purpose of this chapter is to investigation of in-situ leaching using alakline glycine though an electrokinetic experiment.

Chapter 6: Conclusions and recommendationss

This chapter summarises the main outcomes of this research along with the proposition of future work in this area.

References

Bibliography

[1] L. S. Pangum, R. E. Browner, Pressure chloride leaching of a refractory gold ore, Minerals Engineering 9 (5) (1996) 547–556.

[2] M. Jeffrey, Kinetic aspects of gold and silver leaching in ammonia-thiosulfate solutions, Hydrometallurgy 60 (1) (2001) 7–16.

[3] M. G. Aylmore, Alternative lixiviants to cyanide for leaching gold ores, Gold Ore Processing, Project Development and Operation (2005) 501 to 539.

[4] J. A. Heath, M. I. Jeffrey, H. G. Zhang, J. A. Rumball, Anaerobic thiosulfate leaching: Development of in situ gold leaching systems, Minerals Engineering 21 (6) (2008) 424–433.

[5] E. A. Oraby, M. I. Jeffrey, R. E. Browner, The deportment of mercury during thiosulfate leaching and resin-in-pulp recovery of gold from ores, Minerals & Metallurgical Processing Journal 27 (4) (2010) 184–189.

[6] X. Yang, M. S. Moats, J. D. Miller, X. Wang, X. Shi, H. Xu, Thiourea-thiocyanate leaching system for gold, Hydrometallurgy 106 (1) (2011) 58–63.

[7] E. A. Oraby, J. J. Eksteen, The selective leaching of copper from a gold-copper concentrate in glycine solutions, Hydrometallurgy 150 (2014) 14–19.

[8] E. A. Oraby, J. J. Eksteen, The leaching of gold, silver and their alloys in alkaline glycine-peroxide solutions and their adsorption on carbon, Hydrometallurgy 152 (2015) 199–203.

[9] A. Karrech, M. Attar, E. Oraby, J. Eksteen, M. Elchalakani, A. Seibi, Modelling of multicomponent reactive transport in finite columns — application to gold recovery using iodide ligands, Hydrometallurgy 178 (2018) 43 – 53.

[10] D. H. Brown, W. E. Smith, P. Fox, R. D. Sturrock, The reactions of gold (0) with amino acids and the significance of these reactions in the biochemistry of gold, Inorganica Chimica Acta 67 (1982) 27–30.

[11] W. R. Walker, B. J. Griffin, Solubility of copper in human sweat, Search 7 (3) (1976) 100–101.

[12] D. Feng, J. S. J. Van Deventer, The role of amino acids in the thiosulphate leaching of gold, Minerals Engineering 24 (9) (2011) 1022–1024.

[13] E. L. Shock, Stability of peptides in high-temperature aqueous solutions, Geochimica et Cosmochimica Acta 56 (9) (1992) 3481–3491.

[14] J. Amend, E. Shock, Energetics of amino acid synthesis in hydrothermal ecosystems, Science 281 (5383) (1998) 1659–1662.

[15] E. Shock, P. Canovas, The potential for abiotic organic synthesis and biosynthesis at seafloor hydrothermal systems, Geofluids 10 (1-2) (2010) 161–192.

[16] J. P. Amend, D. E. LaRowe, T. M. McCollom, E. L. Shock, The energetics of organic synthesis inside and outside the cell, Phil. Trans. R. Soc. B 368 (1622) (2013) 20120255.

[17] H. C. Helgeson, D. H. Kirkham, Theoretical prediction of the thermodynamic behavior of aqueous electrolytes at high pressures and temperatures; i, summary of the thermodynamic/electrostatic properties of the solvent, American Journal of Science 274 (10) (1974) 1089–1198.

[18] H. C. Helgeson, D. H. Kirkham, Theoretical prediction of thermodynamic properties of aqueous electrolytes at high pressures and temperatures. iii. equation of state for aqueous species at infinite dilution, Am. J. Sci.;(United States) 276 (2).

[19] H. C. Helgeson, D. H. Kirkham, G. C. Flowers, Theoretical prediction of the thermodynamic behavior of aqueous electrolytes by high pressures and temperatures; iv, calculation of activity coefficients, osmotic coefficients, and apparent molal and standard and relative partial molal properties to 600 degrees c and 5kb, American journal of science 281 (10) (1981) 1249–1516.

[20] J. C. Tanger, H. C. Helgeson, Calculation of the thermodynamic and transport properties of aqueous species at high pressures and temperatures; revised equations of state for the standard partial molal properties of ions and electrolytes, American Journal of Science 288 (1) (1988) 19–98.

[21] E. L. Shock, H. C. Helgeson, Calculation of the thermodynamic and transport properties of aqueous species at high pressures and temperatures: Correlation algorithms for ionic species and equation of state predictions to 5 kb and 1000 c, Geochimica et Cosmochimica Acta 52 (8) (1988) 2009–2036.

[22] E. L. Shock, Geochemical constraints on the origin of organic compounds in hydrothermal systems, Origins of Life and Evolution of Biospheres 20 (3) (1990) 331–367.

[23] J. P. Amend, H. C. Helgeson, Calculation of the standard molal thermodynamic properties of aqueous biomolecules at elevated temperatures and pressures part 1l-α-amino acids, Journal of the Chemical Society, Faraday Transactions 93 (10) (1997) 1927–1941.

[24] J. M. Dick, D. E. LaRowe, H. C. Helgeson, Temperature, pressure, and electrochemical constraints on protein speciation: Group additivity calculation of the standard molal thermodynamic properties of ionized unfolded proteins, Biogeosciences 3 (3) (2006) 311–336.

[25] D. E. LaRowe, P. Van Cappellen, Degradation of natural organic matter: a thermodynamic analysis, Geochimica et Cosmochimica Acta 75 (8) (2011) 2030–2042.

[26] E. L. Shock, D. C. Sassani, M. Willis, D. A. Sverjensky, Inorganic species in geologic fluids: correlations among standard molal thermodynamic properties of aqueous ions and hydroxide complexes, Geochimica et Cosmochimica Acta 61 (5) (1997) 907–950.

[27] J. P. Amend, T. M. McCollom, Energetics of biomolecule synthesis on early earth, in: Chemical Evolution II: From the Origins of Life to Modern Society, ACS Publications, 2009, Ch. 4, pp. 63–94.

[28] E. L. Shock, M. D. Schulte, Organic synthesis during fluid mixing in hydrothermal systems, Journal of Geophysical Research: Planets 103 (E12) (1998) 28513–28527.

[29] Z. Jingrong, L. Jianjun, Y. Fan, W. Jingwei, Z. Fahua, An experimental study on gold solubility in amino acid solution and its geological significance, Chinese Journal of Geochemistry 15 (4) (1996) 296–302.

[30] E. L. Shock, C. M. Koretsky, Metal-organic complexes in geochemical processes: Estimation of standard partial molal thermodynamic properties of aqueous complexes between metal cations and monovalent organic acid ligands at high pressures and temperatures, Geochimica et Cosmochimica Acta 59 (8) (1995) 1497–1532.

[31] R. N. Goldberg, N. Kishore, R. M. Lennen, Thermodynamic quantities for the ionization reactions of buffers, Journal of physical and chemical reference data 31 (2) (2002) 231–370.

[32] C. Secretariat, Codata recommended key values for thermodynamics 1977, CODATA Bull 28.

[33] S. Ziemer, T. Niederhauser, E. Merkley, J. Price, E. Sorenson, B. McRae, B. Patterson, M. Origlia-Luster, E. Woolley, Thermodynamics of proton dissociations from aqueous glycine at temperatures from 278.15 to 393.15 k, molalities from 0 to 1.0 mol $\cdot$ kg- 1, and at the pressure 0.35 mpa: apparent molar heat capacities and apparent molar volumes of glycine, glycinium chloride, and sodium glycinate, The Journal of Chemical Thermodynamics 38 (4) (2006) 467–483.

[34] N. Kitadai, Thermodynamic prediction of glycine polymerization as a function of temperature and ph consistent with experimentally obtained results, Journal of molecular evolution 78 (3-4) (2014) 171–187.

[35] E. J. Cohn, J. T. Edsall, Proteins, amino acids and peptides as ions and dipolar ions, Reinhold Publishing Corporation; New York, 1943.

[36] C. J. Downes, A. W. Hakin, G. R. Hedwig, The partial molar heat capacities of glycine and glycylglycine in aqueous solution at elevated temperatures and atp= 10.0 mpa, The Journal of Chemical Thermodynamics 33 (8) (2001) 873–890.

[37] K. Sakata, N. Kitadai, T. Yokoyama, Effects of ph and temperature on dimerization rate of glycine: evaluation of favorable environmental conditions for chemical evolution of life, Geochimica et Cosmochimica Acta 74 (23) (2010) 6841–6851.

[38] M. Häckel, H.-J. Hinz, G. R. Hedwig, Partial molar volumes of proteins: amino acid side-chain contributions derived from the partial molar volumes of some tripeptides over the temperature range 10-90 c, Biophysical chemistry 82 (1) (1999) 35–50.

[39] A. W. Hakin, H. Høiland, G. R. Hedwig, Volumetric properties of some oligopeptides in aqueous solution: partial molar expansibilities and isothermal compressibilities at 298.15 k for the peptides of sequence ala (gly) n, n= 1–4, Physical Chemistry Chemical Physics 2 (21) (2000) 4850–4857.

[40] A. W. Hakin, M. G. Kowalchuck, J. L. Liu, R. A. Marriott, Thermodynamics of protein model compounds: apparent and partial molar heat capacities and volumes of several cyclic dipeptides in water, Journal of solution chemistry 29 (2) (2000) 131–151.

[41] G. R. Hedwig, Thermodynamic properties of peptide solutions 3. partial molar volumes and partial molar heat capacities of some tripeptides in aqueous solution, Journal of solution chemistry 17 (4) (1988) 383–397.

[42] E.-i. Imai, H. Honda, K. Hatori, A. Brack, K. Matsuno, Elongation of oligopeptides in a simulated submarine hydrothermal system, Science 283 (5403) (1999) 831–833.

[43] Y. Qian, M. H. Engel, S. A. Macko, S. Carpenter, J. W. Deming, Kinetics of peptide hydrolysis and amino acid decomposition at high temperature, Geochimica et cosmochimica acta 57 (14) (1993) 3281–3293.

[44] S. Miller, Le orgel the origins of life on the earth (1974).

[45] S. L. Miller, J. L. Bada, Submarine hot springs and the origin of life, Nature 334 (6183) (1988) 609–611.

[46] E. L. Shock, Hydrothermal dehydration of aqueous organic compounds, Geochimica et Cosmochimica Acta 57 (14) (1993) 3341–3349.

[47] J. Oro, C. Guidry, Direct synthesis of polypeptides: I. polycondensation of glycine in aqueous ammonia, Archives of biochemistry and biophysics 93 (1) (1961) 166–171.

[48] M. Hunt, Petroleum geochemistry and geology, WH Freeman and company, 1979.

[49] B. P. Tissot, D. H. Welte, Diagenesis, catagenesis and metagenesis of organic matter, in: Petroleum Formation and Occurrence, Springer, 1984, pp. 69–73.

[50] J. C. Ahluwalia, C. Ostiguy, G. Perron, J. E. Desnoyers, Volumes and heat capacities of some amino acids in water at 25 c, Canadian Journal of Chemistry 55 (19) (1977) 3364–3367.

[51] R. G. Clarke, L. Hnědkovskỳ, P. R. Tremaine, V. Majer, Amino acids under hydrothermal conditions: Apparent molar heat capacities of aqueous α-alanine, β-alanine, glycine, and proline at temperatures from 298 to 500 k and pressures up to 30.0 mpa, The Journal of Physical Chemistry B 104 (49) (2000) 11781–11793.

[52] C. Jolicoeur, J. Boileau, Apparent molal volumes and heat capacities of low molecular weight peptides in water at 25 c, Canadian Journal of Chemistry 56 (21) (1978) 2707–2713.

[53] D. D. Wagman, W. H. Evans, V. B. Parker, R. H. Schumm, I. Halow, The nbs tables of chemical thermodynamic properties. selected values for inorganic and c1 and c2 organic substances in si units, Tech. rep., National Standard Reference Data System (1982).

[54] C. Pistorius, W. Sharp, Properties of water, part vi, entropy and gibbs free energy of water in the range 10-1,000 c and 1-250,000 bars, Am. J. Sci 258 (1960) 757–768.

[55] E. J. King, Thermodynamics of ionization of amino acids. part 6.-the second ionization constants of some glycine peptides, Journal of the Chemical Society, Faraday Transactions 1: Physical Chemistry in Condensed Phases 71 (1975) 88–96.

[56] R. G. Clarke, C. M. Collins, J. C. Roberts, L. N. Trevani, R. J. Bartholomew, P. R. Tremaine, Ionization constants of aqueous amino acids at temperatures up to 250 c using hydrothermal ph indicators and uv-visible spectroscopy: glycine, α-alanine, and proline, Geochimica et Cosmochimica Acta 69 (12) (2005) 3029–3043.

[57] P. Wang, J. L. Oscarson, S. E. Gillespie, R. M. Izatt, H. Cao, Thermodynamics of protonation of amino acid carboxylate groups from 50 to 125 c, Journal of solution chemistry 25 (3) (1996) 243–266.

[58] E. S. Hamborg, J. P. Niederer, G. F. Versteeg, Dissociation constants and thermodynamic properties of amino acids used in co2 absorption from (293 to 353) k, Journal of Chemical & Engineering Data 52 (6) (2007) 2491–2502.

[59] S. Gillespie, J. Oscarson, R. Izatt, P. Wang, J. Renuncio, C. Pando, Thermodynamic quantities for the protonation of amino acid amino groups from 323.15 to 398.15 k, Journal of solution chemistry 24 (12) (1995) 1219–1247.

[60] J. Bujdák, B. M. Rode, Silica, alumina and clay catalyzed peptide bond formation: enhanced efficiency of alumina catalyst, Origins of Life and Evolution of Biospheres 29 (5) (1999) 451–461.

[61] K. I. Zamaraev, V. N. Romannikov, R. I. Salganik, W. A. Wlassoff, V. V. Khramtsov, Modelling of the prebiotic synthesis of oligopeptides: silicate catalysts help to overcome the critical stage, Origins of Life and Evolution of Biospheres 27 (4) (1997) 325–337.

[62] A. H. Pakiari, Z. Jamshidi, Interaction of amino acids with gold and silver clusters, The Journal of Physical Chemistry A 111 (20) (2007) 4391–4396.

[63] A. F. Pearlmutter, J. Stuehr, Kinetics of copper (ii)-glycine interactions in aqueous solution, Journal of the American Chemical Society 90 (4) (1968) 858–862.

[64] S. Aksu, F. M. Doyle, Electrochemistry of copper in aqueous glycine solutions, Journal of the Electrochemical Society 148 (1) (2001) B51–B57.

[65] T. Kiss, I. Sovago, A. Gergely, Critical survey of stability constants of complexes of glycine, Pure and applied chemistry 63 (4) (1991) 597–638.

[66] I. V. Mironov, Stability of gold (i) glycinate complexes in aqueous solution, Russian Journal of Inorganic Chemistry 52 (5) (2007) 791–792.

[67] D. Michel, J. Frenay, Integration of amino acids in the thiosulfate gold leaching process, in: Randol Glod & Silver Forum, 1999, pp. 99–103.

[68] H. L. Riley, Ccxiv.-studies in complex salts. part iii. the effect of alkyl substitution on the stability of the dimalonatocupriate ion, Journal of the Chemical Society (Resumed) (1930) 1642–1652.

[69] A. M. Corrie, G. K. Makar, M. L. Touche, D. R. Williams, Thermodynamic considerations in co-ordination. part xx. a computerised approach as an alternative to graphical normalised curve fitting as a means of detecting oligonuclear complexes in metal ion–ligand solutions and its application to the zinc (ii)–, lead (ii)–, and proton–glycine peptide systems, Journal of the Chemical Society, Dalton Transactions (1975) 105–110.

[70] S. Seal, S. C. Kuiry, B. Heinmen, Effect of glycine and hydrogen peroxide on chemical-mechanical planarization of copper, Thin Solid Films 423 (2) (2003) 243–251.

Chapter 2

Data analysis and estimation of thermodynamic properties of aqueous monovalent metal-glycinate complexes

ABSTRACT

Recently, an aqueous glycine solution has been proposed as a non-toxic environmentally friendly lixiviant to leach precious metals such as gold. In confined spaces, gold can be leached effectively using cyanide as a lixiviant. However, in unconfined applications, cyanide poses detrimental environmental effects due to its high level of toxicity. In order to investigate the effectiveness of lixiviant systems containing glycine and examine their potential, it is essential to identify the thermodynamic properties and stability domains of metal-glycinate complexes. Numerous studies have been conducted on the thermodynamic equilibrium of divalent metal-glycinate formations but those of monovalent metal-glycinate are scarce in general and inexistent for most precious metals including gold. In this study, we use data analysis to relate the standard partial molal properties of metal-glycinate complexes to the standard partial molal properties of various metals and estimate the equilibrium constants of monovalent metal-glycinate formation at ambient conditions. Finally, the standard partial molal properties of the metal-glycinate complexes and their revised Helgeson-Kirkham-Flowers (HKF) equations of state have been estimated and used to deduce the equilibrium constants of metal-glycine systems at different temperatures. The proposed method has been tested using existing experimental data and showed excellent consistency.

2.1 Introduction

Preserving the environment while extracting natural resources is a challenge that requires multi-disciplinary knowledge. Due to the widespread awareness of these problems and the increasingly restrictive legislative measures, scientists have been seeking alternatives to conventional mining methods. The conventional surface and underground mining methods

are highly dependent on the availability of low-cost energy and can leave detrimental footprints in the landscape. In-situ (or in-place) recovery has been recently proposed as a sustainable and economic method to extract precious metals from low-grade subsurface deposits. While precious metals can be effectively leached by cyanide as a standard reagent in confined spaces (i.e. heap leaching), there is no consensus on alternative lixiviants that can be used in un-confined domains (i.e. in-situ recovery) and can fulfil the tight criteria of acceptance based on economics, process availability and tocixity. Scientists are exploring environmentally benign lixiviants to selectively leach precious metals from low-grade ores. Among the available reagents with lower level of toxicity such as thiosulphate, acidic thiocyanate, halides, thiourea, and organic reagents [1–6], glycine has a high potential to be used in the benign hydrometallurgical processes as a non-toxic reagent [7–9]. To assess the performance of lixiviant systems containing glycine, the thermodynamic properties and stability of metal-glycinate formations have to be explored first. Although, numerous studies have been conducted on the reaction of metals with amino acids, a limited number of studies is available on monovalent metals. For instance, the thermodynamic data characterising gold-glycinate systems are yet to be determined despite the few experimental contributions that have been published on reacting glycine with gold. For example, [10] examined the effects of pH on the solubility of gold and copper in the presence of glycine and hydrogen peroxide. These authors observed higher solubility for samples containing gold and copper compared to pure gold bearing samples. This could be due to the increased surface area of gold exposed to glycine as copper dissolves before gold in amino acid solutions [11].

[12] indicated that gold is intensively soluble in amino acids at pH ranging from 6 to 8 and temperature 80^oC. [13] has shown that the recovery rate can be substantially improved in gold leaching by the addition of amino acids (e.g. glycine) to thiosulphate-based solution. Subsequently, [7, 8] studied the application of glycine as a gold lixiviant in an alkaline environment, with the exposure to hydrogen peroxide. They found that glycine is more effective at pH between 10 and 11 and temperature ranging from 60^oC to 70^oC. Thus, the main factors that affect the chemical reaction of gold in direct contact amino acids are temperature, pH and concentration. However, in order to theoretically optimise the reaction conditions at different levels of pH and temperatures, the standard state equilibrium constant of the chemical reaction of gold-glycinate and their thermodynamic data are essential. These physical quantities are instrumental to assess the system's stability in aqueous solutions. They can also be used to deduce thermodynamic potentials such as free energy and entropy and key extensive variables such as entropy and heat capacities.The effects of pH and temperature levels on the enhancement of gold solubility and the rate of gold dissolution can be explored and as a result, the optimum scenarios of recovery can be obtained.

In this study, we present comprehensive results for the standard state equilibrium constants of monovalent metal-glycinate built using the correlation techniques proposed by [14] and [15]. The experimental data from the literature are statistically averaged and used for calculating the revised Helgeson-Kirkham-Flowers (HKF) constants [16]. In order to estimate the standard partial molal Gibbs free energy of the aqueous complexes at the temperature and pressure of interest, values of heat capacities, volumes, standard partial

entropies and conventional Born coefficient of aqueous complexes are needed at the reference temperature and pressure. However, there are many aqueous species for which experimental data are presently lacking. In these cases, correlations among available thermodynamic data can be employed to estimate the properties that have not been obtained experimentally. The thermodynamic properties of minerals and aqueous species calculated using the HKF parameters are instrumental in multi-physics reactive transport tools that rely on forward numerical integration [17, 18]. [14, 15, 19–21] constructed several empirical correlations among available thermodynamic properties of aqueous species which will be used as proxies to estimated the unknown properties of organic and non-organic species at the temperatures and pressures of interest. The novelty of this paper is in the prediction of thermodynamic properties of various metal-glycinate complexes at various pressures and temperatures as well as the standard state equilibrium constants of reaction between them. This outcome is relevant given the importance of glycine as a benign lixiviant that has the potential to play a key role in the in-situ recovery of precious metals. Nevertheless, it is important to note that the standard state equilibrium constant of a metal-glycinate reaction is sensitive to the changes in ionic strength, pH, and temperature. Therefore, any small change in these parameters could influence the dissolution or precipitation of minerals [14].

2.2 Standard state equilibrium constants at 25^{o}C and 1 Bar

The standard state of an aqueous species (other than H_2O) is the hypothetical ideal solution of unit activity or the state it would have in the case of infinite dilution. According to [14], a standard partial molal thermodynamic property ($\bar{\Xi}^o$) of an aqueous species j can be represented by

$$\bar{\Xi}^o_j = \bar{\Xi}^{o_{abs}}_j - Z_j \bar{\Xi}^{o_{abs}}_{H^+} \tag{2.1}$$

where $\bar{\Xi}^{o_{abs}}_j$ is the absolute property, Z is the charge of the species, and $\bar{\Xi}^{o_{abs}}_{H^+}$ is the same property corresponding to the hydrogen ion. Conventionally, the standard partial molal properties of hydrogen are considered zero regardless of temperature and pressure, which permits the calculation of standard partial molal properties of individual ions [22]. The apparent standard partial molal Gibbs free energies of formation ($\Delta\bar{G}^o$ [cal mol^{-1}])can be related to the standard partial molal Gibbs free energy of formation ($\Delta\bar{G}^o_f$) of an aqueous species at reference pressure P_r and temperature T_r of 1 bar and 298.15K as follow [14, 16, 19]

$$\triangle\bar{G}^o = \triangle\bar{G}^o_f + (\bar{G}^o_{P,T} - \bar{G}^o_{P_r,T_r}) \tag{2.2}$$

where $(\bar{G}^o_{P,T} - \bar{G}^o_{P_r,T_r})$ is the difference between the standard partial molal Gibbs free energy of the aqueous species at the temperature and pressure of interest and the corresponding values at the reference conditions (P_r and T_r). These expressions of Gibbs free energy are used to describe stability chemical reactions. In particular, consider the association reaction of metals and ligands that can be represented as follows:

$$M^Z + yL^- \Leftrightarrow ML^{Z-y}_y; \tag{2.3}$$

where Z denotes the charge of metal and y represents the number of L^- in the complex. In this paper, the ligand anion L^- is glycinate (Gly^-). The overall equilibrium constant of the y-th association reaction corresponding to Eq. 2.3 can be expressed as follows:

$$\beta_y = \prod_{i=1}^{3} \{c_i\}^{v_i} = \frac{[ML_y^{Z-y}]}{[M^Z][L^-]^y} \tag{2.4}$$

where $\{c_i\}$ is the activity of species i at the standard conditions and v_i the stoichiometric coefficient of the species which is positive for the products and negative for the reactants. In the particular case of dilute solution, the quantity $\{c_i\}$ reduces to the concentration $[c_i]$ ($[\mathrm{mol\,m^{-3}}]$) of the same species. It is important to note that in this study, the concentrations are small enough to assume that the activity coefficient (ratio between activity and concentration) remains close to unity. At given temperature and pressure conditions, the standard state equilibrium constant of a chemical reaction can be related to the partial molal Gibbs Free energy of reaction through the an expression of the form:

$$\beta_y = \exp\left(-\Delta\bar{G}_r^o/(RT)\right) \tag{2.5}$$

where R = 1.98793 [cal $\mathrm{mol^{-1}\ K^{-1}}$] is the universal gas constant, T [K] is the reaction temperature, and

$$\Delta\bar{G}_r^o = \sum_i \left(v_i \Delta\bar{G}_i^o\right) \tag{2.6}$$

where $\Delta\bar{G}_r^o$ [cal $\mathrm{mol^{-1}}$] is the standard partial molal Gibbs free energy of the reaction and $\Delta\bar{G}_i^o$ is the standard molal Gibbs free energy of the species.

The available standard state dissociation constants of metal-glycinate (i.e. $\log\beta_y$ in Eq. 2.4 when $y = 1, 2, 3$) have been compiled from the literature and presented in Tables 2.1 to 2.4. We can observe that the metal-glycinate complex formation equilibria have been discussed in numerous papers where different methods have been recommended to determine the relevant equilibrium constants [23]. Electrochemical methods (such as pH-metry, potentiometry, polarography, conductance and electrophoresis), spectroscopic methods (such as spectrophotometry and NMR), ion exchange and liquid-liquid distribution methods have been utilised successfully to this purpose [23–35]. Each of these methods has both strengths and weaknesses depending on the particular application it is designed for. It is important to note that pH-metry with glass or hydrogen electrodes has been applied most extensively [23].

In this study, the average standard state equilibrium constants of metal-glycinate association are calculated based on experimental data that are available in the literature (see Table 2.1 to 2.4). The obtained standard state equilibrium constants are summarised in Table 2.5. The corresponding standard deviation (SD) and number of reference values (N) are also presented to indicate the level of certainty and confidence in the data. To achieve a high level of accuracy, the quantities that are available in multiple references and that exhibit minimum SD have been selected for analysis.

Metal	Cu^{2+}			Ni^{2+}			Co^{2+}		
References	$log\beta_1$	$log\beta_2$	$log\beta_3$	$log\beta_1$	$log\beta_2$	$log\beta_3$	$log\beta_1$	$log\beta_2$	$log\beta_3$
[36]				5.69		13.44			
[37]	8.19	14.96							
[38]	8.13	14.97							
[39]	8.13	14.97							
[40]	8.16	14.98							
[41]	8.07	14.88							
[42]		15.28							
[43]	8.07	14.92							
[44]	8.20								
[45]	8.20	15.10							
[46]	8.22	15.14							
[47]	8.23	15.04							
[48]	8.30	15.20							
[49]		15.20							
[50]				5.74	10.7				
[51]				5.69	10.52				
[52]				5.74	10.55				
[53]	8.14	14.96							
[54]				5.79	10.57				
[55]	8.28	15.38							
[56]	8.05	14.84		5.6	10.34				
[57]				5.86	10.84				
[58]	8.79	16.13							
[59]	8.58	15.67							
[60]				6.18	11.25				
[61]	8.11	14.43		5.65	10.51	13.95			
[62]	8.46	15.29		5.94	10.78				
[63]				6.28	11.12		4.95	8.43	
[64]				5.65	10.40				
[65]				5.65	10.40				
[66]				5.83	10.74		4.63	8.50	
[67]	8.23	15.19		5.73	10.56				
[68]				5.77	10.65		4.66	8.64	
[69]	8.22	15.11		5.80	10.65		4.70	8.58	
[70]	8.07	14.84							
[71]				6.19	11.14		4.62	8.60	
[72]	8.25	15.38	19.55	5.74	10.41		5.03	8.97	
[73]	8.27	14.96							
[74]	8.18								
[75]		14.60							
[76]	8.38	15.17		5.86	10.64				
[77]	8.04	15.09							
[78]		15.10							
[79]	8.62	15.59		6.18	11.14		5.02	9.02	
[80]	8.62	15.59		6.18	11.15		5.23	9.25	
[81]		15.10							
[82]		15.10		5.97	10.92				
[83]	8.14	14.9							
[84]		15.03		5.73	10.49		4.95	8.94	
[85]		15.42							
[86]		15.10							
[87]	8.10	15.10	16.88						
[88]				5.80	10.59				
[89]	8.59	15.54							
[90]	8.15	15.1							
[91]	8.51	15.42		6.12	11.15		4.95	8.94	
[92]	8.17			5.50			4.60		
[93]	8.14								
[94]							4.57		
[95]	8.21	15.09		5.75	10.65		4.71	8.76	
[96]				5.66	10.51	14.00			
[97]	8.12	14.87	15.3	5.63	10.48	14.00			
[98]				5.83	10.53				
[99]	8.57	15.83		6.13	11.05	14.23	5.07	9.09	11.63
[23]	8.09	14.85		5.65	10.41		4.66	8.51	
[100]							4.51	8.16	
[101]							5.02		

Table 2.1: The standard state equilibrium constants of reactions containing glycinate and Cu^{2+},Ni^{2+} and Co^{2+} at 25^{o}C and 1 bar. Logβ_1, logβ_2 and β_3 represent the equilibrium constants of reactions that form 1:1, 1:2 and 1:3 metal-glycinates, respectively.

Metal	Mn^{2+}			Zn^{2+}			Cd^{2+}		
References	$log\beta_1$	$log\beta_2$	$log\beta_3$	$log\beta_1$	$log\beta_2$	$log\beta_3$	$log\beta_1$	$log\beta_2$	$log\beta_3$
[102]							3.95	7.17	
[36]						12.02			
[103]				5.00			4.40		
[104]							4.54	8.04	
[105]							4.01	7.49	
[106]							4.25	7.80	
[107]							3.98	7.42	
[108]							3.78	6.00	
[109]							4.50	8.00	
[110]							5.68	8.45	
[111]				5.09	9.78				
[112]				5.05					
[113]				4.85	9.14				
[114]				4.96	9.19				
[56]				4.81	9.00				
[57]				5.24	9.65				
[61]				4.88	9.01	11.02			
[62]				5.19	9.41				
[63]				5.21	9.52				
[65]				4.84	9.02				
[66]				4.96	9.19				
[68]				5.06	9.44				
[71]	3.17								
[77]				5.00	9.30		4.40	7.85	
[79]	3.44			5.52	9.96		4.80	8.83	
[80]	3.45			5.52	9.96				
[115]				5.42	9.94				
[82]									9.94
[84]				5.16	9.9.50				
[116]								8.1	
[91]	3.66	6.63		5.33	9.72		4.74	8.60	
[92]	3.00			5.50					
[95]				4.93	9.26		4.26	8.08	
[96]	2.60	4.58	5.70	4.88	9.01	11.00			
[98]	2.83	4.83		5.08	9.14				
[99]	3.21			5.38	9.81	12.33	4.69	8.40	10.68
[97]	2.65	4.70		4.88	9.11	11.56			
[117]	2.85								
[23]				5.03	9.23		4.28	7.72	
[93]	2.65			4.88					
[100]	2.56	4.27					4.18	7.50	

Table 2.2: The standard state equilibrium constant of reactions containing glycinate and Mn^{2+}, Zn^{2+} and Cd^{2+} at 25^{o}C and 1 bar. Logβ_1, logβ_2 and β_3 represent the equilibrium constants of reactions to form 1:1, 1:2 and 1:3 metal-glycinates, respectively.

Metal	Ag^{+}		Cr^{2+}		Cr^{3+}		Hg^{2+}		Au^{3+}	
References	$log\beta_1$	$log\beta_2$	$log\beta_1$	$log\beta_2$	$log\beta_1$	$log\beta_2$	$log\beta_1$	$log\beta_2$	$log\beta_1$	$log\beta_2$
[118]	3.28	6.96								
[119]	3.15	6.53								
[120]	3.43	6.86								
[80]	3.51	6.89								
[121]	4.28	6.96								
[122]	3.35									
[95]	3.01	6.22								
[123]					8.62	16.27				
[124]					8.40	14.80				
[23]	3.45	6.80								
[125]			7.72	15.26						
[93]			4.21	7.27						
[126]							10.50	19.20		
[127]								18.20		
[128]								18.40		
[129]								19.20		
[130]									7.05	10.57
Metal	Pb^{2+}		Pd^{2+}		Mg^{3+}		Fe^{2+}		Cu^{+}	
References	$log\beta_1$	$log\beta_2$	$log\beta_1$	$log\beta_2$	$log\beta_1$	$log\beta_2$	$log\beta_1$	$log\beta_2$	$log\beta_1$	$log\beta_2$
[131]									6.75	
[49]										10.00
[132]	5.28	8.32								
[77]		7.60								
[79]	5.27	8.59								
[80]	5.28	8.60			2.08					
[121]	5.17									
[88]	4.78	7.66								
[133]	5.04									
[134]	4.91	9.00								
[135]	5.75									
[136]	4.91	8.01								
[137]	5.63	8.10								
[91]	5.53	9.98	9.12	17.55	3.66	6.63				
[94]							3.73	6.65		
[99]							4.31			
[138]	5.46	9.32								
[100]	4.36	7.62			1.34					

Table 2.3: The standard state equilibrium constant of reactions containing glycinate and Ag^{+}, Cr^{2+}, Cr^{3+}, Hg^{2+}, Au^{3+}, Pb^{2+} , Pd^{2+}, Mg^{2+}, Fe^{2+} and Cu^{+} at 25^{o}C and 1 bar. Logβ_1 and logβ_2 represent the equilibrium constants of reactions to form 1:1 and 1:2 metal-glycinate, respectively.

Metal	Au^{+}	Na^{+}	Ti^{+}	$MeHg^{+}$	Sr^{2+}	Ga^{2+}	Ca^{2+}	Ba^{2+}	Fe^{3+}	La^{3+}	Pr^{3+}	Ce^{3+}	Nd^{3+}	Sm^{3+}
References	$log\beta_2$	$log\beta_1$	$log\beta_1$	$log\beta_1$	$log\beta_1$	$log\beta_1$	$log\beta_1$	$log\beta_1$	$log\beta_1$	$log\beta_1$	$log\beta_1$	$log\beta_1$	$log\beta_1$	$log\beta_1$
[139]	18.00													
[140]	15.40													
[141]		-0.40												
[142]		-0.60												
[143]			1.51											
[144]				7.85										
[145]				7.88										
[146]				7.52										
[147]									8.00					
[80]							1.28	0.77						
[148]						9.6								
[149]					0.6									
[150]					0.91									
[151]										5.38	5.55	5.38	5.68	5.84

Table 2.4: The standard state equilibrium constant of reactions containing glycinate and Au^{+}, Na^{+}, Ti^{+}, $MeHg^{+}$ (Methylmercury), Sr^{2+}, Ga^{2+}, Ca^{2+}, Ba^{2+}, Fe^{3+}, La^{3+}, Pr^{3+}, Ce^{3+}, Nd^{3+} and Sm^{2+} at 25^{o}C and 1 bar. Logβ_1 and logβ_2 represent the equilibrium constants of reactions to form 1:1 and 1:2 metal-glycinates, respectively.

Metal	$log\beta_1$	SD	N	$log\beta_2$	SD	N	$log\beta_3$	SD	N
Cu^{2+}	8.26	0.19	39	15.15	0.31	44	17.24	2.15	3
Cu^{+}	6.75		1	10.00		1			
Ni^{2+}	5.83	0.21	33	10.70	0.27	31	13.92	0.29	5
Co^{2+}	4.82	0.22	17	8.74	0.30	14	11.63		1
Mn^{2+}	3.01	0.38	12	5.00	0.93	5	5.70		1
Zn^{2+}	5.10	0.22	27	9.40	0.33	23	11.59	0.59	5
Cd^{2+}	4.40	0.45	16	7.84	0.67	16	10.31	0.52	2
Pb^{2+}	5.18	0.38	13	8.44	0.76	11			
Pd^{2+}	9.12		1	17.55		1			
Mg^{2+}	2.36	1.18	3	6.63		1			
Fe^{2+}	4.02	0.41	2	6.65		1			
Fe^{3+}	8.00		1						
Ca^{2+}	1.36	0.06	4						
Ag^{+}	3.43	0.38	8	6.71	0.28	6			
Au^{3+}	7.05		1	10.57		1			
Au^{+}				16.70	1.84	2			
Na^{+}	-0.50	0.14	2						
Ti^{+}	1.51		1						
Hg^{2+}	10.50		1	18.73	0.50	4			
La^{3+}	5.38		1						
Pr^{3+}	5.55		1						
Ce^{3+}	5.38		1						
Nd^{3+}	5.68		1						
Sm^{3+}	5.84		1						
Sr^{2+}	0.76	0.22	2						
Ga^{3+}	9.60		1						
Cr^{2+}	5.97	2.48	2	11.27	5.65	2			
Cr^{3+}	8.51	0.16	2	15.54	1.04	2			
Ba^{2+}	0.77		1						

Table 2.5: Average standard state equilibrium constant of reactions containing glycinate and metals at 25^{o}C and 1 bar. Logβ_1 and logβ_2 represent the equilibrium constants of reactions to form 1:1 and 1:2 metal-glycinates, respectively. SD and N represent the standard deviation and number of references reporting standard state equilibrium constants.

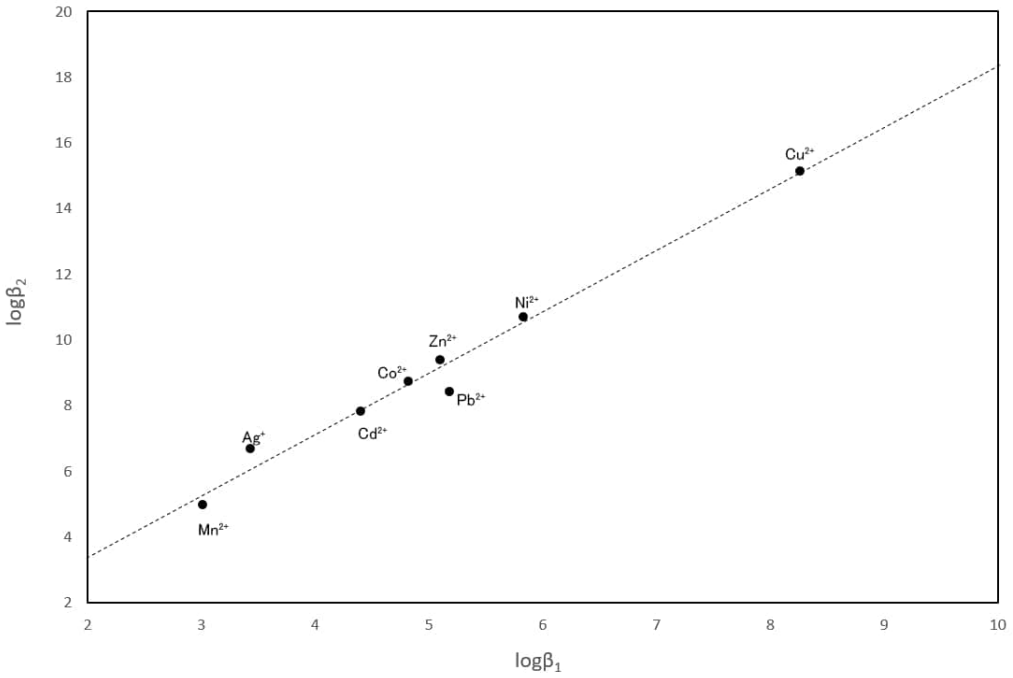

Figure 2.1: The standard state equilibrium constant of association reactions to form 1:2 metal-glycinate (β_2) against the standard state equilibrium constant of association reactions to form 1:1 metal-glycinate (β_1) at temperature 25^{o}C and 1 bar. The regression line can be expressed as $\log\beta_2 = 1.83\ \log\beta_1$ -0.1487

2.3 Isothermal correlations among the standard state equilibrium constants

Table 2.5 shows the standard state equilibrium constants of formation of metal-glycinate complexes, which will be used as inputs to construct correlations among the standard state constants of association (i.e. β_1, β_2 and β_3 as described in Eq. 2.4). This technique has been proposed by [14] who studied many metal-ligand complexes and showed that isothermal correlations among β_1 and β_2 exhibit linear trends with a universal slope of 1.83 with different intercepts.

Given the availability of β_1, β_2 and β_3 for metal-glycinate at 25^{o}C and 1 bar (Table 2.5), the average value of $\log\beta_2$ for metals with $N \geq 5$ have been considered and a correlation among $\log\beta_1$ and $\log\beta_2$ (formation of 1:1 and 1:2 metal-glycinate, respectively) have been regressed as shown in Fig. 2.1. The linear correlation that we obtained can be expressed as

$$\log\beta_2 = 1.83\log\beta_1 - 0.15 \tag{2.7}$$

where the coefficient of determination (also known as R-squared) is equal to 0.98.

We conducted a similar regression analysis to correlate the standard state equilibrium constants of the first and third association reaction constants ($\log\beta_1$ to $\log\beta_3$) of aqueous metal-glycinate at temperature 25^{o}C (Fig. 2.2). Using the same process, the average value of $\log\beta_3$ for metals with $N \geq 2$ has been considered from Table 2.5. We obtained the following expression of linear correlation with an R-squared coefficient of 0.97:

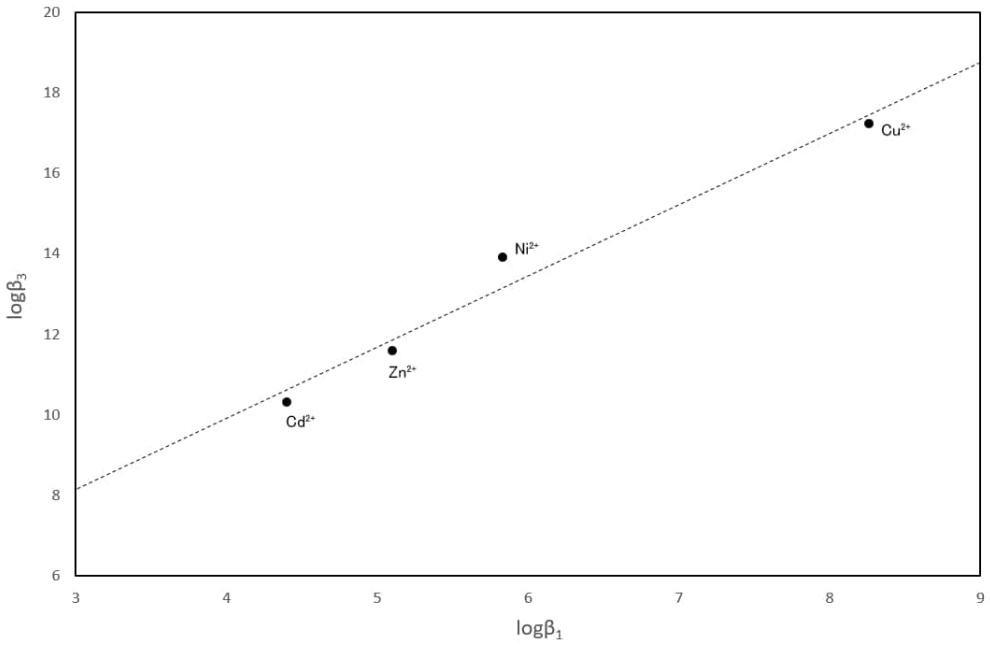

Figure 2.2: The standard state equilibrium constant of association reactions to form 1:3 metal-glycinate (β_3) against the standard state equilibrium constant of association reactions to form aqueous 1:1 metal-glycinate (β_1) at temperature 25^{o}C and 1 bar. The linear correlation can expressed as $\log\beta_3 = 1.83\log\beta_1 + 2.4566$.

$$\log\beta_3 = 1.83\log\beta_1 + 2.46 \tag{2.8}$$

Eqs. 2.7 and 2.8 can be used to predict $\log\beta_3$ and $\log\beta_2$ from $\log\beta_1$ and vice versa. Therefore, the reactions described by Eq. 2.4 are fully characterised at ambient conditions if $\log\beta_1$ is known. Since the standard partial molal Gibbs free energy and the equilibrium constant of reaction are related as shown by Eq. 2.5, it can be seen that $\Delta\bar{G}^o_r = -2.303RT\log\beta_1$ for a reaction forming 1:1 metal-glycinate. To obtain $\log\beta_1$ it is important to first estimate $\Delta\bar{G}^o_r$ through a correlation that involves the standard partial molal Gibbs free energy of formation $\Delta\bar{G}^o_f$. We proceed in accordance with [14] who constructed correlations of $\Delta\bar{G}^o_r$ to form 1:1 metal-ligands against $\Delta\bar{G}^o_f$ of metal ions at 25^{o}C and 1 bar for many ligands. They reported their expressions for different divalent metal-ligands complex formations containing glycolate, alanate and glycinate. The correlation of values of $\Delta\bar{G}^o_r$ to form 1:1 metal-glycinate against $\Delta\bar{G}^o_f$ of divalent metal cations at 25^{o}C and 1 bar can be expressed as:

$$\Delta\bar{G}^o_r = -0.043\Delta\bar{G}^o_f - 78 \tag{2.9}$$

In Eq. 2.9, an uncertainty of ± 500 [cal mol^{-1}] has been considered for specific divalent metal cation complexes [14]. However, no expression has been suggested for the association of monovalent metals with glycinate, mainly because of the lack of experimental data. In this paper, we address this gap and obtain a new correlation of $\Delta\bar{G}^o_r$ to form 1:1 monovalent metal-glycinate against $\Delta\bar{G}^o_f$ of monovalent metal ions at 25^{o}C and 1 bar. Using Eq. 2.7, we estimate the lacking values of $\log\beta_1$ from $\log\beta_2$. For example, the value of $\log\beta_1$

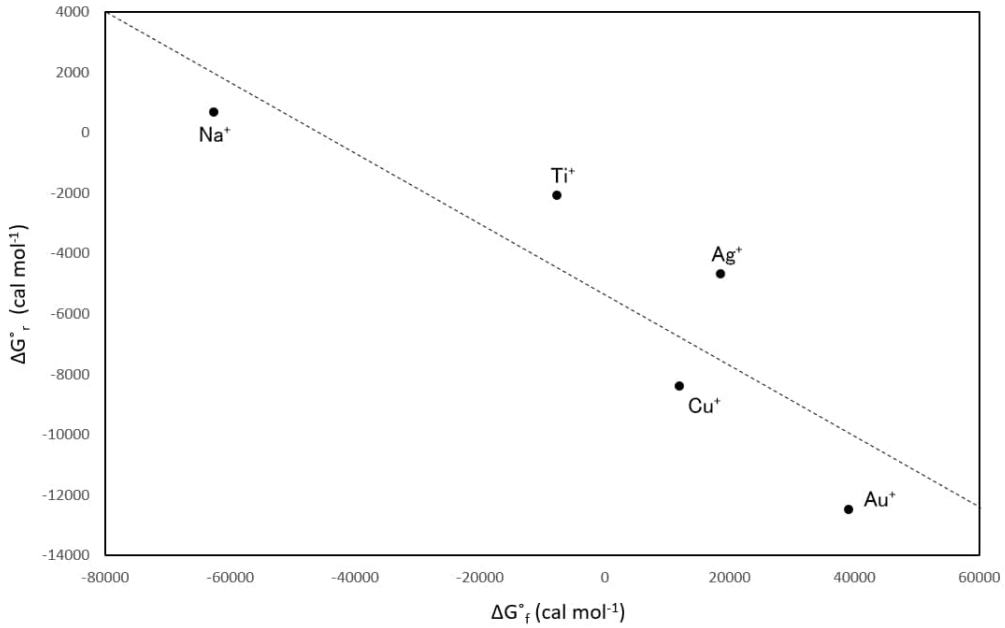

Figure 2.3: The standard partial molal Gibbs free energies of association to form 1:1 monovalent metal-glycinate against the standard partial molal Gibbs free energies of formation of aqueous monovalent metal ions at temperature 25^{o}C and 1 bar. The corresponding equation of regression line for gold-glycinate reaction to estimate $\Delta\bar{G}^o_r$ can expressed as $\Delta\bar{G}^o_r$ = -0.1246$\Delta\bar{G}^o_f$ -5701.1.

corresponding to gold-glycinate can be estimated as 9.21 using the average input data reported by [140] as well as [139]. Similarly, the value of logβ_1 corresponding to Cu^+ can be estimated as 6.15 using the average input data of [131] and [49]. Fig. 2.3 shows the correlation between the standard partial molal Gibbs free energies of reaction to form 1:1 aqueous monovalent metal-glycinate and the standard molal Gibbs free energies of monovalent metals at temperature 25^{o}C and pressure 1 bar. The equation of regression line corresponding to monovalent metal-glycinate formations can expressed as:

$$\Delta\bar{G}^o_r = -0.118\Delta\bar{G}^o_f - 54 \tag{2.10}$$

Fig. 2.3 shows that none of the values coincides with the regression line, which motivates the introduction of an interval of tolerance (or uncertainty). The interval of uncertainty has been identified as $\pm$1616.62 [cal mol^{-1}] which can be used in Eq. 2.10. To obtain this interval, the estimated value of $\Delta\bar{G}^o_r$ was calculated for Na^+, Ti^+, Ag^+, Cu^+ and Au^+ from Eq. 2.10. Consequently, the deviations of the actual values from the estimated ones have been calculated. By taking into account the proposed uncertainty intervals, the constants logβ_1, logβ_2 and logβ_3 corresponding to the formation of gold-glycinate can be estimated as 8.52$\pm$0.59, 15.45$\pm$0.48 and 18.05$\pm$0.89 (the average values of SD from Table 2.5) have been used, respectively.

In addition, to check the estimated values, we plot the correlation between logβ_2 of gold chelate and logβ_1 of Methylmercury ($MeHg^+$) chelate with the available data for various ligands including Cl^-, Br^-, I^- and Gly^- [3, 146]. No coherent data are available for other cations to be used in this paper. This method was originally proposed by [152] to estimate the stability constants of UO_2^{2+} and NpO_2^+ as well as Zn^{2+} and NpO_2^+, which are

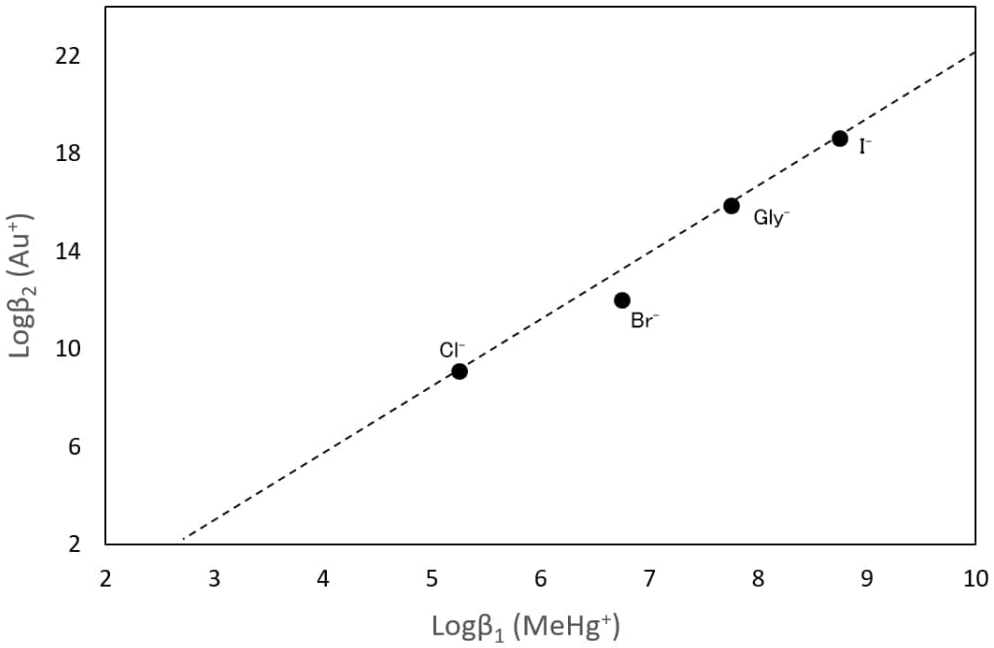

Figure 2.4: Correlation between form 1:2 chelate equilibrium constant of Au^+ ($\log\beta_2$)and 1:1 chelate equilibrium constant of $MeHg^+$ ($\log\beta_1$) at temperature 25^oC.

1:1 metal/metal oxide to chelate reactions. Fig. 2.4 shows that the constants of reaction are all consistent with the regression line.

2.4 Estimating the revised HKF equation of state for monovalent metal-glycinate complex formations

At the reference pressure P_r of 1 bar and temperature T_r of 25^oC, Eqs. 2.7, 2.8 and 2.10 can be used to estimate the standard partial molal Gibbs free energies of reactions to form 1:1, 1:2 and 1:3 monovalent metal-glycinate. These properties are sufficient to deduce the corresponding equilibrium constants that can be deduced using Eq. 2.5. However, the purpose of this section is to estimate β_y for $y = 1$ and 2 in Eq. 2.4 at different values of pressure P and temperature T. To this end, the thermodynamic properties and the revised HKF equations of state are calculated to work out $\Delta\bar{G}^o_r$ for monovalent metal-glycinate complexes at the temperature and pressure of interest. Referring to Eq. 2.2, the quantity $\bar{G}^o_{P,T} - \bar{G}^o_{P_r,T_r}$ can be obtained as [14, 19]

$$\bar{G}^o_{P,T} - \bar{G}^o_{P_r,T_r} = -\bar{S}^o_{P_r,T_r}(T - T_r) + \int_{T_r}^{T} \bar{C}^o_{P_r} dT - T\int_{T_r}^{T} \bar{C}^o_{P_r} dlnT + \int_{P_r}^{P} \bar{V}^o_{T_r} dP \qquad (2.11)$$

where $\bar{S}^o_{P_r,T_r}$ [cal $mole^{-1}K^{-1}$], $\bar{C}^o_{P_r}$ [cal $mole^{-1}K^{-1}$], and $\bar{V}^o_{T_r}$ [m^3 $mole^{-1}$] are the standard partial molal entropy, heat capacities, and volumes of the species, respectively.

In order to calculate $(\bar{G}^o_{P,T} - \bar{G}^o_{P_r,T_r})$ from Eq. 2.11, the properties $\bar{S}^o_{P_r,T_r}$, $\bar{C}^o_{P_r}$, and $\bar{V}^o_{T_r}$ need to be estimated first for which objective we utilise the well-known revised HKF model. In the literature, it has been demonstrated that the revised HKF equations of state

can be used to estimate the standard partial molal thermodynamic properties of aqueous electrolytes at high pressure and temperature with a fair level of accuracy [19]. Therefore, Eq. 2.2 can be substituted into Eq. 2.11 so that $\triangle \bar{G}^o_{P,T}$ can be expressed as

$$\begin{aligned}\triangle \bar{G}^o &= \triangle \bar{G}^o_f - \bar{S}^o_{P_r,T_r}(T-T_r) - c_1[T\ln(\frac{T}{T_r})] - c_2[(\frac{1}{T-\theta}) - (\frac{1}{T_r-\theta})](\frac{\theta-T}{\theta}) \\ &+ c_2(\frac{T}{\theta^2})ln[\frac{T_r(T-\theta)}{T(T_r-\theta)}] + a_1(P-P_r) + a_2 ln(\frac{\Psi+P}{\Psi+P_r}) + (\frac{1}{T+\theta})[a_3(P-P_r) \\ &+ a_4 ln(\frac{\Psi+P}{\Psi+P_r})] + \omega[(\frac{1}{\varepsilon}) - 1] - \omega_{P_r,Tr}[Y_{P_r,T_r}(T_r-T) + (\frac{1}{\varepsilon_{P_r,T_r}}) - 1]\end{aligned} \tag{2.12}$$

where the parameters a_1 [cal mol^{-1} bar^{-1}], a_2 [cal mol^{-1}], a_3 [cal K mol^{-1} bar^{-1}], a_4 [cal K mol^{-1} bar^{-1}], c_1 [cal mol^{-1} K^{-1}], and c_2 [cal K mol^{-1} bar^{-1}] are temperature and pressure independent properties of the species, the parameters $\theta = 228$ ^{o}K and $\Psi = 2600$ bar are intrinsic to the solvent, ω [cal mol^{-1}] denotes the temperature and pressure dependent Born coefficient of the species, and ε stands for the dielectric constant of H_2O. The term $Y = -(\frac{\delta(\frac{1}{\varepsilon})}{\delta T})_P$ represents the partial derivatives of the reciprocal dielectric constant of H_2O at constant pressure.

In order to use Eq. 2.12, the parameters $\bar{S}^o_{P_r,T_r}$, a_1, a_2, a_3, a_4, c_1, c_2 and ω need to be obtained first. The constants a_1, a_2, a_3 and a_4 are directly related to the standard partial molal volume $\bar{V}^o$ of the species, c_1 and c_2 are related to the standard partial molal heat capacity $\bar{C}^o_P$ of species and ω is related to $\bar{S}^o_{P_r,T_r}$.

This method is commonly used to predict the thermodynamic properties of chemical species at different temperatures and pressures. For instance, the thermodynamic data of many aqueous organic species including amino acids have been calculated by [153–156]. The revised HKF parameters have been utilised to predict the polymerization behavior of organic species as a function of temperature, pressure, pH, and redox state [157, 158]. Some studies have been conducted to calculate and predict the thermodynamic properties of aqueous metal complexes using the revised HKF equations of state of aqueous species [22, 159]. Some correlations have been obtained among HKF equations and the standard partial molal properties at 25^{o}C and 1 bar [15, 19–22, 160]. Therefore, it is possible to retrieve the standard partial molal entropies ($\bar{S}^o$), volumes ($\bar{V}^o$), and heat capacities ($\bar{C}^o_p$) of aqueous metal complexes at 25^{o}C and 1 bar [15]. Several empirical correlations constructed by [14, 15, 19–21] among available thermodynamic properties to estimate the behavior of organic and non-organic species at different temperatures and pressures.

The relationship between the standard partial molal entropy of reaction and the absolute standard partial molal of the species corresponding to the reaction can be presented as follows:

$$\Delta \bar{S}^o_{r,P_r,T_r} = \bar{S}^o_{ML_y^{Z-y}} - \bar{S}^o_{ML_{y-1}^{Z-y+1}} - \bar{S}^o_L \tag{2.13}$$

where y, Z and $\bar{S}^o_L$ represent the number of ligands (glycinate), charge of the metals and the standard partial molal entropy of the ligand, respectively. Eq. 2.13 can be used to calculate the entropy of the chemical reaction between glycinate and the metal M when $y = 1$ and between glycinate and the metal-glycinate complex ML^{Z-y+1} when $y \geq 2$. For

$y = 1$ in $\bar{S}^o_L$ and $\bar{S}^o_{M^Z}$ $(Z = 1, 2)$ are presented in Table 2.6. The thermodynamic data of several aqueous formations between metals and ligands including alanate, bicarbonate, acetylacetone and glycinate were estimated by [14]. The regression results of the standard partial molal entropy of the reaction versus the absolute standard molal entropy of divalent metals ($\bar{S}^o_{M^{2+}}{}^{abs}$) at 25^{o}C and 1 bar is given as [14]

$$\Delta\bar{S}^o_{r,P_r,T_r} = 0.37\bar{S}^o_{M^{2+}}{}^{abs} + 26 \tag{2.14}$$

By having the absolute standard partial molal entropy of divalent metals ($\bar{S}^o_{M^{2+}}{}^{abs}$), the standard partial molal entropy of reactions to form 1:1 metal-glycinate ($\Delta\bar{S}^o_{r,P_r,T_r}$) can be obtained. As a result, Eqs. 2.13 and 2.14 can be employed to obtain $\bar{S}^o_{ML^{Z-1}}$. The correlations corresponding to 1:1 monovalent metal-glycinate can be expressed as

$$\Delta\bar{S}^o_{r,P_r,T_r} = 0.31\bar{S}^o_{M^+}{}^{abs} + 9.9 \tag{2.15}$$

The correlations between the standard partial molal entropy of reaction and the absolute standard partial molal entropies of 1:1 complexes ($\bar{S}^o_{ML^+}$) have been regressed by [14] as

$$\Delta\bar{S}^o_{r,P_r,T_r} = 0.31\bar{S}^o_{ML^+}{}^{abs} + 5 \tag{2.16}$$

This regression is valid for metal-alanate and metal-glycinate with divalent metals (e.g. Cu^{2+}). Eq. 2.16 expresses the correlation of the standard partial molal entropy of the reaction to form aqueous 1:2 metal-ligand complexes against the absolute standard partial molal entropy $\bar{S}^o_{ML^+}{}^{abs}$ of the corresponding 1:1 metal-ligand complexes. A similar equation can be obtained for the reactions to form 1:2 metal-glycinate containing monovalent metals (e.g. Au^+)

$$\Delta\bar{S}^o_{r,P_r,T_r} = 0.31\bar{S}^o_{ML}{}^{abs} + 4.9 \tag{2.17}$$

where $\bar{S}^o_{ML}{}^{abs}$ represents the absolute standard partial molal entropy of the corresponding 1:1 monovalent metal-glycinate. Similar to Eq. 2.13, the standard partial molal heat capacities ($\bar{C}^o_{P,ML_y^{Z-y}}$ and $\bar{C}^o_{P,ML_{y-1}^{Z-y+1}}$) and standard partial molal volumes ($\bar{V}^o_{ML_y^{Z-y}}$ and $\bar{V}^o_{ML_{y-1}^{Z-y+1}}$) of all species in the reactions can be related as

$$\Delta\bar{V}_{r,y} = \bar{V}^o_{ML_y^{Z-y}} - \bar{V}^o_{ML_{y-1}^{Z-y+1}} - \bar{V}^o_L \tag{2.18}$$

$$\Delta\bar{C}^o_{r,y} = \bar{C}^o_{P,ML_y^{Z-y}} - \bar{C}^o_{P,ML_{y-1}^{Z-y+1}} - \bar{C}^o_{P,L} \tag{2.19}$$

where $\Delta\bar{V}^o_{r,y}$ represents the standard partial molal volume of reaction, $\Delta\bar{C}^o_{r,y}$ represents the standard partial molal heat capacity of reaction, $\bar{V}^o_L$ [cm^3 mole^{-1}] and $\bar{C}^o_{P,L}$ [cal mole^{-1} K^{-1}] represent the standard partial molal volumes and heat capacities of the ligand, respectively. Similar to Eq. 2.13, Eqs. 2.18 and 2.19 can be applied to obtain the standard partial molal volume and heat capacity of reaction between glycinate and metals when $y = 1$, and between glycine and metal-glycinate complexes when $y \geq 2$. Note that $\bar{V}^o_L$, $\bar{V}^o_{ML_{y-1}^{Z-y+1}}$ (for $y = 1$), $\bar{C}^o_{P,L}$ and $\bar{C}^o_{P,ML_{y-1}^{Z-y+1}}$ (for $y = 1$) are available in Table 2.6. Various correlations have been developed for different groups of complexes containing monovalent

Species	$\triangle\bar{G}_f^{oa}$	$\triangle\bar{H}_f^{oa}$	$\bar{S}_{Pr,Tr}^{ob}$	$\bar{C}_P^{ob}$	$\bar{V}^{oc}$	$a_1^d \times 10$	$a_2^e \times 10^{-2}$	a_3^f	$a_4^g \times 10^{-4}$	c_1^b	$c_2^g \times 10^{-4}$	$\omega^e \times 10^{-5}$
$^{i}Gly^{-}$	-75.27	-112.27	28.57	-0.80	45.70	9.7400	3.5400	20.0700	-4.7300	21.6000	-7.9200	0.69000
$^{j}Cu^{2+}$	15.67	15.70	-23.20	-5.70	-24.60	-1.1021	-10.4726	9.8662	-2.3461	20.3000	-4.3900	1.47690
$^{j}Ni^{2+}$	-10.90	-12.90	-30.80	-11.70	-29.00	-0.1694	-11.9181	10.4344	-2.2863	13.1905	-5.42179	-1.50670
$^{j}Co^{2+}$	-13.00	-13.90	-27.00	-7.80	-24.40	-1.0748	-12.9948	16.4112	-2.2418	15.2014	-4.62235	-1.47690
$^{j}Mn^{2+}$	-54.50	-52.72	-17.60	-4.10	-17.10	-0.1016	-8.0295	8.9060	-2.4471	16.6674	-3.8698	-1.40060
$^{j}Zn^{2+}$	-35.20	-36.66	-26.20	-6.30	-24.30	-0.1067	-10.39	9.8331	-2.3495	15.90009	-4.3179	-1.45740
$^{j}Cd^{2+}$	-18.56	-18.14	-17.40	-3.50	-15.60	-0.0537	-10.7080	16.5176	-2.3363	15.6573	-3.7476	-1.25280
$^{j}Au^{+}$	39.00	47.58	24.50	0.60	11.10	3.3448	0.3856	5.5985	-2.7949	8.1768	-2.9124	0.18000
$^{j}Ag^{+}$	18.43	25.27	17.54	7.90	-0.80	1.7285	-3.5608	7.1496	-2.6318	12.7862	-1.4254	0.21600
$^{j}Na^{+}$	-62.59	-57.43	13.96	9.06	-1.11	1.8390	-2.2850	2.2560	-2.7260	18.1800	-2.9810	0.33060
$^{j}Ti^{+}$	-7.74	1.28	30	-4.20	18.20	4.3063	2.7333	4.6757	-2.8920	5.0890	-3.8901	0.15020
$^{j}Cu^{+}$	11.95	17.13	9.70	13.70	-8.00	0.7835	-5.8682	8.0565	-2.5364	17.2831	-0.2439	0.33510

Table 2.6: The standard partial molal thermodynamic data and the revised HKF equations of various ions reported at 25^{o}C and 1 bar. ^{a} Kcal mol^{-1}, ^{b} cal mol^{-1} K^{-1}, ^{c} cm^3 mol^{-1}, ^{d} cal mol^{-1} bar^{-1}, ^{e} cal mol^{-1}, ^{f} cal K mol^{-1} bar^{-1}, ^{g} cal K mol^{-1}. ^{i}[161], ^{j} [19].

ligands such as chloride and acetate complexes containing monovalent and divalent cations by [15] to estimate heat capacities and volumes of complexes. The regression analysis for the volume of reaction is generally expressed as follows:

$$\Delta \bar{V}^o_{r,y} = 0.11419 \bar{V}^o_{ML_{y-1}^{Z-y+1}} + 8.9432 \tag{2.20}$$

By using the data available in Table A.6 in terms of $\bar{V}^o_L$ and $\bar{V}^o_{ML_{y-1}^{Z-y+1}}$ (for $y = 1$), applying Eq. 2.20 to estimate $\Delta \bar{V}^o_{r,y}$ and substituting the outputs into Eq. 2.18, we obtain $\bar{V}^o_{ML_y^{Z-y}}$ (for $y \geq 1$).

For the reaction to form a 1:1 metal-ligands, the following expression has been proposed by [15] to relate the standard partial molal heat capacity of reaction to the standard molal heat capacity of a metal M when the ligands are Cl^-, Br^-,F^- or I^-:

$$\Delta \bar{C}^o_{r,y} = 1.25 \bar{C}^o_{P,M^Z} + 45.3(Z) - 27.3 \tag{2.21}$$

where $\bar{C}^o_{P,M^Z}$ represents the metal's standard molal heat capacity. Eq. 2.21 can be rewritten for acetate complexes of divalent metals as

$$\Delta \bar{C}^o_{r,y} = 1.25 \bar{C}^o_{P,M^{2+}} + 93.8 \tag{2.22}$$

The regression between the metal's standard molal heat capacity and the standard partial molal heat capacity of reaction to form 1:y metal-ligands—when $y \geq 2$ and the ligands are Cl^-, Br^-,F^- or I^-—is also expressed as

$$\Delta \bar{C}^o_{r,y} = (0.89 \bar{C}^o_{P,M^Z} - 4.9)y + 1.25 \bar{C}^o_{P,M^Z} + 45.3(Z) - 27.3 \tag{2.23}$$

Similarly, in the case of acetate complexes of divalent metals the standard partial molal heat capacity of reaction can be written as

$$\Delta \bar{C}^o_{r,y} = (0.89 \bar{C}^o_{P,M^Z} + 20.6)y + 1.25 \bar{C}^o_{P,M^Z} + 93.8 \tag{2.24}$$

According to [14, 15], the slope and intercept of the correlation that relate the standard molal heat capacity of reaction to the standard molal heat capacity of metal-ligand complexes depend on the ligands' properties. Using these dependences, we deduce the slope and intercept of the correlation that would have been valid when the ligand is glycinate knowing C^o_{P,L^-}. Therefore, based on these dependencies and Eqs. 2.21 and 2.22 we can suggest the following equation that can be used reaction to form 1:1 metal-glycinate:

$$\Delta \bar{C}^o_{r,y} = 1.25 \bar{C}^o_{P,M^Z} + 45.3(Z) - 12.1 \tag{2.25}$$

Following a similar methodology, the standard partial molal heat capacity of reaction to form 1:y metal-glycinate ($y \geq 2$) can be written as

$$\Delta \bar{C}^o_{r,y} = (0.89 \bar{C}^o_{P,M^Z} + 7.8)y + 1.25 \bar{C}^o_{P,M^Z} + 45.3(Z) - 12.1 \tag{2.26}$$

Using the thermodynamic data reported in Table 2.6 in terms of $\bar{C}^o_{P,L}$ and $\bar{C}^o_{P,ML_{y-1}^{Z-y+1}}$ (for $y = 1$), Eqs. 2.19 and 2.25 can be used to calculate the value of $\bar{C}^o_{P,ML_y^{Z-y}}$. As can

be seen in Table 2.7, the values obtained in this study are consistent with those reported [14] for $CuGly^+$, $CuGly_2$, $NiGly^+$, $NiGly_2$, $CoGly^+$, $CoGly_2$, $MnGly^+$, $MnGly_2$, $ZnGly^+$, $ZnGly_2$, $CdGly^+$, and $CdGly_2$. These values are 63.4, 139.0, 49.9, 112.7, 58.7, 129.8, 67.0, 146.1, 62.1, 136.4, 68.4, and 148.7, respectively.

In order to obtain the solvation parameter of the species at the reference pressure and temperature (ω_{P_r,T_r} [cal mole^{-1}]), the following regression has been proposed by [15] based on the experimental data reported by [162]

$$\omega_{P_r,T_r} = -1514.4\bar{S}^o_{P_r,T_r} + \beta_{Z'} \tag{2.27}$$

where Z' represents the charge of the species and $\beta_{Z'} \times 10^{-5}$ [cal mol^{-1}] is equal to 0.5512, 1.0586, 1.5795, -1.6295, 3.2120 and 0 for Z' equal to 1, 2, 3, -1, -2 and 0, respectively. The following equations are also used to calculate temperature and pressure independent properties of the species [15, 19].

$$a_1 = 0.013684(\bar{V}^o + 41.84\omega_{P_r,T_r}Q_{P_r,T_r}) + 0.1765 \tag{2.28}$$

$$a_2 = 33.423(\bar{V}^o + 41.84\omega_{P_r,T_r}Q_{P_r,T_r}) - 347.23 \tag{2.29}$$

$$a_3 = -0.1435(\bar{V}^o + 41.84\omega_{P_r,T_r}Q_{P_r,T_r}) + 7.0274 \tag{2.30}$$

$$a_4 = -138.17(\bar{V}^o + 41.84\omega_{P_r,T_r}Q_{P_r,T_r}) - 26355 \tag{2.31}$$

$$c_1 = 0.6087\bar{C}^o_p + \omega_{P_r,T_r}T_rX_{P_r,T_r} + 5.85 \tag{2.32}$$

$$c_2 = 2037\bar{C}^o_p - 30460 \tag{2.33}$$

The terms $Q_{P_r,T_r} = -(\frac{\delta(\frac{1}{\varepsilon})}{\delta P})_T$ and $X_{P_r,T_r} = (\frac{\delta(Y)}{\delta T})_P$ represent the partial derivatives of the reciprocal dielectric constant of H_2O which are equal to 5.903×10^{-7} bar^{-1} and -3.09×10^{-7} K^{-2}, respectively.

Using the above equations and the input data available in Table 2.6, the thermodynamic properties and the revised HKF equations of state can be calculated for metal-glycinate complexes (Table 2.7) and can be used in Eq. 2.12 to estimate the the apparent standard partial molal Gibbs free energy of formation of various aqueous species at any temperature (T) and pressure (P).

2.5 Predicted equilibrium constants of monovalent metal-glycinates at elevated temperatures

In this section, we use Eqs. 2.12 to calculate the standard state equilibrium constants of monovalent metal-glycinates at temperatures up to 150^{o}C. We also calculate the thermodynamic data of divalent metal-glycinate complexes containing Cu^{2+}, Ni^{2+}, Co^{2+}, Mn^{2+}, Zn^{2+}, and Cd^{2+} to verify the proposed method and assess its accuracy and reliability. Additional experimental data at specific temperatures are used to validate the equilibrium constants obtained in this study. Fig. 2.5, 2.6 and 2.7 show the standard state equilibrium constants of reactions involving 1 : 1 and 1 : 2 metal-glycinates. The results show that the values obtained in this study are consistent with those reported as experimental data.

Species	$\triangle\bar{G}_f^{oa}$	$\triangle\bar{H}_f^{oa}$	$\bar{S}_{Pr,Tr}^{ob}$	$\bar{C}_P^{ob}$	$\bar{V}^{oc}$	$a_1^d \times 10$	$a_2^e \times 10^{-2}$	a_3^f	$a_4^g \times 10^{-4}$	c_1^b	$c_2^g \times 10^{-4}$	$\omega^e \times 10^{-5}$
$CuGly^+$	-70.86	-77.65	22.79	64.87	27.23	5.5614	5.8003	3.0462	-3.0188	43.4404	10.1690	0.20613
$CuGly_2$	-155.36	-174.27	63.42	140.90	84.99	13.0700	24.1424	-4.8279	-3.7770	100.4665	25.6561	-0.96043
$NiGly^+$	-94.12	-97.81	12.37	51.38	22.33	4.9438	4.2942	3.6939	-2.9565	33.7703	7.4191	0.36381
$NiGly_2$	-176.03	-190.87	49.78	109.22	79.53	12.3924	22.4873	-4.1172	-3.7086	79.2799	19.2029	-0.75387
$CoGly^+$	-94.83	-100.08	17.58	60.15	27.4570	5.6185	5.9422	2.9863	-3.0246	39.8379	9.2065	0.28497
$CoGly_2$	-175.45	-192.33	56.60	129.82	85.2354	13.1389	24.3107	-4.9001	-3.7839	92.7658	23.3975	-0.85715
$MnGly^+$	-133.87	-142.95	30.46	68.47	35.5905	6.6656	8.4997	1.8883	-3.1303	46.7021	10.9023	0.08994
$MnGly_2$	-211.86	-233.76	73.47	149.35	94.30	14.2927	27.1287	-6.1100	-3.9004	107.0010	27.3770	-1.11263
$ZnGly^+$	-117.42	-122.99	18.68	63.52	27.57	5.6282	5.9657	2.9762	-3.0256	42.0452	9.8940	0.26837
$ZnGly_2$	-198.56	-215.86	58.04	137.74	85.36	13.1486	24.3342	-4.9102	-3.7849	97.7870	25.0108	-0.87889
$CdGly^+$	-99.83	-108.99	30.73	69.82	37.26	6.8929	9.0548	1.6499	-3.1533	47.5621	11.1773	0.08580
$CdGly_2$	-179.78	-201.80	73.83	152.52	96.16	14.5457	27.7466	-6.3753	-3.9260	108.9895	28.0223	-1.11807
AuGly	-47.88	-68.92	70.56	33.75	67.01	10.5736	18.0425	-2.2099	-3.5242	36.2388	3.8289	-1.06864
$AuGly_2^-$	-132.59	-170.13	125.91	83.57	129.31	18.2641	36.8264	-10.2747	-4.3006	89.2970	13.9768	-3.56227
AgGly	-61.52	-79.84	61.45	50.17	53.75	8.8059	13.7273	-0.3562	-3.3464	44.9646	7.1746	-0.93056
$AgGly_2^-$	-141.26	-175.24	113.97	122.11	114.53	16.3037	32.0405	-8.2189	-4.1035	111.09	21.8282	-3.3554
NaGly	-137.18	-154.10	56.76	52.78	53.41	8.7826	13.6705	-0.3318	-3.3441	45.8990	7.7063	-1.06864
$NaGly_2^-$	-212.09	-244.23	107.82	128.24	114.15	16.2824	31.9887	-8.1966	-4.1014	113.96	23.0758	-3.2624
TiGly	-85.88	-109.07	77.77	22.95	74.92	11.6192	20.5988	-3.3064	–3.6305	30.6701	1.6289	-1.17775
$TiGly_2^-$	-163.34	-203.69	135.35	58.22	138.12	19.4219	39.6567	-11.4888	-4.4183	75.1870	8.8142	-3.67922
CuGly	-71.75	-87.00	51.18	63.22	45.73	7.7607	11.1745	0.7399	-3.2409	51.4752	9.8329	-0.77502
$CuGly_2^-$	-153.81	-183.78	100.51	152.74	105.59	15.1494	29.2213	-7.0084	-3.9869	127.8561	28.0663	-3.15165

Table 2.7: The standard molal thermodynamic data and the revised HKF equations of 1:1 and 1:2 metal-glycinates at 25°C and 1 bar. ^{a} Kcal mol^{-1}, ^{b} cal mol^{-1} K^{-1}, ^{c} cm^3 mol^{-1}, ^{d} cal mol^{-1} bar^{-1}, ^{e} cal mol^{-1}, ^{f} cal K mol^{-1} bar^{-1}, ^{g} cal K mol^{-1}.

For example, the first row of Fig. 2.5 shows the values of $\log\beta_1$ for $CuGly^+$ have been reported as 8.61 at 0.35^{o}C, 8.54 at 15^{o}C, 8.22 at 20^{o}C, 8.17 at 30^{o}C, and 8.07 at 37^{o}C by [62, 67, 127, 163, 164], respectively. These values are in a good agreement with the results obtained in this study. The value of $\log\beta_1$ for $CuGly^+$ has been reported as 8.85 and 8.59 at 10^{o}C and 20^{o}C by [59, 165], respectively, which are close to those obtained in this study. [166] reported $\log\beta_1$ as 7.72 at 30^{o}C which is slightly lower than but close to the value obtained in present study. The figure also shows the values of $\log\beta_2$ for $CuGly_2$ reported by [67, 82, 167] are equal to 15.4, 15 and 14.6 at 20^{o}C, 30^{o}C and 35^{o}C, respectively, which agree well with this study. The values reported by [62, 84, 163] are also close to the values obtained in this study. However, [99] reported slightly higher values but still comparable to the results of the current study.

The second row of Fig. 2.5 shows that the experimental values of $\log\beta_1$ and $\log\beta_2$ for $NiGly^+$ and $NiGly_2$ are close to the data generated in this study. The value of $\log\beta_1$ for $NiGly^+$ is equal to 5.73, 5.9 and 5.72 at 10^{o}C, 35^{o}C, and 40^{o}C as reported by [82, 96, 168], respectively. The value of $\log\beta_2$ for $NiGly_2$ is equal to 10.7 and 10.4 at 20^{o}C and 35^{o}C as reported by [67, 169], respectively. The experimental data of $\log\beta_1$ for $CoGly^+$ is consistent with the data generated using our proposed model as can be seen in the third row of Fig. 2.5. In particular, [36, 166, 169, 170] reported the $\log\beta_1$ of $CoGly^+$ as 4.99, 5.1, 4.77 and 4.6 at 15^{o}C, 20^{o}C, 30^{o}C and 35^{o}C, respectively. [84, 171] reported the $\log\beta_2$ of $CoGly_2$ as 8.9 at 20^{o}C. However, [99, 166] reported slightly higher values of 9.23 and 8.99 at 10^{o}C and 30^{o}C than the data generated in this study. In addition, [36] reported a slightly lower value of 8.57 at 15^{o}C. In the case of $MnGly^+$ and $MnGly_2$, despite the small discrepancy between the current model and the experimental data obtained from literature [96, 99, 172, 173], the average values are still close to the presented results as can be seen in the fourth row of Fig. 2.5.

Fig. 2.6 shows that the experimental values of $\log\beta_1$ and $\log\beta_2$ for $ZnGly^+$ and $ZnGly_2$ reported by [134, 164, 167, 170, 171] agree well with data obtained in this study. Similarly, the values of $\log\beta_1$ and $\log\beta_2$ for $CdGly^+$ and $CdGly_2$ measured by [150, 174–177] are consistent with those calculated in this rsearch. However, [102] reported slightly lower values for $CdGly^+$ and $CdGly_2$ which are equal to 3.86 and 6.78 at 45^{o}C, respectively. The values reported by [127, 166, 175, 176, 178] are consistent with the values obtained in this study.

No equilibrium constants have been found for monovalent metals reacting with glycinate except for Ag^+ (Fig. 2.7). Although the equilibrium constants reported by [120] deviate slightly from the trend predicted in this study, the experimental values of $\log\beta_1$ and $\log\beta_2$ are still close to the results of the current model.

It is obvious that the experimental values of stability constants may change depending on the testing method, ionic strength, and testing conditions. Most experiments are conducted under constant ionic strength conditions. The ionic strength is controlled by using different inert salts such as KNO_3. The most common ionic strengths are 0, 0.1, 0.2, 0.5, 1.0, and 3.0 mol dm^{-3}. As a result, experimental values may differ slightly from the theoretical values obtained using the basic principles of thermodynamics. Overall, the average thermodynamic properties obtained experimentally are close to the results generated in the present study.

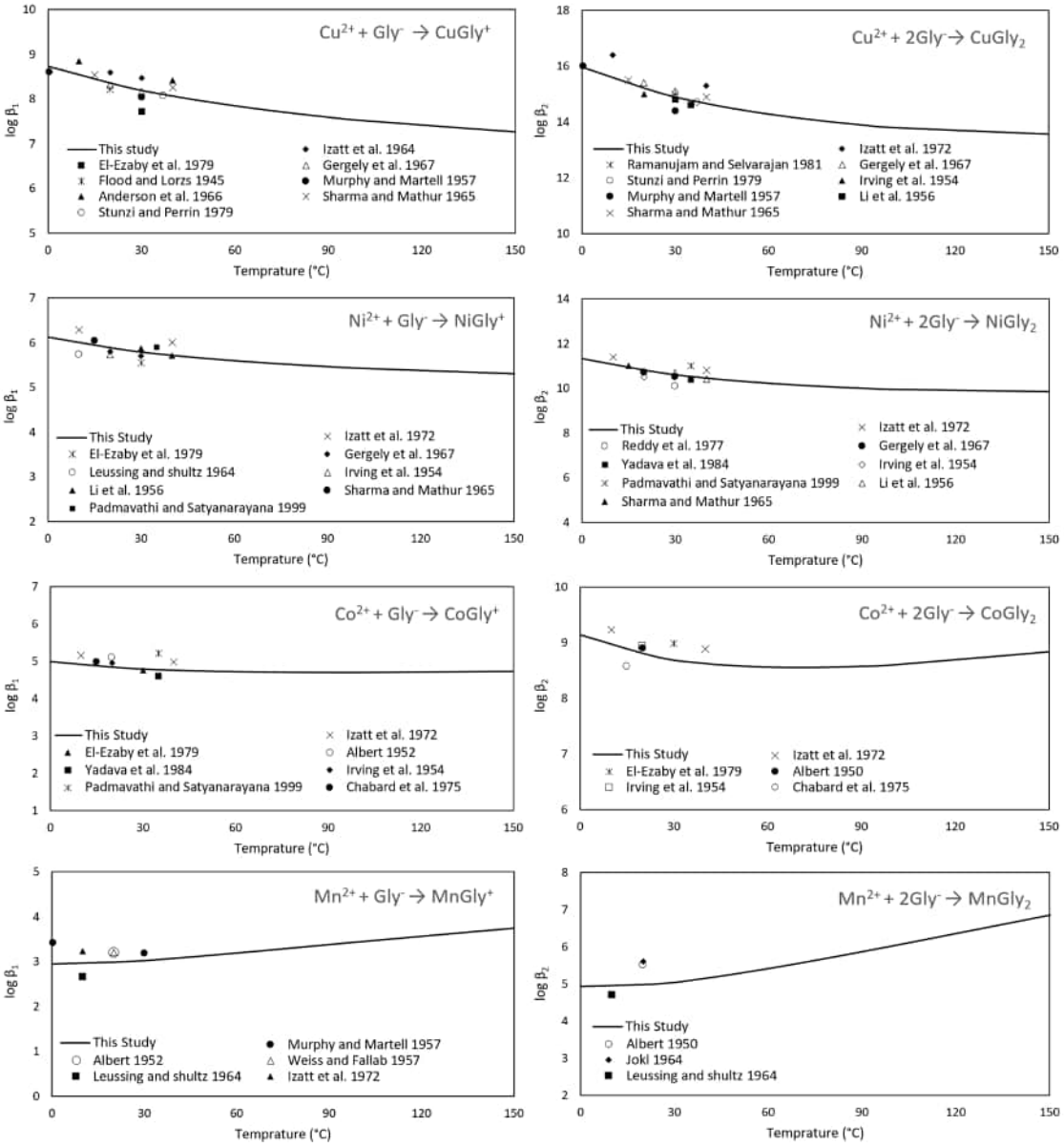

Figure 2.5: The standard state equilibrium constants of association of metal-glycinates at different temperatures up to 150^{o}C and pressure of 1 bar. The graphs on the left side present the standard state equilibrium constants of reactions to form 1:1 metal-glycinate and the graphs on the right side present the standard state equilibrium constants of reaction to form 1:2 metal-glycinate involving the metals Cu^{2+}, Ni^{2+}, Co^{2+} and Mn^{2+}. The markers represent experimental data reported in the literature.

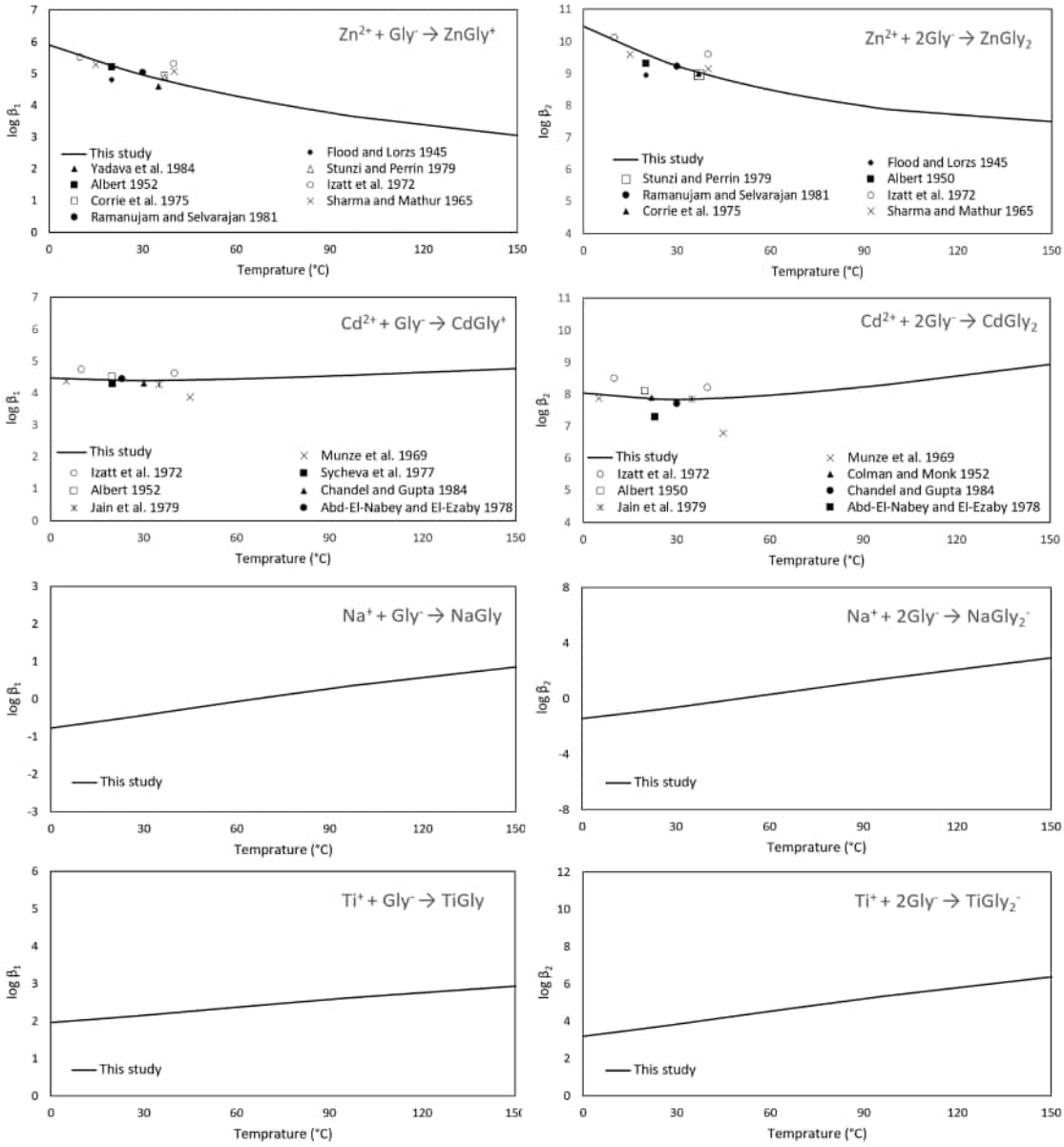

Figure 2.6: The standard state equilibrium constants of association of metal-glycinates at different temperatures up to 150^{o}C and pressure of 1 bar. The graphs on the left side present the standard state equilibrium constants of reaction to form 1:1 metal-glycinate and the graphs on the right side present the standard state equilibrium constants of reaction to form 1:2 metal-glycinate involving the metals Zn^{2+}, Cd^{2+}, Na^+ and Ti^+. The markers represent experimental data reported in the literature.

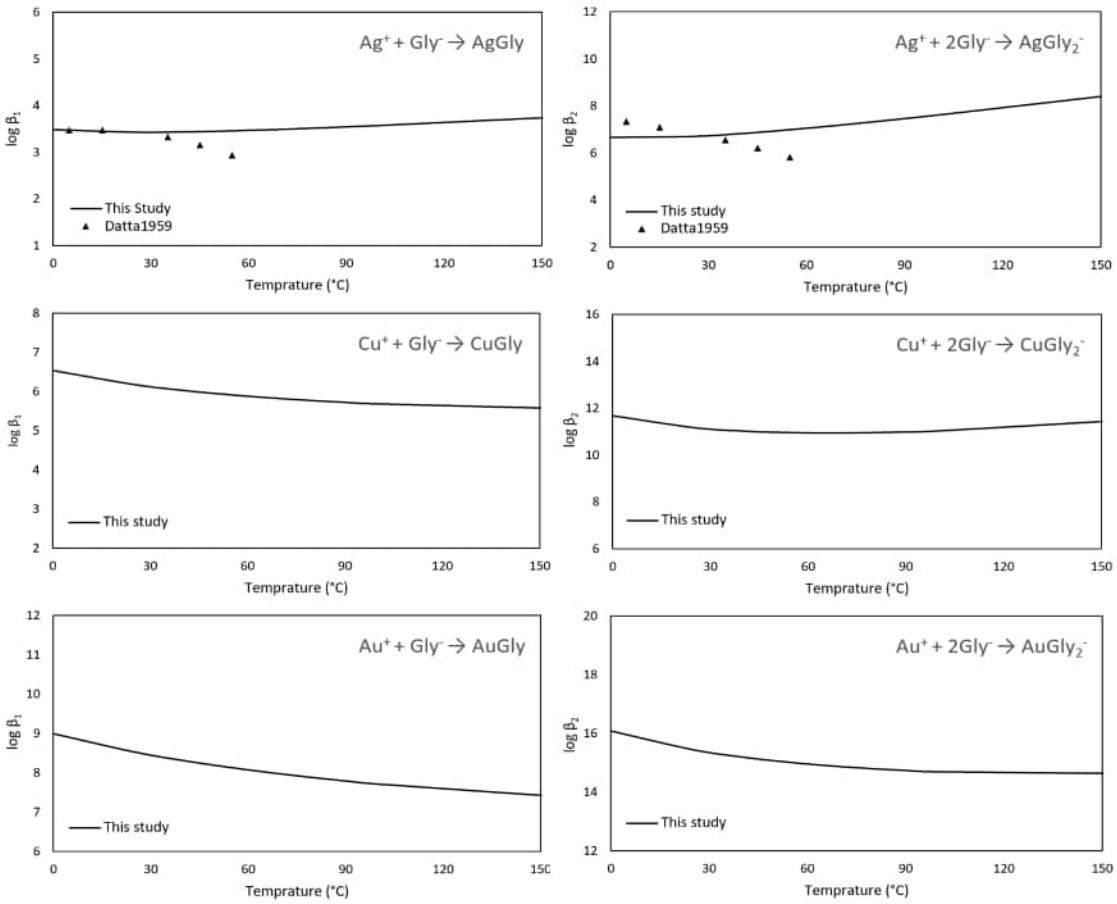

Figure 2.7: The standard state equilibrium constants of association of metal-glycinates at different temperatures up to 150^{o}C and pressure of 1 bar. The graphs on the left side present the standard state equilibrium constants of reaction to form 1:1 metal-glycinate and the graphs on the right side present the standard state equilibrium constants of reaction to form 1:2 metal-glycinate involving the metals Ag^+, Cu^+ and Au^+. The markers represent experimental data reported in the literature.

2.6 Conclusion

Understanding the behaviour of metal-glycine systems is important because aqueous glycine solutions have been proposed as non-toxic environmentally friendly lixiviants to leach precious metals. However, the thermodynamic data that are necessary to predict the behavior of chemical species in these systems are scarce. This study bridges this gap by using data analysis techniques to relate the standard partial molal properties of metal-glycinate complexes to the standard partial molal properties of metals and estimate the equilibrium constants of association of monovalent metal-glycinates. Finally, the standard partial molal properties of the metal-glycinate complexes and their revised HKF equations of state have been deduced. In particular, this work calculates for the first time the thermodynamic data HKF parameters of monovalent metal-glycinate complexes. Therefore this work has the potential to influence the use of glycine in future metal leaching applications. The proposed method has been tested using existing experimental data and showed excellent consistency. The proposed work takes into account the uncertainty that is inherent to various experimental techniques and reports tolerance intervals that offer best likelihood of accuracy.

Acknowledgements

This research was supported by the Australian Research Council through the Discovery grant DP170104205. This support is highly appreciated. The authors would like to acknowledge the financial support provided by Robert and Maude Gledden Postgraduate Scholarships.

References

Bibliography

[1] L. S. Pangum, R. E. Browner, Pressure chloride leaching of a refractory gold ore, Minerals Engineering 9 (5) (1996) 547–556.

[2] M. Jeffrey, Kinetic aspects of gold and silver leaching in ammonia-thiosulfate solutions, Hydrometallurgy 60 (1) (2001) 7–16.

[3] M. G. Aylmore, Alternative lixiviants to cyanide for leaching gold ores, Gold Ore Processing, Project Development and Operation (2005) 501 to 539.

[4] J. A. Heath, M. I. Jeffrey, H. G. Zhang, J. A. Rumball, Anaerobic thiosulfate leaching: Development of in situ gold leaching systems, Minerals Engineering 21 (6) (2008) 424–433.

[5] E. A. Oraby, M. I. Jeffrey, R. E. Browner, The deportment of mercury during thiosulfate leaching and resin-in-pulp recovery of gold from ores, Minerals & Metallurgical Processing Journal 27 (4) (2010) 184–189.

[6] X. Yang, M. S. Moats, J. D. Miller, X. Wang, X. Shi, H. Xu, Thiourea-thiocyanate leaching system for gold, Hydrometallurgy 106 (1) (2011) 58–63.

[7] E. A. Oraby, J. J. Eksteen, The leaching of gold, silver and their alloys in alkaline glycine-peroxide solutions and their adsorption on carbon, Hydrometallurgy 152 (2015) 199–203.

[8] J. Eksteen, E. Oraby, B. Tanda, P. Tauetsile, G. Bezuidenhout, T. Newton, F. Trask, I. Bryan, Towards industrial implementation of glycine-based leach and adsorption technologies for gold-copper ores, Canadian Metallurgical Quarterly (2017) 1–9.

[9] A. Karrech, M. Attar, E. Oraby, J. Eksteen, M. Elchalakani, A. Seibi, Modelling of multicomponent reactive transport in finite columns–application to gold recovery using iodide ligands, Hydrometallurgy 178 (2018) 43–53.

[10] D. H. Brown, W. E. Smith, P. Fox, R. D. Sturrock, The reactions of gold (0) with amino acids and the significance of these reactions in the biochemistry of gold, Inorganica Chimica Acta 67 (1982) 27–30.

[11] W. Walker, B. Griffin, Solubility of copper in human sweat, Search 7 (3) (1976) 100–101.

[12] Z. Jingrong, L. Jianjun, Y. Fan, W. Jingwei, Z. Fahua, An experimental study on gold solubility in amino acid solution and its geological significance, Chinese Journal of Geochemistry 15 (4) (1996) 296–302.

[13] D. Feng, J. S. J. Van Deventer, The role of amino acids in the thiosulphate leaching of gold, Minerals Engineering 24 (9) (2011) 1022–1024.

[14] E. L. Shock, C. M. Koretsky, Metal-organic complexes in geochemical processes: Estimation of standard partial molal thermodynamic properties of aqueous complexes between metal cations and monovalent organic acid ligands at high pressures and temperatures, Geochimica et Cosmochimica Acta 59 (8) (1995) 1497–1532.

[15] D. Sverjensky, E. Shock, H. Helgeson, Prediction of the thermodynamic properties of aqueous metal complexes to 1000 c and 5 kb, Geochimica et Cosmochimica Acta 61 (7) (1997) 1359–1412.

[16] H. C. Helgeson, D. H. Kirkham, G. C. Flowers, Theoretical prediction of the thermodynamic behavior of aqueous electrolytes by high pressures and temperatures; iv, calculation of activity coefficients, osmotic coefficients, and apparent molal and standard and relative partial molal properties to 600 degrees c and 5kb, American journal of science 281 (10) (1981) 1249–1516.

[17] T. Poulet, A. Karrech, K. Regenauer-Lieb, L. Fisher, P. Schaubs, Thermal–hydraulic–mechanical–chemical coupling with damage mechanics using escriptrt and abaqus, Tectonophysics 526-529 (2012) 124 – 132.

[18] A. Karrech, Non-equilibrium thermodynamics for fully coupled thermal hydraulic mechanical chemical processes, Journal of the Mechanics and Physics of Solids 61 (3) (2013) 819 – 837.

[19] E. L. Shock, H. C. Helgeson, Calculation of the thermodynamic and transport properties of aqueous species at high pressures and temperatures: Correlation algorithms for ionic species and equation of state predictions to 5 kb and 1000 c, Geochimica et Cosmochimica Acta 52 (8) (1988) 2009–2036.

[20] E. L. Shock, H. C. Helgeson, D. A. Sverjensky, Calculation of the thermodynamic and transport properties of aqueous species at high pressures and temperatures: Standard partial molal properties of inorganic neutral species, Geochimica et Cosmochimica Acta 53 (9) (1989) 2157–2183.

[21] E. L. Shock, H. C. Helgeson, Calculation of the thermodynamic and transport properties of aqueous species at high pressures and temperatures: Standard partial molal properties of organic species, Geochimica et Cosmochimica Acta 54 (4) (1990) 915–945.

[22] J. C. Tanger, H. C. Helgeson, Calculation of the thermodynamic and transport properties of aqueous species at high pressures and temperatures; revised equations of state for the standard partial molal properties of ions and electrolytes, American Journal of Science 288 (1) (1988) 19–98.

[23] T. Kiss, I. Sovago, A. Gergely, Critical survey of stability constants of complexes of glycine, Pure and applied chemistry 63 (4) (1991) 597–638.

[24] F. J. Rossotti, H. Rossotti, The determination of stability constants: and other equilibrium constants in solution, Tech. rep., McGraw-Hill, (1961).

[25] M. T. Beck, I. Nagypál, D. Williams, Chemistry of complex equilibria, Van Nostrand Reinhold London, 1970.

[26] M. Beck, Critical evaluation of equilibrium constants in solution. stability constants of metal complexes, Pure and Applied Chemistry 49 (1) (1977) 127–136.

[27] G. Anderegg, Critical survey of stability constants of nta complexes, Pure and Applied chemistry 54 (12) (1982) 2693–2758.

[28] M. Beck, Critical survey of stability constants of cyano complexes, Pure and applied chemistry 59 (12) (1987) 1703–1720.

[29] J. Stary, J. Liljenzin, Critical evaluation of equilibrium constants involving acetylacetone and its metal chelates, Pure and applied chemistry 54 (12) (1982) 2557–2592.

[30] D. Tuck, Critical survey of stability constants of complexes of indium, Pure and Applied Chemistry 55 (9) (1983) 1477–1528.

[31] L. Pettit, Critical survey of formation constants of complexes of histidine, phenylalanine, tyrosine, l-dopa and tryptophan, Pure and Applied Chemistry 56 (2) (1984) 247–292.

[32] P. Paoletti, Formation of metal complexes with ethylenediamine: a critical survey of equilibrium constants, enthalpy and entropy values, Pure and applied chemistry 56 (4) (1984) 491–522.

[33] A. Braibanti, G. Ostacoli, P. Paoletti, L. Pettit, S. Sammartano, Recommended procedure for testing the potentiometric apparatus and technique for the ph-metric measurement of metal-complex equilibrium constants, Pure and Applied Chemistry 59 (12) (1987) 1721–1728.

[34] M. Beck, I. Nagypál, Chemistry of complex equilibria, akadémiai kiadó (1990).

[35] G. Anderegg, Critical Survey of Stability Constants of EDTA Complexes: Critical Evaluation of Equilibrium Constants in Solution: Stability Constants of Metal Complexes, Elsevier, 2013.

[36] J. Chabard, G. Besse, D. Pepin, J. Petit, J. andBerger, Study of stability of complexes by thin-layer electrophoresis. 4. metallic mononuclear complexes of glycine, Bulletin De La Societe Chimique De France (1975) 1943.

[37] M. M. Shoukry, E. M. Khairy, A. A. El-Sherif, Ternary complexes involving copper (ii) and amino acids, peptides and dna constituents. the kinetics of hydrolysis of α-amino acid esters, Transition Metal Chemistry 27 (6) (2002) 656–664.

[38] N. Ivičić, V. Simeon, Stability and cd spectra of co2+ and cu2+ complexes with epimeric threonines and isoleucines, Journal of Inorganic and Nuclear Chemistry 43 (10) (1981) 2581–2584.

[39] I. Šoštarić, V. Simeon, Die stabilität der kobalt (ii)-und kupfer (ii)-komplexe mit α-, β-und γ-aminobutyrat, Monatshefte für Chemie/Chemical Monthly 106 (1) (1975) 169–173.

[40] M. S. Mohan, D. Bancroft, E. Abbott, Mixed-ligand complexes of copper (ii) with imidazole and selected ligands, Inorganic Chemistry 18 (6) (1979) 1527–1531.

[41] T. B. Field, W. McBryde, Determination of stability constants by p h titrations: a critical examination of data handling, Canadian Journal of Chemistry 56 (9) (1978) 1202–1211.

[42] G. Nakagawa, H. Wada, T. Hayakawa, Use of the copper (ii)-selective electrode for the determination of the stability constants of copper (ii) complexes, Bulletin of the Chemical Society of Japan 48 (2) (1975) 424–427.

[43] E. Hansen, J. Ruzicka, Selectrode-the universal ion-selective electrode-v. complex formation studies with the cu (ii) selectrode, Talanta 20 (11) (1973) 1105–1115.

[44] O. Yamauchi, Y. Hirano, Y. Nakao, A. Nakahara, Stability of fused rings in metal chelates. vi. structures and stability constants of the copper (ii) chelates of dipeptides containing glycine and/or β-alanine, Canadian Journal of Chemistry 47 (18) (1969) 3441–3445.

[45] O. Yamaughi, H. Miyata, A. Nakahara, The stability of fused rings in metal chelates. viii. solution equilibria of the copper (ii) complexes of glycinamide and related compounds, Bulletin of the Chemical Society of Japan 44 (10) (1971) 2716–2721.

[46] H. Sigel, R. Griesser, Ternäre komplexe in lösung ii. einfluss von 2, 2-bipyridyl auf die stabilität des cu2+-glycin-1: 1-komplexes, Helvetica chimica acta 50 (7) (1967) 1842–1845.

[47] R. Martin, R. Paris, Variation, en fonction de la force ionique, des constantes de stability des chelates simples et mixtes du cuivre avec la glycine et l'alanine, CR Acad. Sci.(Paris) 258 (1964) 3038.

[48] R.-P. Martin, L. Mosoni, B. Sarkar, Ternary coordination complexes between glycine, copper (ii), and glycine peptides in aqueous solution, Journal of Biological Chemistry 246 (19) (1971) 5944–5951.

[49] B. James, R. Williams, 383. the oxidation–reduction potentials of some copper complexes, Journal of the Chemical Society (Resumed) (1961) 2007–2019.

[50] S.-i. Ishiguro, T. Pithprecha, H. Ohtaki, Potentiometric and calorimetric studies on formation of glycinato complexes of nickel (ii) in water and in an aqueous dioxane solution, Bulletin of the Chemical Society of Japan 59 (5) (1986) 1487–1491.

[51] O. Enea, G. Berthon, M. Cromer-Morin, J.-P. Scharff, Thermodynamique des complexes metalliques ternaires des amino acides: Etude du systeme ni (ii)-glycine-dl-α-alanine, Thermochimica Acta 33 (1979) 311–322.

[52] P. Daniele, G. Ostacoli, P. Amico Caldoro, et al., Mixed complexes formed in aqueous solution by nickel (ii) ion with 2, 2'-dipyridyl and glycine, sarcosine and beta-alanine., Annali Di Chimica 66 (1976) 127–138.

[53] P. Daniele, G. Ostacoli, et al., Mixed complexes of copper (ii) with ligand pairs formed by glycine, sarcosine and dl-threonine in aqueous solution, Annali di Chimica 67 (1977) 311–320.

[54] G. Nancollas, M. Lim, Thermodynamics of ion association. xxii. nickel complexes of glycine, diglycine, triglycine, and glycyl-. gamma.-aminobutyric acid, Inorganic Chemistry 10 (9) (1971) 1957–1961.

[55] Y. Z. Hamada, N. Makoni, H. Hamada, Copper complex with the simplest amino acid glycine, Nanomedicine Research.

[56] G. Faraglia, F. Rossotti, H. Rossotti, Potentiometric studies in mixed solvents, ii complexes of nickel (ii), copper (ii) and zinc (ii) with pyridine, ethylenediamine and glycine, Inorganica Chimica Acta 4 (1970) 488–492.

[57] M. Chidambaram, P. Bhattacharya, Amino acid chelates, i, I., J. Indian Chem. Soc 47 (1970) 881–882.

[58] M. Chidambaram, P. Bhattacharya, Studies in amine-amino acid mixed ligand chelates-i, Journal of Inorganic and Nuclear Chemistry 32 (10) (1970) 3271–3275.

[59] K. P. Anderson, W. O. Greenhalgh, R. M. Izatt, Formation constants and enthalpy and entropy values for the association of h+ and cu2+ with glycinate and phenylalanate ions in aqueous solution at 10, 25, and 40, Inorganic Chemistry 5 (12) (1966) 2106–2109.

[60] K. P. Anderson, W. O. Greenhalgh, E. A. Butler, Formation constant, enthalpy, and entropy values for the association of nickel (ii) ion with glycinate, alanate, and phenylalanate ions at 10, 25, and 40. degree., Inorganic Chemistry 6 (5) (1967) 1056–1058.

[61] D. Leussing, E. Hanna, Metal ion catalysis in transamination. iii. nickel (ii) and zinc (ii) mixed complexes involving pyruvate and various substituted aliphatic amino acids1, Journal of the American Chemical Society 88 (4) (1966) 693–696.

[62] V. Sharma, H. Mathur, Thermodynamic properties of coordination complexes of transition metal ions with amino acids, Indian Journal Of Chemistry 3 (11) (1965) 475.

[63] S. Lotfi, A. M. Mazloum, J. B. Ghasemi, Potentiometeric study of protonation and complex formation of some amino acids with zn (ii), co (ii) and ni (ii) in aqueous solution, Journal of the Iranian Chemical Research.

[64] I. Sovago, A. Gergely, J. Posta, Equilibria of alfa-amino acid complexes of transition metal ions vii. effect of the aliphatic carbon ni (ii)-amino acid complexes, Acta Chim. Acad. Sci. Hung 85 (1975) 153–159.

[65] I. Sóvágó, A. Gergely, Factors influencing the formation of mixed ligand complexes of nickel (ii) and zinc (ii), Inorganica Chimica Acta 37 (1979) 233–236.

[66] R. Griesser, H. Sigel, Ternary complexes in solution. xi. complex formation between the cobalt (ii)-, nickel (ii)-, copper (ii)-, and zinc (ii)-2, 2'-bipyridyl 1: 1 complexes and ethylenediamine, glycinate, or pyrocatecholate, Inorganic Chemistry 10 (10) (1971) 2229–2232.

[67] A. Gergely, I. Nagypal, J. Mojzes, A new method for calculation of stability constants, Acta Chimica Academiae Scientarium Hungaricae 51 (4) (1967) 381.

[68] A. Gergely, I. Nagypal, I. Sovago, Equilibria of alpha-amino-acid complexes of transition-metal ions. 3. calorimetric determination of enthalpies and entropies of formation of some amino-acid complexes, Acta Chimica Academiae Scientarium Hungaricae 67 (3) (1971) 241.

[69] A. Gergely, I. Sovago, I. Nagypaál, R. Kiraly, Equilibrium relations of alpha-aminoacid mixed complexes of transition metal ions, Inorganica Chimica Acta 6 (1972) 435–439.

[70] A. Gergely, I. Sóvágó, Log β, δh and δs values of mixed complexes of cu (ii) with histamine and some aliphatic aminoacids, Journal of Inorganic and Nuclear Chemistry 35 (12) (1973) 4355–4365.

[71] J. Brannan, H. Dunsmore, G. Nancollas, 51. thermodynamics of ion association. part xi. some transition-metal glycine salts, Journal of the Chemical Society (Resumed) (1964) 304–310.

[72] A. E. Angkawijaya, A. E. Fazary, S. Ismadji, Y.-H. Ju, Cu (ii), co (ii), and ni (ii)–antioxidative phenolate–glycine peptide systems: an insight into its equilibrium solution study, Journal of Chemical & Engineering Data 57 (12) (2012) 3443–3451.

[73] J. L. d. Miranda, J. Felcman, Study on guanidino–carboxylate interactions in copper (ii) ternary complexes of guanidinoacetic acid with glutamic and aspartic acids, Polyhedron 22 (2) (2003) 225–233.

[74] J. Fan, X. Shen, J. Wang, Determination of stability constants of copper (ii)-glycine complex in mixed solvents by copper (ii)-selective electrode, Electroanalysis 13 (13) (2001) 1115–1118.

[75] M. M. Khalil, A. E. Attia, Potentiometric studies on the binary and ternary complexes of copper (ii) containing dipicolinic acid and amino acids, Journal of Chemical & Engineering Data 44 (2) (1999) 180–184.

[76] F. Basolo, Y. T. Chen, Steric effects and the stability of complex compounds. iii. the chelating tendencies of n-alkylglycines and n-dialkylglycines with copper (ii) and nickel (ii) ions1, Journal of the American Chemical Society 76 (4) (1954) 953–955.

[77] D. Mellor, H. McKenzie, The polarography of glycine metal complexes and the determination of stepwise formation constants, Australian Journal of Chemistry 14 (4) (1961) 562–576.

[78] H. Laitinen, E. Onstott, J. Bailar, S. Swann, Polarography of copper complexes. i. ethylenediamine, propylenediamine, diethylenetriamine and glycine complexes, Journal of the American Chemical Society 71 (5) (1949) 1550–1552.

[79] W. Evans, C. Monk, Electrolytes in solutions of amino acids. part 6.-dissociation constants of some triglycinates by emf and ph measurements, Transactions of the Faraday Society 51 (1955) 1244–1250.

[80] C. Monk, Electrolytes in solutions of amino acids. part iv.-dissociation constants of metal complexes of glycine, alanine and glycyl-glycine from ph titrations, Transactions of the Faraday Society 47 (1951) 297–302.

[81] N. C. Li, E. Doody, Metal-amino acid complexes. ii. polarographic and potentiometric studies on complex formation between copper (ii) and amino acid ion1, 2, Journal of the American Chemical Society 74 (16) (1952) 4184–4188.

[82] N. C. Li, J. M. White, R. L. Yoest, Some metal complexes of glycine and valine1, Journal of the American Chemical Society 78 (20) (1956) 5218–5222.

[83] H. Irving, H. Rossotti, 680. methods for computing successive stability constants from experimental formation curves, Journal of the Chemical Society (Resumed) (1953) 3397–3405.

[84] H. Irving, R. Williams, D. Ferrett, A. Williams, The influence of ring size upon the stability of metal chelates, Journal of the Chemical Society (Resumed) (1954) 3494–3504.

[85] R. Keefer, Polarographic determination of cupric glycinate and cupric alaninate complex ions, Journal of the American Chemical Society 68 (11) (1946) 2329–2331.

[86] H. L. Riley, V. Gallafent, Cclxxiv.-studies in complex salts. part iv. the effect of alkyl substitution on the tendency of the aminoacetate ion to co-ordinate with copper, Journal of the Chemical Society (Resumed) (1931) 2029–2034.

[87] D. D. Perrin, Stability constants of metal-ion complexes: organic ligands, no. 22, Pergamon, 1979.

[88] E. Bottari, C. Severini, Amino-acids as ligands: the system lead (ii)-aminoacetate, Journal of Coordination Chemistry 8 (2) (1978) 69–74.

[89] A. Brunetti, M. Lim, G. Nancollas, Thermodynamics of ion association. xvii. copper complexes of diglycine and triglycine, Journal of the American Chemical Society 90 (19) (1968) 5120–5126.

[90] L. Davis, F. Roddy, D. E. Metzler, Metal chelates of imines derived from pyridoxal and amino acids1, Journal of the American Chemical Society 83 (1) (1961) 127–134.

[91] L. Maley, D. Mellor, The relative stability of internal metal complexes. ii. metal derivatives of 8-hydroxyquinoline 5-sulphonic acid and a series of monocarboxylic mono-α-amino acids including histidine, Australian Journal of Chemistry 2 (4) (1949) 579–594.

[92] Z. M. Anwar, H. A. Azab, Ternary complexes in solution. comparison of the coordination tendency of some biologically important zwitterionic buffers toward the binary complexes of some transition metal ions and some amino acids, Journal of Chemical & Engineering Data 44 (6) (1999) 1151–1157.

[93] K. Micskei, F. Debreczeni, I. Nagypál, Equilibria in aqueous solutions of some chromium (2+) complexes, Journal of the Chemical Society, Dalton Transactions (1983) 1335–1338.

[94] K. Micskei, Equilibria in aqueous solutions of some iron (ii) complexes, Journal of the Chemical Society, Dalton Transactions (1987) 255–257.

[95] M. Israeli, L. Pettit, Complex formation between unsaturated α-aminoacids and silver (i) and some divalent transition metal ions, Journal of Inorganic and Nuclear Chemistry 37 (4) (1975) 999–1003.

[96] D. Leussing, D. Shultz, Metal ion catalysis in transamination. ii. pyruvate-glycinate equilibrium systems with some divalent metal ions, Journal of the American Chemical Society 86 (22) (1964) 4846–4850.

[97] D. L. Leussing, K. S. Bai, N-salicylideneglycinato complexes. comparison with pyridoxal, Analytical Chemistry 40 (3) (1968) 575–581.

[98] K.-K. Mui, W. McBryde, E. Nieboer, The stability of some metal complexes in mixed solvents, Canadian Journal of Chemistry 52 (10) (1974) 1821–1833.

[99] R. M. Izatt, H. D. Johnson, J. J. Christensen, Log k, $\delta\ h^o$, and $\delta\ s^o$ values for the interaction of glycinate ion with h^+, mn^{2+}, fe^{2+}, co^{2+}, ni^{2+}, cu^{2+}, zn^{2+}, and cd^{2+} at

10, 25, and 40 ^{o}, Journal of the Chemical Society, Dalton Transactions 3 (11) (1972) 1152–1157.

[100] D. Hopgood, D. Leussing, Kinetic and equilibrium studies of formation of n-salicylidene-glycinato complexes. the promnastic [matchmaker] effect of the divalent ions of magnesium, manganese, zinc, cadmium, and lead, Journal of the American Chemical Society 91 (14) (1969) 3740–3750.

[101] R. Gillard, Stereoselectivity and reactivity in complexes of amino-acids and peptides, Inorganica Chimica Acta Reviews 1 (1967) 69–86.

[102] R. Münze, A. Güthert, H. Matthes, Potentiometrische bestimmung von komplexkonstanten einiger aminosäuren mit cd++, Zeitschrift für Physikalische Chemie 241 (1) (1969) 240–243.

[103] D. Perkins, A study of some simple peptide complexes with zinc and cadmium ions in aqueous solution, Biochemical Journal 57 (4) (1954) 702.

[104] V. Mundra, G. Rao, C. Murthy, Polarography of mixed ligand complexes of cadmium (ll) containing ethylenediamine and amino acids, Polish Journal of Chemistry 58 (1-6) (1984) 53.

[105] H. Matsui, H. Ohtaki, A potentiometric study on mixed ligand cadmium (ii) complexes with 2-amino carboxylic acids, Bulletin of the Chemical Society of Japan 55 (2) (1982) 461–465.

[106] H. Matsui, Determination of the stability constants of the complexes of cd (ii) ion with α-amino acids, Journal of Inorganic and Nuclear Chemistry 43 (9) (1981) 2187–2189.

[107] V. Nikitenko, K. Litovchenko, V. Kublanovskij, Chronopotentiometric determination of stability of cadmium (2) complexes with glycine, Zhurnal Neorganicheskoj Khimii 24 (3) (1979) 662–665.

[108] G. B. Gavioli, L. Benedetti, G. Grandi, G. Marcotrigiano, G. Pellacani, M. Tonelli, Comparison of the pologràphic behavior of the cd^{2+}-glycine, n-acetyl-and n-benzoyl-glycine systems in aqueous and ethanolic solution, Inorganica Chimica Acta 37 (1979) 5–9.

[109] G. Heijne, W. Van der Linden, Determination of stability constants of cadmium (ii) with some amino-acids by use of an ion-selective electrode, Talanta 22 (10-11) (1975) 923–925.

[110] J. H. Smith, A. M. Cruickshank, J. T. Donoghue, J. F. Pysz Jr, A polarographic study of cadmium (ii)-amino acid complexes, Inorganic Chemistry 1 (1) (1962) 148–150.

[111] N. Vlasova, N. Davidenko, Heteroligand complexes of magnesium (ii) and manganese (ii) with anions of orotic-acid and amino-acid, Zhurnal Neorganicheskoi Khimii 30 (7) (1985) 1738–1744.

[112] G. Reinhard, R. Dreyer, R. Münze, Thermodynamische funktionen der komplexbildung von 3 d-metallen und aminosäuren, Zeitschrift für Physikalische Chemie 254 (1) (1973) 226–236.

[113] W. Felty, C. Ekstrom, D. Leussing, Equilibrium studies involving schiff base complexes. the zinc (ii)-pyridoxal phosphate-glycine and-. alpha.-alanine systems, Journal of the American Chemical Society 92 (10) (1970) 3006–3011.

[114] P. Daniele, G. Ostacoli, V. Zelano, et al., Mixed complexes of zinc (2+) ion with 2, 2-dipyridyl and glycine or sarcosine in aqueous solution., Annali Di Chimica 65 (1975) 455–463.

[115] N. C. Li, R. A. Manning, Some metal complexes of sulfur-containing amino acids1, 2, Journal of the American Chemical Society 77 (20) (1955) 5225–5228.

[116] E. Martell, Chemistry of the metal chelate compounds, Prentice-hall Chemistry Series.

[117] H. Kroll, Manganous complexes of several amino acids1, Journal of the American Chemical Society 74 (8) (1952) 2034–2036.

[118] H. Ohtaki, M. Zama, H. Koyama, S.-i. Ishiguro, A potentiometric study on complex formation of silver (i) ion with glycine and β-alanine in aqueous solution, Bulletin of the Chemical Society of Japan 53 (10) (1980) 2865–2867.

[119] G. Thiers, L. Van Poucke, M. Herman, Ag (i) complexes of some ω-aminocarboxylic acids, Journal of Inorganic and Nuclear Chemistry 30 (6) (1968) 1543–1552.

[120] S. Datta, A. Grzybowski, 222. the stability constants of the silver complexes of some aliphatic amines and amino-acids, Journal of the Chemical Society (Resumed) (1959) 1091–1095.

[121] R. Keefer, H. Reiber, Interaction of ions and dipolar ions. iii. solubility of thallous salts in glycine and in alanine solutions, Journal of the American Chemical Society 63 (12) (1941) 3504–3507.

[122] V. Isaeva, V. Naumov, Z. F. Gesse, V. Sharnin, Complex formation of silver (i) with glycinate ion in aqueous ethanol and dimethyl sulfoxide solutions, Russian Journal of Coordination Chemistry 34 (8) (2008) 624–628.

[123] H. Matsukawa, M. Ohta, S. Takata, R. Tsuchiya, The formation constants of chromium (iii)-glycinato and α-alaninato complexes, Bulletin of the Chemical Society of Japan 38 (8) (1965) 1235–1239.

[124] A. Khan, W. U. Malik, Current sci.(india), 29 (1960) 135, J. Indian Chem. Soc 40 (1963) 565.

[125] Y. Fukuda, E. Kyuno, R. Tsuchiya, Formation constants of chromium (ii) complexes with (o, o)-,(o, n)-and (n, n)-type ligands and comparison with those of the other first transition metal complexes, Bulletin of the Chemical Society of Japan 43 (3) (1970) 745–749.

[126] R. S. Reid, B. Podányi, A proton nmr study of the glycine-mercury (ii) system in aqueous solution, Journal of inorganic biochemistry 32 (3) (1988) 183–195.

[127] H. Flood, V. Lorzs, Tids. tcjemi, berg (1945).

[128] M. Maeda, M. Tsunoda, Y. Kinjo, Coordination of mercury (ii) to amino acids under physiological conditions, Journal of inorganic biochemistry 48 (3) (1992) 227–232.

[129] D. Perkins, A study of the amino-acid complexes formed by metals of group ii of the periodic classification, Biochemical Journal 51 (4) (1952) 487.

[130] O. Farooq, N. Ahmad, Stability and binding of au (iii) to certain amino acids using sodium chloroaurate, Journal of Electroanalytical Chemistry and Interfacial Electrochemistry 53 (3) (1974) 457–460.

[131] Y. He, M. Luo, X. Zhang, J. Meng, Determination of stability constants of complexes of cu2+ and cu+ with glycine using zero current potentiometry through electrogenerating copper ions, Electrochimica Acta 165 (2015) 416–421.

[132] M. Maeda, Y. Tanaka, G. Nakagawa, Potentiometric investigation of complex formation of lead (ii) with glycine and dl-alanine, Journal of Inorganic and Nuclear Chemistry 41 (5) (1979) 705–709.

[133] J. Berggren, O. Bortin, S. Gobom, A potentiometric study on the complex-formation of the lead (ii)-glycine system, Acta chemica scandinavica. Series A. Physical and inorganic chemistry 42 (10) (1988) 685–690.

[134] A. M. Corrie, G. K. Makar, M. L. Touche, D. R. Williams, Thermodynamic considerations in co-ordination. part xx. a computerised approach as an alternative to graphical normalised curve fitting as a means of detecting oligonuclear complexes in metal ion–ligand solutions and its application to the zinc (ii)–, lead (ii)–, and proton–glycine peptide systems, Journal of the Chemical Society, Dalton Transactions (1975) 105–110.

[135] A. M. Corrie, D. R. Williams, Thermodynamic considerations in co-ordination. part xxiv. gibbs free-energy changes, enthalpies, and entropies of formation of complexes of glycinate, glycylglycinate, glycylglycylglycinate, cysteinate, and glutathionate with hydrogen and lead (ii) ions and suggested aqueous structures, Journal of the Chemical Society, Dalton Transactions (1976) 1068–1072.

[136] M. C. Dos Santos, M. S. Gonçalves, Electroanalytical chemistry of copper, lead and zinc complexes of amino acids at the ionic strength of seawater (0.70 m naclo4 part iii, Journal of Electroanalytical Chemistry and Interfacial Electrochemistry 208 (1) (1986) 137–152.

[137] R. Diezcaballero, J. A. Valentin, A. A. Garcia, P. S. Batanero, Potentiometric determination of stability-constants binary and ternary complexes of zn (ii) and pb (ii), Bulletin De La Societe Chimique De France (1985) 688–694.

[138] Y. Khayat, M. Cromer-Morin, J.-P. Scharff, Stability constants for lead (ii) complexes of glycine, serine, aspartic acid and glycyl-l-leucine, Journal of Inorganic and Nuclear Chemistry 41 (10) (1979) 1496–1498.

[139] D. Michel, J. Frenay, Integration of amino acids in the thiosulfate gold leaching process, in: Randol Glod & Silver Forum, 1999, pp. 99–103.

[140] I. V. Mironov, Stability of gold (i) glycinate complexes in aqueous solution, Russian Journal of Inorganic Chemistry 52 (5) (2007) 791–792.

[141] A. Casale, A. De Robertis, C. De Stefano, A. Gianguzza, G. Patanè, C. Rigano, S. Sammartano, Thermodynamic parameters for the formation of glycine complexes with magnesium (ii), calcium (ii), lead (ii), manganese (ii), cobalt (ii), nickel (ii), zinc (ii) and cadmium (ii) at different temperatures and ionic strengths, with particular reference to natural fluid conditions, Thermochimica acta 255 (1995) 109–141.

[142] C. De Stefano, S. Sammartano, A. Gianguzza, Mixed proton complexes of aminoacids and carboxylic ligands in aqueous solution, Talanta 40 (5) (1993) 629–635.

[143] V. U. F.J. Kulba, Z. J.B. Jakovlev, Zhurnal Neorganicheskoi Khimii 19 (1974) 1758.

[144] L. Alderighi, P. Gans, S. Midollini, A. Vacca, Co-ordination chemistry of the methylmercury (ii) ion in aqueous solution: a thermodynamic investigation, Inorganica chimica acta 356 (2003) 8–18.

[145] D. L. Rabenstein, R. Ozubko, S. Libich, C. A. Evans, M. T. Fairhurst, C. Suvanprakorn, Nuclear magnetic resonance studies of the solution chemistry of metal complexes. x. determination of the formation constants of the methylmercury complexes of selected amines and aminocarboxylic acids, Journal of Coordination Chemistry 3 (4) (1974) 263–271.

[146] M. Jawaid, F. Ingman, D. Liem, Studies on the hydrolysis of methylmercury (ii) and its complex formation with some aliphatic carboxylic and aminocarboxylic acids, Acta Chem. Scand. A 32 (1978) 333–343.

[147] G. Anderegg, The stability of iron (iii) complexes formed below ph= 3 with glycinate, iminodiacetate, β-hydroxyethyliminodiacetate, n, n-di-(hydroxyethyl)-glycinate, nitrilotriacetate and triethanolamine, Inorganica chimica acta 121 (2) (1986) 229–231.

[148] P. Bianco, J. Haladjian, R. Pilard, Complexation du gallium par la glycine ou l'isoleucine, Journal of the Less Common Metals 42 (1) (1975) 127–135.

[149] J. Schubert, A. Lindenbaum, Stability of alkaline earth-organic acid complexes measured by ion exchange1, Journal of the American Chemical Society 74 (14) (1952) 3529–3532.

[150] C. Colman-Porter, C. Monk, 836. dissociation constants of the alkaline-earth salts of some monocarboxylic acids, Journal of the Chemical Society (Resumed) (1952) 4363–4368.

[151] S. N. Limaye, M. C. Saxena, Relative complexing tendencies of o-o, o-n, and o-s donor (secondary) ligands in some lanthanide-edta mixed-ligand complexes, Canadian journal of chemistry 64 (5) (1986) 865–870.

[152] Y. Inoue, O. Tochiyama, Study of the complexes of np (v) with organic ligands by solvent extraction with tta and 1, 10-phenanthroline, Polyhedron 2 (7) (1983) 627–630.

[153] J. P. Amend, H. C. Helgeson, Calculation of the standard molal thermodynamic properties of aqueous biomolecules at elevated temperatures and pressures part 1l-α-amino acids, Journal of the Chemical Society, Faraday Transactions 93 (10) (1997) 1927–1941.

[154] J. M. Dick, D. E. LaRowe, H. C. Helgeson, Temperature, pressure, and electrochemical constraints on protein speciation: Group additivity calculation of the standard molal thermodynamic properties of ionized unfolded proteins, Biogeosciences 3 (3) (2006) 311–336.

[155] D. E. LaRowe, P. Van Cappellen, Degradation of natural organic matter: a thermodynamic analysis, Geochimica et Cosmochimica Acta 75 (8) (2011) 2030–2042.

[156] E. L. Shock, D. C. Sassani, M. Willis, D. A. Sverjensky, Inorganic species in geologic fluids: correlations among standard molal thermodynamic properties of aqueous ions and hydroxide complexes, Geochimica et Cosmochimica Acta 61 (5) (1997) 907–950.

[157] J. P. Amend, T. M. McCollom, Energetics of biomolecule synthesis on early earth, in: Chemical Evolution II: From the Origins of Life to Modern Society, ACS Publications, 2009, Ch. 4, pp. 63–94.

[158] E. L. Shock, M. D. Schulte, Organic synthesis during fluid mixing in hydrothermal systems, Journal of Geophysical Research: Planets 103 (E12) (1998) 28513–28527.

[159] E. L. Shock, Stability of peptides in high-temperature aqueous solutions, Geochimica et Cosmochimica Acta 56 (9) (1992) 3481–3491.

[160] E. H. Oelkers, H. C. Helgeson, E. L. Shock, D. A. Sverjensky, J. W. Johnson, V. A. Pokrovskii, Summary of the apparent standard partial molal gibbs free energies of formation of aqueous species, minerals, and gases at pressures 1 to 5000 bars and temperatures 25 to 1000 c, Journal of Physical and Chemical Reference Data 24 (4) (1995) 1401–1560.

[161] N. Kitadai, Thermodynamic prediction of glycine polymerization as a function of temperature and ph consistent with experimentally obtained results, Journal of molecular evolution 78 (3-4) (2014) 171–187.

[162] P. Kebarle, Gas-phase ion equilibria and ion solvation, in: Modern Aspects of Electrochemistry, Springer, 1974, pp. 1–46.

[163] C. Murphy, A. Martell, Metal chelates of glycine and glycine peptides, Journal of Biological Chemistry 226 (1) (1957) 037–050.

[164] H. Stünzi, D. Perrin, Stability constants of metal complexes of phosphonoacetic acid, Journal of Inorganic Biochemistry 10 (4) (1979) 309–316.

[165] R. M. Izatt, J. J. Christensen, V. Kothari, Acid dissociation constant, formation constant, enthalpy, and entropy values for some copper (ii)-α-amino acid systems in aqueous solution, Inorganic Chemistry 3 (11) (1964) 1565–1567.

[166] M. S. El-Ezaby, H. M. Marafie, S. Fareed, Complexes of vitamin b6, part vii: Ternary complexes of cobalt (ii), nickel (ii), and copper (ii) involving pyridoxamine and some amino acids, Journal of Inorganic Biochemistry 11 (4) (1979) 317–326.

[167] V. Ramanujam, V. Selvarajan, Equilibrium studies on the formation of mixed-ligand complexes in solution. 3., Journal of the Indian Chemical Society 58 (12) (1981) 125–128, 1131–1134.

[168] M. Padmavathi, S. Satyanarayana, Potentiometric and proton nmr studies on ternary metal (ii) complexes containing thiaminepyrophosphate and a series of secondary ligands.

[169] H. Yadava, S. Singh, P. Prasad, R. Singh, P. Yadava, K. Yadava, Bulletin de la Societe Chimique de France (1984) I–314.

[170] A. Albert, Quantitative studies of the avidity of naturally occurring substances for trace metals. 2. amino-acids having three ionizing groups, Biochemical Journal 50 (5) (1952) 690.

[171] A. Albert, Quantitative studies on the avidity of naturally occurring substances for trace metals. 1. amino-acids having only two ionizing groups, Biochemical Journal 47 (5) (1950) 531.

[172] A. Weiss, S. Fallab, Das komplexbildungsvermögen von acylierten aminosäuren, Helvetica Chimica Acta 40 (3) (1957) 576–579.

[173] V. Jokl, Studium der komplexverbindungen in lösung mittels papierelektrophorese: Ii. elektrophoretische beweglichkeit und stabilität der einkernigen komplexe, Journal of Chromatography A 14 (1964) 71–78.

[174] S. Jain, J. Kishan, R. Kapoor, Polarographic study of mixed-ligand complexes-cadmium-glycinate-bicinate system, Indian Journal Of Chemistry Section A-inorganic Bio-inorganic Physical Theoretical & Analytical Chemistry 18 (2) (1979) 133–135.

[175] Abd-El-Nabey, B. A, El-Ezaby, M. S, Complexes of vitamin b6-iv: Polarographic determination of the stability constants of the mixed-ligand complexes of cadmium (ii) with amino acids and pyridoxamine, Journal of Inorganic and Nuclear Chemistry 40 (4) (1978) 739–744.

[176] C. P. S. Chandel, C. M. Gupta, Mixed chelates of cadmium (ii) with n-(2-hydroxyethyl) ethylenediamine and some amino acids, Bulletin of the Chemical Society of Japan 57 (8) (1984) 2303–2306.

[177] G. Sycheva, A. Y. Fridman, Y. A. Afanas' ev, Formation of certain mixed cadmium complexes, Koordinatsionnaya Khimiya 3 (8) (1977) 1161–1163.

[178] D. Reddy, B. Sethuram, T. Rao, Physicochemical studies of ternary chelates in solution. 2. stability-constants of ternary chelates of cu (ii), ni (ii), zn (ii), cd (ii), co (ii) and mn (ii) with 2, 2'-bipyridyl as primary ligand and 2-phenylacetohydroxamic acid as secondary ligand, Indian Journal Of Chemistry Section A-inorganic Bio-inorganic Physical Theoretical & Analytical Chemistry 15 (4) (1977) 333–336.

Chapter 3

Microfluidic study of sustainable gold leaching using a glycine solution

ABSTRACT

The purpose of this paper is to investigate the in-situ leaching of gold using a microfluidic system with controlled flow, temperature and fluid composition. The microfluidic system is a microchannel embedding a nano-scale layer of gold over which the fluid can flow and etch (erode) gold at various temperatures and concentrations of lixiviant. The lixiviant in this case is an alkaline glycine system that has been identified as an environmentally friendly substance to dissolve precious metals, it is used to extract gold within the engineered micro-cavity. As the fluid flows in the microchannel, the thickness of the gold layer is monitored to control its reduction with respect to time and space. The experimental conditions were varied to evaluate their effects on the recovery rate. The results show that compared to traditional methods being used in laboratory testing, this technique can provide real time measurements with low consumption of chemicals and the results can be obtained in shorter periods of time.

3.1 Introduction

Microelectronics technology has been developing over more than 60 years and has produced valuable devices for a broad range of applications [1–5]. In particular, microfluidic systems have been instrumental in biochemistry and microbiology and have helped characterising the chemical and physical mechanisms that occur at the micro-scale [6–9]. As they can be used to manipulate small amounts of fluids in micro-scale channels [10], microfluidic systems have been used to extract some metals such as Ag [11], Cu/Cr [12–14], Co [15], Pt [16], Pd [17], and rare earth elements [18, 19].

In hydrometallurgy, leaching is the main stage of mineral processing and often has significant effects on subsequent steps [20, 21]. Many studies have been conducted on metal dissolution in order to understand the behaviour of leachates and lixiviants, identify the kinetic parameters, and optimize the overall efficiency of hydrometallurgical operations [21].

Recently, [22] conducted a pioneering experimental study on gold leaching by amonium thiosulfate using microchannels and monitored the etching rate of gold in real time under controlled conditions. In comparison with traditional leaching experiments, this new technique offers a visual and quantitative monitoring in a confined space with under controlled laminar flow rates. [22] conducted their experiment using a high aspect ratio microchannel to mimic a crack in a mineralised sample. In the current paper, we upgrade the design by including a temperature controlled system and we use alkaline glycine solutions instead of amonium thiosulfate. The flow rate can vary based on the joint aperture and the flow is assumed to be analogous and laminar between two highly smooth parallel plates. However, as real surfaces are not necessarily smooth or parallel enough and they converge abruptly at their ends, turbulent flow may also occur [23, 24]. In this work, the flow is laminar within the range of fluid velocities imposed in the micro-channel, size of the aperture and physical properties of the water-glycine system. We present a visual and quantitative analysis of gold leaching by alkaline glycine in confined and high aspect ratio channels under controlled fluid flow rates, pH and temperature.

3.2 Materials and methods

3.2.1 Microchannel preparation

The microchannel preparation has been conducted at the Western Australian Centre for Semiconductor Optoelectronics and Microsystems (WACSOM) at The University of Western Australia. The WACSOM fabrication facility is a cleanroom environment that has a low level of environmental pollutants such as dust, airborne microbes, aerosol particles and chemical vapors. In this study, we used a transparent and colourless poly(methyl-methacrylate)(PMMA) material to make the substrate/chip. A groove was included in the chip to represent the microchannel and PMMA cover sheets were used to confine the flow. The PMMA sheets—purchased from Goodfellow (UK)—were cut to fit the chip size (150×150×2mm). PMMA has good abrasion and UV resistance and excellent optical clarity. It is inert to the chemicals used in this study and to the heat applied in the preparation process. PMMA characteristics have been examined and discussed in numerous studies [25–28]. Inlet and outlet holes (1.6mm) were drilled in the chip to circulate the fluid. The distance between two holes has been adjusted with respect to the channel size (4mm×40mm). To avoid scratching the surface after removing the plastic cover, a small tong was used to carry the substrate all the time. The substrate was washed with running water, dried by air and checked under microscope for any dirts.

Fig. 3.1 shows a schematic representation of the microchannel preparation process. For the first step of fabrication, the substrate needed to be covered by photoresist to avoid etching outside the channel area. For this purpose, the photoresist AZ 4562 was selected. The substrate was placed in a spinning machine, covered with photoresist and allowed to spin for about 40 seconds at an angular speed of 2000 rpm. The substrate was then placed on a hot plate (90^{o}C) for 120 mins to bake the layer of photoresist (8.8μm). Using a mask, only the channel area was exposed to UV light for 1 min and washed up with the developer photoresist AZ 340. The substrate was then scanned under the microscope to make sure no photoresist was left in the channel area. To built a channel on the substrate,

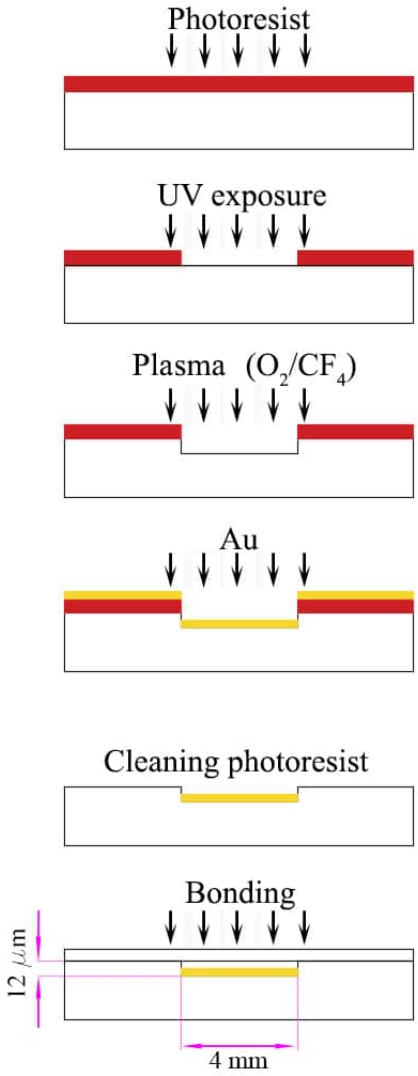

Figure 3.1: Schematic process of microchannel parapration steps. Oxygen plasma machine was used to etch the PMMA substarte to make the channel. Photoresist was used to protect the surface of PMMA rather than the channel area. Au (60nm) was caoted on the channel using thermal evaporation techniques. The UV glue was applied to bond two substrates.

we used an oxygen plasma machine (Plasma100) and a practical recipe (60% O_2 and 5% CF_4) to etch the surface of the PMMA substrate (12μm). Thermal evaporation was used to deposit a layer of 5nm Cr (for adherence between substrate and gold) and a layer of 60nm of gold on the channel. Thermal evaporation is a the physical vapor deposition (PVD) technique in which the metal is heated in a vacuum chamber until its surface atoms have sufficient energy to leave the surface. At this point they will traverse the vacuum chamber, at thermal energy (less than 1 eV), and coat on the substrate positioned above the chamber.

The rest of the photoresist was then cleaned up from the substrate with the developer AZ 340. The final step was bonding two PMMA substrates together. There are many different methods to bond two PMMA substrates including thermal bonding, chemical bonding using acetone/ethanol, oxygen plasma activation, pressure bonding and UV assisted bonding [29–36]. Among the above methods, we used UV assisted glue because it was easy to apply manually. In this method, a small amount of glue was applied on the surface and carefully spread on the substrate while care was taken to keep the channel clean of glue. In the next step, two substrates were bonded by applying a load of 1kg while curing by UV exposure. The thickness of the gold layer and the depth of microchannel were checked by profilometer Dektak 150 and high resolution microscope ZYGO 6300.

3.2.2 Choice of lixiviant

In recent years, there have been an increasing interest in studying in-situ leaching (ISL) of gold using non-cyanideation system such as iodine [37–39]. Finding an environmentally friendly chemicals as a replacement for cyanide can make ISL more viable. A considerable number of studies have been conducted on the amino acids (including glycine) and metals reactions [40–46]. The effect of pH and temperature on the solubility of gold in amino acids has been examined by [47]. It has been shown that the presence of hydrogen peroxide can enhance the solubility of gold in amino acids [48]. The effect of adding amino acids to thiosulphate for leaching gold has been evaluated by [49]. These authors found that gold recovery increases as amino acids are added to thiosulphate solutions. The following equations have been suggested by [50] as an example of gold dissolution reactions where the amino acid glycine is a ligand:

$$4Au + 8\,NH_2CH_2COOH + 4NaOH + O_2 = 4Na[Au(NH_2CH_2COO)_2] + 6H_2O \quad (3.1)$$

$$2Au + 4\,NH_2CH_2COOH + 2NaOH + H_2O_2 = 2Na[Au(NH_2CH_2COO)_2] + 4H_2O \quad (3.2)$$

Recently, experimental studies have been carried out to investigate the application of glycine as an eco-friendly lixiviant for gold leaching in alkaline environment with the exposure to hydrogen peroxide [51, 52]. The experimental data suggest that glycine is more effective at pH between 10 and 11 and temperature of 60^oC.

In this study, we evaluate the gold leaching using alkaline-glycine. For this purpose, deionized (DI) water and glycine (ReagentPlus, $\geq$99% HPLC) were used to prepare the solutions. Sodium hydroxide has been used to adjust the pH and hydrogen peroxide has been added to the solution right before exposure with gold. All chemicals have been

Lixiviant no.	Glycine (mole)	H_2O_2 (%)	pH	Temperature ($\pm 2^oC$)	Flow rate (ml/h)
Sample 1	1.0	0.56	11	60	7.0
Sample 2	1.5	0.56	11	60	7.0
Sample 3	1.0	0.56	12	60	7.0
Sample 4	0.5	0.56	10	60	7.0
Sample 5	1.0	0.56	9	60	7.0
Sample 6	1.0	0.40	12	75	7.0
Sample 7	1.2	0.40	12	75	7.0
Sample 8	0.1	0.40	12	75	7.0
Sample 9	0.5	0.40	12	75	7.0

Table 3.1: The list of lixiviant samples used in the experiment at different temperature, pH, glycine and H_2O_2 concentrations.

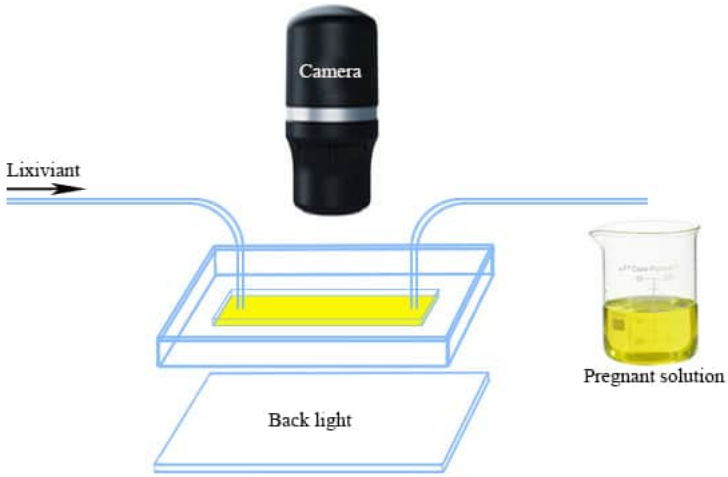

Figure 3.2: Experimental set-up: alkaline glycine solution injected through a microchannel to leach gold. The thickness of the gold layer is monitored by a camera from the top and illuminated with LED backlight under the micochannel.

purchased from Sigma-Aldrich. In this experiment, nine different specimens of aqueous glycine (see Table 3.1) have been examined to evaluate the effect of pH, temperature, and glycine concentration on the leaching process. All sample were prepared using a beaker with a magnetic stirrer on a hot plate. The stirring process lasted for at least 1 hour until a clear solution was obtained. Temperature and pH were regularly checked until stable conditions were reached.

3.2.3 Experiment set-up

Fig. 3.1 is a schematic representation of the experiment in which the aqueous glycine is injected at a rate of 7ml/h through the microchannel (4mm×50mm×12μm) to leach gold from the 60nm gold layer coated in the channel. To keep the temperature constant over the experiment duration, a heating pad was used and temperature was controlled by an infrared thermometer during the experiment process. A white LED backlight was used to illuminate the device and the thickness of the gold layer was monitored using a microscope camera (Digitech) that captures the etching process in real time. Video files were recorded using the MicroCapture software through a 4mm×30mm window.

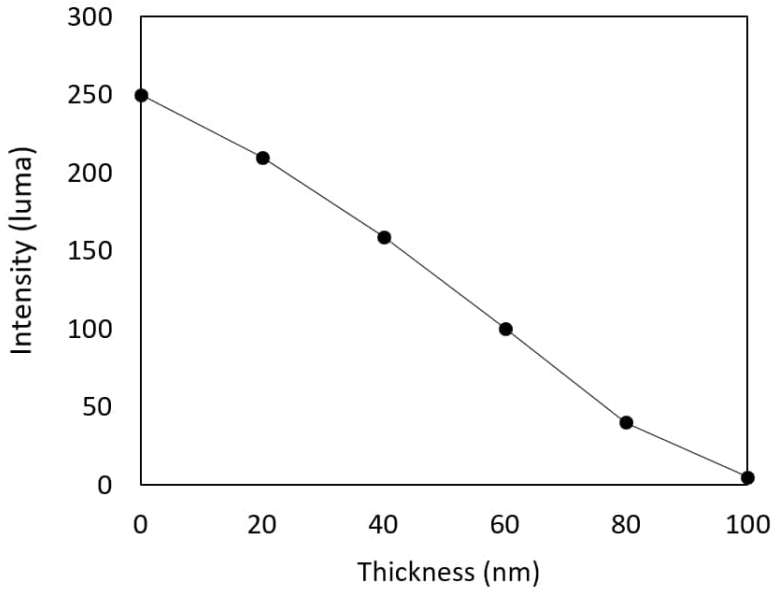

Figure 3.3: Calibration curve of gold thickness versus luminosity.

3.2.4 Method of analysis

The gold layer thickness was monitored by a camera recording video files from the top of the microchannel. The video files were analysed using Video Tracker 5.0.5 in which the brightness (luma) of a point can be tracked over a period of time. Samples with known gold layers thicknesses were prepared and used to calibrate the thickness-luminosity relationship as shown in Fig. 3.3. A thickness of 60nm was selected because it represents the opacity threshold as suggested by [22].

Image analysis was conducted on the three different points, A, B and C shown in Fig. 3.4 to see if the distance from the injection point has an effect on the leaching process. Additional images were processed to analyse the whole area of the micorchannel and examine the fingering patterns that are produced according to the fluid flow pathways.

3.3 Results and discussions

The experiment was conducted with 9 samples (see Table 3.1) to check the effect of temperature, pH and glycine concentration on gold leaching. Fig. 3.5 shows the experimental results of obtained with different leaching conditions. Samples 4, 5 and 8 had the least effects after 12 hours (no changes were observed on the gold thickness to be analyzed). Samples 6 and 7 had the most significant effects on the leaching process; the gold layer thicknesses decreased to zero after 30 mins. In the cases of Samples 1, 3 and 9 the the gold layer thicknesses reduced to zero after 12 hours. As can be seen in Fig. 3.5, the leaching process was more effective at point A that is spatially closer to the injecting point. This could be attributed to the decrease of flow velocity towards the end of the channel. Sample 2 also shows a low leaching rate, although glycine concentration is as high as 1.5 M. This may be explained by the passivated layers of gold dissolution and/or the reduction of the velocity of the flow by crystallization of glycine as the result of high concentration of glycine. Fig. 3.6 shows the solid crystals of glycine that appeared as dark

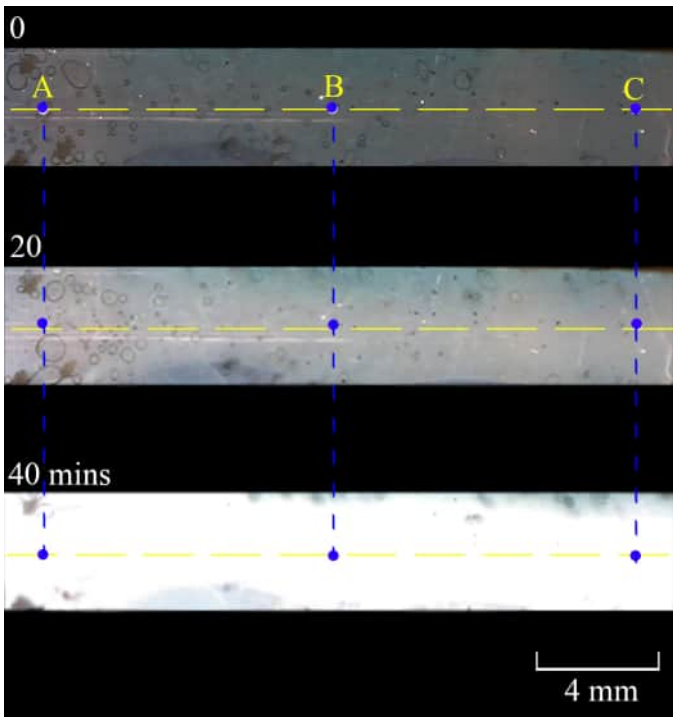

Figure 3.4: Images of gold layers captured after 0, 20 and 40 mins of leaching. The points A, B and C shows the distance from the injecting point. The fluid is injected from left to right with a flow rate 7 ml/h. The lixiviant contains 1M glycine 0.4% H_2O_2, pH 12 and the temperature was controlled at 75±2^{o}C.

stains on the image.

3.3.1 Effect of pH

Glycine can react with metals in different ranges of pH [43]. In aqueous solutions containing amino acids such as glycine, increasing the pH increases the solubility of gold [47, 48, 51]. By comparing the results corresponding to samples 1 , 3 and 5, it can be seen from Fig. 3.6 that increasing pH increases the leaching rate. Fig. 3.7 shows the graph of gold thickness versus time; the gold layer thickness decreases in less time as pH increases. It can be seen that pH beyond 11 can be more effective for recovery using alkaline glycine lixiviant.

3.3.2 Effect of temperature

As it can be seen from Fig. 3.5, Samples 6 and 7 show dramatical increase in the rate of gold dissolution at pH 12 and temperature 75±2^{o}C. Some experimental studies on the solubility of gold in amino acid solutions at different temperatures have been conducted by [47], which have shown the maximum solubility of gold is produced at 80^{o}C. The effect of temperature on the gold leaching in alkaline glycine solutions have been experimentally studied by [51] who conducted beaker-scale experiments over periods of time up to 48 h. Their results indicate that the gold dissolution increases dramatically as temperature increases. Comparing the outputs of Samples 3 and 9 (see Fig. 3.5), it can be seen that the recovery rates are close although the temperatures are 60^{o}C and 75^{o}C, respectively while

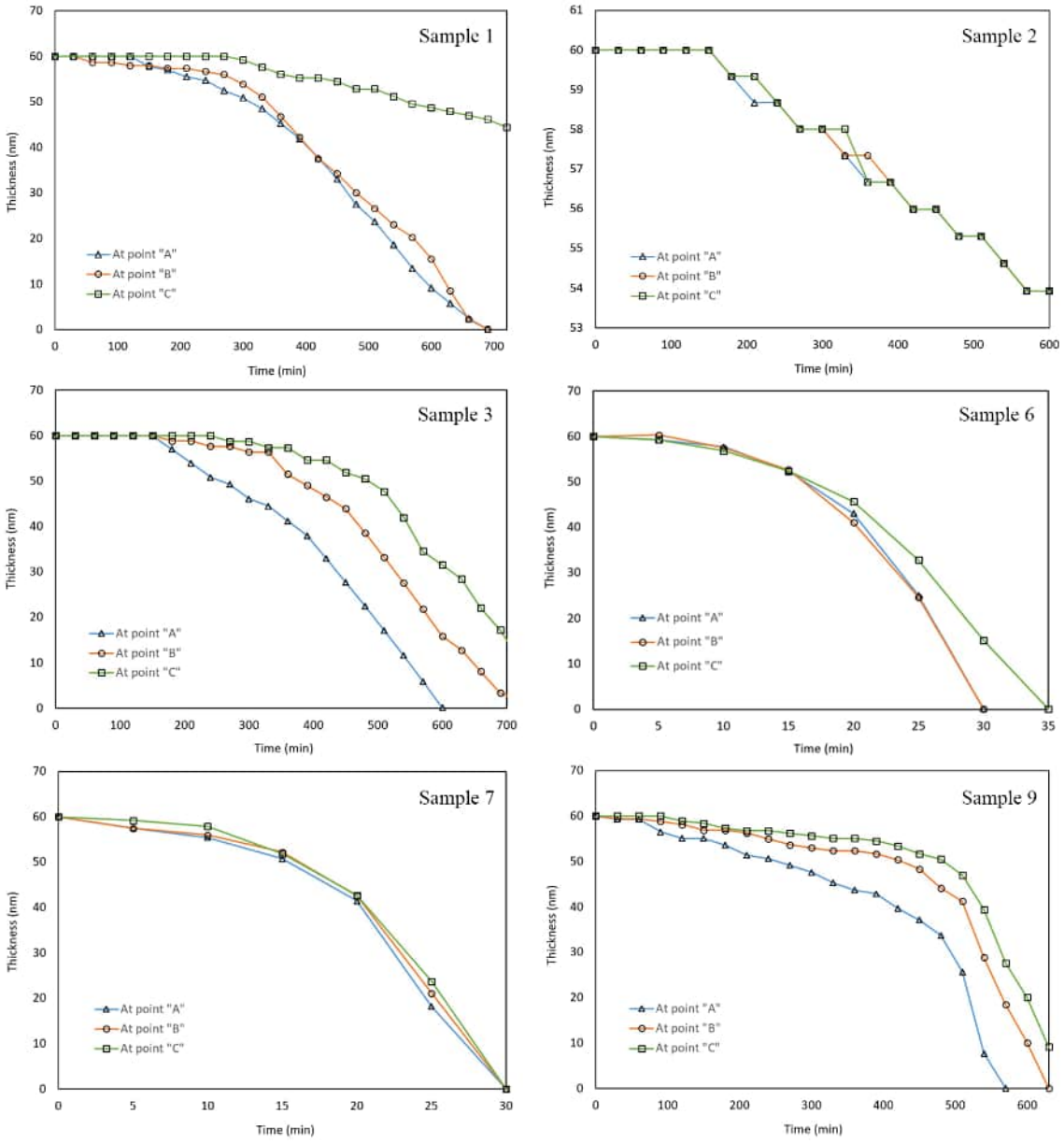

Figure 3.5: Gold thickness versus time at different conditions of temperature and glycine concentration corresponding to Table 3.1. The points A, B and C shows the distance from the injecting point through the microchannel, respectively.

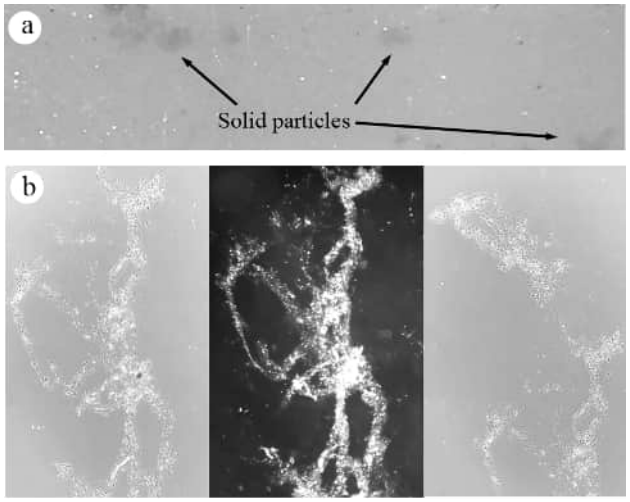

Figure 3.6: Polymerisation of glycine that blocks the microchannel and reduces the velocity of flow corresponding to sample 2 (Table 3.1). It may explained by the high concentration of glycine.

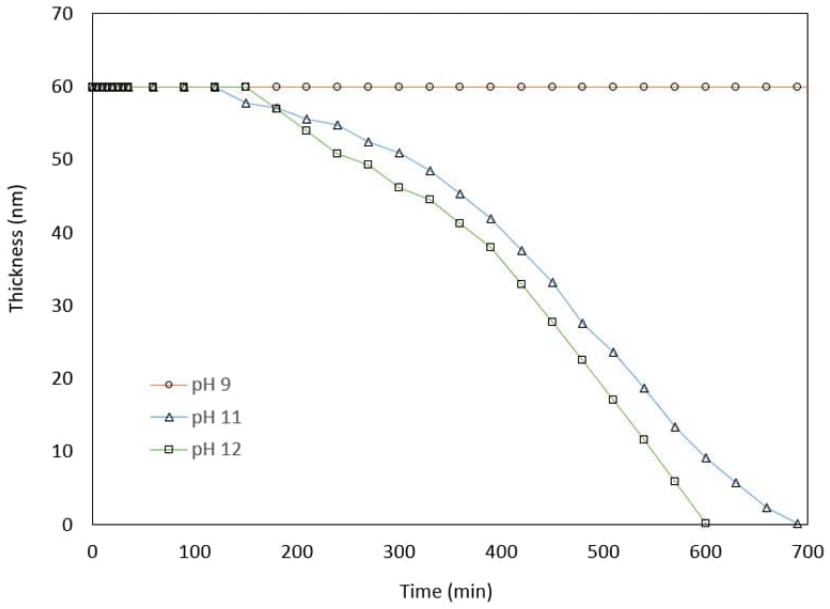

Figure 3.7: Effect of pH on gold dissolution corresponding to samples 1, 3 and 5 (Table 3.1). It shows that inceasing pH increases the rate of gold dissolution as the thickness of gold layer is reduced.

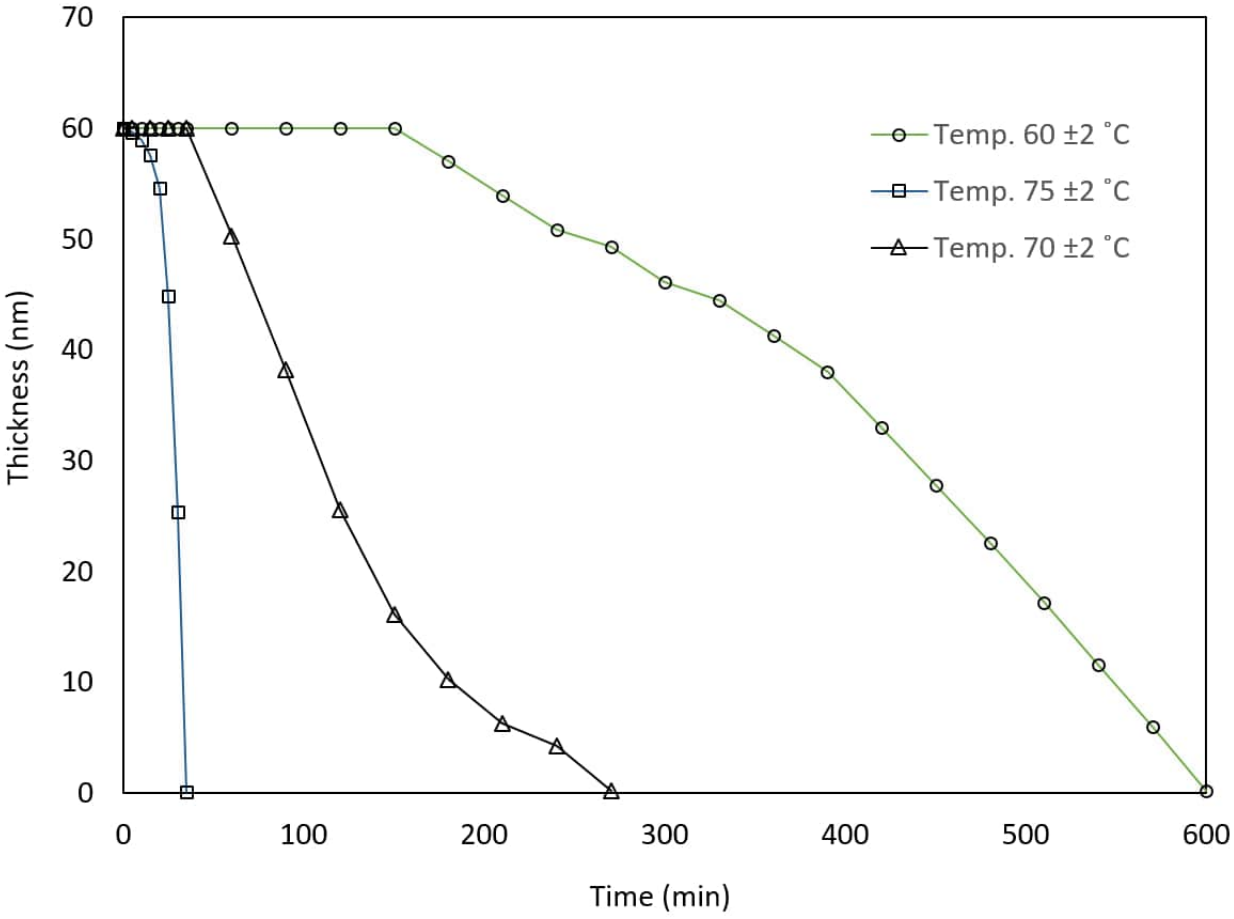

Figure 3.8: Effect of temperature on gold dissolution corresponding to Samples 3 and 6 (Table 3.1).

the glycine concentrations are 1M and 0.5M, respectively. Fig. 3.8 obtained by comparing the outputs of Samples 3 and 6 shows a dramatical increase of gold recovery by increasing temperature from 60±2 to 75±2^{o}C.

3.3.3 Effect of glycine concentration

Our experimental results indicate that increasing the concentration of glycine increases the gold dissolution rate, provided that the concentration remains below the polymerisation level that depends on temperature and pH [53]. Excessively high glycine concentrations may result in adverse effects because if glycine polymerises, it hinders the flow. In addition, surface passivation may reduce the rate of etching/leaching [22, 54, 55]. Note that the solubility of glycine in water can be increased by increasing temperature [56]. Fig. 3.9 shows that increasing the glycine concentration up to 1.2 M increases the gold dissolution corresponding to Samples 6, 7, 8 and 9 at 75^{o}C (Table 3.1). However, Fig. 3.10 shows that increasing the glycine concentration from 1 to 1.5 M (corresponding to Sample 1 and 2, respectively) reduces the rate of gold dissolution. As mentioned before, high concentration of glycine may cause passivation of the gold surface which can reduce the dissolution rate.

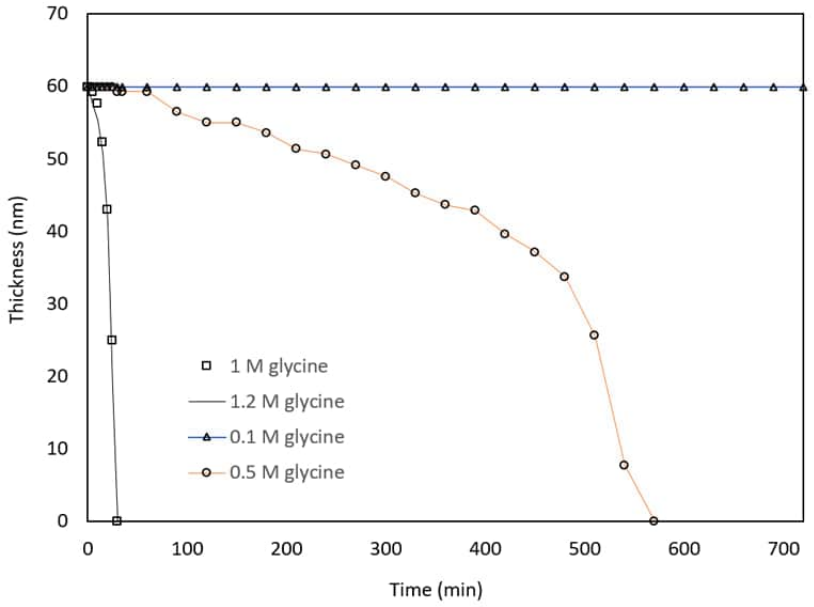

Figure 3.9: Effect of glycine concentration on gold dissolution corresponding to Samples 6, 7, 8 and 9 (Table 3.1). Increasing glycine concentration at temperature 75±2^{o}C increases the rate of gold dissolution.

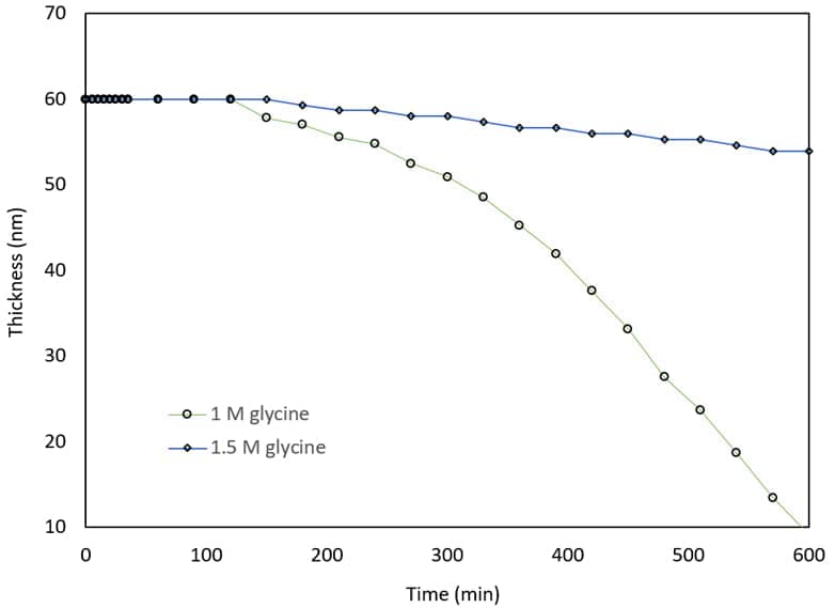

Figure 3.10: Effect of glycine concentration on gold dissolution corresponding to Samples 1 and 2 (Table 3.1). Increasing the glycine concentration at temperature 60±2^{o}C from 1 to 1.5 M decreases the rate of gold dissolution.

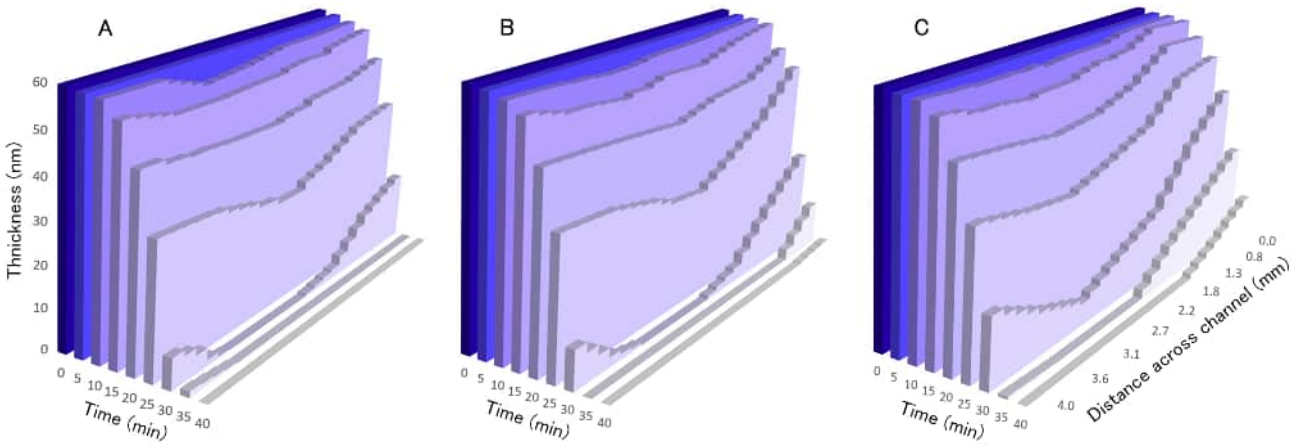

Figure 3.11: Etch profile lines of Au thickness versus time and space corresponding to sample 6 (Table 3.1). A, B and C are specific points located away from the injection point as can be seen in Fig. 3.4.

3.4 Monitoring the leaching throughout the channel

In the previous sections, we show that the microchannel system is instrumental to evaluate the effects of temperature, pH and glycine concentration on gold recovery within a confined space that mimics micro-cracks. One of the main advantages of using the michrochannel is the ability to monitor leaching rates during the experiment and the possibility to observe the finger-like pattern that characterises the etching process in real time. Fig. 3.11 shows the three etch profiles across the microchannel corresponding to Sample 6. As can be seen, the leaching rate is fully monitored with respect to space and time within the microchannel. The figure also shows that the leaching rate reduces close to the walls because the lowest flow velocity occurs in these areas. The leaching rate also decreases from profiles A to C (see Fig. 3.4) because of the distance from the injecting point.

To evaluate the effects of friction on the velocity of flow and consequently on the leaching rate, more profile lines were drawn across the channel corresponding to Sample 6. By combining the profile lines and measuring the gold thickness at 300 points within the microchannel surface, contour plots of gold thickness were obtained at intervals of 5 minutes (Fig. 3.12). It can be seen in Fig. 3.12 that leaching started in the left area close to the injecting points and moved towards the right side. In addition, the results indicte that leaching intensified in the middle of the microchannel and decreased at the areas close to the lateral sides. Video Tracker 5.0.5 and Surfur 10 were employed to obtain the gold thickness across the channel and the contour graphs.

Compared to other laboratory tests, this method mimics the in-situ gold etching process in micro-cavities. Yet, the system has certain limitations and can be improved in the future. For example, selecting the right material to make the substrates and covering sheets can be critical as some materials can be opaque to the light, react with the lixiviants or sensitive to temperature. Controlling the temperature within a small range throughout the channel can be difficult with the current technology where a single thermocouple is used to measure

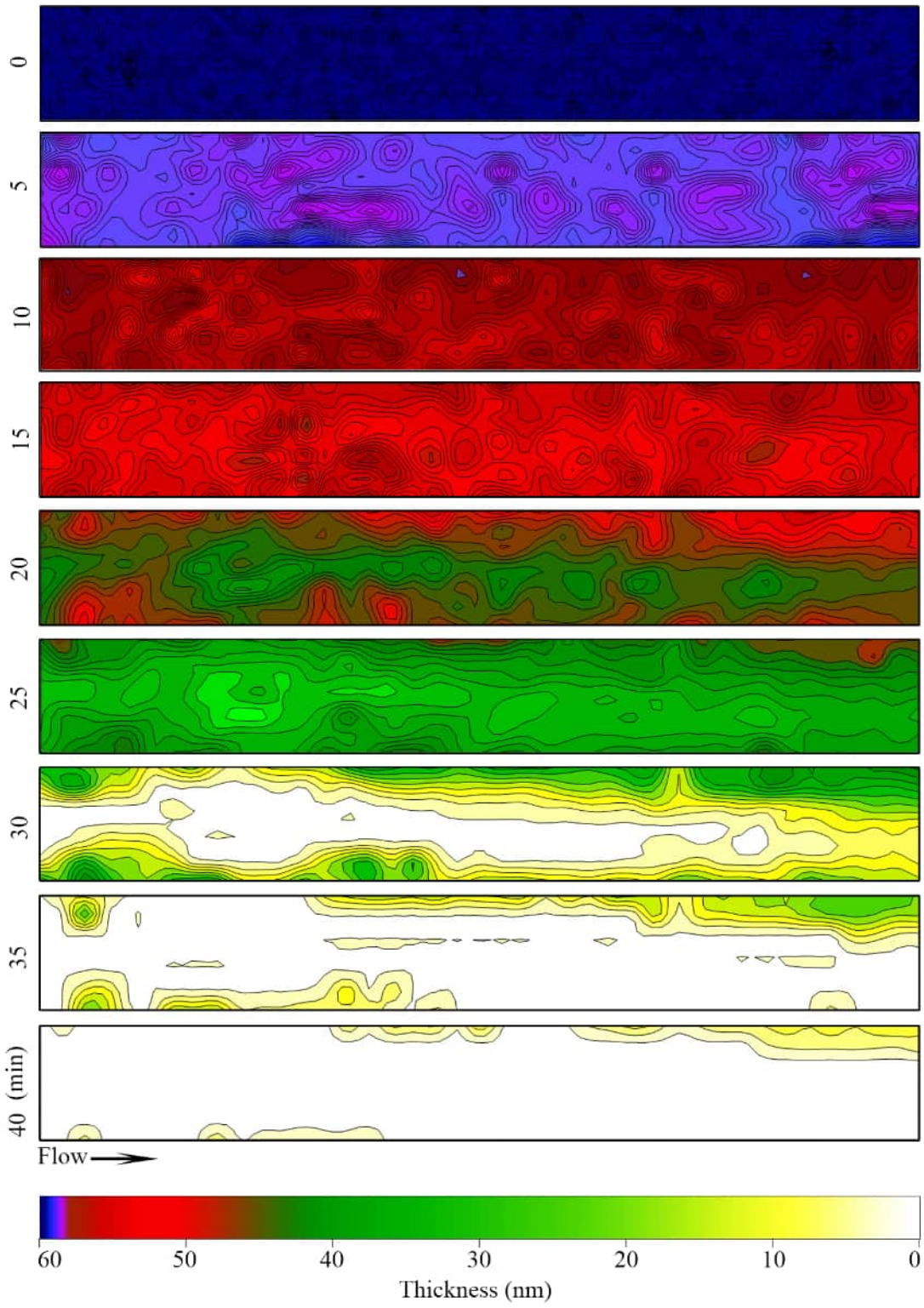

Figure 3.12: Contour plots of Au thickness across the microchannel at 5 mins intervals corresponding to sample 6 (Table 3.1).

temperature. In addition, preparing proper microchannels is challenging, expensive, and dependent on the type of metal or elements to be leached.

3.5 Conclusion

A microfluidic device has been developed to mimic the conditions of in-situ leaching of gold using an alkaline glycine system at various temperatures and lixiviant concentrations. The device builds on an existing device developed by [22] where amonium thiosulfate has been used to extract gold at room temperature. The device was instrumental to conduct the experiment and quantitatively monitor the leaching process under controlled conditions at full scale. It has been shown that increasing temperature around 75^oC dramatically increases the leaching rate of gold in alkaline glycine solutions. It has also been noticed that increasing pH to 11 and beyond can increase the leaching rate. Although increasing glycine concentration improves the rate of leaching to some extend, excessively high concentrations of glycine can reduce the recovery. This study shows that microchannel systems have a great potential for future mining and metallurgy studies where in-situ leaching under controlled conditions is relevant.

Acknowledgements

This project was supported by the Australian Research Council through the Discovery Project DP170104205. This support is highly appreciated. M.R. Azadi would like to acknowledge the financial support provided by Robert and Maude Gledden Postgraduate Scholarships. In addition, the authors thank Dr. Mariusz Martyniuk, Dr. Adrian Keating, Dr. Dhirendra Tripathi, Dr. Xiao Sun and Dr. Martin Hill for valuable advices and great assistance in making the microchannels.

References

Bibliography

[1] G. E. Moore, Cramming more components onto integrated circuits. electronics 38 (8): 114–117 (1965).

[2] A. Manz, N. Graber, H. á. Widmer, Miniaturized total chemical analysis systems: a novel concept for chemical sensing, Sensors and actuators B: Chemical 1 (1-6) (1990) 244–248.

[3] A. C. Henry, T. J. Tutt, M. Galloway, Y. Y. Davidson, C. S. McWhorter, S. A. Soper, R. L. McCarley, Surface modification of poly (methyl methacrylate) used in the fabrication of microanalytical devices, Analytical chemistry 72 (21) (2000) 5331–5337.

[4] H. Becker, L. E. Locascio, Polymer microfluidic devices, Talanta 56 (2) (2002) 267–287.

[5] Y. Temiz, R. D. Lovchik, G. V. Kaigala, E. Delamarche, Lab-on-a-chip devices: How to close and plug the lab, Microelectronic Engineering 132 (2015) 156–175.

[6] J. Melin, S. R. Quake, Microfluidic large-scale integration: the evolution of design rules for biological automation, Annu. Rev. Biophys. Biomol. Struct. 36 (2007) 213–231.

[7] L. Y. Yeo, H.-C. Chang, P. P. Chan, J. R. Friend, Microfluidic devices for bioapplications, small 7 (1) (2011) 12–48.

[8] E. K. Sackmann, A. L. Fulton, D. J. Beebe, The present and future role of microfluidics in biomedical research, Nature 507 (7491) (2014) 181.

[9] S. Halldorsson, E. Lucumi, R. Gómez-Sjöberg, R. M. Fleming, Advantages and challenges of microfluidic cell culture in polydimethylsiloxane devices, Biosensors and Bioelectronics 63 (2015) 218–231.

[10] G. M. Whitesides, The origins and the future of microfluidics, Nature 442 (7101) (2006) 368.

[11] H. Nagai, N. Miwa, M. Segawa, S.-i. Wakida, K. Chayama, Quantification of ag (i) and kinetic analysis using ion-pair extraction across a liquid/liquid interface in a laminar flow by fluorescence microscopy, Journal of Applied Physics 105 (10) (2009) 102015.

[12] C. Priest, J. Zhou, R. Sedev, J. Ralston, A. Aota, K. Mawatari, T. Kitamori, Microfluidic extraction of copper from particle-laden solutions, International Journal of Mineral Processing 98 (3-4) (2011) 168–173.

[13] C. Priest, J. Zhou, S. Klink, R. Sedev, J. Ralston, Microfluidic solvent extraction of metal ions and complexes from leach solutions containing nanoparticles, Chemical Engineering & Technology 35 (7) (2012) 1312–1319.

[14] C. Priest, S. F. Hashmi, J. Zhou, R. Sedev, J. Ralston, Microfluidic solvent extraction of metal ions from industrial grade leach solutions: extraction performance and channel aging, Journal of Flow Chemistry 3 (3) (2013) 76–80.

[15] T. Minagawa, M. Tokeshi, T. Kitamori, Integration of a wet analysis system on a glass chip: determination of co (ii) as 2-nitroso-1-naphthol chelates by solvent extraction and thermal lens microscopy, Lab on a Chip 1 (1) (2001) 72–75.

[16] F. H. Kriel, G. Holzner, R. A. Grant, S. Woollam, J. Ralston, C. Priest, Microfluidic solvent extraction, stripping, and phase disengagement for high-value platinum chloride solutions, Chemical Engineering Science 138 (2015) 827–833.

[17] C.-Y. Yin, A. N. Nikoloski, M. Wang, Microfluidic solvent extraction of platinum and palladium from a chloride leach solution using alamine 336, Minerals Engineering 45 (2013) 18–21.

[18] E. Kolar, R. P. Catthoor, F. H. Kriel, R. Sedev, S. Middlemas, E. Klier, G. Hatch, C. Priest, Microfluidic solvent extraction of rare earth elements from a mixed oxide concentrate leach solution using cyanex® 572, Chemical Engineering Science 148 (2016) 212–218.

[19] Z. Chen, W.-T. Wang, F.-N. Sang, J.-H. Xu, G.-S. Luo, Y.-D. Wang, Fast extraction and enrichment of rare earth elements from waste water via microfluidic-based hollow droplet, Separation and Purification Technology 174 (2017) 352–361.

[20] F. K. Crundwell, Extractive metallurgy of nickel, cobalt and platinum group metals, Elsevier, 2011.

[21] F. Crundwell, The dissolution and leaching of minerals: Mechanisms, myths and misunderstandings, Hydrometallurgy 139 (2013) 132–148.

[22] S. Kotova, B. Follink, L. Del Castillo, C. Priest, Leaching gold by reactive flow of ammonium thiosulfate solution in high aspect ratio channels: Rate, passivation, and profile, Hydrometallurgy 169 (2017) 207–212.

[23] A. F. Gangi, Variation of whole and fractured porous rock permeability with confining pressure, in: International Journal of Rock Mechanics and Mining Sciences and Geomechanics Abstracts, Vol. 15, Elsevier, 1978, pp. 249–257.

[24] S. R. Brown, C. H. Scholz, Closure of random elastic surfaces in contact, Journal of Geophysical Research: Solid Earth 90 (B7) (1985) 5531–5545.

[25] A. C. Henry, R. L. McCarley, S. S. Das, C. G. K. Malek, Characteristics of commercial pmma sheets used in the fabrication of extreme high-aspect-ratio microstructures, Journal of The Electrochemical Society 146 (7) (1999) 2631–2636.

[26] A. C. Henry, Surface modification and characterization of pmma used in the construction of microelectromechanical systems.

[27] A. Mathur, S. Roy, M. Tweedie, S. Mukhopadhyay, S. Mitra, J. McLaughlin, Characterisation of pmma microfluidic channels and devices fabricated by hot embossing and sealed by direct bonding, Current Applied Physics 9 (6) (2009) 1199–1202.

[28] S. Prakash, S. Kumar, Fabrication of microchannels on transparent pmma using co 2 laser (10.6 μm) for microfluidic applications: An experimental investigation, International Journal of Precision Engineering and Manufacturing 16 (2) (2015) 361–366.

[29] C. Leonard, J. Halary, L. Monnerie, Hydrogen bonding in pmma-fluorinated polymer blends: Fti. r. investigations using ester model molecules, Polymer 26 (10) (1985) 1507–1513.

[30] K. F. Lei, S. Ahsan, N. Budraa, W. J. Li, J. D. Mai, Microwave bonding of polymer-based substrates for potential encapsulated micro/nanofluidic device fabrication, Sensors and Actuators A: Physical 114 (2-3) (2004) 340–346.

[31] Y.-C. Hsu, T.-Y. Chen, Applying taguchi methods for solvent-assisted pmma bonding technique for static and dynamic μ-tas devices, Biomedical microdevices 9 (4) (2007) 513–522.

[32] N. Harris, A. Keating, M. Hill, A lateral mode flow-through pmma ultrasonic separator.

[33] K. Kim, S. W. Park, S. S. Yang, The optimization of pdms-pmma bonding process using silane primer, BioChip Journal 4 (2) (2010) 148–154.

[34] H. H. Tran, W. Wu, N. Y. Lee, Ethanol and uv-assisted instantaneous bonding of pmma assemblies and tuning in bonding reversibility, Sensors and Actuators B: Chemical 181 (2013) 955–962.

[35] H. Yu, Z. Chong, S. Tor, E. Liu, N. Loh, Low temperature and deformation-free bonding of pmma microfluidic devices with stable hydrophilicity via oxygen plasma treatment and pva coating, RSC Advances 5 (11) (2015) 8377–8388.

[36] A. Wan, T. A. Moore, E. Young, Solvent bonding for fabrication of pmma and cop microfluidic devices., Journal of visualized experiments: JoVE (119).

[37] A. Karrech, M. Attar, E. Oraby, J. Eksteen, M. Elchalakani, A. Seibi, Modelling of multicomponent reactive transport in finite columns-application to gold recovery using iodide ligands, Hydrometallurgy 178 (2018) 43–53.

[38] E. Martens, H. Zhang, H. Prommer, J. Greskowiak, M. Jeffrey, P. Roberts, In situ recovery of gold: Column leaching experiments and reactive transport modeling, Hydrometallurgy 125 (2012) 16–23.

[39] M. Z. Wu, D. A. Reynolds, H. Prommer, A. Fourie, D. G. Thomas, Numerical evaluation of voltage gradient constraints on electrokinetic injection of amendments, Advances in water resources 38 (2012) 60–69.

[40] C. Monk, Electrolytes in solutions of amino acids. part iv.-dissociation constants of metal complexes of glycine, alanine and glycyl-glycine from ph titrations, Transactions of the Faraday Society 47 (1951) 297–302.

[41] R.-P. Martin, L. Mosoni, B. Sarkar, Ternary coordination complexes between glycine, copper (ii), and glycine peptides in aqueous solution, Journal of Biological Chemistry 246 (19) (1971) 5944–5951.

[42] O. Farooq, N. Ahmad, Stability and binding of au (iii) to certain amino acids using sodium chloroaurate, Journal of Electroanalytical Chemistry and Interfacial Electrochemistry 53 (3) (1974) 457–460.

[43] T. Kiss, I. Sovago, A. Gergely, Critical survey of stability constants of complexes of glycine, Pure and applied chemistry 63 (4) (1991) 597–638.

[44] I. V. Mironov, Stability of gold (i) glycinate complexes in aqueous solution, Russian Journal of Inorganic Chemistry 52 (5) (2007) 791–792.

[45] V. Isaeva, V. Naumov, Z. F. Gesse, V. Sharnin, Complex formation of silver (i) with glycinate ion in aqueous ethanol and dimethyl sulfoxide solutions, Russian Journal of Coordination Chemistry 34 (8) (2008) 624–628.

[46] A. E. Angkawijaya, A. E. Fazary, S. Ismadji, Y.-H. Ju, Cu (ii), co (ii), and ni (ii)–antioxidative phenolate–glycine peptide systems: an insight into its equilibrium solution study, Journal of Chemical & Engineering Data 57 (12) (2012) 3443–3451.

[47] Z. Jingrong, L. Jianjun, Y. Fan, W. Jingwei, Z. Fahua, An experimental study on gold solubility in amino acid solution and its geological significance, Chinese Journal of Geochemistry 15 (4) (1996) 296–302.

[48] D. H. Brown, W. E. Smith, P. Fox, R. D. Sturrock, The reactions of gold (0) with amino acids and the significance of these reactions in the biochemistry of gold, Inorganica Chimica Acta 67 (1982) 27–30.

[49] D. Feng, J. S. J. Van Deventer, The role of amino acids in the thiosulphate leaching of gold, Minerals Engineering 24 (9) (2011) 1022–1024.

[50] M. G. Aylmore, Alternative lixiviants to cyanide for leaching gold ores, Gold Ore Processing, Project Development and Operation (2005) 501 to 539.

[51] E. A. Oraby, J. J. Eksteen, The leaching of gold, silver and their alloys in alkaline glycine-peroxide solutions and their adsorption on carbon, Hydrometallurgy 152 (2015) 199–203.

[52] J. Eksteen, E. Oraby, B. Tanda, P. Tauetsile, G. Bezuidenhout, T. Newton, F. Trask, I. Bryan, Towards industrial implementation of glycine-based leach and adsorption technologies for gold-copper ores, Canadian Metallurgical Quarterly (2017) 1–9.

[53] K. Sakata, N. Kitadai, T. Yokoyama, Effects of ph and temperature on dimerization rate of glycine: evaluation of favorable environmental conditions for chemical evolution of life, Geochimica et Cosmochimica Acta 74 (23) (2010) 6841–6851.

[54] L. M. Fairley, A survey of conventional and novel processes for the treatment of refractory gold, Ph.D. thesis, University of British Columbia (1998).

[55] D. Feng, J. Van Deventer, Oxidative pre-treatment in thiosulphate leaching of sulphide gold ores, International journal of mineral processing 94 (1-2) (2010) 28–34.

[56] S. Budavari, M. O Neil, A. Smith, P. Heckelman, J. Kinneary, The merck index. an encyclopedia of chemicals, drugs and biologicals. whitehouse station, nj. merck research laboratories division of merck and co, Inc. Monograph (2006) (1996) 4175.

Chapter 4

Microchannel - a useful device for experimental hydrometallurgy

4.1 Introduction

The development of microfluidic devices has been attracting increasing interest from scientists over the past decades. Microfluidic systems enable many areas of science such as engineering, physics, chemistry, biotechnology, and medicine [1, 2] to manipulate fluids especially where small scale experiments (roughly 100 nanometers to 100 micrometers) are relevant [3]. Microchannels are devices that are manufactured to accomodate microfluids; they allow to downscale analytical systems which enhances the performance of analysis using smaller amounts of samples with higher analysis speed [4]. Some microchannels have the advantage of offering a high surface-volume ratio, which allows multiphase reactions to be established on the interface area between different phases such as gas-liquid-solid [5]. Microfluidic devices are able to combine multiple processes such as separation and pre/post-column reactions on a single device [6]. Microfluidic systems provide high quality monitoring of processes under realistic conditions of temperature, pressure and composition, which has proven difficult in current combinatorial approaches. Moreover, the small dimensions imply laminar flow which allows high heat and mass transfer and help extract chemical kinetic parameters [7].

The benefit of microfluidic devices is obvious in the field of chemistry [8] as they reduce the consumption of expensive reagents and other components. A large number of studies reported the use of michrochannels in chemical processing due to the various advantages of microfluidic systems. Some of these examples include solvent extractions in gas-liquid [9] for rare earth elements [10] and solid-liquid phases [11], liquid-liquid extraction [8, 12] and separation of species such as Co^{2+} and Ni^{2+} [13] as well as Ce^{3+} and Pr^{3+} [14], Cu^{2+} [15]. Liquid-liquid extraction is one of the separation processes that benefits the most from studies based on microfluidic systems. For instance, the conventional solvent extraction for low-concentration rare earth elements (REEs) has some limitations related to large factories, long mixing times and high energy consumption. [10] investigated a solvent extraction system to recover Nd^{3+} using a microfluidic system. They showed that the introduction of nitrogen gas greatly increased the efficiency by increasing the mass transfer rate through a microfluidic device. Conventional solvent extraction SX is

mainly used to extract metals from mineral leached solutions, which is carried out in a two stage vessel called a mixer-settler [16]. Some studies have been conducted in order to compare the conventional SX with microfludic system extraction in which the advantages of fast mass transferring in mirochannels have been hinted [15, 17, 18]. Microfluidics offer many advantages and only few limitations including relatively higher pressure drops when handling a solution that contains solid particles [19].

Leaching is sometimes the main stage of mineral processing operations; it is often the initial operation and thereby plays an important role in the success of a hydrometallurgical business [20, 21]. Although, the usefulness of using microfluidic systems in chemical engineering studies has been proven, the potential impact of this technology in the leaching and hydrometallurgy needs more investigations. Recently, few studies have been carried out on the leaching of metals using microchannels. For example, [22, 23] conducted experimental studies on leaching of gold by ammonium thiosulfate solution using microchannels. They monitored the etching rate of gold layers under controlled visual and quantitative monitoring. Their studies showed the potential of michrochannel chips to improve the leaching precess by controlling the leaching experiment in a real time.

In this paper, we explain the benefits of using microchannels in comparison with other common laboratory leaching experiments using examples from literature. We describe methods and techniques of fabrication of microchannel chips step-by-step and present an experimental example of microchannel fabrication for leaching gold in order to illustrate this method.

4.2 An overview of laboratory leaching tests

There are various testing techniques that have known success hylometallurgy including the bottle roll, column leach, pressure leach, bioleach, albion process, electrowinning, solvent extraction tests to mention a few. Among these techniques, bottle roll tests are widely employed to determine the ability of chemical solutions (from acid to basic) to leach specific metals and to evaluate conventional mill leaching processes and investigate. The procedure of bottle roll is relatively easy to set up and it usually provides reliable and quick data that would form the basis for further assessment of a particular ore with respect to a prospective leaching process and scaling-up of leaching methods/procedures. Batch laboratory bench scale tests, either rolled bottles or in stirred vessels are generally used to estimate the recovery, leach residence time and chemical consumption. Bottle roller tests and stirred reactor are commonly used for evaluating gold cyanidation [24–29].

Column test is used for evaluating ore samples and simulating heap leaching conditions. Particle size, reagent consumption, final constituent mass balance and recovery can be determined during this test by daily sampling over leach cycle which can range up to months and years. Column tests have been used by many researchers and companies to evaluate the leaching of precious metals, copper, uranium, and other constituents [30–33]. The leaching column test is a valid and standard method to evaluate and simulate the risk of leaching of inorganic elements from the soil [34].

Leaching experiments using microchannel chips are a new method to evaluate chemical reactions and their correponding rates which can optimise the leaching conditions. In this

method, a reagent in a small scale is injected through a microchannel containing a layer of etchable metal. The whole process can be monitored under controlled conditions of pH, temperature and injection rate. The results can be obtained as the experiment is running from the start to the end. However, this method has some limitations beside its significant benefits. To explain the benefits and limitations of this method, we selected three conventional methods to compare it with including bottle roll, column and stirrer reactor leaching. A considerable number of experiments have been conducted using these three methods for different metals and minerals. Some of these experiments have been selected and summarised in Table A.1 to emphasize the outputs of the leaching test methods and subsequently compare the methods with respect to those outputs. It needs to be mentioned that the experiments presented in Table A.1 have been selected based on leaching method, leached metal, and experimental purpose.

By reviewing the published literature meticulously, we noticed that most leaching experiments have been conducted using stirrer reactors. The first part of Table A.1 presents gold leaching experiments using different experimental methods. It can be seen that the experimental time duration using ammonia thiosulphate in microchannel is less than the duration of stirrer reactor and bottle roll based tests. In all experiments, chemical analysis is the way to evaluate the recovery except for microchannels where optical observation is the way of monitoring. Despite the accuracy of chemical analysis, optical observation is much faster and more traceable since it can be recorded in real time. As can be seen in Table A.1, experimental outputs are commonly used to optimise the conditions of pH, temperature, agitation rates and composition. The kinetic studies, passivation, rate of recovery and effect of specific mineral or catalysers are also commonly studied and have been investigated in those experiments. It is clear that different ranges of samples whether pure elements or ores, and various reagents from base to acid have been employed in those methods. The durations of experiments can be varied based on their reaction rates. However, column tests are usually more complex and may be carried out over longer periods. Conditions of pH, temperature and agitation rates are of paramount importance for researchers focusing on leaching processes. Therefore, these conditions need to be controlled during the experiments. In this context, stirrer reactors showed high reliability and practicability. For example, the effect of ultrasonic waves on the leaching process and metal recovery have been investigated using stirrer reactors. Despite careful survey, we could not find temperature-controlled and pressure-controlled experiments that involve bottle roll and/or column tests. In this section, the leaching methods and their outputs are discussed. It is important to evaluate the microchannel system, its efficiency and ability to produce relevant outputs under controlled conditions. For example, we address questions such as; can kinetic studies be conducted using microchannel chips? and how to deal with wide ranges of pH, temperature, pressure, and composition?

4.3 Advantages and disadvantages of microchannel systems

Laboratory research is expensive and high costs are driven by the requirement for specialised equipment, reagents, and consumables that are necessary to provide the appropriate testing conditions. Equipment can be very expensive depending on the required level of

Method	Leached element	Sample type	Reagents	Time[a]	Method of analysis	Output	Comment	Ref.
Stirrer reactor	Au	Gold ores	Ammonia thiosulphate	3.5 hours	ICP	Optimisation	kinetic	[35]
Stirrer reactor	Au	Concentrated ores	Alkaline cyanide	8 hours	XRD	Optimisation	Fully controlled conditions	[36]
Bottle roller	Au	Gold ores	Ammonia thiosulphate	24 hours	AAS	Optimisation	Using Ni as a ctalyt	[37]
Stirrer reactor	Au	Refractory gold	Alkaline cyanide	24 hours	XRD	Pre-treatment (NaOH)	Effect of pyrite and sphalerite	[38]
Stirrer reactor	Au	Gold ores	Alkaline cyanide	24 hours	MP-AES	Effect of iron oxide	Passivation	[39]
Stirrer reactor	Au	Concentrated ores	Chloride	30 mins	ICP	Optimisation	Pre milling (480 mins)	[40]
Stirrer reactor	Au	ores	Ammonia thiosulphate	6 hours	ICP-OES	Optimisation	Pressure oxidized concentrate	[41]
Stirrer reactor	Au	Refractory gold	Thiourea	4 hours	ICP	Physical beneficiation	Applied pressure	[42]
Stirrer reactor	Au	Gold ore	Bromide	4 hours	AAS	Optimisation		[43]
Stirrer reactor	Au	Gold foil	Thiosulphate	60 hours	AAS	Effect of tetrathionate		[44]
Column	Au	Gold ores	Iodine	200 days	ICP-OES	Optimisation	Transport modelling	[33]
Microchannel	Au	Coated gold	Ammonia thiosulphate	35 mins	Optical monitoring	Passivation	Effect of $CuSO_4$	[22]
Stirrer reactor	Co/Zn/Cu	Copper slag	Sulfuric acid	2-4 hours	XRD	Optimisation	Applied pressure	[45]
Stirrer reactor	Cu	Malachite	Alkaline glycine	180 mins	AAS	Optimisation	Kinetic	[46]
Stirrer reactor	Cu	Chalcocite	Alkaline glycine	48 hours	ASS/UV-Vis	Optimisation	Kinetic	[47]
Bottle roller	Cu	Copper ores	Alkaline glycine	48 hours	ICP-OES	Optimisation		[48]
Stirrer reactor	Ge	Roasted zinc residue	$HCl/CaCl_2$	120 mins	Spectrometer	Recovery	Effect of ultrasonic	[49]
Stirrer reactor	K	Phosphorus potassium	Sulfuric acid	7 hours	AAS	Recovery	Effect of ultrasonic	[50]
Stirrer reactor	Fe	Waste bauxite	HCl	240 mins	XRD	Optimisation		[51]
Stirrer reactor	Zn-Pb	Ores	NaOH	1.5 hours	AAS	Optimisation	Kinetic	[52]
Stirrer reactor	Mn	Serpantine	$H_2SO_4/HCl/HNO_3$	2 hours	XRD	Optimisation		[53]
Column	Na/K/Mg/Ca	Caliche	Reverse osmosis brine	23 days	XRD	Recovery		[54]
Stirrer reactor	Ni	Laterite ores	Sulfuric acid	1.5 hours	XRD	effect of Na_2SO_4	High temperature/pressure	[55]
Stirrer reactor	Li/Co	Secondary batteries	H_2SO_4/Cyanecx272	2 hours	AAS	Recovery	Effect of pH	[56]
Column	Mn/Fe/Ca	Manganiferous ore	H_2SO_4/glucose	24 hours	ICP	Optimisation	Particle size	[57]

Table 4.1: Some common laboratory leaching tests. [a] Time for one round of the experiment.
ICP: Inductively coupled plasma mass spectrometry
XRD: X-ray diffraction
AAS: Atomic absorption spectroscopy
OES: Optical emission spectrometers
MP-AES: Microwave plasma atomic emission spectroscopy

precision. Sampling and analyses to examine the outputs are very costly and often require collaboration with various teams with special skills. Most of these costs–including the cost of energy–can be avoided in microchannels. In microchannel experiments, optical observation using microscopic camera (see the section A.3) is a cost effective of measuring recovery as opposed to advanced chemical analyses that would be required otherwise. In microfluidic systems, the consumption of chemicals (e.g. lixivian) is reduced to millilitres while such consumption can two order of magnitude higher in common larger scales. Hence, the corresponding costs can be reduced considerably.

Environmental and safety issues related to the use of chemicals and complex equipment used in conventional experiments need to be managed carefully. Using lower amounts of chemicals can facilitate the laboratory management and the adherence to safety regulations, protections and guidelines of using chemicals. For example, cyanide which is a highly toxic chemical can be challenging to control in a laboratory setting because of the risks it poses when it evaporates, gets handled, or enters in contact with human skin and/or organs. However it can be of lower risk when manipulated at small scale.

Direct analysis significantly reduces the experiment duration because it is practical to stop the test when enough information is available. Conventionally, sampling takes place on a regular basis and prepare and analysis are time consuming. When samples are extracted from the solution, they need to be replaced with equivalent amounts of solvents and solutes to balance the concentrations which requires extra care and time.

Chemical resistivity is one of the important factors that need to be taken into consideration when selecting equipment and devices to handle leaching solutions safely. As can be seen in Table A.1, specific methods and handling equipment can be used depending on the types of chemicals to be handled. Nevertheless, selecting large equipment such as column or bottle roll tests can be costly and non justifiable especially in the case of precious metals, in which case microchannels can represent a viable alternative. Microchannel chips can be made of materials that are resistant to acids and bases. New fabrication technologies fit these devices to the desired conditions and make them amenable to modern monitoring techniques including microscopic cameras, electronic analysers, and injection pumps with controlled flow rates. Employing a technology with high quality monitoring at larger scales would be prohibitively expensive.

It is obvious that commercial-scale recovery and other informations can not be available prior to the plant being built and operated at steady state. Therefore, laboratory results have to be scaled up to estimate production rates. To establish a database of valid scale-up factors, having benchmark of laboratory test results against production plant operating data is indispensable and often not readily available in the literature or directly from operators [58]. The actual scale of leaching may differ from the laboratory scale of an experiment. One of the main reasons of using large scale experiments such as column tests is to simulate a real process. However, the results cannot be directly applied to calculate a rough recovery in the actual scale, and normally, empirical uncertainty factors are used to estimate the recovery with a proposed leaching technique. Notwithstanding the benefits of large scale experiments, it is important to realise that scaling up the experiments does not cover all aspects of the leaching process in details. Studying the micro-scale to simulate the leaching process through a small parameters-window in details is significant.

Method	Set up	Full-time monitoring	Particle size	Temperature control	pH control	Concentration control	Pressure control	Flow rate agitation rate	Full-time sampling	Time period	Scale up the result	Low chemical consumption
Bottle roller	√√√	√	√√	√	√√	√√√	√	√√√	√√		√√	
Column test	√√√	√	√√√	√√	√√	√√	√	√√√	√√		√√√	
Stirrer reactor	√√√	√	√	√√√	√√√	√√√	√√√	√√√	√√√		√	
Microchannel	√√√	√√√	√	√√	√√√	√√√	√√	√√√	√√√		√	

Table 4.2: A comparison between laboratory leaching test methods. The symbols of √√√, √√ and √ show the high to low reliability, respectively. The colours is to show how convenient and easy the factor is to be applied. , , and are used for very convenient, convenient, difficult and very difficult to apply, respectively. This data is relatively estimated in comparison with only four common methods.

Conventional leaching experiments are conducted for three main purposes, namely kinetic, recovery, and optimisation of reaction conditions such as pH, temperature, concentration and agitation rate. The kinetic mechanism and the rate of reaction are of primary importance in hydrometallurgy as they help understand the mechanism of dissolution. Usually, the reaction pathways need to be determined up to the slowest step in a series of experiments to examine the kinetic mechanism of a reaction [21]. Defined surface area of a metal and controlled flow rate are two factors that make kinetic studies possible in microchannel systems. Passivated surface can reduce the rate of dissolution of minerals. Passivation has been studied by many researchers to examine the proposed model and reasons of passivation [59–61]. Microchannel systems with a full-time monitoring high resolution microscopic camera also has the ability to examine the passivation for some metals such as gold which has been evaluated recently by [22].

As mentioned above, it is beneficial for a number of reasons to combine leaching experiments with michrofluidic systems. The main motivation is to have a real time and monitoring of the leaching process where traceability is ensured by recording. By recording the leaching process whether using a microscopic camera or other detection devices, reviewing the whole process can be possible to reduce errors. The results of the leaching tests depend on the sampling for the purpose of chemical analysis. However, the number of samples is limited by time and the amount of samples especially for fast reactions. In this case, the benefit of direct and recordable monitoring is clear which is well adopted to microfluidic systems. One of the normal methods to continuously monitor the flow regimes is to use a high speed camera on the top of the microchannel chips while the experiment is running. All videos can be recorded and then videos and images can be used for image analysis. In this case, a back light (e.g. LED), may assist and improve the quality of monitoring. This method has been used in liquid-liquid extraction [12, 17, 62] and in gold leaching [22, 23] using microchannel chips.

As this method has been used only recently by hydrometallurgists, its full judiciousness needs to be examined experimentally. Applying pressure in the leaching process has been examined using stirrer reactor (see Table A.1), microchannel chips showed the ability of being under pressure (see Table A.8). However, the effect of ultrasonic [49], microwave [63] and shaking assistance [64] in leaching experiments has not been evaluated using microchannel chips.

Apart from the various advantages of microfluidic systems, there are some limitations to using micro-size scale devices. One of the obvious issues is the particle size of the materials which is limited to microns (less than the size of a typical channel). In other words, particle size is difficult to investigate using leaching experiments that require microchannel devices. In most leaching experiments using conventional methods, ore samples need to be ground to less than 75-100μm. Leaching metals from ore samples using microfluidic system have not been reported yet. In the field of agriculture, [65] conducted an experiment to leach potassium K from soil samples using a microchannel. Therefore, it is not illusory to imagine the use ore samples in microchannel devices to examine a leaching process in the future.

Another important limitation is the sampling for the purpose of chemical analysis. Although direct analysis such as optical monitoring is applied in microfluidic system, evaluating the recovery of leached materials is very important. As the amount of injected

reagents through the microchannel is very low (millilitres), the output amount of chemicals in each desired time increment is not enough for chemical analysis. However, it is possible to take one or two samples at the end of experiments when the pregnant solution is enough to be taken for chemical analysis.

By reviewing leaching experiments from the literature and referring to Table A.1, a comparison between four different methods of leaching experiments including bottle roll, column, stirrer reactor, and microchannel chips has been summarised in Table A.2 in terms of ease and reliability of testing. It can be seen in Table A.2 that stirrer reactor is an easy and reliable method to be used for leaching tests. Column test is the most reliable test for scaling up the results. Similarly, microchannel systems are reliable and easy to use for leaching in controlled conditions of pH, temperature, concentration, pressure and injection rate. However, this device needs considerable research work and future studies to showcase its full relevance to leaching tests.

4.4 Manufacturing microchannel chips

In Appendix A, we describe the techniques of making microchannel chips step-by-step to facilitate the process of laboratory fabrication.

4.5 Summary

The fabrication processes of microchannel chips have been reviewed in details to make them accessible for hydrometallurgical applications. The main advantages of this device have been identified as the real time monitoring, low consumption of reagents, safe use of the environment, easy control of experimental conditions (i.e. pH, temperature, injection rate, and composition), controllable heat and mass transfer, potential to use advanced imaging technologies (e.g. high resolution microscopes) in real time, and the direct and fast acquisition of analytical results. This review has also identified a number of limitations that are mainly the inadequacy for ore samples of large particle size, the difficulty of real time sampling for chemical analysis, and the challenging scale-up to engineering apparatus sizes. Overall the advantages are sufficient to overcome the possible limitations of microfluidic system. Therefore, this technology can become a powerful tool for the laboratory testing of leaching processes. Through this survey, a number of gaps in the literature have been identified; addressing them may enhance of status of microchannels as common tools in hydrometallugy. The scientific community would benefit from research activities that examine

1. the up-scaling of results obtained through microchannels to engineering scale applications;

2. the applicability of micro-fluidic systems to alloys because of the difficulty of evaporating such materials;

3. competing leachable metals in a single microchannel;

4. the phenomenon of passivation in microchannels;

5. the process of in-situ leaching by controlling pressure, temperature and composition at the same time.

6. different regimes of flow and their impact on the leaching process within a microchannel.

Bibliography

[1] Y. Liu, D. Ganser, A. Schneider, R. Liu, P. Grodzinski, N. Kroutchinina, Microfabricated polycarbonate CE devices for DNA analysis, Analytical Chemistry 73 (17) (2001) 4196–4201.

[2] E. K. Sackmann, A. L. Fulton, D. J. Beebe, The present and future role of microfluidics in biomedical research, Nature 507 (7491) (2014) 181.

[3] G. M. Whitesides, The origins and the future of microfluidics, Nature 442 (7101) (2006) 368.

[4] B. Grass, A. Neyer, M. Jöhnck, D. Siepe, F. Eisenbeiß, G. Weber, R. Hergenröder, A new pmma-microchip device for isotachophoresis with integrated conductivity detector, Sensors and Actuators B: Chemical 72 (3) (2001) 249–258.

[5] J. Kobayashi, Y. Mori, S. Kobayashi, Multiphase organic synthesis in microchannel reactors, Chemistry–An Asian Journal 1 (1-2) (2006) 22–35.

[6] S. C. Jacobson, L. B. Koutny, R. Hergenroeder, A. W. Moore, J. M. Ramsey, Microchip capillary electrophoresis with an integrated postcolumn reactor, Analytical Chemistry 66 (20) (1994) 3472–3476.

[7] K. F. Jensen, Microchemical systems: status, challenges, and opportunities, AIChE Journal 45 (10) (1999) 2051–2054.

[8] H. Breisig, M. Schmidt, H. Wolff, A. Jupke, M. Wessling, Droplet-based liquid–liquid extraction inside a porous capillary, Chemical Engineering Journal 307 (2017) 143–149.

[9] J. Tan, Y. Lu, J. Xu, G. Luo, Mass transfer performance of gas–liquid segmented flow in microchannels, Chemical Engineering Journal 181 (2012) 229–235.

[10] Z. Chen, W.-T. Wang, F.-N. Sang, J.-H. Xu, G.-S. Luo, Y.-D. Wang, Fast extraction and enrichment of rare earth elements from waste water via microfluidic-based hollow droplet, Separation and Purification Technology 174 (2017) 352–361.

[11] S. De Loos, J. van der Schaaf, M. de Croon, T. Nijhuis, J. Schouten, Enhanced liquid–solid mass transfer in microchannels by a layer of carbon nanofibers, Chemical engineering journal 167 (2-3) (2011) 671–680.

[12] J. Tang, X. Zhang, W. Cai, F. Wang, Liquid–liquid extraction based on droplet flow in a vertical microchannel, Experimental Thermal and Fluid Science 49 (2013) 185–192.

[13] L. Zhang, V. Hessel, J. Peng, Liquid-liquid extraction for the separation of Co (ii) from Ni (ii) with Cyanex 272 using a pilot scale re-entrance flow microreactor, Chemical Engineering Journal 332 (2018) 131–139.

[14] S. Yin, K. Chen, C. Srinivasakannan, S. Li, J. Zhou, J. Peng, L. Zhang, Microfluidic solvent extraction of Ce (iii) and Pr (iii) from a chloride solution using EHEHPA (P507) in a serpentine microreactor, Hydrometallurgy 175 (2018) 266–272.

[15] C. Priest, J. Zhou, R. Sedev, J. Ralston, A. Aota, K. Mawatari, T. Kitamori, Microfluidic extraction of copper from particle-laden solutions, International Journal of Mineral Processing 98 (3-4) (2011) 168–173.

[16] J. M. Coulson, J. F. Richardson, J. R. Backhurst, J. H. Harker, Particle technology and separation processes, Vol. 2, Pergamon Press, 1991.

[17] A. Sahu, A. B. Vir, L. S. Molleti, S. Ramji, S. Pushpavanam, Comparison of liquid-liquid extraction in batch systems and micro-channels, Chemical Engineering and Processing: Process Intensification 104 (2016) 190–200.

[18] K. Singh, A. Renjith, K. Shenoy, Liquid–liquid extraction in microchannels and conventional stage-wise extractors: a comparative study, Chemical Engineering and Processing: Process Intensification 98 (2015) 95–105.

[19] M. Darekar, N. Sen, K. Singh, S. Mukhopadhyay, K. Shenoy, S. Ghosh, Liquid–liquid extraction in microchannels with Zinc–D2EHPA system, Hydrometallurgy 144 (2014) 54–62.

[20] F. K. Crundwell, Extractive metallurgy of nickel, cobalt and platinum group metals, Elsevier, 2011.

[21] F. Crundwell, The dissolution and leaching of minerals: Mechanisms, myths and misunderstandings, Hydrometallurgy 139 (2013) 132–148.

[22] S. Kotova, B. Follink, L. Del Castillo, C. Priest, Leaching gold by reactive flow of ammonium thiosulfate solution in high aspect ratio channels: Rate, passivation, and profile, Hydrometallurgy 169 (2017) 207–212.

[23] D. Yang, C. Priest, Microfluidic platform for high-throughput screening of leach chemistry, Analytical Chemistry.

[24] P. Kondos, G. Deschênes, R. Morrison, Process optimization studies in gold cyanidation, Hydrometallurgy 39 (1-3) (1995) 235–250.

[25] H. Yilmaz, Stream sediment geochemical exploration for gold in the Kazdağ dome in the Biga Peninsula, western Turkey, Turkish Journal of Earth Sciences 16 (1) (2007) 33–55.

[26] W. Srithammavut, S. Luukkanen, A. Laari, T. Kankaanpää, I. Turunen, Kinetic modelling of gold leaching and cyanide consumption in intensive cyanidation of refractory gold concentrate., Journal of the University of Chemical Technology & Metallurgy 46 (2).

[27] A. M. Nazari, A. Ghahreman, S. Bell, A comparative study of gold refractoriness by the application of QEMSCAN and diagnostic leach process, International Journal of Mineral Processing 169 (2017) 35–46.

[28] E. Oraby, J. Eksteen, B. Tanda, Gold and copper leaching from gold-copper ores and concentrates using a synergistic lixiviant mixture of glycine and cyanide, Hydrometallurgy 169 (2017) 339–345.

[29] M. C. Cetin, N. E. Altun, M. Ü. Atalay, K. Büyüktanır, Bottle roll testing for cyanidation of gold ores: Problems related to standardized procedures on difficult-to-process ores, Proceedings of the 3rd World Congress on Mechanical, Chemical, and Material Engineering.

[30] L. Saria, T. Shimaoka, K. Miyawaki, Leaching of heavy metals in acid mine drainage, Waste Management & Research 24 (2) (2006) 134–140.

[31] P. Schwab, D. Zhu, M. Banks, Heavy metal leaching from mine tailings as affected by organic amendments, Bioresource Technology 98 (15) (2007) 2935–2941.

[32] V. Cappuyns, R. Swennen, The use of leaching tests to study the potential mobilization of heavy metals from soils and sediments: a comparison, Water, air, and soil pollution 191 (1-4) (2008) 95–111.

[33] E. Martens, H. Zhang, H. Prommer, J. Greskowiak, M. Jeffrey, P. Roberts, In situ recovery of gold: Column leaching experiments and reactive transport modeling, Hydrometallurgy 125 (2012) 16–23.

[34] W. Hartley, N. M. Dickinson, R. Clemente, C. French, T. G. Piearce, S. Sparke, N. W. Lepp, Arsenic stability and mobilization in soil at an amenity grassland overlying chemical waste (St. Helens, UK), Environmental pollution 157 (3) (2009) 847–856.

[35] C. Abbruzzese, P. Fornari, R. Massidda, F. Veglio, S. Ubaldini, Thiosulphate leaching for gold hydrometallurgy, Hydrometallurgy 39 (1-3) (1995) 265–276.

[36] R. K. Asamoah, W. Skinner, J. Addai-Mensah, Alkaline cyanide leaching of refractory gold flotation concentrates and bio-oxidised products: The effect of process variables, Hydrometallurgy 179 (2018) 79–93.

[37] H. Arima, T. Fujita, W.-T. Yen, Using nickel as a catalyst in ammonium thiosulfate leaching for gold extraction, Materials Transactions 45 (2) (2004) 516–526.

[38] E. Bidari, V. Aghazadeh, Alkaline leaching pretreatment and cyanidation of arsenical gold ore from the Carlin-type Zarshuran deposit, Canadian Metallurgical Quarterly (2018) 1–11.

[39] A. D. Bas, E. Ghali, Y. Choi, A review on electrochemical dissolution and passivation of gold during cyanidation in presence of sulphides and oxides, Hydrometallurgy 172 (2017) 30–44.

[40] M. G. Hasab, S. Raygan, F. Rashchi, Chloride-hypochlorite leaching of gold from a mechanically activated refractory sulfide concentrate, Hydrometallurgy 138 (2013) 59–64.

[41] M. Lampinen, A. Laari, I. Turunen, Ammoniacal thiosulfate leaching of pressure oxidized sulfide gold concentrate with low reagent consumption, Hydrometallurgy 151 (2015) 1–9.

[42] D. Murthy, V. Kumar, K. Rao, Extraction of gold from an indian low-grade refractory gold ore through physical beneficiation and thiourea leaching, Hydrometallurgy 68 (1-3) (2003) 125–130.

[43] R. Sousa, A. Futuro, A. Fiúza, M. Vila, M. Dinis, Bromine leaching as an alternative method for gold dissolution, Minerals Engineering 118 (2018) 16–23.

[44] C. Shi, Y. Nie, F. Zi, Q. Wang, Y. Chen, H. Yu, Effect of tetrathionate on thiosulfate leaching of gold in copper–ammonia system, Asia-Pacific Journal of Chemical Engineering 13 (2) (2018) e2173.

[45] S. Anand, R. Das, P. Jena, Sulphuric acid pressure leaching of Cu/Ni/Co matte obtained from copper converter slag-optimisation through factorial design, Hydrometallurgy 26 (3) (1991) 379–388.

[46] B. Tanda, E. Oraby, J. Eksteen, Kinetics of malachite leaching in alkaline glycine solutions, Mineral Processing and Extractive Metallurgy (2018) 1–9.

[47] B. Tanda, J. Eksteen, E. Oraby, Kinetics of chalcocite leaching in oxygenated alkaline glycine solutions, Hydrometallurgy 178 (2018) 264–273.

[48] B. Tanda, J. Eksteen, E. Oraby, An investigation into the leaching behaviour of copper oxide minerals in aqueous alkaline glycine solutions, Hydrometallurgy 167 (2017) 153–162.

[49] L. Zhang, W. Guo, J. Peng, J. Li, G. Lin, X. Yu, Comparison of ultrasonic-assisted and regular leaching of germanium from by-product of zinc metallurgy, Ultrasonics sonochemistry 31 (2016) 143–149.

[50] Y.-F. Zhang, J. Ma, Y.-H. Qin, J.-F. Zhou, L. Yang, Z.-K. Wu, T.-L. Wang, W.-G. Wang, C.-W. Wang, Ultrasound-assisted leaching of potassium from phosphorus-potassium associated ore, Hydrometallurgy 166 (2016) 237–242.

[51] R. Swain, R. B. Rao, Application of response surface methodology on leaching of iron from partially laterised khondalite rocks: A bauxite mining waste, Journal of The Institution of Engineers (India): Series D (2017) 1–9.

[52] S. M. S. Ghasemi, A. Azizi, Alkaline leaching of lead and zinc by sodium hydroxide: kinetics modeling, Journal of Materials Research and Technology 7 (2) (2018) 118–125.

[53] V. Singh, R. Rautela, K. S. Durbha, Y. R. Murthy, Study of the kinetics of the magnesium leaching from serpentine bearing chromite overburden rocks for mineral carbonation, Mineral Processing and Extractive Metallurgy (2018) 1–8.

[54] J. I. Ordóñez, L. Moreno, J. F. González, L. A. Cisternas, Use of discharged brine from reverse osmosis plant in heap leaching: Opportunity for caliche mining industry, Hydrometallurgy 155 (2015) 61–68.

[55] J. Johnson, B. Cashmore, R. Hockridge, Optimisation of nickel extraction from laterite ores by high pressure acid leaching with addition of sodium sulphate, Minerals Engineering 18 (13-14) (2005) 1297–1303.

[56] J. Kang, G. Senanayake, J. Sohn, S. M. Shin, Recovery of cobalt sulfate from spent lithium ion batteries by reductive leaching and solvent extraction with Cyanex 272, Hydrometallurgy 100 (3-4) (2010) 168–171.

[57] F. Veglio, M. Trifoni, C. Abbruzzese, L. Toro, Column leaching of a manganese dioxide ore: a study by using fractional factorial design, Hydrometallurgy 59 (1) (2001) 31–44.

[58] M. Brittan, G. Plenge, Estimating process design gold extraction, leach residence time and cyanide consumption for high cyanide-consuming gold ore., Minerals & Metallurgical Processing 32 (2).

[59] E. Ahlberg, A. E. Broo, Electrochemical reaction mechanisms at pyrite in acidic perchlorate solutions, Journal of The Electrochemical Society 144 (4) (1997) 1281–1286.

[60] C. Weisener, R. Smart, A. R. Gerson, Kinetics and mechanisms of the leaching of low fe sphalerite, Geochimica et Cosmochimica Acta 67 (5) (2003) 823–830.

[61] Y. Liu, Z. Dang, P. Wu, J. Lu, X. Shu, L. Zheng, Influence of ferric iron on the electrochemical behavior of pyrite, Ionics 17 (2) (2011) 169–176.

[62] M. Sattari-Najafabadi, M. N. N. Esfahany, Intensification of liquid-liquid mass transfer in a circular microchannel in the presence of sodium dodecyl sulfate, Chemical Engineering and Processing: Process Intensification 117 (2017) 9–17.

[63] S. Simi, M. Janaki, K. Bhat, P. Das, Microwave acid leaching of beneficiated ilmenite for the production of synthetic rutile.

[64] W. Astuti, T. Hirajima, K. Sasaki, N. Okibe, Comparison of effectiveness of citric acid and other acids in leaching of low-grade indonesian saprolitic ores, Minerals Engineering 85 (2016) 1–16.

[65] D. Ciceri, A. Allanore, Microfluidic leaching of soil minerals: Release of K+ from K feldspar, PloS one 10 (10) (2015) e0139979.

Chapter 5

Electrokinetic study on leaching gold using alkaline glycine

ABSTRACT

In-situ leaching is gaining potential as an alternative mining method for metal ores. In particular, electrokinetic in-situ leaching (EK-ISL) is a technique that has been introduced fairly recently in the mining and minerals realm with promising outcomes so far. This method consists of using a voltage gradient to enhance the transport of ions from low-permeable ore bodies by applying electric current through the reagents (lixiviant and porous ore). In this study, we examine the potential of Gly^- as a lixiviant to leach gold through materials of low-permeability consisting of micro-silica sand and gold powder. An experimental campaign was designed based on five different stages by varying the difference of voltage: 0, 5, 10, 20 and 30 V. Each stage took 4 days irrespective of the level of leaching. The effects of copper and sulfide minerals were evaluated by adding 10% chalcopyrite and pyrite to the system. The results show that gold recovery increases when the difference of voltage increases. In addition, the obtained data suggest that gold recovery decreases in the presence of chalcopyrite and pyrite.

5.1 Introduction

It has become increasingly challenging to excavate ore bodies using open pit or underground mining due to the environmental footprint that these conventional methods entail. Moreover, the deletion of close to surface resources has driven operators to target deeper ore bodies, which requires the management of larger amounts of waste at greater depth. Depending on the commodity and the conditions of mining, the extraction process can be prohibitively costly compared to ore bodies at accustomed depth. Increasing costs of processing, accumulation of tailing, monitoring and management along with the variable commodity prices concern the mining industry as they can potentially lead to reduced profitability [1]. In situ leaching (ISL) is gaining momentum as an alternative mining method that reduces the cost and environmental footprint of mining operations. ISL is the "removal of valuable components of a mineral deposit without physical extraction of the rock" [2]. In ISL, reagents are injected into the ore body through a network of bores;

pregnant solution are then extracted through production bores and treated at plants to produce a high concentrate solution of the target metal [1]. However, the ore body is required to have high permeability and to be hydrogeologically confined to allow a uniform distribution of fluids that interact with valuable metals and prevent the loss of lixiviant [3].

Sandstone uranium deposits are favourable conditions for ISL mining in several countries including Kazakhstan, Uzbekistan, Australia, China, Russia, and USA [1]. Copper recovery with ISL has also been successfully undertaken in North America [4]. However, it has been revealed that sufficient permeability is required for reagents to reach the minerals of interest in the ore body [2, 5, 6]. In the late 1980s, seepage of very weak cyanide solutions into a mine workings from tailings caused the leaching of gold in the Northwest Territories (Canada). The pregnant cyanide-gold solution was discovered when water was pumped from the mine underground workings. It was the first known gold ISL using processing water and resulting in gold recovery [4]. Gold ISL was also proposed at Eastville (central Victoria, Australia) in 1980 [7]. After initial pump and dye tracer tests all approvals were denied because of raising concerns of possible groundwater contamination with cyanide [8].

Unlike uranium deposits that are permeable enough for lixiviants to reach the mineral, the majority of gold deposits have low hydraulic conductivities [3]. It should be mentioned that there is a distinction between porosity and permeability enhancement in ore bodies prone to ISL. For example, fracturing improves lixiviant distribution rather than porosity. However, the reaction of lixiviant with gangue can either increase porosity by dissolution or decrease it by precipitation. For ores with low porosity, fracturing can play a key role in permeating the rock mass in order to reach target metals such as gold, copper, and nickel [4]. Many challenging methods have been proposed to enhance permeability at depth including hydraulic fracturing [9, 10], horizontally oriented fracture pattern [11] and even nuclear underground blasting [12], often causing controversies. Recently, Orica Australia discussed the possibility to create confined ISL compartments in the ore bodies by drilling and blasting [13].

[3] proposed to employ electrokinetic in-situ leaching (EK-ISL) to accelerate the transport of ions where ISL has limited impact on low-permeability ore bodies. The concept consists of using an electric field to induce a uniform migration of ions through from target metals to collection reservoirs. These authors conducted an experimental campaign using iodide and tri-iodide mixture to leach gold in a low-permeability conditions. Their experimental work shows a full gold recovery within 4 days. Identifying an eco-friendly solution to leach metals such as gold, silver and copper from ores is of ultimate significance to the research community. Cyanide is the standard and robust substance that leaches gold from low grade secondary processing pads. However, it has toxicity limitation to be used for in-situ recovery. Therefore, other reagents that have less toxicity and environmental footprint have been investigated through recent research initiatives. For example, thiosulphate, acidic thiocyanate, halides, thiourea, organic reagents, and glycine have been examined as potential alternatives to cyanide [14–18]. In recent years, there is an increasing interest in studying the ISL of gold using non-cyanide systems such as iodide [3, 19]. Given the progress on understanding the interaction of amino acids with precious metals [20], we evaluate EK-ISL approach using glycine as an environmentally friendly lixviant. The effect of pH and temperature on the leach of gold in amino acids has been examined by [21]. It

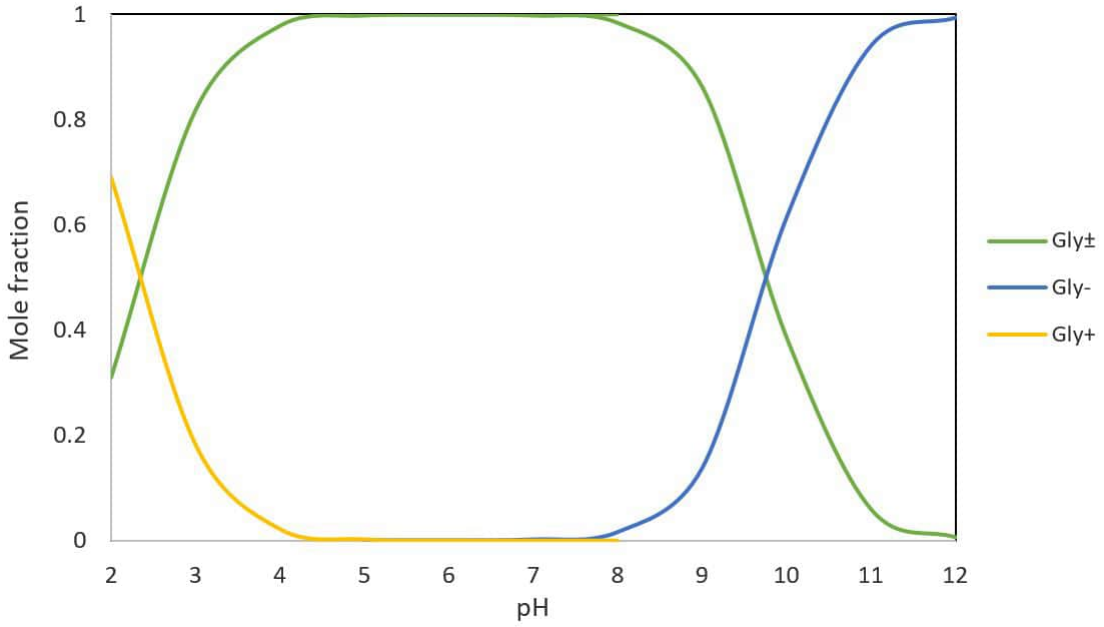

Figure 5.1: Mole fraction and dissociation change of Gly as a function of pH at 25^{o}C. It can be seen that $Gly^{\pm}$ and Gly^{-} exist in approximately equal mole fraction at pH values of about 9.79. $GlyGly^{\pm}$ and $GlyGly^{-}$ are equal at pH values of about 8.27 at 25^{o}C.

has been shown that the presence of hydrogen peroxide can enhance the recovery of gold using amino acids [22]. Recently, new studies have been conducted on the leaching of gold using alkaline glycine as an environmentally friendly lixiviant [18, 23–25]. The results are promising and seems to attract the interest of major mining operators. In this study, we designed and constructed an experimental apparatus inspired by [3] and modified to apply temperature up to 60^{o}C.

5.2 Choice of lixiviant

Behaviour of glycine in aqueous solutions under various conditions of pH and temperature has been explained in chapter 1 of this thesis. Despite the importance of glycine as a promising substance of mineral processing, its behaviour in aqueous solution has not been investigated comprehensively yet. Therefore, we intend to bridge this gap by evaluating the role of alkaline glycine in the leaching of gold in chapter 1 of this thesis.

Glycine (NH_2CH_2COOH) has three dissociation states in water, namely glycinium cation $^+H_3NCH_2COOH$ (Gly^+), zwitterion $^+H_3NCH_2COO^-$ ($Gly^{\pm}$), and glycinate anion H2NCH2COO$^-$ (Gly^-). The equilibrium concentration of Non-Zwitterionic forms is negligible at room temperature [41].

Fig.5.1 shows the dissociation states of Gly and how they change with respect to pH at temperatures 25^{o}C [42]. It can be seen that $Gly^{\pm}$ and Gly^{-} exist in approximately equal mole fractions at pH values of about 9.79. Similarly, the mole fraction of Gly^pm and Gly^+ are equal at pH values of about 2.34 at 25^{o}C.

Many studies have been done on the stability of metal and glycine complexes. Although metals can react with three dissociation states of Gly, existing studies have revealed that the reaction with the glycinate anion (Gly^-) is the most effective [44–46]. The following

equation shows the gold dissolution reaction where the amino acid glycine is a ligand [47]:

$$2\mathrm{Au} + 4\,\mathrm{NH_2CH_2COOH} + 2\mathrm{NaOH} + \mathrm{H_2O_2} = 2\mathrm{Na[Au(NH_2CH_2COO)_2]} + 4\mathrm{H_2O} \quad (5.1)$$

or in simple notation

$$\mathrm{Au} + 2\mathrm{Gly}^- \Leftrightarrow \mathrm{Au(Gly)}_2^- \quad (5.2)$$

where $\log_{10} K$ for the Eq. 5.1 is equal to 15.45±0.48 at temperature 25^{o}C [20].

As explained in chapter 1 of this thesis, and given the range of temperature from 25^{o}C to 100^{o}C and the corresponding pH from 10.4 to 12, a temperature-pH domain centred around 60^{o}C and pH 11 is the optimal window where Gly can be used as an alkaline lixiviant for metals such as Au (Fig. 1.9). Using high temperatures has its own shortcomings as water reaches its boiling point, but also because the process becomes more energy demanding and less cost-effective. However, for in-situ leaching, temperature may play an important role depending on the ore body depth as temperature increases with depth. Factors such temperature and pH have a direct influence on metal-glycinate reactions and need to be studied extensively both in terms of kinetics and thermodynamics.

5.3 Experimental design

The apparatus is an upgraded version of the design of [3, 49] to take the temperature into account. The apparatus made of Ploy vinyl chloride (PVC) pipes (ϕ = 70mm) consists of five reservoirs as shown in Fig. 5.2. Cathode and anode electrodes were placed in the outer reservoirs (mixed metal-oxide titanium from McCoy Engineering - Osborne Park, Australia). Deionized (DI) water and 100mM NaCl were used to make the electrolyte solutions as recommended by [3]. The source reservoir contained an alkaline glycine solution (1M glycine, 0.5% H_2O_2, 0.1M NaCl, pH= 10 to 11). The target reservoir was filled with the electrolyte solution. The middle reservoir was used to resemble very low permeability ore which contained a slurry mixed of a non-reactive quartz powder (<10μm), gold powder (<10μm and purity >99.9) and 0.1M NaCl solution. It should be mentioned that NaCl was used to enhance the conductivity of the liquid throughout the apparatus. All chemicals were purchased from Sigma-Aldrich. All solution samples were prepared using a beaker with a magnetic stirrer on a hot plate. The stirring process lasted for at least 1 hour until a clear solution was obtained. Temperature and pH were regularly checked until stable conditions were reached. The apparatus was placed in a water bath to keep the temperature at about 57±2^{o}C. The water bath was covered by a transparent sheet and all reservoir were capped to avoid evaporation. However, a small amount of evaporation was unavoidable due to regular monitoring and sampling. The effect of copper and sulfide minerals were evaluated by using 10% fine chalcopyrite and by adding 10% fine pyrite to the source reservoir in two separate experiments.

The experiment is to apply Direct Current (DC) power with a constant voltage through the electrodes. Consequently, Gly^- ions from the source reservoir is transported in the Cathode-Anode direction through the low permeability media in the middle reservoir (hosting the gold powder). Gly^- ions leaches the gold, AuGly_2^- is formed and migrated in the same direction toward the target reservoir. A cation exchange membrane (CEM) was

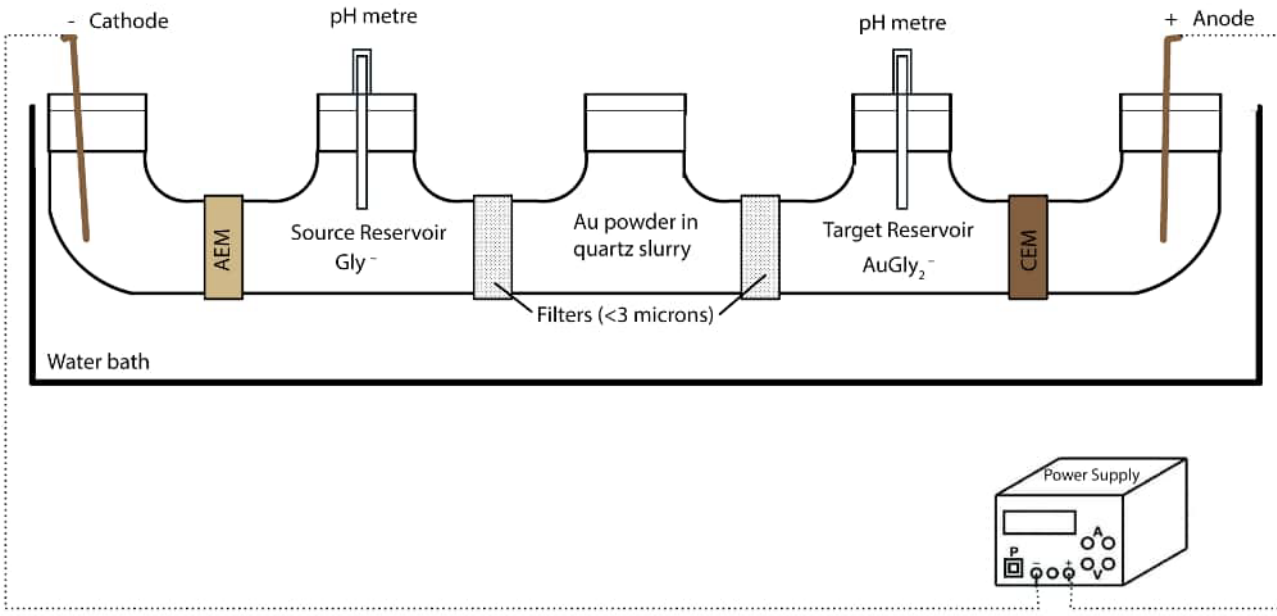

Figure 5.2: Laboratory-sacled of an experimental EK-ISL to leach the gold using alkaline glycine. AEM and CEM are anion exchange and cation exchange membranes, respectively.

used to avoid gold-glycine complexes reaching to the anode electrode. An anion exchange membrane (AEM) was used to separate the cathode and the source reservoir. These membranes were purchased from Membrane International Inc. (Ringwood, USA).

As [3] recommended, hydrochloric acid (4M HCl) and sodium hydroxide (4M NaOH) were regularly added to the cathode and anode reservoirs, respectively, to control the pH. This compensates for the electrolysis of water which produces hydroxyl (OH^-) and hydrogen (H^+) ions in the cathode and anode reservoirs, respectively [50]. A small hole was made in the anode and cathode caps to allow produced gases (H_2, O_2) to escape. All reservoirs were filled the same level, and refilled using DI-water in the case of evaporation.

To fill and place the gold powder in the middle reservoir, care was taken to prevent loosing gold mass during the placement. Quartz slurry was made by mixing silica powder with a 0.1 mol/l NaCl solution and placed in the reservoir. About halfway up, 20mg of gold powder mixed with the quartz slurry was embedded in the middle of the reservoir in the form of a planar layer. Over time, silica powder settled down and about 10mm liquid formed at the top, which was kept in place. 3μm-meshed filter sheets (Sefar Pty Ltd, Australia) and geotextile fabrics were fixed by plastic rings to separate the middle reservoir from the source and target reservoirs.

Seven sets of experiments were designed to examine the potential of gold EK-ISL using alkaline glycine. Table 5.1 shows the different stages of 0 to 30 Volts that were applied. In the first five experiments, only voltage was changed as the control parameter. In the last two experiments, 10% chalcopyrite and 10% pyrite were added separately to the source reservoir to evaluate their effects on gold leaching in the presence of glycine. Each experiment was undertaken for 4 days and samples were taken after every 24 hours. It needs to be mentioned that 4-days period was selected to have safe conditions of leaching; longer periods may loosen the connections between the different PVC compartments while

Experiment No.	Time Periode	Voltage
EK-0	4 day	0 V
EK-5	4 day	5 V
EK-10	4 day	10 V
EK-20	4 day	20 V
EK-30	4 day	30 V
EK-20 (10% Chalcopyrite)	4 day	20 V
EK-20 (10% Pyrite)	4 day	20 V

Table 5.1: Experimental design in 5 different stages of voltage.

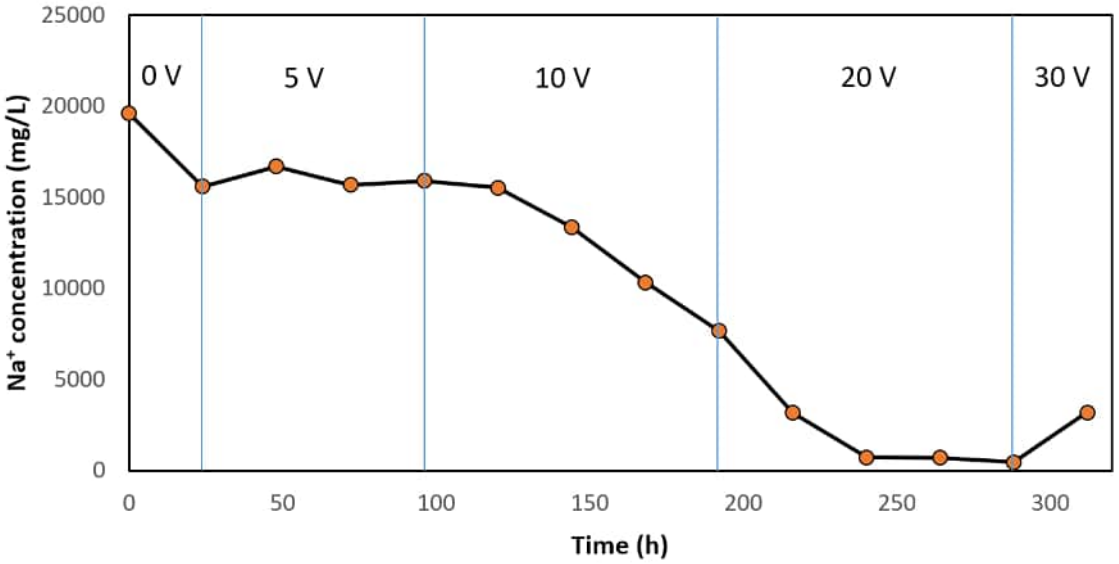

Figure 5.3: Na^+ concentration in the target reservoir at each stage of applied voltage.

the apparatus was placed in a water bath with 57±2^{o}C. Each time, a 10ml sample was taken, diluted in a 100ml pycnometer and sent for chemical analysis using ICP-MS at School of Agriculture and Environment, the University of Western Australia. Samples were taken from source and target at each stage. When the experiment was completed, quartz slurry, AEM, CEM and electrodes are washed, and samples were taken from the liquids for chemical analysis.

5.4 Results and discussions

EK-ISL produces a voltage gradient that transports ions through low permeability media [3]. In our experiment, Gly^- was used as the lixiviant in the electrokinetic process. It should be mentioned that we used the term “low permeability" instead of “impermeability" as the middle reservoir (gold and sands) contains essentially small size particles. To verify the apparatus, a first test named EK-0 with 0 voltage was remained for 4 days. The results show no Au recovery, which means there is no ion transport through the middle reservoir. Fig.5.3 and Fig.5.4 show the Na^+ and Cl^- concentrations in target reservoir. It can be seen that Na^+ decreases and Cl^- increases in target reservoir due to the applied current.

Fig.5.5 shows an overview of Au recovery, which is increasing with voltage over 16 days. As can be seen in Fig.5.6, EK-10 (10 V) exhibits higher recovery rate during 4 days in

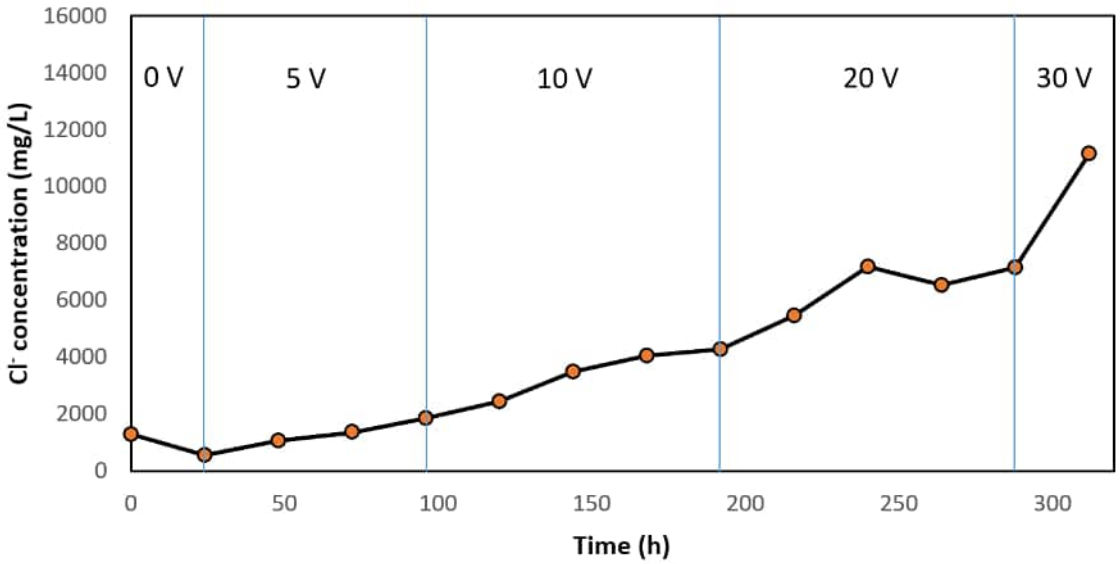

Figure 5.4: Cl^- concentration in the target reservoir at each stage of applied voltage.

comparison with EK-5 and EK-20. This behaviour can be explained by the pH changes in the target reservoir that may have affected the voltage gradient.

After applying a voltage gradient through the apparatus (tests EK-5, EK-10, EK20 and EK-30), Au concentration in target reservoir increased over time, which suggests that the voltage gradient causes ions to migrate through the middle reservoir in the cathode-anode direction. Samples were collected from the source and target reservoirs and analysed, but no Au was detected in source reservoir. As shown in Fig.5.6, ramping up the voltage increases the concentration of Au in the target reservoir. The maximum accumulated recovery of Au for each stage (5 V, 10 V, 20 V and 30 V) after 16 days of leaching is shown in Fig.5.5. Although the maximum recovery of gold is enhanced by voltage increment, the concentration of gold slowly grows in each experiment day-by-day.

Fig. 5.7 depicts the variation of Au recovery with respect to time based on different applied voltages. This figure confirms that the maximum rate of recovery has been obtained at EK-10, but does not necessarily suggest that this voltage is the optimum because the concentration of gold reduces with time. It certainly indicates that enhancing the voltage gradient during the process can boost the recovery after the transition from 5 V to 10 V. Fig. 5.8 shows the variation of pH in target reservoir, which was initially adjusted to around 11. The pH in the source reservoir was controlled to be around 11 and the pH in the target reservoir was monitored continuously. As can be seen in Fig. 5.8, pH dropped when voltage increased, demonstrating the transportation of anions to the target reservoir. Anions could not reach to the anode because of CEM barrier. Therefore, it is possible that increasing anion in target reservoir influences the rate of ion transportation as shown in Fig.5.7, in which EK-10 (10 V) shows higher growth compared to EK-20 and EK-30.

The total recovery of Au after 16 days is not stellar; the reason could be attributed to the use of H_2O_2 as an oxidant. Although the size of H_2O_2 molecules is small enough to reach to the gold particles in the middle reservoir, it cannot be transport by voltage gradient. An alternative oxidant that is amenable to electrokinetic transport may increase the efficiency of EK-ISL. However, the benefit of using Gly^- is that it can leach metals such as gold

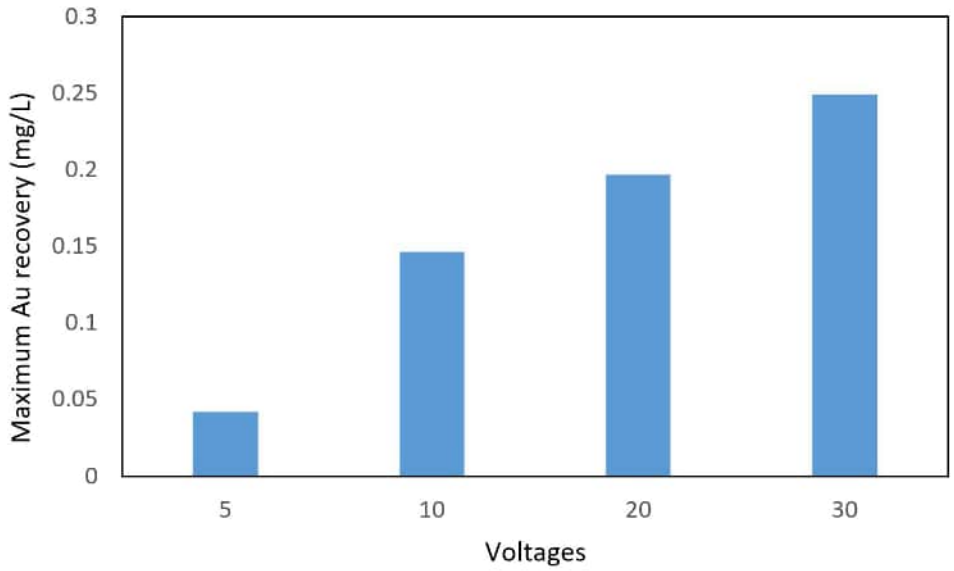

Figure 5.5: Maximum accumulated Au recovery at each stage of applied voltage during 16 days of leaching

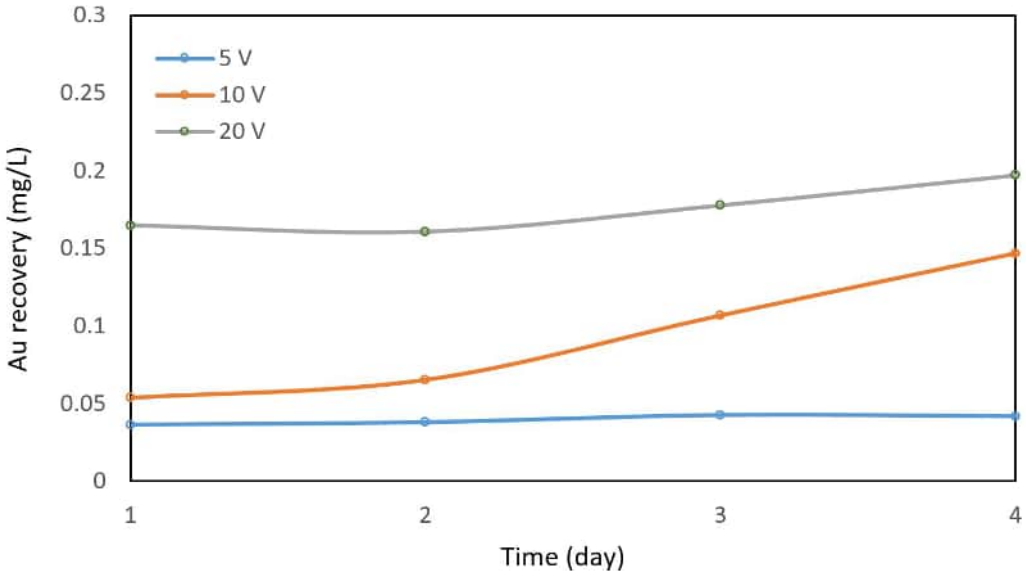

Figure 5.6: Au recovery in 4 days for different voltages.

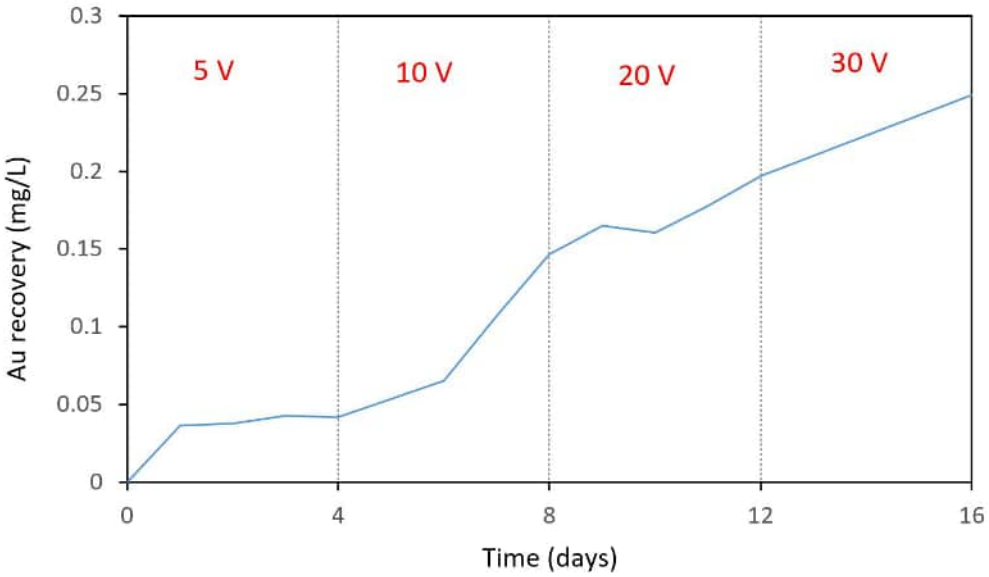

Figure 5.7: Total Au recovery in 16 days for all voltages.

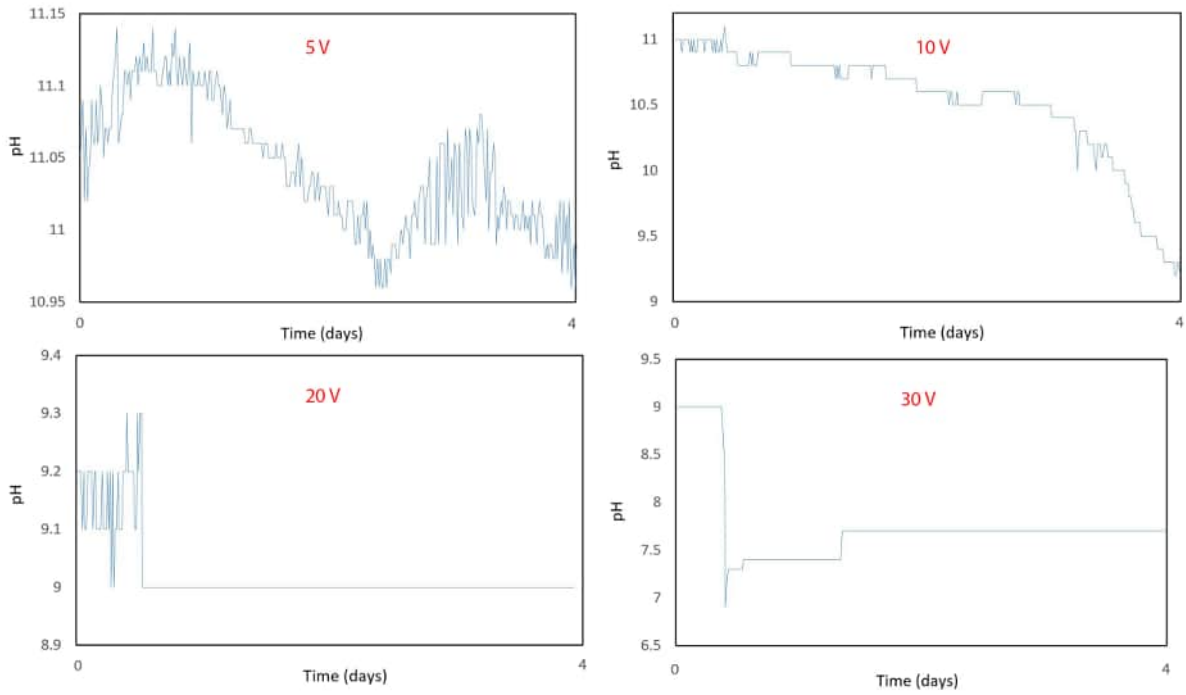

Figure 5.8: pH changes in the target reservoir during each experimental phase.

even without oxygen, but the process is relatively slow in the absence of oxygen [20]. It is important to note that most of reagents introduced for ISL applications need oxygen, which may be challenging at the depth.

5.5 Effect of pyrite and chalcopyrite on leaching gold

The existence of gangue minerals in the ore body may affect the leaching of gold [51]. Pyrite (FeS_2) is a common mineral that is known to decrease the gold leaching possibly due to the consumption of oxygen by pyrite. Although amino acids can dissolve gold even in the absence of oxygen, the rate of leaching decreases dramatically in such circumstances. Pyrite can consume large quantities of oxygen, which jeopardises the gold leaching using glycine. Eq. 5.3 depicts the oxidation of pyrite in hydrogen peroxide [52].

$$FeS2 + 15/2H2O2 = Fe^{3+} + 2SO_4^{2-} + H^+ + 7H2O \tag{5.3}$$

[53] studied the electrochemical dissolution of gold using cyanide in the presence of sulfide minerals including pyrite. The data indicated that these sulfide minerals are more noble than gold (they are not oxidized at more negative potentials than gold). This study explained the effects of sulfide minerals on gold leaching by two mechanisms, namely the galvanic interaction and the dissolution of sulphide minerals. The first mechanism of galvanic interaction is relevant when gold is contact with a sulfide mineral; higher cathodic currents shift the mixed potential more positively, which increases the leaching rate of gold. The second mechanism is related to the dissolution of sulfide minerals in cyanide, which generates new species and thereby impacts the leaching of gold.

Gold leaching in the presence of pyrite can be complicated as dissolved species can hinder the process. When glycine is a reagent, Fe^{3+} can make complexes with Gly^- [20] and affect gold leaching by consuming the Gly^-. In this study, 10% pyrite was used to evaluate its impact on gold leaching through EK-ISL (Table 5.1). The results show that adding pyrite to the system dramatically reduces gold leaching as indicated in Fig.5.9. The figure shows that the concentration of gold in the target reservoir increases with time, but at a much lower rate than in the absence of pyrite. Fe^3+ can be shifted to the cathode side and made complexes with Gly^-. Fe^3+ can also make neutral ions/complexes, which cannot be transferred through electric current and may prevent gold from reacting with Gly^- in the source reservoir. Analysis of the possible anions and cations in the system can be complicated due to existing current in the system affecting transfer towards the anodic or cathodic sides. However, our experiment shows low gold recovery in the presence of pyrite. Fig.5.10 indicates the total N concentration in the target reservoir, which can be represent Gly that contains N. The figure shows a maximum concentration of 3.4 g/L which is very low compared to gold recovery in the absence of pyrite (about 10 g/L). This difference shows that the presence of pyrite reduces the electrokinetic transport of Gly^-.

Copper can be leached from chalcopyrite in an alkaline glycine solution at various temperatures in the presence of oxygen [54]. By using an ore sample from the cyclone underflow of a copper-gold plant in Western Australia, these authors reported the presence of intact pyrite and very low concentration of iron in the pregnant solution. Eq. 5.4 describes the leaching of copper in an alkaline glycine solution. Copper glycinate can form

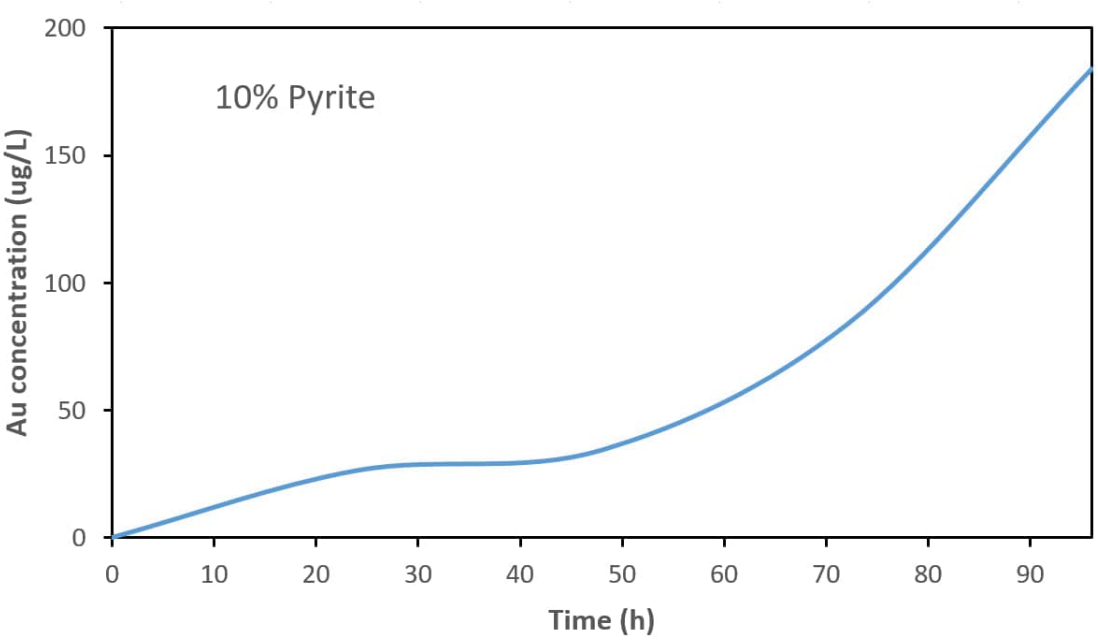

Figure 5.9: leaching gold in the presence of 10% pyrite.

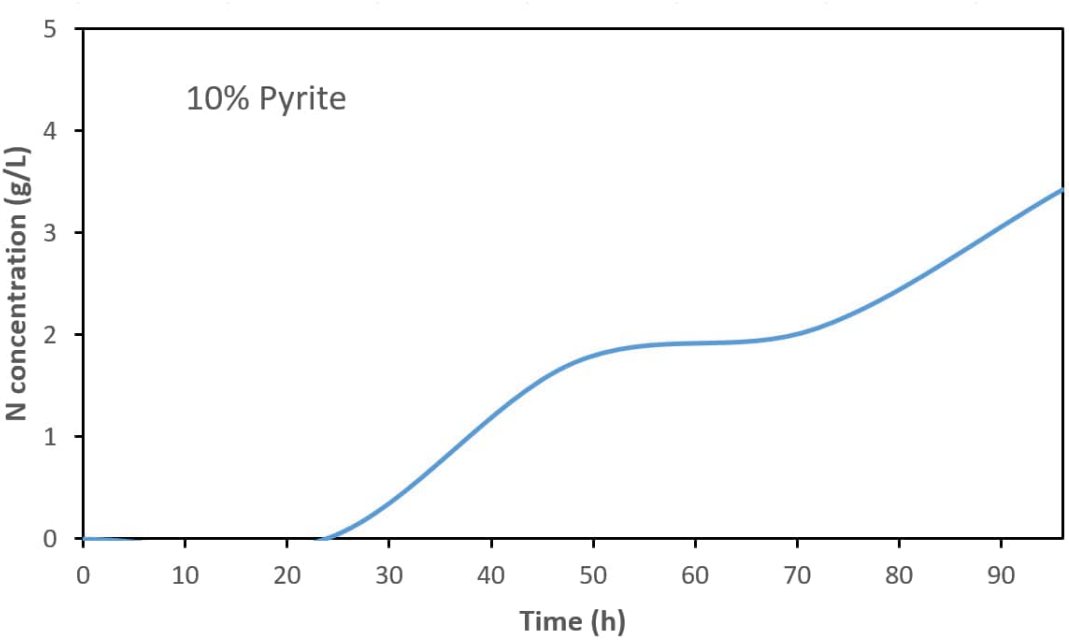

Figure 5.10: Concentration of total N in the target reservoir representing the concentration of Gly.

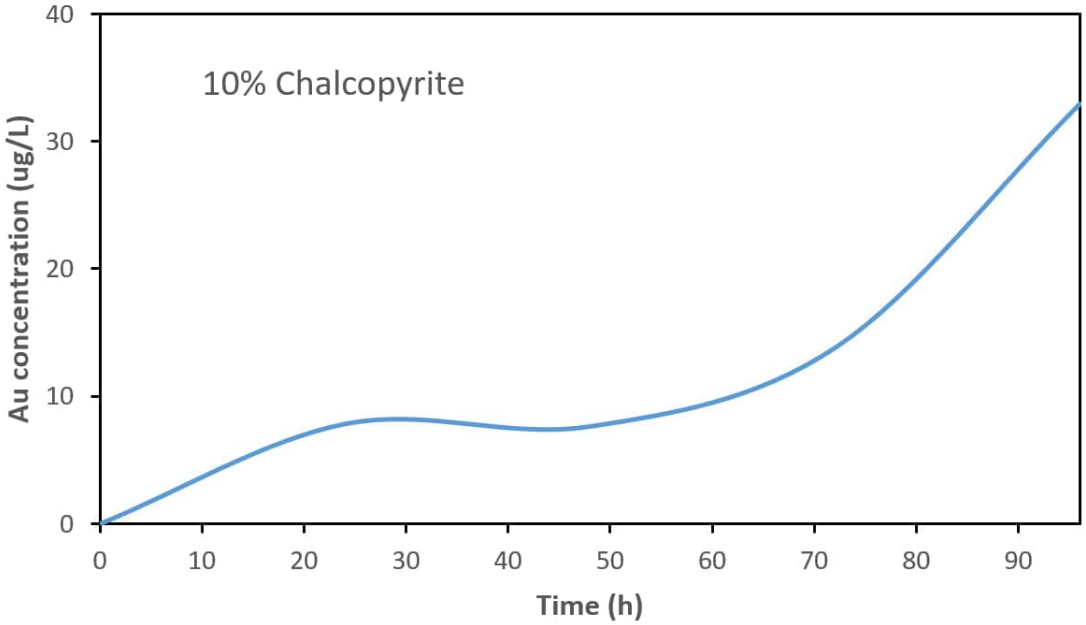

Figure 5.11: Au concentration in the target reservoir.

through Eqs. 5.5 and 5.6 depending on the concentration of copper and glycine [20].

$$CuFeS_2+2NH_2CH_2COO^-+4.25O_2+3OH^- = Cu(NH_2CH_2COO)_2+FeO(OH)+2SO_4{}^{2-}+2H_2O \tag{5.4}$$

$$Cu^{2+} + 2NH_2CH_2COO^- \Leftrightarrow Cu(NH_2CH_2COO)_2 \tag{5.5}$$

$$Cu^{2+} + NH_2CH_2COO^- \Leftrightarrow Cu(NH_2CH_2COO)^+ \tag{5.6}$$

As shown in Fig.5.11, the recovery of gold is reduced remarkably in the presence of chalcopyrite. This can be attributed to the more favourable reactivity of alkaline glycine with copper than gold as explained above [55]. It also may be explained by the precipitation of copper oxides on the surface of the mineral. Copper and iron precipitates can occur in glycine solutions in the form of CuO, Cu_2O, and iron oxy-hydroxides [**? ?**]. Precipitates can form on mineral surfaces adjacent to the glycine solution, which can reduce the recovery of gold. Fig.5.13 shows the total nitrogen concentration representing the glycine concentration in the presence of chalcopyrite; it can be seen that the concentration of glycine (indicated by the concentration of N) increases over the time. This increasing concentration remains lower than ones recorded in the absence of chalcopyrite. The voltage measured during the experiment was quite different from the applied voltage, which was fixed at 20 V all the time. This reduction may be explained by the cathodic current shift affecting the voltage potential due to the production of cations. Fig.5.11 shows the existing voltage changes during the experiment.

Based on the results of this experiment, EK-ISL for gold leaching may be more effective for weathered ores rich in oxides. It should be mentioned that the only transporting force in this experiment is electric current. Therefore, the effect of pyrite and chalcopyrite on the gold leaching using alkaline glycine may be addressed by other factors if EK is not applied. These factors include agitation and fluid flow.

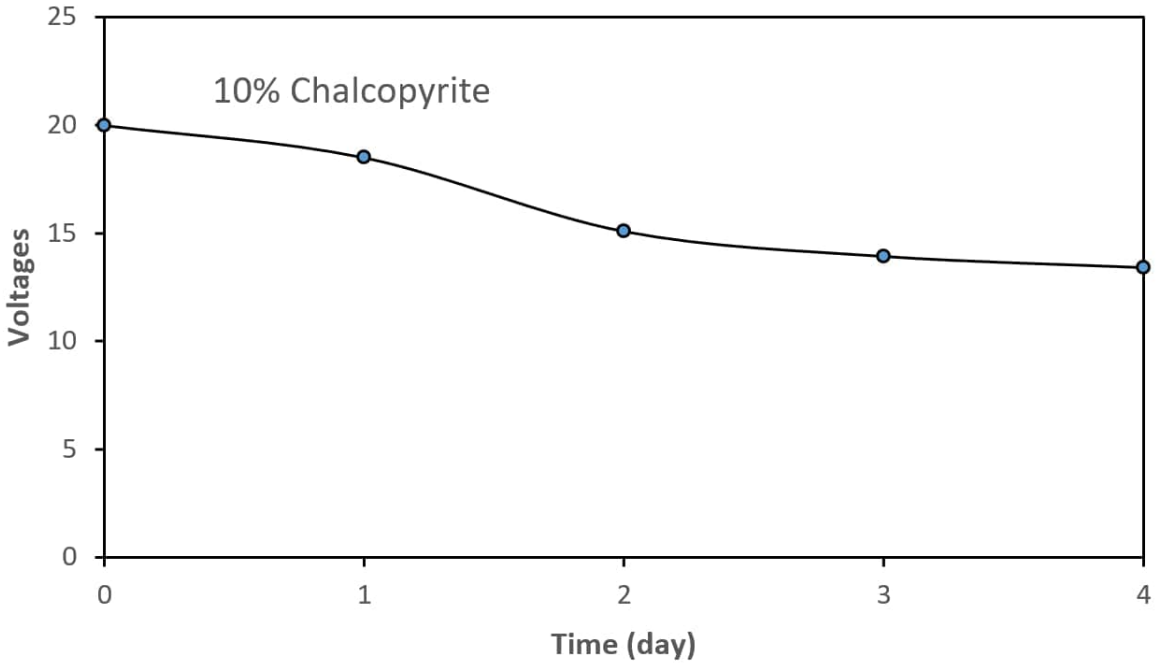

Figure 5.12: Voltage changes during the experiment inside the system. Although 20V has been applied to the system, this voltage needed to be adjusted during the experiment due to ion transportation inside the system. This graph presents those required adjustment.

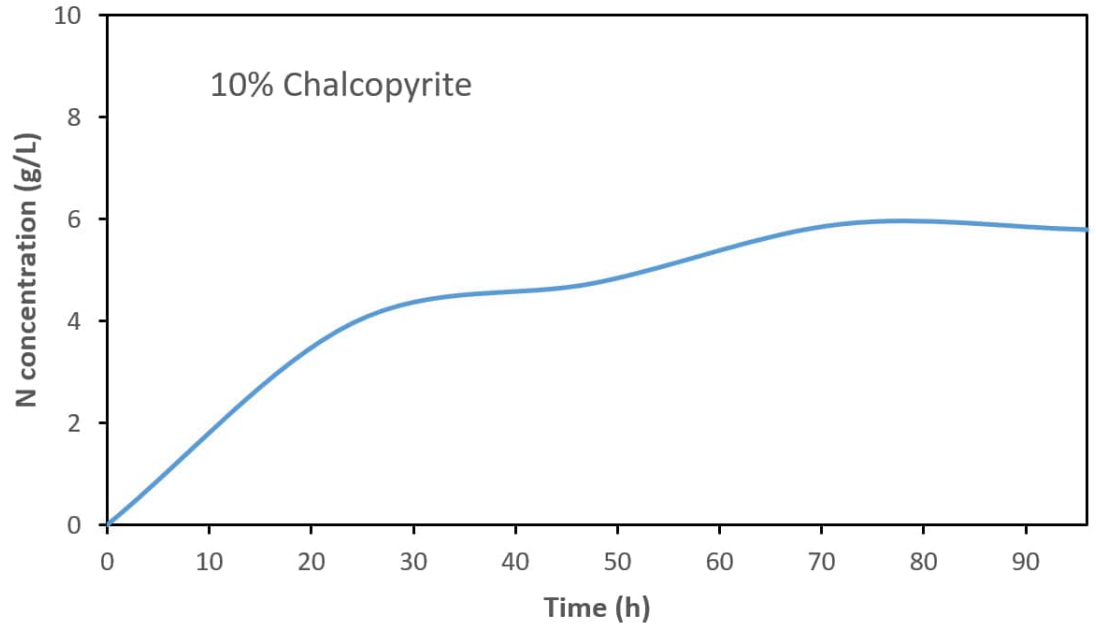

Figure 5.13: concentration of total N in the target reservoir representing the Gly concentration. It is clear that Gly inos have been transported to the target which needed to be in anion formation.

5.6 Conclusion

This chapter investigated the feasibility of gold EK-ISL using alkaline-glycine in order to the pave the road for environmentally-conscious mining methods that can replace the conventional rock moving approaches and/or reduce the use of cyanide. The behaviour of glycine in aqueous solutions in terms of pH and temperature was also examined to identify windows of propitious leaching. An experiment was conducted by designing and constructing a laboratory scale apparatus consisting of compartments representing the cathode, source, middle (low-permeable medium), target and anode reservoirs. The proposed set-up is an upgraded version of an existing apparatus that was limited to isothermal EK-ISL experiments. The constructed set-up was used to evaluated the performance of the leaching gold using alkaline glycine by an electric current to the anode and cathode in order to create a voltage gradient easing the transport of ions through porous media mediums of low permeability in the cathode-anode direction. The experiment consisted of five stages characterised by voltage increment from 0 to 30 V. Gly^- was proposed as the reagent that interacts with the gold while migrating through the middle reservoir. The results shown that Au recovery increases when the voltage is increased. Although the size of H_2O_2 molecules is small enough to reach the gold particles in the middle reservoir, it cannot be transported by voltage gradient. An alternative oxidant to be transported in anion form can increase the efficiency of EK-ISL. Finally, the effect of pyrite and chalcopyrite on the EK-ISL of gold was evaluated. Au recovery dramatically reduced by adding 10% of chalcapyrite or pyrite. Hence, EK-ISL may be more effective in weathered ores where oxides are more abundant.

Acknowledgements

This project was supported by the Australian Research Council through the Discovery Project DP170104205. This support is highly appreciated.

References

Bibliography

[1] M. Seredkin, A. Zabolotsky, G. Jeffress, In situ recovery, an alternative to conventional methods of mining: exploration, resource estimation, environmental issues, project evaluation and economics, Ore Geology Reviews 79 (2016) 500–514.

[2] T. National Academies Press, Evolutionary and revolutionary technologies for mining, National Academies Press, 2002.

[3] E. Martens, H. Prommer, X. Dai, M. Z. Wu, J. Sun, P. Breuer, A. Fourie, Feasibility of electrokinetic in situ leaching of gold, Hydrometallurgy 175 (2018) 70–78.

[4] G. O'Gorman, H. von Michaelis, G. J. Olson, Novel in-situ metal and mineral extraction technology, Tech. rep., Little Bear Laboratories, Inc.(US) (2004).

[5] K. Coyne, J. B. Hiskey, In situ recovery of minerals, no. 88, New York, United Engineering Foundation, 1989.

[6] R. Bartlett, Solution Mining: Leaching and fluid recovery of materials, Amsterdam: Gordon and Breach Science Publishers., 1998.

[7] A. Bell, Checking the safety of solution mining, Ecos 39 (1984) 19–22.

[8] G. M. Mudd, Critical review of acid in situ leach uranium mining: 1. usa and australia, Environmental Geology 41 (3-4) (2001) 390–403.

[9] C. Jacoby, In-situ extraction of mineral values from ore deposits, uS Patent 3,822,916 (Jul. 9 1974).

[10] A. Jones, S. Greene, Process for solution mining, u.S. Patent 4,561,696 (1986).

[11] C. W. Graves, In situ recovery of mineral values, uS Patent 4,561,696 (Dec. 31 1985).

[12] L. Girard, R. Hard, Stimulation of production well for in situ metal mining, uS Patent 3,841,705 (Oct. 15 1974).

[13] ALTA, Enhancing isr permeability, mining3, orica, csiro, Perth, Australia, 2019.

[14] L. S. Pangum, R. E. Browner, Pressure chloride leaching of a refractory gold ore, Minerals Engineering 9 (5) (1996) 547–556.

[15] M. Jeffrey, Kinetic aspects of gold and silver leaching in ammonia-thiosulfate solutions, Hydrometallurgy 60 (1) (2001) 7–16.

[16] J. A. Heath, M. I. Jeffrey, H. G. Zhang, J. A. Rumball, Anaerobic thiosulfate leaching: Development of in situ gold leaching systems, Minerals Engineering 21 (6) (2008) 424–433.

[17] X. Yang, M. S. Moats, J. D. Miller, X. Wang, X. Shi, H. Xu, Thiourea-thiocyanate leaching system for gold, Hydrometallurgy 106 (1) (2011) 58–63.

[18] E. A. Oraby, J. J. Eksteen, The leaching of gold, silver and their alloys in alkaline glycine-peroxide solutions and their adsorption on carbon, Hydrometallurgy 152 (2015) 199–203.

[19] A. Karrech, M. Attar, E. Oraby, J. Eksteen, M. Elchalakani, A. Seibi, Modelling of multicomponent reactive transport in finite columns–application to gold recovery using iodide ligands, Hydrometallurgy 178 (2018) 43–53.

[20] M. Azadi, A. Karrech, M. Attar, M. Elchalakani, Data analysis and estimation of thermodynamic properties of aqueous monovalent metal-glycinate complexes, Fluid Phase Equilibria 480 (2019) 25–40.

[21] Z. Jingrong, L. Jianjun, Y. Fan, W. Jingwei, Z. Fahua, An experimental study on gold solubility in amino acid solution and its geological significance, Chinese Journal of Geochemistry 15 (4) (1996) 296–302.

[22] D. H. Brown, W. E. Smith, P. Fox, R. D. Sturrock, The reactions of gold (0) with amino acids and the significance of these reactions in the biochemistry of gold, Inorganica Chimica Acta 67 (1982) 27–30.

[23] J. Eksteen, E. Oraby, B. Tanda, P. Tauetsile, G. Bezuidenhout, T. Newton, F. Trask, I. Bryan, Towards industrial implementation of glycine-based leach and adsorption technologies for gold-copper ores, Canadian Metallurgical Quarterly (2017) 1–9.

[24] M. Azadi, A. Karrech, M. Elchalakani, M. Attar, Microfluidic study of sustainable gold leaching using glycine solution, Hydrometallurgy 185 (2019) 186–193.

[25] K. Barani, M. Dehghani, M. Azadi, A. Karrech, Leaching of a polymetal gold ore and reducing cyanide consumption using cyanide-glycine solutions, Minerals Engineering 163 (2021) 106802.

[26] E. L. Shock, Stability of peptides in high-temperature aqueous solutions, Geochimica et Cosmochimica Acta 56 (9) (1992) 3481–3491.

[27] J. Amend, E. Shock, Energetics of amino acid synthesis in hydrothermal ecosystems, Science 281 (5383) (1998) 1659–1662.

[28] E. Shock, P. Canovas, The potential for abiotic organic synthesis and biosynthesis at seafloor hydrothermal systems, Geofluids 10 (1-2) (2010) 161–192.

[29] J. P. Amend, D. E. LaRowe, T. M. McCollom, E. L. Shock, The energetics of organic synthesis inside and outside the cell, Phil. Trans. R. Soc. B 368 (1622) (2013) 20120255.

[30] H. C. Helgeson, D. H. Kirkham, Theoretical prediction of the thermodynamic behavior of aqueous electrolytes at high pressures and temperatures; i, summary of the thermodynamic/electrostatic properties of the solvent, American Journal of Science 274 (10) (1974) 1089–1198.

[31] H. C. Helgeson, D. H. Kirkham, Theoretical prediction of thermodynamic properties of aqueous electrolytes at high pressures and temperatures. iii. equation of state for aqueous species at infinite dilution, Am. J. Sci.;(United States) 276 (2).

[32] H. C. Helgeson, D. H. Kirkham, G. C. Flowers, Theoretical prediction of the thermodynamic behavior of aqueous electrolytes by high pressures and temperatures; iv, calculation of activity coefficients, osmotic coefficients, and apparent molal and standard and relative partial molal properties to 600 degrees c and 5kb, American journal of science 281 (10) (1981) 1249–1516.

[33] J. C. Tanger, H. C. Helgeson, Calculation of the thermodynamic and transport properties of aqueous species at high pressures and temperatures; revised equations of state for the standard partial molal properties of ions and electrolytes, American Journal of Science 288 (1) (1988) 19–98.

[34] E. L. Shock, H. C. Helgeson, Calculation of the thermodynamic and transport properties of aqueous species at high pressures and temperatures: Correlation algorithms for ionic species and equation of state predictions to 5 kb and 1000 c, Geochimica et Cosmochimica Acta 52 (8) (1988) 2009–2036.

[35] E. L. Shock, Geochemical constraints on the origin of organic compounds in hydrothermal systems, Origins of Life and Evolution of Biospheres 20 (3) (1990) 331–367.

[36] J. P. Amend, H. C. Helgeson, Calculation of the standard molal thermodynamic properties of aqueous biomolecules at elevated temperatures and pressures part 1l-α-amino acids, Journal of the Chemical Society, Faraday Transactions 93 (10) (1997) 1927–1941.

[37] J. M. Dick, D. E. LaRowe, H. C. Helgeson, Temperature, pressure, and electrochemical constraints on protein speciation: Group additivity calculation of the standard molal thermodynamic properties of ionized unfolded proteins, Biogeosciences 3 (3) (2006) 311–336.

[38] D. E. LaRowe, P. Van Cappellen, Degradation of natural organic matter: a thermodynamic analysis, Geochimica et Cosmochimica Acta 75 (8) (2011) 2030–2042.

[39] E. L. Shock, D. C. Sassani, M. Willis, D. A. Sverjensky, Inorganic species in geologic fluids: correlations among standard molal thermodynamic properties of aqueous ions and hydroxide complexes, Geochimica et Cosmochimica Acta 61 (5) (1997) 907–950.

[40] E. L. Shock, C. M. Koretsky, Metal-organic complexes in geochemical processes: Estimation of standard partial molal thermodynamic properties of aqueous complexes between metal cations and monovalent organic acid ligands at high pressures and temperatures, Geochimica et Cosmochimica Acta 59 (8) (1995) 1497–1532.

[41] E. J. Cohn, J. T. Edsall, Proteins, amino acids and peptides as ions and dipolar ions, Reinhold Publishing Corporation; New York, 1943.

[42] N. Kitadai, Thermodynamic prediction of glycine polymerization as a function of temperature and ph consistent with experimentally obtained results, Journal of molecular evolution 78 (3-4) (2014) 171–187.

[43] C. J. Downes, A. W. Hakin, G. R. Hedwig, The partial molar heat capacities of glycine and glycylglycine in aqueous solution at elevated temperatures and atp= 10.0 mpa, The Journal of Chemical Thermodynamics 33 (8) (2001) 873–890.

[44] A. H. Pakiari, Z. Jamshidi, Interaction of amino acids with gold and silver clusters, The Journal of Physical Chemistry A 111 (20) (2007) 4391–4396.

[45] A. F. Pearlmutter, J. Stuehr, Kinetics of copper (ii)-glycine interactions in aqueous solution, Journal of the American Chemical Society 90 (4) (1968) 858–862.

[46] S. Aksu, F. M. Doyle, Electrochemistry of copper in aqueous glycine solutions, Journal of the Electrochemical Society 148 (1) (2001) B51–B57.

[47] M. G. Aylmore, Alternative lixiviants to cyanide for leaching gold ores, Gold Ore Processing, Project Development and Operation (2005) 501 to 539.

[48] K. Sakata, N. Kitadai, T. Yokoyama, Effects of ph and temperature on dimerization rate of glycine: evaluation of favorable environmental conditions for chemical evolution of life, Geochimica et Cosmochimica Acta 74 (23) (2010) 6841–6851.

[49] D. Hodges, A. Fourie, D. Reynolds, D. Thomas, Development of an apparatus for ph-isolated electrokinetic in situ chemical oxidation, Journal of Environmental Engineering 137 (9) (2011) 809–816.

[50] Y. B. Acar, A. N. Alshawabkeh, Principles of electrokinetic remediation, Environmental science & technology 27 (13) (1993) 2638–2647.

[51] J. Eksteen, E. Oraby, The leaching and adsorption of gold using low concentration amino acids and hydrogen peroxide: effect of catalytic ions, sulphide minerals and amino acid type, Minerals Engineering 70 (2015) 36–42.

[52] P. Chirita, Pyrite oxidation by hydrogen peroxide in phosphoric acid solutions., European Journal of Mineral Processing & Environmental Protection 4 (3).

[53] X. Dai, M. I. Jeffrey, The effect of sulfide minerals on the leaching of gold in aerated cyanide solutions, Hydrometallurgy 82 (3-4) (2006) 118–125.

[54] J. Eksteen, E. Oraby, B. Tanda, A conceptual process for copper extraction from chalcopyrite in alkaline glycinate solutions, Minerals Engineering 108 (2017) 53–66.

[55] E. Oraby, J. Eksteen, The selective leaching of copper from a gold–copper concentrate in glycine solutions, Hydrometallurgy 150 (2014) 14–19.

Chapter 6

Conclusions and recommendation

6.1 Closing remarks

This thesis contains six chapters, the first chapter is an introduction to the basic thermodynamics of glycine and the importance of its alkaline form in leaching metals. Chapter two presents a data analysis approach to estimate the equilibrium constant and the thermodynamic behaviour of gold-glycinate. The third chapter presents an experimental study using microchips to evaluate the rate of gold leaching by alkaline glycine. The fourth chapter covers the advantages of using micro-channel as real time monitoring device in leaching experiments. The fifth chapter presents an electro-kinetic study to evaluate the effect of electric current on gold ion transportation using alkaline glycine. The last chapter focuses on remarks, conclusion and future studies. In this Chapter, a summary of the main findings is presented as closing remarks:

6.1.1 Best leaching conditions of aqueous glycine in terms of pH and temperature

Using the revised HKF equations of state and thermodynamic dada that are reported in the literature, the stability of Gly is presented as a function of pH and temperature. The data shows that increasing temperature and pH can improve the leaching of metal using alkaline glycine (Gly^-). Gly^- is more stable at pH 12 (resp. 10.4) and temperature 25^oC (resp. 100^oC). Hydrogen peroxide, which facilitates the oxidative dissolution of metals, can increase the recovery of gold during leaching.

6.1.2 Thermodynamic data for monovalent metal glycinate complexes

The thermodynamic data that are necessary to predict the behavior of chemical species in aqueous solution are scarce. This gap was bridged by using data analysis techniques to relate the standard partial molal properties of metal-glycinate to the standard partial molal properties of metals and estimate the equilibrium constants of monovalent metal-glycinates. In this work, the thermodynamic data HKF parameters of monovalent metal-glycinate complexes was calculated including gold-glycinate by taking into account the uncertainty of input parameters.

6.1.3 Kinetic study of leaching gold using alkaline glycine

A microfluidic device mimicked the conditions of in-situ leaching of gold using alkaline glycine. The experiment was undertaken at various temperatures and lixiviant concentrations. The results showed that increasing temperature can dramatically increase the leaching rate of gold in alkaline glycine solutions. In addition, increasing pH to 11 and beyond can increase the leaching rate. However, increasing glycine concentration improves the recovery rate to some extend, and excessively high concentrations of glycine can reduce the recovery.

6.1.4 Electrokinetic study of gold leaching using alkaline glycine

The feasibility of gold EK-ISL using alkaline-glycine was evaluated by increasing voltages from 0 to 30 V. The experiment has been achieved by designing and constructing a laboratory scale apparatus using PVC pipes. The apparatus consisted of compartments representing the cathode, source, middle (low-permeable medium), target and anode reservoirs. Gly^- was proposed as the reagent that leaches gold while migrating through the low-permeability medium by transporting the ions. The results showed that increasing the voltage increases the Au recovery. As H_2O_2 molecules cannot be transported by voltage gradient, it is recommended to use other oxidants instead. Alkaline-glycine can be used without H_2O_2, but the recovery rate is very slow. Yet, the size of H_2O_2 molecules is small enough to reach the gold particles in the middle reservoir. The results showed that pyrite and chalcopyrite dramatically reduce the recovery of gold. Therefore, EK-ISL might be more effective in weathered ores where oxides are more abundant.

6.2 Future research

Recent studies (Appendix B) show that glycine can be very effective in sulphide ores where cyanide is the main reagent for leaching purposes. The role of glycine in the leaching systems using cyanide is not clear yet. However, the experimental results show that cyanide consumption can be reduced by adding glycine to the system with the same gold leaching rate.

Appendix A

Appendix A

A.1 Manufacturing microchannel chips

In the following sections, we describe the techniques of making microchannel chips step-by-step to facilitate the process of laboratory manufacturing. The first step is to select a proper substrate based on the experimental conditions and the employed chemicals. Fabrication of the channels, deposition, and bonding are the next steps, respectively.

A.1.1 Materials

Materials for microfluidic devices can be selected by some factors. They must be easy to work with using current technology. The transparency is also important if optical observations are required for the study. Materials must have resistance to the solvents and other experimental conditions such as pH and temperature. They must also have acceptable amenability to geometry modifications during the fabrication process through specific steps such as etching and bonding processes. Some of the materials which have been used in microchip applications include glass, quartz, ceramic, organically modified ceramics (ORMOCERs), silicon, elastomer polymers such as poly(dimethylsiloxane) PMMS, thermoplastic polymers including poly(methyl methacrylate) PMMA, polycarbonate PC, polyethylene PE, polystyrene PS, polyethylene terephthalate PET, polypropylene PP, polyurethane PU, polysulfone PSU nylon NY, polysulfone PSU, poly(acrylonitrile-butadiene-styrene) ABS, cyclic olefin polymers COP or copolymers COC, polyetheretherketone PEEK, polytetrafluoroethylene PTFE, fluorinated ethylene propylene FEP, polyvinylidene chloride PVDC and polyvinyl chloridePVC [1–3]. A summary of properties of most common materials in microfluidic chips is presented in Table A.1. Polymers can be classified based on polymer molecular weight, the amount of additives included in the formulation and the method of polymer sheet manufacturing [1]. Therefore, manufacturer's information of the materials need to be checked for the chemicals and conditions used in the experiment.

The first material that has been used for microfluidic applications is silicon [4]. Silicon has a high elastic modulus and it is transparent to infrared with invisible light. It makes fluorescence detection or fluid imaging challenging. This issue can be solve by bonding silicon to polymer or glass in a hybrid system [3]. One of the special advantages of using silicon is its usefulness in fabricating membranes with reduced thermal mass which enables high temperature ramp-rates [5].

Glass has also been used for many years in microscopic studies. Glass has high temperature stability and it is resistant to most chemicals except HF. Glass has low background fluorescence, it is compatible with biological samples, it has very low nonspecific absorption, it is not gas permeable and it has a large elastic modulus [3]. High quality glass is costly although it is fragile [6], yet the high transparency of glass is an advantage that makes it particularly useful as a substrate. Glass can also be bond to other materials such as PMMS using different techniques depends on the materials. Although glass and quartz substrates meet most of the criteria such as transparency to be used in microfluidic chips, the limitation of choices in fabrication techniques makes their use limited compared to polymers [1].

Ceramic can be used as a substrate when the optical transparency is not required. Ceramics used in microchannels are usually made of aluminium borosilicate, which is less expensive than glass and of the same price as many plastics [7].

ORMOCERs are inorganic-organic hybrid materials. Since silicon was always used in the material, [8] called it organically modified silicon ORMOSIL. However, it was called ORMOCER later because of its ceramic nature [9]. ORMOCERs cure into glass-like films which have high optical properties, and thermal and mechanical stability [10, 11]. The structures of these materials are well explained by [12].

Polymers such as PMMA, PDMS and PC are long-chain organic-based materials that have been used significantly in microfluidic chips over the past two decades. Using polymer in microfluidic device fabrications is advantageous because they are relatively inexpensive, amenable to mass production processes, and adaptable through formulation changes and chemical modification [3].

COC and COP have been highly attractive to be used in microfluidic materials due to their high optical transparency, low water absorption, and good resistance to solvents such as acetonitrile [2, 13, 14]. In addition, COC has good moldability and low background fluorescence [3]. PS, PEEK, PEP and PTFE are amorphous materials with transparency over a wide range of wavelengths [2]. PET can be either transparent or opaque based on grade and processing conditions [15]. PET has a high stiffness, low water absorption and good chemical resistance except to alkalis, which hydrolyses it. PS is an amorphous thermoplastic, relatively hard, but brittle. It has good electrical properties, excellent gamma radiation resistance and can be radiation sterilised. PP is semi-crystalline, white, semiopaque with wide variety of grades and modifications. PU has the elasticity of rubber as well as the toughness and durability of metal. It has an excellent solvents resistance and a very high resistance to mechanical impact. NY is a white semi-crystalline material with slightly low extensibility and impact strength. PSU is hard, but rigid with high strength transparency and high temperature resistant. PSU is excellent acid, base and salt solution resistant, but not inert to polar organic solvents (ketones,chlorinated hydrocarbons and aromatic hydrocarbons). ABS is white greyish amorphous, relatively hard, easy to be processed and bonded. However, ABS has poor solvent and fatigue resistances [1].

PMMA and PC are widely used as substrates in microchip applications. PMMA and PC, are amorphous and clear transparent thermoplastics. PC has a good temperature resistance compared to PMMA . Although PMMA has a good stiffness, it is notch-sensitive and can be fragile. Some advantages of PMMA include biological compatibility, gas impermeability

Materials	Working temperature (^{o}C)	Water absorption[a] (%)	Acid resistance	Base resistance	Solvent resistance	Transparency	Ref.
PMMA	50-90	0.2	Good-Poor	Good	Good-Poor	Excellent	©Goodfellow
PDMS	200-260		Good-Poor	Good-Fair	Good-Poor	Excellent	©Goodfellow
COC/COP	130-170	0.01	Good	Good	Good	Excellent	©Goodfellow
PC	115-130	0.1	Good	Good-Poor	Good-Poor	Excellent	©Goodfellow
PS	50-95	0.4	Good-Poor	Good-Fair	Good-Poor	Excellent	©Goodfellow
PP	90-120	0.03	Good-Fair	Good	Good-Poor	Good	©Goodfellow
PEEK	250	0.2	Good-Poor	Good	Good-Poor	Poor	©Goodfellow
PET	115-170	0.1	Good-Poor	Poor	Good-Poor	Good	©Goodfellow
PE	55-120	0.01	Good-Fair	Good	Good-Poor	Fair	©Goodfellow
PVC	50-75	0.04	Good-Poor	Good	Good-Poor	Good	©Goodfellow
PVDC	80-100	0.1	Good-Fair	Good	Good-Fair	Good	©Goodfellow
PSU	150-180	0.85	Good-Fair	Good	Good-Poor	Fair	©Goodfellow
Quartz	1100-1400	0	Good[b]	Fair[b]	Good	Excellent	©Goodfellow

Table A.1: Summary of physical properties for commonly used microfluidic materials. [a] water absorption is over 24 hours. [b] Quartz and glass can be dissolved in HF/NaOH. Glass and ceramic have a wide variety of types and based on the component they may have different physical properties.

and ease of fabrication at low temperature as 100^{o}C [3].

Silicones contain a repeating chain of SiO with various organic groups attached to the silicon. PDMS [$(CH_3)_2SiO$] has two methyl groups attached to the silicon. PDMS has been extensively used for microchannel applications. It is an elastomer polymer with a low elastic modulus [3], which makes it easy to work with, and it can be moulded to produce complex fluidic circuits. PDMS is gas permeable, transparent, soft and deformable, non-toxic and fully bio-compatible. PDMS can be strongly and permanently bonded to a glass [16] or plastic by plasma or thermal curing [17]. PMMA and PC are cost-effective polymers compared with PDMS which is a fairly high-cost material [18].

Paper is a flexible cellulose-based material that has been recently employed in microfluidic chips and its capability has been investigated in several experiments [19–23]. Some of the advantages of using paper have been reported by [3] include availability and low cost, easy disposal, easy pattern definition by ink jet and solid wax printing. Paper combines functionalities related to flow, filtering, and separation because of its porous nature. Hence, paper is biologically compatible and its chemical modifications offer flexibility for proper processing. For example, a white background provides a contrast for color-based detection methods.

A.1.2 Fabrication

There are various ways of making microfluidic chips, which differ based on the fabrication materials and the destined use. A microfluidic chip is made of two substrates that are bonded together to avoid fluid leakage. Established techniques are used to make microchannel patterns on the substrate before bonding. These techniques can be categorised as wet or dry etching, thermoforming, polymer ablation and polymer casting. Table A.2 shows some of the fabrication methods applied on different materials.

Etching

Etching is the process of using chemical solution to cut into a solid surface. Etching is commonly used to make profiles over silicon or glass substrates and can used for polymer

casting or microfluidic chip manufactoring. In the latter, the etching process includes attacking some parts of the substrate to remove a desired depth of the material and make the targeted channel. Before the etching precess, other areas of substrate rather than etched parts are protected by masking materials such as photoresists using a photolithography process. Generally, there are two types of etching including wet and dry etching. Masking materials for wet etching of glass include photoresist, amorphous Si, LPCVD polysilicon, Cr/Au, Cr/photoresist, bulk Si, amorphous SiC/PECVD, Ag, Mo, and Ti [24–31].

Wet etching consists of applying liquid chemicals that are corrosive to the substrate. For instance, HF with different concentrations can be used for glass/quartz substrates with different compositions. HCl or H_3PO_4 can also be added to HF solutions to etch the glass containing oxides such as CaO, MgO, and Al_2O_3. The wet etching of glass is isotropic, and the etch rate is a parabolic function of HF concentration which is strongly dependent on the glass composition. By reducing the concentration of HF, the rate of etching can be decreased. The etching rate can also be increased by raising temperature, by using ultrasonic agitation or by annealing the glass wafer before etching [27, 32–35]. HNA solutions which is a mixture of HNO_3, HF, and CH_3COOH can be used for the isotropic etching of silicon and aqueous potassium hydroxide (KOH) solution can be instrumental for the orientation-dependent etching of silicon [36–38]. The etching rates of different materials using different etchants have been investigated by [32].

Dry etching consists of applying plasmas or etchant gasses to remove material at the surface of a targeted substrate. The ablation reaction can be physical (with high kinetic energy), chemical or a combination of both (most widely used). The dry etching rate of glass can be relatively slow and it is usually performed in inductively coupled plasma deep reactive ion etching RIE reactors. The large amount of energy needed to etch the glass material generates strong temperature gradients causing a poor control of the process and a reduced etch selectivity of glass over the masking material [31]. Oxygen plasma etching is used to remove layers of materials in order to create microchannels on the surface of substrates over pattern masks such as photoresists. In a vacuum chamber, high power radio waves are used at low pressure to ionise oxygen molecules and form plasma. Etching using oxygen plasma is also known as ashing because it turns photoresists into ash.

Other gas precursors can be used to etch materials such as XeF_2 for silicon and SF_6, C_4F_8, CF_4, CHF_3, He, H_2, or Ar for glass. They also can be used as mixed depends on the materials to control chamber pressure or for improving the quality of the etching process. Based on the etching rate and desired depth, different thicknesses of masking layers may be required to protect the parts of the substrate that are intended to be intact during etching [39**?** –42].

Laser ablation

Laser ablation consists of removing materials from the surface of a substrate by irradiating it with a laser beam. This direct (or physical) technique is faster than etching processing when used to fabricate microchannels on polymers and plastics. Laser ablation (or photoablation) causes the absorption of a short wavelength pulse and the breakage of covalent bonds in long chains of polymer molecules [43]. [44] introduced a technique using UV excimer laser photoablation which can be used for making miniaturized capillary

electrophoresis CE [45] instrumentation for liquid-handling platform. The processes of making micro-scale capillary electrophoresis μ-CE for generating micro-scale total analytical systems μ-TAS [46] are costly and need to be done in a clean room which has extra costs [44]. Laser ablation can be an alternative method for generating micro systems by the fabrication of photoablated polymer capillaries and their subsequent sealing using a low-temperature lamination process [44]. Although using laser ablation in the microfabrication of polymers has been used and examined in some experiments [47–50], the resolution of the channels and the thermal effects of laser irradiation on the stability of materials need to be investigated [43, 51].

Thermoforming and casting

In general, thermoforming can be done by injection moulding or hot embossing to make plastic materials soft and turn them into particular desired forms. Soft lithography is also involved in elastometric polymer (PMMS) moulding technique [52]. The formation of microchannels by moulding techniques consists of two primary steps, namely the fabrication of a master then the use of the master to transfer patterns into the substrate. Various techniques exist to produce the masters such as computer numerical control machining CNC, electroplates of silicon wafer or photoresist on nickel-cobalt materials and lithography [53–55]. Accomplishment of the moulding process can be applied by injection moulding, embossing and casting. The injection moulding process turns thermoplastic pellets into a heated mould. The melted polymers then injected against the master in the moulding chamber to create the chip with low cost [56, 57]. The embossing process consists in pressing heated embosses (made of silicon or metal ribs) against a heated thermoplastic sheets such as PMMA or COC [14, 58–61]. Casing is easier to apply than other methods but it requires contact with the master often over extended durations [62].

A.1.3 Masks

Microchannel fabrication requires the creation of micro-patterns on the substrates to facilitate the flow of fluids. These patterns can be applied directly by masks or indirectly by photoresists which are light-sensitive polymers. Some thick photoresists such as SU-8 can be used as masks. SU-8 is a high-contrast epoxy-based negative photoresist designed to make ultra-thick structures [81]. The surface of the substrate can be covered by the masks or photoresists to protect the zones that are meant to remain intact and subject the channel profile to etching. Pattern generating by photoresist is known as photolithography in which photoresist is exposed to ultraviolet UV light with wavelengths in the range of 193-436 nm [81]. Generally, the substrate is placed on a spinning machine while a photoresist is applied on the substrate. Increasing the spinning rate decreases the thickness of the photoresist. The substrate is then baked on a hot plate for 90–120 seconds at a temperature of 100–130^{o}C (temperature can be varied based on the substrate material). The subsequent exposure to UVcauses the photoresist to be chemically modified, so that the exposed areas (not covered by mask) either becomes soluble in the developers (positive photoresist) or becomes insoluble (negative photoresist). Developers are aqueous alkaline solutions that can dissolve UV exposed photoresists. Another possible use for the patterned photoresist layer is to lift-off the thin metal layers after exposure on the substrates. Both

Materials	Fabrication methods	comment	Ref.
PDMS	Casting	cured at 65^oC for 1 hour Channel size: $> 20\mu m$	[16]
PDMS	Laser ablation	$50\mu m$	[63]
PDMS	Thermoforming	Soft lithography	[64] [65] [66] [67] [68]
Silicon	Wet etching	Anisotropic KOH Channel size: Channel size: $20 - 40\mu m$	[69]
Silicon	Wet etching	Isotropic HNA (HNO_3-HF-CH_3COOH)	[36]
Silicon	Dry etching	Bosch/Cryogenic	[70]
Fused silica	Wet etching	Concentration of etchant is important (HF/HF-NH_4F)	[71] [72]
Glass	Wet etching	HF. High etch rate achieved mainly by using highly concentrated HF	[35] [39] [26]
Glass	Wet etching	HF/HCL. The composition of the glass is an important factor for the quality of generated surface	[73]
Glass	Wet etching	HF-HNO_3	[74]
Glass	Dry etching	$SF_6/C_4F_8/CF_4/CHF_3$ $0.5 - 0.8\mu m$/min based on glass composition	[39] [40] [42] [75] [41] [73]
PMMA	Dry etching	O_2-CF_4 $0.2 - 0.3\mu m$/min	This study
PMMA	Laser ablation	Fabrication parameters/speed affect Size and shape of microchannels	[76] [77] [78]
PMMA	Termoforming	Embossing (110^oC/3kN for 5 mins) (115^oC/5-15kN for 5 mins)	[79] [80]
PC	Laser ablation	50 Hz/250 pulses/mm ($37\mu m$)	[44]

Table A.2: Summary of some fabrication techniques on different materials.

Masks	Fabrication method	Comments	Ref.
SU-8	Wet etching of glass	Max depth of 20μm/3min	[26]
Cr/Cu	Wet etching of glass	Max depth of 100μm/15min	[82]
Cr/Au	Wet etching of glass	Max depth of 50μm/7min	[27]
Cr/Au/photoresist	Wet etching of glass	Max depth of 250μm/40min	[83]
α :Si(PECVD)[a]	Wet etching of glass	Max depth of 70μm/10min	[84]
α :Si/photoresist	Wet etching of glass	Max depth of 500μm/1min	[85]

Table A.3: Summary of some examples of masks for different substrate materials. [a] An alternative process to create thin SiO_2 films at significant low temperatures and on nearly arbitrary substrates is the plasma-enhanced chemical vapour deposition (PECVD)

Photoresist	Thickness (μm) at 2000 rpm	Thickness (μm) at 6000 rpm	Developer	Comments
Thin positive				
AZ 111 XFS	1.41	0.82	AZ 303	
AZ 1529	4.10	2.37	AZ 340	Wet etching
AZ ECI 3012	1.70	0.90	AZ 351	
AZ MiR 701	2.25	1.25	AZ 300MIF	Dry etching
Thick positive				
AZ 4562	8.77	5.06	AZ 340	
AZ 9260	11.50	6.00	AZ 400	
AZ 4903	17.00	7.00	AZ 400	
AZ IPS-6050	60 (at 1000 rpm)	30 (at 2500 rpm)	AZ 326	Dry etching
Negative				
AZ 125nXT-10A	120 (at 600 rpm)	38 (at 2500 rpm)	AZ 326	
AZ 15nXT-450CPS	18 (at 1000 rpm)	8 (at 3000 rpm)	AZ 326	
AZ nLof 2070	11.8 (at 500 rpm)	5.5 (at 4000 rpm)	AZ 726	

Table A.4: Some examples of common photoresists. All information retrieved from data sheet provided by Microchemicals GmbH for photoresist.

layers of thin metal and photoresist are removed together and the metal remains in the uncovered areas (channels). It is recommended to use standard laser laboratory safety equipment including protective eye wear before working with UV light. UV laser energy is dangerous and staring at UV light is not recommended.

A.1.4 Deposition

Deposition techniques include physical vapour deposition PVD, chemical vapour deposition CVD, electroplating, spin-cast and epitaxial. PVD and CVD are the most common techniques of deposition. PVD can take place by either evaporation or sputtering techniques. Thermal evaporation can be used to deposit thin metal layers by heating the precursor metal in a vacuum chamber until its atoms have sufficient energy to leave the surface. At this point, they will traverse the vacuum chamber, at thermal energy (less than 1 eV), and coat on the substrate positioned above the chamber. Although, thermal evaporation is a simple and cheap technique, some disadvantages can be counted for this technique. The deposition rate varies and the thin metal films are not quite homogeneous, limited to materials with lower melting points compared with crucible. Common evaporable metals

include gold, silver, aluminium, chrome, nickel, titanium, and platinum. It is difficult to use alloys because of their stoichiometry control as they have different melting points [81].

In the case of sputtering, the target metal with negative potential is bombarded with positive argon ions created in a plasma due to a high electric direct-current voltage. The substrate and the wall of vacuum chamber are on positive potential to release uncharged target atoms. The accelerated atoms are then deposited onto the substrate. Sputtering has some obvious advantages: it applies to a wide variety of materials, has a better step coverage, and usually offers better adhesion to the substrate compared to evaporation [81].

CVD process is a vapour-transfer process which is considered to be one of the most powerful tools for producing advanced materials including metals, metal alloys and their compounds [86]. This method is also used for depositing thin SiO_2 films on nearly arbitrary substrates in a process called plasma-enhanced chemical vapour deposition PE CVD. Silicon nitride Si_3N_4 can be deposited by using both PE CVD and a low pressure chemical vapour deposition LP CVD which takes place in a vertical diffusion furnace [81].

A.1.5 Measurement of dimensions

In microchannel fabrication, it is necessary to check the dimensions of the channel as well as the surface and thickness of the deposited metals. Although the equipment required for fabrication has high accuracy, small errors can occur and it is recommended to check the sample under high resolution microscopes at every fabrication stage. For instance, when photoresist is used before etching, it is important to check that the channel is clean of any photoresist materials to be etched. Optical profilometers and surface profilers are powerful tools for characterizing and quantifying surface roughness, step heights, critical dimensions, and other topographical features. All measurements are, non-contact, fast, and do not require sample preparation. The system analyses a wide range of surfaces, including smooth, rough, flat, sloped, and stepped, and provides profile heights ranging from sub-nanometre to millimetres at high speed.

A.1.6 Bonding

There are many types of bonding approaches that have been used in the fabrication of microfludic chips based on different materials. Depending on the material used as a substrate, the patterns of the microchannels and the required channel resolution, specific bonding methods can be selected. In this section, the common methods that apply to popular substrate materials are presented. In general, there are two types of bonding approaches including indirect [78] and direct bonding [87].

Indirect bonding

Indirect bonding consists of using an adhesive layer which is placed between two substrates to bond them together. This approach is widely used for many types of materials. Using different types of glues or other liquid adhesives can be categorised as a simplest adhesive bonding technique [2, 60, 88]. In this technique, curing time depends on the bonding agent and may need extra heat or pressure. UV curing adhesives are among the most commonly used bonding agents. The adhesive can be performed by applying a thin layer of a highly

viscous liquid between two completely clean surfaces; the glued area and is formed and cured by UV light exposure. Some experiments have been conducted to control the liquid adhesives against clogging the channels [89–92]. Thermal lamination, which is normally used to seal grooves in microfluidic devices, can also be used for bonding well matching materials [54].

Direct bonding

Direct bonding is applied without any additional materials at the interface [93]. Thermal bonding and solvent bonding are the most common techniques of direct bonding. In thermal bonding, a temperature near to or above glass transition temperature T_g is applied to substrates [94–96], such as PMMA or PC [97]. Thermal boding along with pressure is also commonly used method for plastic/polymer materials such as PMMA [48, 98–100]. Although using thermal bonding techniques for polymers has been well investigated [1, 93, 101–103] and some issues associated to this technique such as the deformation have been examined [100, 104–106], selecting appropriate process parameters still need to must be optimised to limit the collapse of micro-channels during direct bonding [2]. Annealing the moulded plate directly to another plate can be performed at room temperature [16, 58].

Solvent bonding consists of using a strong chemical solvent to soften and dissolve materials at the interface of two (or more) solid pieces. As they dissolve the surface molecules mix up and form continuous chains while the solvent evaporates. Solvent bonding depends on various parameters such as temperature, composition, and molecule size [107]. The Hildebrandt parameter is often used to assess the interaction between materials and to provide a quantitative indication of solubility especially for nonpolar materials [108]. This technique is commonly used for polymers [109–111] such as PMMA; if the solubility parameter of PMMA and the solvent are substantially different, the bonding process could be done without significant channel deformation [2].

Surface treatment involves increasing surface energy to enhance the bonding potential between two surfaces. In the case of polymers, high specific energy in the form of polar functional groups causes hydrogen or covalent bonds providing bond strengths [2]. There are many methods of surface treatment including acid treatment [112], surface grafting [113], vacuum plasmas [114, 115], atmospheric plasmas [116], and plasma treatment [117–120]. In these methods, bonding process has to be carried out immediately after treatment as the surface properties of the polymer change quickly with time and humidity.

There are many other practical techniques for bonding such laser bonding [121, 122] and microwave bonding [123] in which electromagnetic waves being absorbed by the polymer materials. Ultrasonic welding for thermoplastic polymer has also been used successfully in various applications for decades [15, 124, 125]. In fusion techniques, the assembly of glass/metal is heated to a temperature near the annealing point of glass (500^oC), and a DC voltage across the glass-metal assembly so that the glass is negative with respect to the metal [126]. A surface treatment can be applied by combining two or more techniques such as UV light assisted [127–129], UV/ozone [130, 131], or UV assisted ethanol [132] which has been proved as exceptionally high bond strengths for thermoplastic materials. Table A.5 presents some bonding techniques applied on different types of materials.

Materials	Bonding technique	Temperature	Pressure	Comments	Ref.
PDMS-PDMS/glass	Surface treatment	30^oC	-	O_2 plasma	[16]
Glass-metal	Fusion	500^oC	-	-	[126]
Glass-glass	Fusion	650^oC	-	Strong bonding	[133]
Glass-glass	Surface treatment	400^oC	-	N_2/O_2 plasma	[134]
Glass-glass	Thermal/anodic bonding	530^oC	-	Using Ti film	[135]
Glass-silicon	Thermal/anodic bonding	350^oC	0.05 MPa	Strong bonding	[136]
Glass-glass Glass-silicon	Adhesive bonding	150^oC	0.15MPa	SU-8 adhesive layer	[137] [138]
PMMA-PMMA	Solvent bonding	Room temperature	1 kg mass	takes 15 mins to bond	[139]
PMMA-PDMS	Surface treatment	$65\text{-}85^oC$	-	O_2 plasma/3-APTES[a] /corona discharge	[140]
PMMA-silicon PMMA-PMMA	Adhesive bonding using microwave	Not mentioned	-	Sn-Pb/Au film	[92]
COC	Solvent bonding	25^oC	-	1-decanol-DPA[b] /UV assisted	[14]
PMMA/PC/COC	Solvent bonding	Low temperature	-	High bond strength	[141] [118] [142] [143]
PMMA-PMMA	Solvent bonding	Room temperature	-	Ethanol/UV assisted	[132]
PMMA-PMMA	Adhesive bonding	Room temperature	1 kg mass	UV assisted glue	this study
PMMA-PMMA	Ultrasonic	$25 - 70^oC$	0.147-0.297 MPa	Thermal/Solvent assisted	[125]
PMMA/PC	Surface treatment	$75 - 110^oC$	300 psi	O_2 plasma	[144]
PMMA/PC/PS/ PSU/COC	Thermal bonding	Depends on materials		Fusion	[129] [145] [146] [147] [105] [148]

Table A.5: Some bonding techniques on different materials. [a] 3-aminopropyl triethoxysilane. [b] 1-decanol ($C_{10}H_{22}O$)Diphenylamine ($C_{12}H_{11}N$)

Substrate materials	Method	reusable	Max. pressure	Comments	Ref.
PDMS/glass	Contact-based	Yes	634.3 kPa	Chemically inert	[162]
PDMS	Ports	Yes	less than 450 kPa	PDMS molding	[163]
Silicon-glass	Adhesive	No	40000 kPa	Epoxy resin	[164]
PDMS	Couplers	Yes	600 kPa	Multiple in/outputs	[161]
PDMS/PMMA	Molding	No	103 kPa	Multiple in/outputs	[165]
PMMA	Press-fit	Yes	600 kPa	Needle-tubing[a]	[166]
PDMS	Casting	Yes	220 kPa	Silicon wafer mold	[167]
PMMA	Plug n play	No	700 kPa	Using ring	[168]
PDMS/glass	O-ring	No	250 kPa	3D-printed	[169]
Silicon	Thermal	No	2171 kPa	Using epoxy also	[154]
Silicon	Thermal	Yes	200 kPa	Heat-shrink/silastic tubing	[170]
PMMA	Adhesive	No	not measured	UV-curing glue	This study
Silicon	Solder-based/thermal	No	12666	Using ferrule	[171]

Table A.6: Some examples of common interconnection. [a] In this method, first tubing is placed and then a needle with larger diameter than tubing is inserted into tubing.

A.1.7 Fittings

One of the most important parts of microfluidic fabrication are the connections for inlet and outlet liquids. Microfuidic connectors are known as interconnections or chip-to-word interfaces CWI. A considerable research work is currently dedicated to connectors to produce easy, cost-effective and reliable ways to produce them [149]. There is no universally-accepted connection but a wide variety of techniques have been produced to support this application such as Luer Lock and Luer Cone [150]. As this area of fabrication is still developing, the standardisation of connections is important to reduce the cost [151, 152]. The microfluidic interconnect permits liquid connections from a microchip to observatory devises which are not necessarily in the micro-scale. Therefore, the connection points are very important parts in microfluidic systems. Successful connections have to meet certain criteria such as chemical resistance, high sealing performance, high fluid flow, heat and pressure capabilities, and ease of fabrication. Fitting connections can be permanent using adhesive joints such as dry adhesive film [153], epoxy [154], UV curable glue [155] and moulding techniques [156, 157] or non permanent such as couplers [158, 159], magnetic connectors [149], insertion-based [160**?** , 161] and contact-based interconnects [162]. Table 7 presents some examples of connection techniques which have been reported in the literature. However, interconnecting methods are not limited to these examples.

A.2 Cleanroom

As microchannel fabrication is sensitive to nano/macro size impurities; a small pollution can have a huge effect on the process. Therefore, cleanrooms have been established to mitigate this issue. A cleanroom environment has a low level of pollutants such as dust,

airborne microbes, aerosol particles and chemical vapours. Cleanrooms are classified according to the number and size of particles permitted per volume of air. As safety is an overriding concern in all laboratory activities, reasonable measures have been implemented to ensure that the laboratory provides a clean and safe working environment. Access to cleanrooms and the rules of using the facility are highly restrictive for all users. Cleanroom has a dress code that requires all users to follow the designated procedure of gowning in order to avoid generating unnecessary particles when they are in the cleanroom. Clothing should be clean of dusts and dirts before entering the laboratory and not to shed a lot of fibers like fur, fake fur, mohair, etc. Normal paper, pencil, leather cases, drinks and food are prohibited in cleanrooms. As in other chemical laboratories where safety regulations are strict in terms of using chemicals, cleanrooms have standard guidelines for using the facilities and chemicals under professional supervision. Different protections such as gloves, face shield, safety glasses, nitrile apron and so on are provided to be used to handle chemicals. All acids, bases, and solvents are classified and controlled in the facility based on the Materials Safety Data Sheet MSDS which is a convenient source for information on the properties of any chemical provided by the manufacturer or seller of a chemical.

A.3 An experimental method to leach precious metals

Recently, we conducted an experiment to evaluate the ability of a microfluid system to leaching a gold layer of thickness 60 nm using alkaline glycine in controlled conditions. In this section, the microchannel fabrication part is presented to illustrate the processes described in the previous sections. The fabrication process has been carried out in the Western Australian Centre for Semiconductor Optoelectronics and Microsystems (WACSOM) known as the cleanoom at The University of Western Australia. We used transparent and colourless PMMA sheets purchased from Goodfellow (UK) to manufacture the microchannel device. Fig. A.1 shows a schematic image of the process of preparation including photoresist, UV treatment, etching, deposition and bonding stages. It is essential to use a small tong to carry the substrates to avoid contamination. Small amounts of contaminants on the surface can cause significant problems including non-uniform evaporation or etching. For cleaning the surface of the substrates, isopropanol is used. However, the resistivity of materials to the chemical cleaners has to be checked. For instance, PMMA is sensitive to alcohol such as ethanol. Therefore, running water on the surface of substrate can be a safe option.

It needs to cut the PMMA sheet to the expected size of microchannel chip PMMA sheets need to be cut to the expected size of the microchannel chip (12mm×50mm). The tubing holes are punched right after the cutting stage (rather than the end of the process) to avoid scratching the substrate or making edges on it. The distance between the inlet and outlet holes can be adjusted with respect to the channel size (4mm×40mm). Following the cutting and hole punching phases, the PMMA substrate is placed on spinning machine and holds it by vacuum applied under substrate (see Fig. A.1). A suitable photoresist (AZ 4562) is then applied on the spinning substrate for about 1 min to cover the whole surface of (see Fig. A.2-a). It is important to examine the thickness of photoresist required for etching as photoresist protects the surface rather than the channel against etching. Different photoresists with different viscosities can apply various thicknesses when the

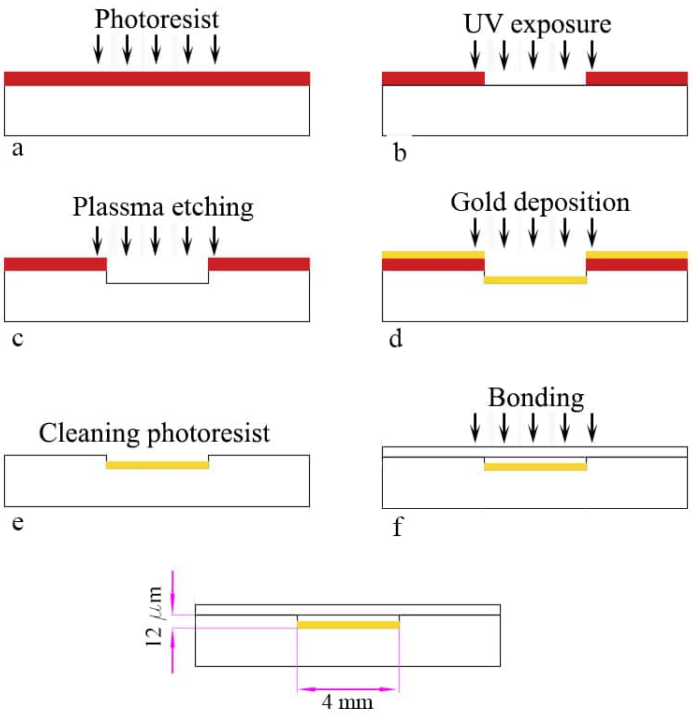

Figure A.1: Microchannel fabrication processes.

Spin rate (rpm)	2000	3000	4000	5000	6000
Thickness (μm)	8.77	7.16	6.20	5.55	5.06

Table A.7: Photoresist thickness as a function of spin rate.

spinning rate is changed. Table A.7 and tab:8 present guidelines on the application of photoresist AZ 4562 used in this experiment. This information is provided by the suppliers and can be verified in the laboratory through scanning probes. As the expected depth of the channel is about 12 μm, a maximum thickness of 8.77 μm can considered for photoresist. It should be mentioned that the photoresist can spread more level on the substrate with less aspect ratio such as rounded or square shapes. The substrate needs to be baked at 115^{o}C for 50 seconds on a hotplate before UV exposure. However, because of the heating limitation of PMMA, it was baked at 90 ^{O}C for 110 seconds (Fig. A.2-b). These processes can be repeated once or twice to reach the desirable thickness of photoresist.

A mask is used to protect the photoresist against UV exposure except the channel area. This mask can be made of any material which is UV resistant and flexible to be used (Fig. A.2-c). After UV exposure for 60 seconds, the substrate is washed with developer AZ326 for 60 seconds to remove the photoresist in the channel and baked for 110 seconds at 90^{O}C.

Prebake	100^{O}C for 50 seconds on hotplate
UV exposure	60 seconds (for this study)
Developer	AZ 340 or AZ326 30 to 60 seconds
Postbake	115^{O}C for 50 seconds on hotplate
Removal	AZ 100

Table A.8: Photoresist processing guidelines.

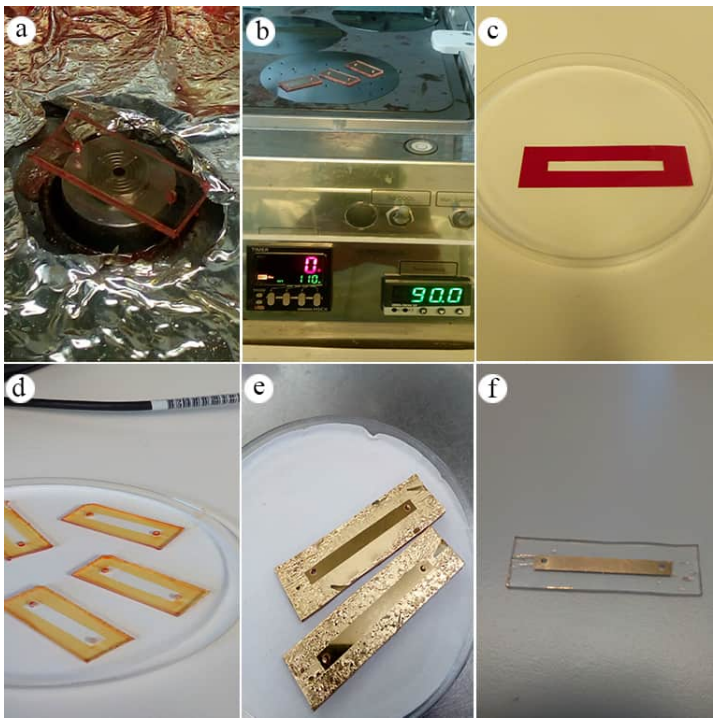

Figure A.2: Photos of microchannel chip fabrication; a-spinning machine, b-hot plate, c-mask, d-substrate after applying photoresist, e-after deposition stage, and f-substrate after removing photoresist.

Fig. A.2-d shows the substrates after the photoresist process. In any failed cases required process can be repeated, removal liquids such as AZ 100 which is a strong developer can be used. Another way to remove photoresist completely is to expose it to UV light directly without using a mask.

Using a Plassma100 machine, the channel is etched by a practical recipe (60% O_2 and 5% CF_4). In this recipe, oxygen is the main effective gas for etching PMMA, and CF_4 is useful to obtain a smooth surface. It is important to understand that photoresist and substrate (the channel area) are etched the same time, but with different rates because of different structure, and PMMA is etched faster than the photoresist. In practice, considering this recipe PMMA can be etched12mum after 30 minutes while a thin layer of photoresist remains on substrate which can protect the rest of surface against etching. The depth of the channel can be verified by Optical profilometers (Zygo 6300) and surface profilers (Dektak 150).

As can be seen in Fig. **??**-c and d, the layer of photoresist is needed for etching and deposition. It needs to be mentioned that if the photoresist is cleaned during the etching process, the substrate has to be covered by photoresist again using a mask. After etching, the substrate is placed in the thermal evaporation machine to deposit a layer of gold on the channel. To use this machine, the properties of the metal coating on substrate have to be input. Therefore, in the case of alloys, the properties of the metal mixture have to be measured carefully. This machine requires restricted guidelines for the users and all stages have to be performed carefully in the specific order. As the gold may not have strong adherence to the PMMA or other similar materials, it is recommended to deposit a very thin layer of Cr first (about 5 nm) on the substrate before depositing gold.

The substrate covered by the layer of gold (Fig A.2-e) is then processed to remove the rest of the photoresist. It can be seen in Fig A.2-e that the smooth area (channel) hosts the direct deposition on substrate and the rest is deposition over photoresist. As mentioned before, AZ 100 can be used to removed the photoresist. Caution is need at this stage as the removal part is not a fast process. However, if the substrate is exposed to the UV light from the back of substrate which is not covered by gold, the photoresist can be removed faster in developers. Fig. A.2-f shows the substrate after removal of the photoresist.

The last part of the fabrication is bonding. Many methods of bonding such as plasma treatment, thermal treatment, and adhesive solutions have been tested to glue PMMA to PMMA. However, UV glue proved to be the best option because it can be applied easily without leaking to the channel. However, the above mentioned bonding methods can be more appropriate for other materials. For instance, plasma treatment is recommended to bond PDMS and glass. Although the above process may sound long, the equipment that are currently available to make few microchannel chips in parallel which makes the task less tedious.

A.4 Conclusion

In this paper, the fabrication processes of microchannel chips have been reviewed in details to make them accessible for hydrometallurgical applications. The main advantages of this device have been identified as the real time monitoring, low consumption of reagents, safe use of the environment, easy control of experimental conditions (i.e. pH, temperature, injection rate, and composition), controllable heat and mass transfer, potential to use advanced imaging technologies (e.g. high resolution microscopes) in real time, and the direct and fast acquisition of analytical results. This review has also identified a number of limitations. Overall the advantages are sufficient to overcome the possible limitations of microfluidic system. Therefore, this technology can become a powerful tool for the laboratory testing o leaching processes. Through this survey, a number of gaps in the literature have been identified. The scientific community would benefit from addressing

Acknowledgements

This project was supported by the Australian Research Council through the Discovery Project DP170104205. The authors would like to acknowledge the financial support provided by Robert and Maude Gledden Postgraduate Scholarships. The authors also would like to appreciate Dr. Mariusz Martyniuk, Dr. Adrian Keating, Dr. Dhirendra Tripathi, Dr. Xiao Sun and Dr. Martin Hill for valuable advice and great assistance.

References

Bibliography

[1] H. Shadpour, H. Musyimi, J. Chen, S. A. Soper, Physiochemical properties of various polymer substrates and their effects on microchip electrophoresis performance, Journal

of Chromatography A 1111 (2) (2006) 238–251.

[2] C.-W. Tsao, D. L. DeVoe, Bonding of thermoplastic polymer microfluidics, Microfluidics and Nanofluidics 6 (1) (2009) 1–16.

[3] P. N. Nge, C. I. Rogers, A. T. Woolley, Advances in microfluidic materials, functions, integration, and applications, Chemical reviews 113 (4) (2013) 2550–2583.

[4] S. C. Terry, J. H. Jerman, J. B. Angell, A gas chromatographic air analyzer fabricated on a silicon wafer, IEEE transactions on electron devices 26 (12) (1979) 1880–1886.

[5] R. M. Tiggelaar, P. Van Male, J. Berenschot, J. Gardeniers, R. Oosterbroek, M. De Croon, J. Schouten, A. van den Berg, M. C. Elwenspoek, Fabrication of a high-temperature microreactor with integrated heater and sensor patterns on an ultrathin silicon membrane, Sensors and Actuators A: Physical 119 (1) (2005) 196–205.

[6] D. J. Harrison, K. Fluri, K. Seiler, Z. Fan, C. S. Effenhauser, A. Manz, Micromachining a miniaturized capillary electrophoresis-based chemical analysis system on a chip, Science 261 (5123) (1993) 895–897.

[7] C. Henry, S. Lunte, J. Santiago, et al., Ceramic microchips for capillary electrophoresis–electrochemistry, Analytical Communications 36 (8) (1999) 305–307.

[8] H. Schmidt, Organically modified silicates by the sol-gel process, MRS Online Proceedings Library Archive 32.

[9] S. Aura, T. Sikanen, T. Kotiaho, S. Franssila, Novel hybrid material for microfluidic devices, Sensors and Actuators B: Chemical 132 (2) (2008) 397–403.

[10] S. Obi, M. Gale, A. Kuoni, N. De Rooij, Replication of optical MEMS structures in sol-gel materials, Microelectronic engineering 73 (2004) 157–160.

[11] R. Buestrich, F. Kahlenberg, M. Popall, P. Dannberg, R. Müller-Fiedler, O. Rösch, Ormocer® s for optical interconnection technology, Journal of Sol-Gel Science and Technology 20 (2) (2001) 181–186.

[12] H. Schmidt, New type of non-crystalline solids between inorganic and organic materials, Journal of Non-Crystalline Solids 73 (1-3) (1985) 681–691.

[13] A. Piruska, I. Nikcevic, S. H. Lee, C. Ahn, W. R. Heineman, P. A. Limbach, C. J. Seliskar, The autofluorescence of plastic materials and chips measured under laser irradiation, Lab on a Chip 5 (12) (2005) 1348–1354.

[14] K. W. Ro, J. Liu, D. R. Knapp, Plastic microchip liquid chromatography-matrix-assisted laser desorption/ionization mass spectrometry using monolithic columns, Journal of chromatography A 1111 (1) (2006) 40–47.

[15] A. B. Strong, B. Strong, Plastics: materials and processing, Prentice Hall Upper Saddle River, 2000.

[16] D. C. Duffy, J. C. McDonald, O. J. Schueller, G. M. Whitesides, Rapid prototyping of microfluidic systems in poly (dimethylsiloxane), Analytical chemistry 70 (23) (1998) 4974–4984.

[17] S. Halldorsson, E. Lucumi, R. Gómez-Sjöberg, R. M. Fleming, Advantages and challenges of microfluidic cell culture in polydimethylsiloxane devices, Biosensors and Bioelectronics 63 (2015) 218–231.

[18] L. R. Volpatti, A. K. Yetisen, Commercialization of microfluidic devices, Trends in biotechnology 32 (7) (2014) 347–350.

[19] A. W. Martinez, S. T. Phillips, G. M. Whitesides, E. Carrilho, Diagnostics for the developing world: microfluidic paper-based analytical devices (2009).

[20] Z. Nie, F. Deiss, X. Liu, O. Akbulut, G. M. Whitesides, Integration of paper-based microfluidic devices with commercial electrochemical readers, Lab on a Chip 10 (22) (2010) 3163–3169.

[21] S. A. Klasner, A. K. Price, K. W. Hoeman, R. S. Wilson, K. J. Bell, C. T. Culbertson, based microfluidic devices for analysis of clinically relevant analytes present in urine and saliva, Analytical and bioanalytical chemistry 397 (5) (2010) 1821–1829.

[22] H. Liu, R. M. Crooks, Three-dimensional paper microfluidic devices assembled using the principles of origami, Journal of the American Chemical Society 133 (44) (2011) 17564–17566.

[23] N. K. Thom, K. Yeung, M. B. Pillion, S. T. Phillips, Fluidic batteries as low-cost sources of power in paper-based microfluidic devices, Lab on a Chip 12 (10) (2012) 1768–1770.

[24] M.-A. Grétillat, F. Paoletti, P. Thiebaud, S. Roth, M. Koudelka-Hep, N. De Rooij, A new fabrication method for borosilicate glass capillary tubes with lateral inlets and outlets, Sensors and Actuators A: Physical 60 (1-3) (1997) 219–222.

[25] T. Corman, P. Enoksson, G. Stemme, Deep wet etching of borosilicate glass using an anodically bonded silicon substrate as mask, Journal of micromechanics and microengineering 8 (2) (1998) 84.

[26] D. Bien, P. Rainey, S. Mitchell, H. Gamble, Characterization of masking materials for deep glass micromachining, Journal of Micromechanics and Microengineering 13 (4) (2003) S34.

[27] F. E. Tay, C. Iliescu, J. Jing, J. Miao, Defect-free wet etching through pyrex glass using Cr/Au mask, Microsystem technologies 12 (10-11) (2006) 935–939.

[28] V. Saarela, M. Haapala, R. Kostiainen, T. Kotiaho, S. Franssila, Glass microfabricated nebulizer chip for mass spectrometry, Lab on a Chip 7 (5) (2007) 644–646.

[29] F. Ceyssens, R. Puers, Deep etching of glass wafers using sputtered molybdenum masks, Journal of Micromechanics and Microengineering 19 (6) (2009) 067001.

[30] H. W. Lee, D. C. Bien, S. A. M. Badaruddin, A. S. Teh, Thin film Ag masking for deep glass micromachining, Electrochemical and Solid-State Letters 13 (11) (2010) H399–H402.

[31] C. Iliescu, H. Taylor, M. Avram, J. Miao, S. Franssila, A practical guide for the fabrication of microfluidic devices using glass and silicon, Biomicrofluidics 6 (1) (2012) 016505.

[32] K. R. Williams, K. Gupta, M. Wasilik, Etch rates for micromachining processing-part ii, Journal of microelectromechanical systems 12 (6) (2003) 761–778.

[33] A. Berthold, F. Laugere, H. Schellevis, C. R. De Boer, M. Laros, R. M. Guijt, P. M. Sarro, M. J. Vellekoop, Fabrication of a glass-implemented microcapillary electrophoresis device with integrated contactless conductivity detection, Electrophoresis 23 (20) (2002) 3511–3519.

[34] H. Zhang, H. Guo, Z. Chen, G. Zhang, Z. Li, Application of PECVD SiC in glass micromachining, Journal of Micromechanics and Microengineering 17 (4) (2007) 775.

[35] C. Iliescu, B. Chen, J. Miao, On the wet etching of pyrex glass, Sensors and actuators A: Physical 143 (1) (2008) 154–161.

[36] B. Schwartz, H. Robbins, Chemical etching of silicon iii. A temperature study in the acid system, Journal of the electrochemical society 108 (4) (1961) 365–372.

[37] J. Haneveld, H. Jansen, E. Berenschot, N. Tas, M. Elwenspoek, Wet anisotropic etching for fluidic 1D nanochannels, Journal of micromechanics and microengineering 13 (4) (2003) S62.

[38] C. Easter, C. B. O'Neal, Characterization of High-Pressure- Vapor-Phase silicon etching for MEMS processing, Journal of Microelectromechanical Systems 18 (5) (2009) 1054–1061.

[39] X. Li, T. Abe, Y. Liu, M. Esashi, Fabrication of high-density electrical feed-throughs by deep-reactive-ion etching of Pyrex glass, Journal of Microelectromechanical Systems 11 (6) (2002) 625–630.

[40] J. Park, N.-E. Lee, J. Lee, J. Park, H. Park, Deep dry etching of borosilicate glass using SF6 and SF6/Ar inductively coupled plasmas, Microelectronic engineering 82 (2) (2005) 119–128.

[41] T. Akashi, Y. Yoshimura, Deep reactive ion etching of borosilicate glass using an anodically bonded silicon wafer as an etching mask, Journal of Micromechanics and Microengineering 16 (5) (2006) 1051.

[42] K. Kolari, V. Saarela, S. Franssila, Deep plasma etching of glass for fluidic devices with different mask materials, Journal of Micromechanics and Microengineering 18 (6) (2008) 064010.

[43] L. G. Reyna, J. R. Soběhart, Laser ablation of multilayer polymer films, Journal of applied physics 76 (7) (1994) 4367–4371.

[44] M. A. Roberts, J. S. Rossier, P. Bercier, H. Girault, Uv laser machined polymer substrates for the development of microdiagnostic systems, Analytical chemistry 69 (11) (1997) 2035–2042.

[45] P. Arquint, M. Koudelka-Hep, B. H. van der Schoot, P. van der Wal, N. de Rooij, Micromachined analyzers on a silicon chip., Clinical chemistry 40 (9) (1994) 1805–1809.

[46] A. Manz, N. Graber, H. á. Widmer, Miniaturized total chemical analysis systems: a novel concept for chemical sensing, Sensors and actuators B: Chemical 1 (1-6) (1990) 244–248.

[47] J. Rossier, M. Roberts, R. Ferrigno, H. Girault, Electrochemical detection in polymer microchannels, Analytical chemistry 71 (19) (1999) 4294–4299.

[48] J.-Y. Cheng, C.-W. Wei, K.-H. Hsu, T.-H. Young, Direct-write laser micromachining and universal surface modification of PMMA for device development, Sensors and Actuators B: Chemical 99 (1) (2004) 186–196.

[49] Y.-C. Lin, H.-C. Ho, C.-K. Tseng, S.-Q. Hou, A poly-methylmethacrylate electrophoresis microchip with sample preconcentrator, Journal of Micromechanics and Microengineering 11 (3) (2001) 189.

[50] P.-P. Shiu, G. K. Knopf, M. Ostojic, S. Nikumb, Rapid fabrication of tooling for microfluidic devices via laser micromachining and hot embossing, Journal of Micromechanics and Microengineering 18 (2) (2008) 025012.

[51] H. Niino, A. Yabe, Excimer laser polymer ablation: formation of positively charged surfaces and its application into the metallization of polymer films, Applied surface science 69 (1-4) (1993) 1–6.

[52] H. Becker, L. E. Locascio, Polymer microfluidic devices, Talanta 56 (2) (2002) 267–287.

[53] W. Ehrfeld, D. Münchmeyer, Three-dimensional microfabrication using synchrotron radiation, Nuclear Instruments and Methods in Physics Research Section A: Accelerators, Spectrometers, Detectors and Associated Equipment 303 (3) (1991) 523–531.

[54] V. Dolnik, S. Liu, S. Jovanovich, Capillary electrophoresis on microchip, Electrophoresis: an international journal 21 (1) (2000) 41–54.

[55] V. Dolnik, S. Liu, Applications of capillary electrophoresis on microchip, Journal of separation science 28 (15) (2005) 1994–2009.

[56] R. M. McCormick, R. J. Nelson, M. G. Alonso-Amigo, D. J. Benvegnu, H. H. Hooper, Microchannel electrophoretic separations of DNA in injection-molded plastic substrates, Analytical Chemistry 69 (14) (1997) 2626–2630.

[57] C. H. Ahn, J.-W. Choi, G. Beaucage, J. H. Nevin, J.-B. Lee, A. Puntambekar, J. Y. Lee, Disposable smart lab on a chip for point-of-care clinical diagnostics, Proceedings of the IEEE 92 (1) (2004) 154–173.

[58] C. S. Effenhauser, G. J. Bruin, A. Paulus, M. Ehrat, Integrated capillary electrophoresis on flexible silicone microdevices: analysis of DNA restriction fragments and detection of single dna molecules on microchips, Analytical Chemistry 69 (17) (1997) 3451–3457.

[59] M. Heckele, W. Bacher, K. Müller, Hot embossing-the molding technique for plastic microstructures, Microsystem technologies 4 (3) (1998) 122–124.

[60] O. Rötting, W. Röpke, H. Becker, C. Gärtner, Polymer microfabrication technologies, Microsystem Technologies 8 (1) (2002) 32–36.

[61] H. Becker, U. Heim, Hot embossing as a method for the fabrication of polymer high aspect ratio structures, Sensors and Actuators A: Physical 83 (1-3) (2000) 130–135.

[62] D. Zhang, L. Men, Q. Chen, Microfabrication and applications of opto-microfluidic sensors, Sensors 11 (5) (2011) 5360–5382.

[63] M. Li, S. Li, J. Wu, W. Wen, W. Li, G. Alici, A simple and cost-effective method for fabrication of integrated electronic-microfluidic devices using a laser-patterned PDMS layer, Microfluidics and nanofluidics 12 (5) (2012) 751–760.

[64] J. C. McDonald, D. C. Duffy, J. R. Anderson, D. T. Chiu, H. Wu, O. J. Schueller, G. M. Whitesides, Fabrication of microfluidic systems in poly (dimethylsiloxane), Electrophoresis: An International Journal 21 (1) (2000) 27–40.

[65] D. Qin, Y. Xia, G. M. Whitesides, Rapid prototyping of complex structures with feature sizes larger than 20 μm, Advanced Materials 8 (11) (1996) 917–919.

[66] Y. Xia, G. M. Whitesides, Soft lithography, Angewandte Chemie International Edition 37 (5) (1998) 550–575.

[67] D. Qin, Y. Xia, J. A. Rogers, R. J. Jackman, X.-M. Zhao, G. M. Whitesides, Microfabrication, microstructures and microsystems, in: Microsystem technology in chemistry and life science, Springer, 1998, pp. 1–20.

[68] K. Hosokawa, T. Fujii, I. Endo, Hydrophobic microcapillary vent for pneumatic manipulaiton of liquid in μtas, Micro Total Analysis Systems 98 (1998) 307–310.

[69] P. Wilding, J. Pfahler, H. H. Bau, J. N. Zemel, L. J. Kricka, Manipulation and flow of biological fluids in straight channels micromachined in silicon., Clinical Chemistry 40 (1) (1994) 43–47.

[70] H. V. Jansen, M. J. de Boer, S. Unnikrishnan, M. Louwerse, M. C. Elwenspoek, Black silicon method X: a review on high speed and selective plasma etching of silicon with profile control: an in-depth comparison between bosch and cryostat drie processes as a roadmap to next generation equipment, Journal of Micromechanics and Microengineering 19 (3) (2009) 033001.

[71] L. Wong, T. Suratwala, M. Feit, P. Miller, R. Steele, The effect of HF/NH4F etching on the morphology of surface fractures on fused silica, Journal of Non-Crystalline Solids 355 (13) (2009) 797–810.

[72] Z. Zheng, X. Zu, X. Jiang, X. Xiang, J. Huang, X. Zhou, C. Li, W. Zheng, L. Li, Effect of HF etching on the surface quality and laser-induced damage of fused silica, Optics & Laser Technology 44 (4) (2012) 1039–1042.

[73] C. Iliescu, J. Jing, F. E. Tay, J. Miao, T. Sun, Characterization of masking layers for deep wet etching of glass in an improved HF/HCl solution, Surface and Coatings Technology 198 (1-3) (2005) 314–318.

[74] Y. Mourzina, A. Steffen, A. Offenhäusser, The evaporated metal masks for chemical glass etching for BioMEMS, Microsystem technologies 11 (2-3) (2005) 135–140.

[75] A. Baram, M. Naftali, Dry etching of deep cavities in Pyrex for MEMS applications using standard lithography, Journal of Micromechanics and Microengineering 16 (11) (2006) 2287.

[76] D. Day, M. Gu, Microchannel fabrication in PMMA based on localized heating by nanojoule high repetition rate femtosecond pulses, Optics express 13 (16) (2005) 5939–5946.

[77] S. Prakash, S. Kumar, Fabrication of microchannels on transparent PMMA using CO2 laser (10.6 μm) for microfluidic applications: An experimental investigation, International Journal of Precision Engineering and Manufacturing 16 (2) (2015) 361–366.

[78] H. Y. Tan, W. K. Loke, N.-T. Nguyen, A reliable method for bonding polydimethylsiloxane (PDMS) to polymethylmethacrylate (PMMA) and its application in micropumps, Sensors and Actuators B: Chemical 151 (1) (2010) 133–139.

[79] J. Liu, H. Qiao, C. Liu, Z. Xu, Y. Li, L. Wang, Plasma assisted thermal bonding for PMMA microfluidic chips with integrated metal microelectrodes, Sensors and Actuators B: Chemical 141 (2) (2009) 646–651.

[80] A. Mathur, S. Roy, M. Tweedie, S. Mukhopadhyay, S. Mitra, J. McLaughlin, Characterisation of PMMA microfluidic channels and devices fabricated by hot embossing and sealed by direct bonding, Current Applied Physics 9 (6) (2009) 1199–1202.

[81] M. Leester-Schädel, T. Lorenz, F. Jürgens, C. Richter, Fabrication of microfluidic devices, in: Microsystems for Pharmatechnology, Springer, 2016, pp. 23–57.

[82] C. Iliescu, J. Miao, F. E. Tay, Stress control in masking layers for deep wet micromachining of Pyrex glass, Sensors and Actuators A: Physical 117 (2) (2005) 286–292.

[83] M. Bu, T. Melvin, G. J. Ensell, J. S. Wilkinson, A. G. Evans, A new masking technology for deep glass etching and its microfluidic application, Sensors and Actuators A: Physical 115 (2-3) (2004) 476–482.

[84] C. Iliescu, J. Miao, F. E. Tay, Optimization of an amorphous silicon mask PECVD process for deep wet etching of Pyrex glass, Surface and Coatings Technology 192 (1) (2005) 43–47.

[85] C. Iliescu, B. Chen, J. Miao, Deep wet etching-through 1mm pyrex glass wafer for microfluidic applications, Micro Electro Mechanical Systems, 2007. MEMS. IEEE 20th International Conference on (2007) 393–396.

[86] M. S. El-Eskandarany, 1 - introduction, in: M. S. El-Eskandarany (Ed.), Mechanical Alloying (Second Edition), second edition Edition, William Andrew Publishing, Oxford, 2015, pp. 1 – 12. doi:https://doi.org/10.1016/B978-1-4557-7752-5.00001-2.
URL http://www.sciencedirect.com/science/article/pii/B9781455777525000012

[87] P. Gu, K. Liu, H. Chen, T. Nishida, Z. H. Fan, Chemical-assisted bonding of thermoplastics/elastomer for fabricating microfluidic valves, Analytical chemistry 83 (1) (2010) 446–452.

[88] H. Becker, C. Gärtner, Polymer microfabrication methods for microfluidic analytical applications, Electrophoresis: An International Journal 21 (1) (2000) 12–26.

[89] F. Dang, S. Shinohara, O. Tabata, Y. Yamaoka, M. Kurokawa, Y. Shinohara, M. Ishikawa, Y. Baba, Replica multichannel polymer chips with a network of sacrificial channels sealed by adhesive printing method, Lab on a Chip 5 (4) (2005) 472–478.

[90] J. Han, S. Lee, A. Puntambekar, S. Murugesan, J. Choi, G. Beaucage, C. Ahn, Uv adhesive bonding techniques at room temperature for plastic lab-on-a-chip, 7th International Conference of Miniaturized Chemical and Biochemical Analysis Systems.

[91] C. Lu, L. J. Lee, Y.-J. Juang, Packaging of microfluidic chips via interstitial bonding technique, Electrophoresis 29 (7) (2008) 1407–1414.

[92] S. Lai, X. Cao, L. J. Lee, A packaging technique for polymer microfluidic platforms, Analytical chemistry 76 (4) (2004) 1175–1183.

[93] S. Yu, S. P. Ng, Z. Wang, C. L. Tham, Y. C. Soh, Thermal bonding of thermoplastic elastomer film to PMMA for microfluidic applications, Surface and Coatings Technology 320 (2017) 437–440.

[94] B. Bilenberg, M. Hansen, D. Johansen, V. Özkapici, C. Jeppesen, P. Szabo, I. Obieta, O. Arroyo, J. Tegenfeldt, A. Kristensen, Topas-based lab-on-a-chip microsystems fabricated by thermal nanoimprint lithography, Journal of Vacuum Science & Technology B: Microelectronics and Nanometer Structures Processing, Measurement, and Phenomena 23 (6) (2005) 2944–2949.

[95] J. Steigert, S. Haeberle, T. Brenner, C. Müller, C. Steinert, P. Koltay, N. Gottschlich, H. Reinecke, J. Rühe, R. Zengerle, et al., Rapid prototyping of microfluidic chips in COC, Journal of Micromechanics and Microengineering 17 (2) (2007) 333.

[96] C. K. Fredrickson, Z. Xia, C. Das, R. Ferguson, F. T. Tavares, Z. H. Fan, Effects of fabrication process parameters on the properties of cyclic olefin copolymer microfluidic devices, Journal of microelectromechanical systems 15 (5) (2006) 1060–1068.

[97] S. Roy, C. Y. Yue, Z. Wang, L. Anand, Thermal bonding of microfluidic devices: Factors that affect interfacial strength of similar and dissimilar cyclic olefin copolymers, Sensors and Actuators B: Chemical 161 (1) (2012) 1067–1073.

[98] A. Muck, J. Wang, M. Jacobs, G. Chen, M. P. Chatrathi, V. Jurka, Z. Vỳbornỳ, S. D. Spillman, G. Sridharan, M. J. Schöning, Fabrication of poly (methyl methacrylate) microfluidic chips by atmospheric molding, Analytical chemistry 76 (8) (2004) 2290–2297.

[99] Z. Chen, Y. Gao, J. Lin, R. Su, Y. Xie, Vacuum-assisted thermal bonding of plastic capillary electrophoresis microchip imprinted with stainless steel template, Journal of Chromatography A 1038 (1-2) (2004) 239–245.

[100] R. T. Kelly, A. T. Woolley, Thermal bonding of polymeric capillary electrophoresis microdevices in water, Analytical chemistry 75 (8) (2003) 1941–1945.

[101] L. E. Locascio, C. E. Perso, C. S. Lee, Measurement of electroosmotic flow in plastic imprinted microfluid devices and the effect of protein adsorption on flow rate, Journal of chromatography A 857 (1-2) (1999) 275–284.

[102] Z. Chen, Y. Gao, R. Su, C. Li, J. Lin, Fabrication and characterization of poly (methyl methacrylate) microchannels by in situ polymerization with a novel metal template, Electrophoresis 24 (18) (2003) 3246–3252.

[103] C.-W. Tsao, J. Liu, D. L. DeVoe, Droplet formation from hydrodynamically coupled capillaries for parallel microfluidic contact spotting, Journal of Micromechanics and Microengineering 18 (2) (2008) 025013.

[104] Y. Sun, Y. C. Kwok, N.-T. Nguyen, Low-pressure, high-temperature thermal bonding of polymeric microfluidic devices and their applications for electrophoretic separation, Journal of Micromechanics and Microengineering 16 (8) (2006) 1681.

[105] Z. Nie, Y. S. Fung, Microchip capillary electrophoresis for frontal analysis of free bilirubin and study of its interaction with human serum albumin, Electrophoresis 29 (9) (2008) 1924–1931.

[106] D. Olivero, Z. H. Fan, Chips tips: lamination of plastic microfluidic devices, Lab Chip. http://www. rsc. org/Publishing/Journals/lc/Chips_and_Tips/lamination. asp.

[107] J. A. Brydson, Plastics materials, Elsevier, 1999.

[108] J. Hildebrand, R. Scott, The solubility of nonelectrolytes, Reinhold Pub, Co., New York 3.

[109] H. V. Fuentes, A. T. Woolley, Phase-changing sacrificial layer fabrication of multilayer polymer microfluidic devices, Analytical chemistry 80 (1) (2008) 333–339.

[110] W. Ryu, S. W. Min, K. E. Hammerick, M. Vyakarnam, R. S. Greco, F. B. Prinz, R. J. Fasching, The construction of three-dimensional micro-fluidic scaffolds of

biodegradable polymers by solvent vapor based bonding of micro-molded layers, Biomaterials 28 (6) (2007) 1174–1184.

[111] F. Umbrecht, D. Müller, F. Gattiker, C. Boutry, J. Neuenschwander, U. Sennhauser, C. Hierold, Solvent assisted bonding of polymethylmethacrylate: Characterization using the response surface methodology, Sensors and Actuators A: Physical 156 (1) (2009) 121–128.

[112] S. Wu, Polymer interfaces and adhesion Marcel Dekker, New York.

[113] S. Hu, W. J. Brittain, Surface grafting on polymer surface using physisorbed free radical initiators, Macromolecules 38 (15) (2005) 6592–6597.

[114] A. Kruse, G. Krüger, A. Baalmann, O.-D. Hennemann, Surface pretreatment of plastics for adhesive bonding, Journal of adhesion science and technology 9 (12) (1995) 1611–1621.

[115] M. Collaud, P. Groening, S. Nowak, L. Schlapbach, Plasma treatment of polymers: the effect of the plasma parameters on the chemical, physical, and morphological states of the polymer surface and on the metal-polymer interface, Journal of adhesion science and technology 8 (10) (1994) 1115–1127.

[116] M. Shenton, M. Lovell-Hoare, G. Stevens, Adhesion enhancement of polymer surfaces by atmospheric plasma treatment, Journal of Physics D: Applied Physics 34 (18) (2001) 2754.

[117] L. Klintberg, M. Svedberg, F. Nikolajeff, G. Thornell, Fabrication of a paraffin actuator using hot embossing of polycarbonate, Sensors and Actuators A: Physical 103 (3) (2003) 307–316.

[118] L. Brown, T. Koerner, J. H. Horton, R. D. Oleschuk, Fabrication and characterization of poly (methylmethacrylate) microfluidic devices bonded using surface modifications and solvents, Lab on a Chip 6 (1) (2006) 66–73.

[119] M. A. Eddings, M. A. Johnson, B. K. Gale, Determining the optimal PDMS–PDMS bonding technique for microfluidic devices, Journal of Micromechanics and Microengineering 18 (6) (2008) 067001.

[120] Y. Wang, H. Chen, Q. He, S. A. Soper, A high-performance polycarbonate electrophoresis microchip with integrated three-electrode system for end-channel amperometric detection, Electrophoresis 29 (9) (2008) 1881–1888.

[121] A. Boglea, A. Olowinsky, A. Gillner, Fibre laser welding for packaging of disposable polymeric microfluidic-biochips, Applied Surface Science 254 (4) (2007) 1174–1178.

[122] J. Kim, X. Xu, Excimer laser fabrication of polymer microfluidic devices, Journal of Laser Applications 15 (4) (2003) 255–260.

[123] K. F. Lei, S. Ahsan, N. Budraa, W. J. Li, J. D. Mai, Microwave bonding of polymer-based substrates for potential encapsulated micro/nanofluidic device fabrication, Sensors and Actuators A: Physical 114 (2-3) (2004) 340–346.

[124] J. Kim, B. Jeong, M. Chiao, L. Lin, Ultrasonic bonding for MEMS sealing and packaging, IEEE transactions on Advanced Packaging 32 (2) (2009) 461–467.

[125] Y. Luo, Z. Zhang, X. Wang, Y. Zheng, Ultrasonic bonding for thermoplastic microfluidic devices without energy director, Microelectronic Engineering 87 (11) (2010) 2429–2436.

[126] G. Wallis, Direct-current polarization during field-assisted glass-metal sealing, Journal of the American Ceramic Society 53 (10) (1970) 563–567.

[127] M. A. Witek, S. Wei, B. Vaidya, A. A. Adams, L. Zhu, W. Stryjewski, R. L. McCarley, S. A. Soper, Cell transport via electromigration in polymer-based microfluidic devices, Lab on a Chip 4 (5) (2004) 464–472.

[128] R. Truckenmuller, P. Henzi, D. Herrmann, V. Saile, W. Schomburg, A new bonding process for polymer micro-and nanostructures based on near-surface degradation, Micro Electro Mechanical Systems, 2004. 17th IEEE International Conference on. (2004) 761–764.

[129] D.-W. Park, M. Hupert, M. Witek, B. You, P. Datta, J. Guy, J.-B. Lee, S. Soper, D. Nikitopoulos, M. Murphy, A titer plate-based polymer microfluidic platform for high throughput nucleic acid purification, Biomedical microdevices 10 (1) (2008) 21–33.

[130] C. Tsao, L. Hromada, J. Liu, P. Kumar, D. DeVoe, Low temperature bonding of PMMA and COC microfluidic substrates using UV/ozone surface treatment, Lab on a Chip 7 (4) (2007) 499–505.

[131] J. Liu, S. Yang, C. S. Lee, D. L. DeVoe, Polyacrylamide gel plugs enabling 2-D microfluidic protein separations via isoelectric focusing and multiplexed sodium dodecyl sulfate gel electrophoresis, Electrophoresis 29 (11) (2008) 2241–2250.

[132] H. H. Tran, W. Wu, N. Y. Lee, Ethanol and uv-assisted instantaneous bonding of PMMA assemblies and tuning in bonding reversibility, Sensors and Actuators B: Chemical 181 (2013) 955–962.

[133] V. Saarela, M. Haapala, R. Kostiainen, T. Kotiaho, S. Franssila, Microfluidic heated gas jet shape analysis by temperature scanning, Journal of Micromechanics and Microengineering 19 (5) (2009) 055001.

[134] M. Howlader, S. Suehara, T. Suga, Room temperature wafer level glass/glass bonding, Sensors and Actuators A: Physical 127 (1) (2006) 31–36.

[135] P. Mrozek, Anodic bonding of glasses with interlayers for fully transparent device applications, Sensors and Actuators A: Physical 151 (1) (2009) 77–80.

[136] M. Haapala, V. Saarela, J. Pól, K. Kolari, T. Kotiaho, S. Franssila, R. Kostiainen, Integrated liquid chromatography–heated nebulizer microchip for mass spectrometry, Analytica chimica acta 662 (2) (2010) 163–169.

[137] C. Iliescu, D. P. Poenar, M. Carp, F. C. Loe, A microfluidic device for impedance spectroscopy analysis of biological samples, Sensors and Actuators B: Chemical 123 (1) (2007) 168–176.

[138] L. Yu, F. E. Tay, G. Xu, B. Chen, M. Avram, C. Iliescu, Adhesive bonding with SU-8 at wafer level for microfluidic devices, Journal of Physics: Conference Series 34 (2006) 776.

[139] N. Harris, A. Keating, M. Hill, A lateral mode flow-through pmma ultrasonic separator, Sensors & Actuators.

[140] K. Kim, S. W. Park, S. S. Yang, The optimization of PDMS-PMMA bonding process using silane primer, BioChip Journal 4 (2) (2010) 148–154.

[141] X. Sun, B. A. Peeni, W. Yang, H. A. Becerril, A. T. Woolley, Rapid prototyping of poly (methyl methacrylate) microfluidic systems using solvent imprinting and bonding, Journal of Chromatography A 1162 (2) (2007) 162–166.

[142] C.-H. Lin, C.-H. Chao, C.-W. Lan, Low azeotropic solvent for bonding of PMMA microfluidic devices, Sensors and Actuators B: chemical 121 (2) (2007) 698–705.

[143] S. Ng, R. Tjeung, Z. Wang, A. Lu, I. Rodriguez, N. F. de Rooij, Thermally activated solvent bonding of polymers, Microsystem Technologies 14 (6) (2008) 753–759.

[144] Y. H. Tennico, M. T. Koesdjojo, S. Kondo, D. T. Mandrell, V. T. Remcho, Surface modification-assisted bonding of polymer-based microfluidic devices, Sensors and Actuators B: Chemical 143 (2) (2010) 799–804.

[145] J. S. Buch, C. Kimball, F. Rosenberger, W. E. Highsmith, D. L. DeVoe, C. S. Lee, DNA mutation detection in a polymer microfluidic network using temperature gradient gel electrophoresis, Analytical chemistry 76 (4) (2004) 874–881.

[146] H. Shadpour, M. L. Hupert, D. Patterson, C. Liu, M. Galloway, W. Stryjewski, J. Goettert, S. A. Soper, Multichannel microchip electrophoresis device fabricated in polycarbonate with an integrated contact conductivity sensor array, Analytical chemistry 79 (3) (2007) 870–878.

[147] L. Riegger, M. Grumann, J. Steigert, S. Lutz, C. Steinert, C. Mueller, J. Viertel, O. Prucker, J. Rühe, R. Zengerle, et al., Single-step centrifugal hematocrit determination on a 10 dollars processing device, Biomedical microdevices 9 (6) (2007) 795–799.

[148] L. P. Hromada, B. J. Nablo, J. J. Kasianowicz, M. A. Gaitan, D. L. DeVoe, Single molecule measurements within individual membrane-bound ion channels using a polymer-based bilayer lipid membrane chip, Lab on a Chip 8 (4) (2008) 602–608.

[149] J. Atencia, G. A. Cooksey, A. Jahn, J. M. Zook, W. N. Vreeland, L. E. Locascio, Magnetic connectors for microfluidic applications, Lab on a Chip 10 (2) (2009) 246–249.

[150] Y. Temiz, R. D. Lovchik, G. V. Kaigala, E. Delamarche, Lab-on-a-chip devices: How to close and plug the lab?, Microelectronic Engineering 132 (2015) 156–175.

[151] H. Becker, One size fits all?, Lab on a Chip 10 (15) (2010) 1894–1897.

[152] H. van Heeren, Standards for connecting microfluidic devices?, Lab on a Chip 12 (6) (2012) 1022–1025.

[153] A. C. Glavan, R. V. Martinez, E. J. Maxwell, A. B. Subramaniam, R. M. Nunes, S. Soh, G. M. Whitesides, Rapid fabrication of pressure-driven open-channel microfluidic devices in omniphobic RF paper, Lab on a Chip 13 (15) (2013) 2922–2930.

[154] A. V. Pattekar, M. V. Kothare, Novel microfluidic interconnectors for high temperature and pressure applications, Journal of Micromechanics and Microengineering 13 (2) (2003) 337.

[155] D. M. Hartmann, J. T. Nevill, K. I. Pettigrew, G. Votaw, P.-J. Kung, H. C. Crenshaw, A low-cost, manufacturable method for fabricating capillary and optical fiber interconnects for microfluidic devices, Lab on a Chip 8 (4) (2008) 609–616.

[156] D. A. Mair, E. Geiger, A. P. Pisano, J. M. Fréchet, F. Svec, Injection molded microfluidic chips featuring integrated interconnects, Lab on a Chip 6 (10) (2006) 1346–1354.

[157] H.-l. Chang, F. Zhang, J.-l. Ding, F.-l. Chen, S.-j. Hong, M. Kraft, W.-z. Yuan, A highly reliable integrated PDMS interconnector with a long cast flange for microfluidic systems, Microsystem technologies 18 (6) (2012) 723–730.

[158] B. Gray, D. Jaeggi, N. Mourlas, B. Van Drieenhuizen, K. Williams, N. Maluf, G. Kovacs, Novel interconnection technologies for integrated microfluidic systems1, Sensors and Actuators A: Physical 77 (1) (1999) 57–65.

[159] A. A. S. Bhagat, P. Jothimuthu, A. Pais, I. Papautsky, Re-usable quick-release interconnect for characterization of microfluidic systems, Journal of Micromechanics and Microengineering 17 (1) (2007) 42.

[160] C.-H. Chiou, G.-B. Lee, Minimal dead-volume connectors for microfluidics using PDMS casting techniques, Journal of Micromechanics and Microengineering 14 (11) (2004) 1484.

[161] D. Van Swaay, J.-P. Mächler, C. Stanley, et al., A chip-to-world connector with a built-in reservoir for simple small-volume sample injection, Lab on a Chip 14 (1) (2014) 178–181.

[162] E. Wilhelm, C. Neumann, T. Duttenhofer, L. Pires, B. E. Rapp, Connecting microfluidic chips using a chemically inert, reversible, multichannel chip-to-world-interface, Lab on a Chip 13 (22) (2013) 4343–4351.

[163] A. Waldbaur, J. Kittelmann, C. P. Radtke, J. Hubbuch, B. E. Rapp, Microfluidics on liquid handling stations (μF-on-LHS): an industry compatible chip interface between

microfluidics and automated liquid handling stations, Lab on a Chip 13 (12) (2013) 2337–2343.

[164] R. M. Tiggelaar, F. Benito-López, D. C. Hermes, H. Rathgen, R. J. Egberink, F. G. Mugele, D. N. Reinhoudt, A. van den Berg, W. Verboom, H. J. Gardeniers, Fabrication, mechanical testing and application of high-pressure glass microreactor chips, Chemical Engineering Journal 131 (1-3) (2007) 163–170.

[165] A. Scott, A. K. Au, E. Vinckenbosch, A. Folch, A microfluidic D-subminiature connector, Lab on a chip 13 (11) (2013) 2036–2039.

[166] D. Sabourin, M. Dufva, T. Jensen, J. Kutter, D. Snakenborg, One-step fabrication of microfluidic chips with in-plane, adhesive-free interconnections, Journal of Micromechanics and Microengineering 20 (3) (2010) 037001.

[167] V. Saarela, S. Franssila, S. Tuomikoski, S. Marttila, P. Östman, T. Sikanen, T. Kotiaho, R. Kostiainen, Re-usable multi-inlet PDMS fluidic connector, Sensors and Actuators B: Chemical 114 (1) (2006) 552–557.

[168] G. Perozziello, F. Bundgaard, O. Geschke, Fluidic interconnections for microfluidic systems: a new integrated fluidic interconnection allowing plug n play functionality, Sensors and Actuators B: Chemical 130 (2) (2008) 947–953.

[169] O. Paydar, C. Paredes, Y. Hwang, J. Paz, N. Shah, R. Candler, Characterization of 3D-printed microfluidic chip interconnects with integrated O-rings, Sensors and Actuators A: Physical 205 (2014) 199–203.

[170] T. Pan, A. Baldi, B. Ziaie, A reworkable adhesive-free interconnection technology for microfluidic systems, Journal of Microelectromechanical Systems 15 (1) (2006) 267–272.

[171] E. R. Murphy, T. Inoue, H. R. Sahoo, N. Zaborenko, K. F. Jensen, Solder-based chip-to-tube and chip-to-chip packaging for microfluidic devices, Lab on a Chip 7 (10) (2007) 1309–1314.

Appendix B

Appendix B

Co-authored paper :*Barani, Kianoush, Morteza Dehghani, M. R. Azadi, and Ali Karrech. "Leaching of a polymetal gold ore and reducing cyanide consumption using cyanide-glycine solutions." Minerals Engineering 163 (2021): 106802.*